

**Innovative approaches towards the optimization of particle
emission monitoring and operating behavior of
pulse-jet cleaned filters in gas cleaning applications**

Zur Erlangung des akademischen Grades eines
DOKTORS DER INGENIEURWISSENSCHAFTEN

von der KIT-Fakultät für Chemieingenieurwesen und Verfahrenstechnik des
Karlsruher Instituts für Technologie (KIT)

genehmigte

DISSERTATION

von
Peter Wolfgang Bächler
aus Würzburg

Tag der mündlichen Prüfung: 23.07.2024

Erstgutachter: Prof. Dr.-Ing. habil. Achim Dittler

Zweitgutachter: Prof. Dr.-Ing. habil. Eberhard Schmidt

ABSTRACT

Pulse-jet cleaned filters are well established in gas cleaning processes for the separation of particles from dust-laden gas streams in many industrial sectors. Due to the efficient particle separation enabled by the development of a dust cake on the medium surface of installed filter elements, emission limits can be reliably met provided the filters are operated under suitable conditions and no leaks enable direct bypass of particulate matter from the raw-gas side to the clean gas side. Small leaks in the range of only several parts per million of installed filter area can contribute greatly to the total dust emission and serve as spatial particle emission hotspots. The identification of such leaks is one of the greatest challenges of the filter industry and suitable (spatially resolved) online measurement technology has the potential to improve process monitoring for pulse-jet cleaned filters facilitating troubleshooting and maintenance procedures for plant operators. In addition to leaks, filter operation is rarely optimized apart from the initial plant layout. Unsuitable regeneration strategies (e.g. high tank pressures or too long / short cycle times between individual filter regenerations) can lead to increased dust emissions or an increased power consumption.

This dissertation deals with these two current problems (identification of particle emission hotspots and efficient filter operation regarding energy demand and particle emissions) of baghouse filtration application. The emission behavior of pulse-jet cleaned filters was investigated by application of spatially deployed online particle emission measurement technology with the goal to identify particle emission hotspots. Additionally, an evaluation of the energy demand of the filtration process in the context of particle emission was performed in order to identify favorable operating conditions to potentially lower dust emissions and improve energy efficiency of the separation process.

For the evaluation of the spatially resolved transient particle emission behavior commercially available “low-cost” PM-sensors that could be installed locally on the clean gas side of baghouses due to their compact size for simultaneous online process monitoring were utilized. The sensors are prominently applied under ambient conditions for air quality monitoring. The operation under demanding conditions in a technical process challenges the limits and accuracy of the low-cost measurement technology regarding the measurement of concentration peaks, as well as the maximum specified particle concentration (e.g. 3000 #/cm³ for the Sensirion sensor) and particle size categorization of the dust emission. For the initial testing of the general suitability of the sensors to measure and quantify the characteristic transient particle emission behavior of pulse-jet cleaned filters, different sensors were installed in a filter test rig for surface filter media based on DIN ISO 11057. Out of a wide selection of commercially available low-cost PM-sensors, the model OPC-N3 manufactured by Alphasense and the model SPS30 of the manufacturer Sensirion were selected in the experiments due to their comprehensive datasheets (including e.g. information on sensor calibration) and different specifications. The Sensirion sensor offers mainly mass & number resolved particulate matter (PM_x) concentrations as measurement outputs and is very limited regarding size categorization (5 size classes). These corresponding outputs and the limited amount of size-information are typical for the larger share of available low-cost PM-sensors. The Alphasense sensor on the other hand offers a larger variety of (measurement) data outputs whereby particle density can be considered in the determination of mass resolved particulate matter concentrations. Furthermore, counting events over a total of 24 size classes enable the determination of particle size distributions.

Three different filter media with different properties and surface treatments (membrane lamination; sined upstream side; hydro entangled micro-filaments) were selected to investigate the impact of filter media properties on different particle emission levels applying low-cost PM-sensors. The test dust for all experiments was an aluminum oxide hydroxide powder “Pural SB” of the manufacturer Sasol. During the validation measurements in the filter test rig, both tested sensors measured the characteristic particle emission peak caused by particle penetration through the filter medium directly after filter regeneration and a subsequent concentration decay with increasing cake formation on the surface of the filter medium until no particles can penetrate to the clean gas side (zero concentration). In comparison to a highly developed reference aerosol spectrometer (Promo[®]2000 with welas[®]2100 sensor of the manufacturer Palas[®]), quantitative differences regarding the detected particle concentrations (e.g. peak height, decay behavior / shape of the emission peak and emitted dust mass per filter area) could be shown. Despite these quantitative differences, the sensors were in good agreement with the reference regarding the general characterization of the particle emission, enabling the identification of different particle emission levels (e.g. caused by filter aging or the application of the three different filter media) and the corresponding particle size distribution in case of the Alphasense sensor (albeit with a lower size resolution compared to the reference).

After the initial validation under defined conditions in the filter test rig, multiple low-cost PM-sensors were spatially deployed in a pilot-plant scale baghouse filter with nine filter bags. Due to the more comprehensive size categorization compared to other low-cost PM-sensors (including the previously investigated SPS30 of the manufacturer Sensirion), the OPC-N3 sensor of the manufacturer Alphasense was selected for these further experiments. A beneficial application scenario for online particle emission monitoring is the spatial identification of small leaks (in the range of several parts per million of installed filter area) and particle emission hotspots that contribute greatly to the total dust emission and are difficult to pinpoint on an industrial scale where hundreds of filter elements are installed. Early detection and localization of a potential leak can enable well directed and fast maintenance procedures (e.g. exchanging the corresponding filter bag) as well as avoid premature replacement of intact filter bags that would (without leak identification) be exchanged as a precaution. For larger baghouses monitoring for each filter bag is economically not feasible (e.g. monitoring of individual rows only), but smaller facilities with fewer filter elements can profit from local online emission monitoring.

“Emission hotspots” were created in the baghouse filter by installing an individual factory-new membrane filter bag with seams. The seams of the filter bag act similar to pinhole leaks and are a source of particle penetration, especially at a low filter age. One factory-new bag with the corresponding seams was installed at each of the different installment positions over multiple experiments. The remaining eight filter elements were made from an efficient membrane filter medium with sealed seams. Particle penetration through these filter elements is very low compared to the increased particle penetration through the seams of the factory-new bag. This filter bag serving as particle emission hotspot could be reliably identified based on the detected particle concentrations by the low-cost PM-sensors. In another investigated application scenario, several leaks were generated within an individual filter bag. The leaks caused a high increase in (continuous) particle emission, pushing the limits of the detection capabilities of the sensor regarding the maximum particle concentration (coincidence probability of 0.84% at 1000 #/cm³ for the Alphasense sensor) and demonstrating limitations in sensor accuracy

regarding size categorization. While an increasing average PM_{10} concentration served as a reliable indication for the growing number of leaks, an illegitimate decrease in $PM_{2.5}$ concentration was proof for a coincidence error. Despite this error, the overall suitability of the sensors and their potential as cheap monitoring tool regarding spatial leak detection was demonstrated.

Under more defined conditions at a lower particle emission level (application of membrane filter elements with sealed seams for all nine installment positions in the baghouse filter), the sensors characterized the spatial particle emission behavior in accordance to the expected transient behavior known from literature and the validation experiments in the filter test rig. After the regeneration of the corresponding filter element, a particle emission peak was detected by the sensor at the measurement position. The peak quickly declined to a zero level after a couple of seconds mainly due to the high efficiency of the membrane filter bag and the fast cake formation. Measurements applying the reference aerosol spectrometer showed the same qualitative trend, whereby quantitative differences regarding the exact particle concentrations were shown.

Further experiments regarding the (spatial) particle emission behavior were investigated in the pilot-plant scale baghouse filter for regular filter bags without sealed seams. The overall (qualitative) trends measured by the low-cost PM-sensors were in good agreement with the trends detected by the reference aerosol spectrometer. The low-cost PM-sensors measured a decreasing particle emission with increasing filter age due to deposition of particles within the filter matrix and clogging of the seams at the individual filter element according to the typical behavior known from literature and application. Increasing the tank pressure above suitable operation points causes a “random” spatial and temporal increase of (continuous) particle emissions. This behavior is linked to the seams of the filter element that de-clog due to the high pulse-intensity enabling renewed particle penetration. This spatio-temporal behavior was validated applying the reference aerosol spectrometer. Differences in the average particle emission level caused by application of filter bags made from different filter media (identical filter media compared to validation experiments) and variation of cycle time could also be derived based on measurements with low-cost PM-sensors and are in agreement with the results from the filter test rig. The particle size distribution calculated from the counting events registered by the Alphasense OPC-N3 low-cost sensor was in overall agreement with the reference but only gives a limited amount of information due to the lower number of size classes compared to the reference device. The general spatial particle emission behavior of the pilot plant scale baghouse filter that was characterized by the low-cost PM-sensors was put into context of an industrial field measurement, where a qualitatively corresponding emission behavior was observed at individual filter bags.

Investigations concerning the operating behavior of pulse-jet cleaned filters in the combined context of energy-demand and particle emissions was the second focus of this work (no spatial PM-monitoring). The total power for filter operation was calculated based on the required fan power and an average power representing the consumption of pressurized air for filter regeneration. An experimental parameter study was performed for several raw-gas concentrations, filter face velocities and regeneration tank pressures varying the cycle time between individual filter regenerations for each set of parameters. A dedicated power minimum at a corresponding cycle time (ranging from 30 to 120 seconds) could be identified for each set of parameters. A suitable operating point should be selected at or above the cycle time for the power minimum, as shorter cycle times cause higher dust emissions at no energetic benefit. The

total particle emission decreases hyperbolically with increasing cycle time, as fewer particle emission peaks occur over a certain time. Too short cycle times create a state of near constant regeneration, where particle emissions increase strongly and the consumption of pressurized air dominates the total power. For exceedingly long cycle times the differential pressure / fan power contribute greatly to the total power pushing the limits of the maximum blower capacity. Larger filter face velocities and raw-gas concentrations cause a shift of the power minimum to shorter cycle times / more frequent regenerations. Increasing the tank pressure, while causing an increase of the cycle time at the power minimum, creates no clear energetic benefit at the cost of strongly increased particle emissions. The results of the experimental parameter study were modeled applying the fundamental equations for the operating behavior of pulse-jet cleaned filters. After the selection of a suitable fit parameter (filter medium resistance as a function of cycle time), the results between model and experiment were in good agreement.

GERMAN ABSTRACT - ZUSAMMENFASSUNG

Druckstoßregenerierte Oberflächenfilter werden konventionell zur Abscheidung von Partikeln aus Feststoff beladenen Gasströmen in der Gasreinigung eingesetzt. Aufgrund der effizienten Partikelabscheidung durch den Aufbau eines Staubkuchens auf der Medienoberfläche der installierten Filterelemente können Emissionsgrenzwerte zuverlässig eingehalten werden, sofern die Filter unter geeigneten Bedingungen betrieben werden und keine Lecks den direkten Staubdurchtritt von der Rohgasseite auf die Reingasseite ermöglichen. Selbst kleine Lecks mit einer Fläche mehrere Größenordnungen unterhalb der installierten Filterfläche können signifikant zur Gesamtemission der Filteranlagen beitragen und fungieren als lokaler Emissions-Hotspot. Die Identifikation solcher Fehlstellen ist eine der größten Herausforderungen der Filterindustrie. Geeignete (räumlich verteilte) Online-Messtechnik hat das Potential die Prozessüberwachung und Wartung der Schlauchfilteranlagen zu verbessern. Neben dem Emissionsbeitrag von Lecks, ist der Filterbetrieb abseits der ursprünglichen Auslegung selten optimiert. Ungünstige Betriebseinstellungen (wie beispielsweise zu hohe Tankdrücke für die Regenerierung oder zu lange / kurze Zykluszeiten zwischen Regenerierungen der einzelnen Filterelemente) können zu erhöhten Emissionen oder einem erhöhten Energiebedarf führen.

Diese Dissertation beschäftigt sich mit diesen zwei aktuellen Problemstellungen (Identifikation von Emissionshotspots und effizienter Filterbetrieb im Hinblick auf Energiebedarf und Partikelemission) beim Betrieb von Schlauchfilteranlagen. Das Emissionsverhalten von druckstoßregenerierten Oberflächenfiltern wurde durch den Einsatz von räumlich verteilter online Partikelmesstechnik untersucht. Das Ziel dieser Untersuchungen war die zuverlässige Detektion und lokale Identifikation von Partikel-Emissionshotspots. Außerdem wurde der Energiebedarf von Filteranlagen im Kontext der Partikelemission untersucht um günstige Betriebsbedingungen zu identifizieren und so die Energieeffizienz der Anlagen zu verbessern und Emissionen zu verringern.

Für die Untersuchung des zeitlich und räumlich aufgelösten Partikelemissionsverhaltens wurden kommerziell erhältliche, kostengünstige Partikelzählsensoren (Low-Cost PM-Sensoren) verwendet, welche aufgrund der kompakten Bauweise potentiell als Online-Messtechnik auf der Reingasseite von Filterhäusern (bei Umgebungsbedingungen) geeignet wären. Ein bisher weit verbreitetes Einsatzfeld der Sensoren war die Messung der Partikelkonzentration in der Umgebungsluft. Ein Einsatz unter herausfordernden Bedingungen in technischen Prozessen stellt die Messgrenzen und die Genauigkeit der Sensoren im Hinblick auf die Messung von kurzen Emissionsspitzen, des maximalen Konzentrationsbereichs (z.B. 3000 #/cm³ für den Sensirion Sensor) und der Erfassung der Größenverteilung der Staubemission auf die Probe. Im Rahmen einer ersten Validierung im Hinblick auf die Eignung der Sensoren zur Erfassung des charakteristischen Emissionsverhaltens von druckstoßregenerierten Oberflächenfiltern wurden die Sensoren in einem Filterprüfstand angelehnt an die DIN ISO 11057 eingesetzt. Aus einer hohen Anzahl an kommerziell verfügbaren Low-Cost PM-Sensoren wurden der Sensor OPC-N3 des Herstellers Alphasense und der Sensor SPS30 des Herstellers Sensirion für die Untersuchungen ausgewählt. Die beiden ausgewählten Sensormodelle zeichnen sich durch ein umfassendes Datenblatt (z.B. mit Hinweisen zur Kalibrierung) und verschiedene Spezifikationen aus. Der Sensirion Sensor ermöglicht die Bestimmung von masse- und anzahlbezogenen (PM_x) Feinstaubkonzentrationen und hat lediglich eine grobe Auflösung der Partikelgrößenverteilung (5 Klassen). Diese ausgegebenen Messdaten des Sensors und die geringe Auflösung einer

Partikelgrößenverteilung sind charakteristisch für den Großteil verfügbarer Low-Cost PM-Sensoren. Der Alphasense Sensor liefert eine größere Anzahl an Messdaten wobei bei der Bestimmung von massebezogenen PM_x Feinstaubkonzentrationen die Partikeldichte in den Einstellungen berücksichtigt werden kann. Weiterhin kann anhand von Zählereignissen in insgesamt 24 Größenklassen eine Partikelgrößenverteilung des Messaerosols bestimmt werden.

Es wurde das Emissionsverhalten bei drei verschiedenen Filtermedien mit verschiedenen Eigenschaften und Oberflächenbehandlungen (auflaminierte Membran, gesengte Anströmseite, wasserstrahlverfestigte Mikrofilamente) mit Hilfe von Low-Cost PM-Sensoren untersucht. Der Teststaub für alle Untersuchungen dieser Arbeit war der Aluminium-Oxid-Hydroxid Staub „Pural SB“ des Herstellers Sasol. Bei den Validierungsuntersuchungen im Filterprüfstand konnten die Sensoren den Emissionspeak auf Basis von Partikeldurchtritt durch das Filtermedium nach der Regenerierung und den darauffolgenden Konzentrationsabfall durch fortschreitenden Kuchenaufbau, bis keine Partikeln mehr auf die Reingasseite penetrieren können (Konzentration sinkt auf null ab), messen. Im Vergleich zu einem Referenz-Aerosolspektrometer (Promo[®]2000 mit welas[®]2100 Sensor des Herstellers Palas[®]) wurden quantitative Abweichungen der erfassten Partikelkonzentrationen (z.B. Höhe und Form des Emissionspeaks, Abklingverhalten und emittierte Staubmasse pro Filterfläche) festgestellt. Trotz der quantitativen Abweichungen wurden äquivalente Emissionsniveaus (z.B. durch Filteralterung oder durch die Verwendung der verschiedenen Filtermedien) zwischen den Low-Cost PM-Sensoren und dem Referenz-Aerosolspektrometer erfasst. Im Falle des Alphasense Sensors stimmte auch die Größenverteilung der Partikelemission (wenn auch mit geringerer Auflösung) mit der Referenz überein.

Nach der ursprünglichen Validierung der Sensoren unter definierten Bedingungen im Filterprüfstand wurden die Sensoren in einer Schlauchfilteranlage im Technikumsmaßstab mit neun Filterschläuchen zur lokalen und simultanen Emissionserfassung eingesetzt. Aufgrund der besseren Auflösung der Partikelgrößenverteilung im Vergleich zu anderen verfügbaren Low-Cost PM-Sensoren (u.A. auch dem vorher untersuchten SPS30 des Herstellers Sensirion) wurde der OPC-N3 des Herstellers Alphasense für diese weiteren Experimente ausgewählt. Ein wichtiges Anwendungsszenario für die Online-Überwachung der Partikelemission ist die Identifikation von kleinen Lecks (im Bereich weniger Millionstel Fläche in Bezug auf die installierte Filterfläche) und anderen Emissions-Hotspots, die stark zur Gesamtemission beitragen. Im industriellen Maßstab, wo unter Umständen Hunderte von Filterelementen installiert sind, ist die genaue Identifikation eines Lecks mit enormen Aufwand verbunden. Frühzeitige Detektion und Lokalisierung eines möglichen Lecks würden die zielgerichtete und schnelle Wartung (z.B. den Austausch des defekten Filterelements) ermöglichen und den vorzeitigen Austausch intakter Filterelemente, welche ohne genaue Identifikation des Lecks als Sicherheitsmaßnahme ausgetauscht werden würden, vermeiden. Zwar können bei großen Anlagen nicht alle Schläuche (wirtschaftlich) mit Low-Cost Sensoren ausgestattet werden (ggf. lediglich Überwachung einzelner Reihen), besonders kleine Anlagen mit wenigen Elementen können aber von einer lokalen Überwachung profitieren.

In den Untersuchungen wurden gezielt lokale Emissions-Hotspots im Schlauchfilter eingebracht. Hierbei wurden die Nähte von fabrikneuen Filterschläuchen, welche äquivalent zu kleineren „Pinhole“ Lecks einen erhöhten Partikeldurchtritt (insbesondere bei einem geringen Filteralter) ermöglichen, verwendet. Ein einzelner fabrikneuer Filterschlauch mit entsprechender Naht wurde über mehrere Messreihen an verschiedenen Stellen eingebaut, wobei die restlichen acht Filterelemente aus einem effizienten Membranfiltermedium mit

versiegelten Nähten gefertigt waren, welche ein geringes Emissionsniveau ermöglichen und Partikeldurchtritt im Vergleich zu den Nähten des fabrikneuen Schlauchs nur in sehr geringem Maß auftritt. Dieser Partikelemissions-Hotspot konnte anhand der gemessenen Partikelkonzentrationen durch die kostengünstigen PM-Sensoren zuverlässig identifiziert werden. In einem weiteren Versuch wurde eine steigende Anzahl an Lecks über mehrere Versuchsdurchläufe in einem einzelnen Filterschlauch erzeugt. Die Lecks verursachten einen starken Anstieg der (kontinuierlichen) Partikelemission an der zugehörigen Messposition und der Gesamtemission, was die Messgenauigkeit der Sensoren im Hinblick auf die maximale Partikelkonzentration an ihre Grenzen brachte und die Größenklassierung des Aerosols beeinflusste. Eine steigende mittlere PM₁₀-Konzentration war ein zuverlässiger Indikator für die steigende Anzahl der Lecks. Ein scheinbarer und fälschlicherweise detektierter Rückgang der PM_{2,5}-Konzentration am Emissions-Hotspot war ein deutliches Anzeichen für das Auftreten von Koinzidenz bei der Partikelzählung des Sensors (Koinzidenzwahrscheinlichkeit von 0,84% bei lediglich 1000 #/cm³ für den Alphasense Sensor). Trotz der Messungenauigkeiten wurde das Potential der Sensoren als kostengünstiges Überwachungstool für die räumliche Detektion von Lecks aufgezeigt.

Unter definierten Bedingungen bei einem geringeren Emissionsniveau (Einsatz von Membranfilterelementen mit versiegelten Nähten für alle neun Einbaupositionen der Filteranlage) wurde das räumlich und zeitlich aufgelöste Emissionsverhalten durch die Messung mit verteilten Sensoren einhergehend mit dem erwarteten Verhalten aus der Literatur und der Validierungsmessungen im Filterprüfstand erfasst. Nach der Regenerierung des entsprechenden Filterelements wurde vom Sensor an der zugehörigen Messposition ein Emissionspeak detektiert. Aufgrund des hohen Abscheidegrads des Membranfilterelements und dem direkten Kuchenaufbau klingt die Partikelemission bereits nach einigen Sekunden auf ein Nullniveau ab. Die Messungen mit dem Referenz-Aerosolspektrometer zeigten einen äquivalenten qualitativen Trend, wobei erneut quantitative Unterschiede hinsichtlich der exakten Partikelkonzentrationen zwischen Low-Cost Sensoren und der Referenz aufgezeigt wurden.

Weitere Trends im räumlichen Partikelemissionsverhalten wurden in der Schlauchfilteranlage bei Verwendung von regulären Filterschläuchen ohne versiegelte Nähte untersucht und die Messergebnisse der Low-Cost PM-Sensoren stimmten (qualitativ) mit dem Referenz-Aerosolspektrometer überein. So hat die Messung mit verteilten Sensoren den bekannten Trend einer abnehmenden Partikelemission mit zunehmendem Filteralter aufgrund von Partikeleinlagerungen innerhalb der Filtermatrix und der Verstopfung der Nähte lokal am einzelnen Filterelement aufgezeigt. Eine Erhöhung des Tankdrucks oberhalb geeigneter Betriebspunkte hinaus führt zu einem "zufälligen" lokalen und zeitlich begrenzten Auftreten von Partikelemissionen an einzelnen Filterelementen. Diese Daueremission wurde mit den Nähten des Filterelements in Verbindung gebracht, wobei sich vorherige Verstopfungen der Nähte aufgrund der hohen Druckstoßintensität lösen können und somit erneuten Partikeldurchtritt ermöglichen. Das Auftreten der umlaufabhängigen Daueremission, welche primär bei den erhöhten Tankdrücken auftritt wurde auch durch eine lokale Messung mit dem Referenz-Aerosolspektrometer validiert. Durch den Einsatz von Filterschläuchen aus verschiedenen Filtermedien (gleiche Filtermedien wie bei den Validierungsmessungen im Filterprüfstand) und der Variation der Zykluszeit zwischen den einzelnen Filterregenerierungen wurden, äquivalent zur Messung im Filterprüfstand, verschiedene Emissionsniveaus durch Messungen mit Low-Cost PM-Sensoren untersucht. Die ermittelte Partikelgrößenverteilung,

welche aus den registrierten Zählereignissen des Alphasense Sensors berechnet wurde, stimmte qualitativ mit der Referenz überein, lieferte aber aufgrund der im Vergleich zum Referenzgerät geringeren Anzahl von Größenklassen begrenzte Informationen. Das von den Low-Cost PM-Sensoren erfasste lokale Partikelemissionsverhalten in der Schlauchfilteranlage im Technikumsmaßstab wurde mit Feldmessungen in einer industriellen Anlage in einen Kontext gesetzt, wobei ein äquivalentes lokales Verhalten bei der Messung der Partikelemission am Einzelschlauch für verschiedene Filtermedien aufgezeigt wurde.

Im Rahmen des zweiten Schwerpunkts der Arbeit (außerhalb der lokalen Emissionserfassung mit Low-Cost PM-Sensoren) wurden der Energiebedarf und die Partikelemissionen beim Betrieb von Schlauchfilteranlagen untersucht und gegenübergestellt. Die Gesamtleistung für den Filterbetrieb wurde aus der Lüfterleistung und einer mittleren repräsentativen Leistung für den Druckluftverbrauch bei der Regenerierung berechnet. Eine experimentelle Parameterstudie wurde für verschiedene (konstante) Rohgaskonzentrationen, Filteranströmgeschwindigkeiten und Tankdrücke für die Filterregenerierung durchgeführt, wobei die Zykluszeit zwischen den einzelnen Regenerierungen für jeden Parametersatz variiert wurde. Dabei konnte für jeden Parametersatz ein dediziertes Leistungsminimum bei einer entsprechenden Zykluszeit (zwischen 30 und 120 Sekunden) ermittelt werden. Ein günstiger Betriebspunkt liegt bei Zykluszeiten am oder oberhalb des Leistungsminimums, da Zykluszeiten unterhalb des Leistungsminimums zu höheren Staubemissionen ohne Leistungseinsparung führen. Die Partikelemission nimmt mit zunehmender Zykluszeit hyperbolisch ab, da in einer bestimmten Zeit weniger Emissionspeaks auftreten. Zu kurze Zykluszeiten erzeugen einen Betriebszustand nahezu konstanter Regenerierung, bei dem die Partikelemissionen stark ansteigen und der Druckluftverbrauch einen hohen Anteil an der Gesamtleistung ausmacht. Bei sehr langen Zykluszeiten dominieren der Differenzdruck und die Lüfterleistung die Gesamtleistung, was zum Einbrechen des Volumenstroms beim Überschreiten der maximalen Kapazität des Gebläses führen kann. Höhere Filteranströmgeschwindigkeiten und höhere Rohgaskonzentrationen bewirken eine Verschiebung des Leistungsminimums hin zu kürzeren Zykluszeiten / häufigerer Regenerierung. Eine Erhöhung des Tankdrucks führt zwar zu einer Verlängerung der Zykluszeit am Leistungsminimum, bringt aber keinen eindeutigen energetischen Vorteil auf Kosten stark erhöhter Partikelemissionen. Im Anschluss an die experimentelle Parameterstudie wurden die experimentell erfassten Daten für die Modellierung des Filtrationsbetriebs verwendet. Das Modell basierte dabei auf den Grundgleichungen der Oberflächenfiltration, welche durch die Berücksichtigung der experimentellen Daten, des Energiebedarfs und der Partikelemission erweitert wurden. Nach der Wahl eines geeigneten Anpassungsparameters (Medienwiderstand als Funktion der Zykluszeit) stimmten die Ergebnisse der Modellierung mit den experimentellen Daten gut überein.

TABLE OF CONTENTS

ABSTRACT	I
GERMAN ABSTRACT - ZUSAMMENFASSUNG	V
TABLE OF CONTENTS	IX
List of Symbols and Abbreviations	xi
1 INTRODUCTION	1
1.1 Motivation and Objective	1
1.2 Research questions	4
1.3 Structure and Scope	4
2 THEORETICAL PART	6
2.1 Fundamentals of particle separation for surface filter media	6
2.2 Design of baghouse filters	7
2.3 Operating behavior of pulse-jet cleaned filters	9
2.3.1 Differential pressure behavior	9
2.3.2 Particle emission behavior of pulse-jet cleaned filters	11
2.4 Particle emission measurement technology	13
3 MATERIALS AND METHODS.....	15
3.1 Filter test rig.....	17
3.2 Pilot-plant scale baghouse filter	18
3.3 Aerosol measurement technology for particle emission measurement	20
3.3.1 Reference aerosol spectrometer Promo®2000 with welas®2100 sensor manufactured by Palas®	21
3.3.2 Low-cost PM-sensors.....	22
3.4 Test dust	24
3.5 Filter media	25
4 POTENTIAL AND LIMITATIONS OF LOW-COST PARTICULATE MATTER SENSORS FOR PARTICLE EMISSION MEASUREMENTS FOR PULSE-JET CLEANED FILTERS	26
4.1 Validation of scattered light based low-cost PM-sensors for the detection of the characteristic particle emission behavior in a filter test rig	26
4.1.1 Extensive summary of publication I.....	26
4.1.2 Main conclusions of publication I.....	29
4.2 The potential of low-cost PM-sensors for the detection and spatial identification of particle emission hotspots in baghouse filters	30

4.2.1	Extensive summary of publication II	30
4.2.2	Main conclusions of publication II	34
5	CHARACTERIZATION OF THE TRANSIENT AND SPATIALLY RESOLVED PARTICLE EMISSION BEHAVIOR OF PULSE-JET CLEANED FILTERS.....	35
5.1	Characterization of the spatial particle emission behavior in a pilot-plant scale baghouse filter at a low particle emission level (membrane filter bags with sealed seams)	35
5.1.1	Extensive summary of publication III	35
5.1.2	Main conclusions of publication III	39
5.2	Characterization of the spatial particle emission behavior in a pilot-plant scale baghouse filter applying regular filter bags made from different filter media (without sealed seams)	40
5.2.1	Extensive summary of publication IV	40
5.2.2	Main conclusions of publication IV	43
6	TRADE-OFF BETWEEN ENERGY DEMAND AND PARTICLE EMISSIONS FOR THE OPERATION OF PULSE-JET CLEANED FILTERS	45
6.1	Experimental parameter study for the evaluation of filter operation regarding energy demand and particle emissions	45
6.1.1	Extensive summary of publication V	45
6.1.2	Main conclusions of publication V	49
6.2	Modeling of filter operation regarding energy demand and particle emissions.....	51
6.2.1	Extensive summary of publication VI.....	51
6.2.2	Main conclusions of publication VI.....	53
7	DISCUSSION	54
7.1	Suitability of low-cost PM-sensors for (local) particle emission monitoring and the identification of particle emission hotspots in baghouse filters.....	54
7.1.1	Quantitative performance of low-cost PM-sensors during filter emission measurements regarding transient particle concentration peaks and potential measurement errors.....	54
7.1.2	Qualitative assessment of the spatially resolved particle emission measurement applying low-cost PM-sensors	59
7.1.3	Comparison of the local particle emission behavior of the pilot-plant scale baghouse filter with an industrial baghouse filtration process	60
7.1.4	Origin of local particle emissions after the regeneration of consecutive filter bags in the cleaning procedure.....	62
7.2	Trade-off between energy-demand and particle emissions for pulse-jet cleaned filters.....	64
7.2.1	The combination of energy demand and particle emissions as a guideline for the selection of suitable operating regions for pulse-jet cleaned filters	64
7.3	Summarizing conclusions in the context of the research questions (chapter 1.2.)	66
8	OUTLOOK	67
	REFERENCES	69
	LIST OF TABLES	73
	LIST OF FIGURES	74

APPENDIX	77
Publication I	78
Publication II.....	79
Publication III	80
Publication IV.....	81
Publication V	82
Publication VI.....	83
ACKNOWLEDGEMENTS.....	84
LIST OF PUBLICATIONS.....	86

List of Symbols and Abbreviations

$c_n / (\#/cm^3)$	Particle number concentration
$c_{\text{raw-gas}} / (g/m^3)$	Raw-gas dust concentration
CPC	Condensation particle counter
MPPS	Most penetrating particle size
OPC	Optical particle counter
$\Delta p / \text{Pa}$	Differential pressure
$\Delta p_{\text{max}} / \text{Pa}$	Maximum differential pressure (trigger for filter regeneration)
$\Delta p_r / \text{Pa}$	Residual differential pressure after filter regeneration
PM	Particulate matter
$PM_{10} / (\mu g/m^3)$	Particulate matter concentration penetrating the upper respiratory system (median aerodynamic diameter of penetration curve at 10 μm)
$PM_{2.5} / (\mu g/m^3)$	Respirable particulate matter concentration penetrating deeper into the lungs (median aerodynamic diameter of penetration curve at 2.5 μm)
$PM_x / (\mu g/m^3)$	Particulate matter concentration with a median aerodynamic diameter of the penetration curve at “x” μm .
$p_{\text{tank}} / \text{bar}$	Tank pressure for filter regeneration
$Q_i / -$	Cumulative particle size distribution (i = 0 number based; i = 3 volume based)
SMPS	Scanning mobility particle sizer
t / s	Time
$\Delta t / \text{s}$	Cycle time (time interval between individual filter regenerations)
$w_{\text{filter}} / (\text{cm/s})$	Filter face velocity
x / μm	Particle diameter
$x_{50,3} / \mu\text{m}$	Mass / volume median diameter

1 INTRODUCTION

1.1 Motivation and Objective

Pulse-jet cleaned filters have remained one of the most prominent unit operations for the separation of particles from dust-laden gas streams for several decades [Peukert, 2022]. The field of applications for pulse-jet cleaned filters ranges across a wide variety of processes from industrial de-dusting for environmental protection from dust emissions [Cora & Hung, 2002] (e.g. power plants; waste / biomass incineration [Steiner & Lanzerstorfer, 2023; Schott et al. 2022; Stabile et al., 2020; Schiller & Schmid, 2015]), aluminum production [Huang et al., 2015], wood processing [Simon et al., 2014], to product recovery in cement plants [Wilanowicz et al., 2013] and life sciences [Litchwark et al., 2015] or the protection of dust-sensitive machinery [Schwarz et al., 2022; Mauschitz et al., 2018]. In the historical context of environmental protection within the past century, the filters greatly helped combat air pollution from industrial processes.

With increasing technological progress regarding the development of filter media for surface filtration applications as well as expertise about filter layout and operation strategies, the filters improved in separation efficiency. The technological break-throughs in gas-cleaning technology regarding particle separation can be illustrated by the development of statutory limits specified in guidelines such as TA-Luft in Germany [TA-Luft, 2021]. The limits regarding the emission of particulate matter from industrial processes into the environment decreased significantly over the course of the past century and are displayed in Figure 1 in the form of the total dust mass concentration as a function of exhaust gas volume flow.

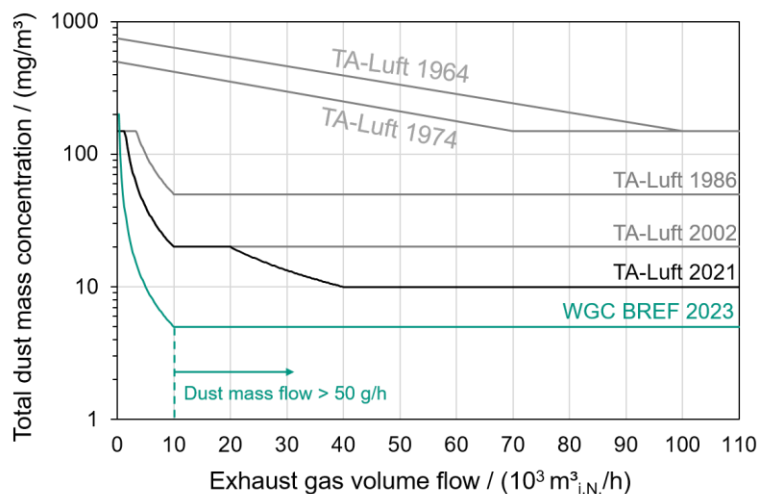


Figure 1 – Historical evolution of statutory limits for the dust mass concentration of particle emissions as a function of exhaust gas volume flow. Image adapted from [Schmidt, 2003].

Note that the mass concentration of these limits is not size resolved and features only the total dust emission. Several other hazardous substances may be subject of individual regulations (e.g. lead or nickel). Larger jumps in the emission limits are clearly visible over the latter half of the 20th century. The aggravation of statutory limits in the 21st century progresses at a slower pace, however there is clear drive towards lower emissions. With the publication of the best available techniques reference document for common waste gas management and treatment systems in the chemical sector (WGC BREF), dust emissions from processes where cleanable fabric filters can be applied are limited at a gravimetric mass concentration of 1-5 mg/m³ (for significant dust-mass flows exceeding 50 g/h at each stack with unique conditions) [European Commission, 2023].

While pulse-jet cleaned filters are generally able to provide low emission levels below the statutory limits [Steiner & Lanzerstorfer, 2023], energy efficient operation of baghouse filters is still subject to research [Klein et al., 2012]. Current incentives regarding digitalization in the process industry and mechanical process engineering also affect the operation and maintenance of pulse-jet cleaned filters, aiming to improve process and separation efficiency, avoid unfavorable operating conditions, or improving process monitoring and maintenance for plant operators for small and large scale applications.

Nonetheless, in many cases, the filters are treated as a mere necessity to meet the corresponding requirements regarding stable process management and potential emission limits. As a consequence, filter operation is rarely optimized and process monitoring and control is kept at a bare minimum (Figure 2). The baghouse filter itself is practically a “black box” and kept to its own devices unless problems are noted.

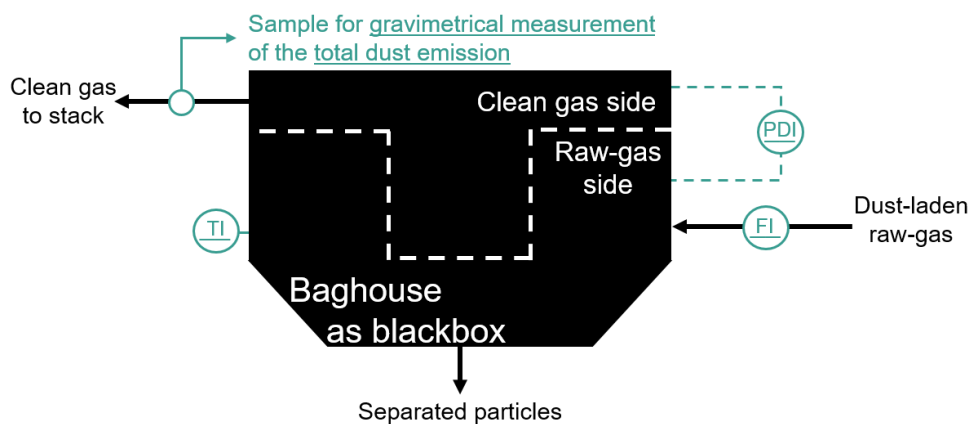


Figure 2 – Concept of a baghouse filter as a “black box” with only rudimentary process monitoring and control.

Provided the filter is operated within a reasonable operating window and unfavorable process conditions are avoided (e.g. unstable filter operation and too frequent regenerations [Leubner & Riebel, 2003] or excessively high tank pressures for filter regeneration [Kurtz et al., 2016]), low particle emission levels can be realized due to the high separation efficiency of the dust cake formed during filter operation. However, a wide variety of other emission sources relevant for the real application outside the scope of ideal filter operation can greatly impact the total dust emission at the stack. Leaks of the size of several parts per million of the installed filter area can be the cause of continuous dust emissions and cause a significant increase of clean-gas dust concentrations [Kurtz et al., 2017].

The prevention and reliable detection of leaks is one of the largest challenges of the filter industry to minimize plant downtime and facilitate maintenance procedures. Conventional detection procedures include online monitoring of the dust emission for individual filter houses via the use of e.g. triboelectric sensors (so-called filter guards) to identify remarkably high emissions [Wiegler, 2016]. While this method may offer online information, the lack of spatial resolution makes the exact identification of leaks a laborious effort. Fluorescent dust can be used to highlight regions of increasing dust penetration for easier manual inspection during plant shutdown but a suitable online measurement tool that provides spatially resolved online information on particle emissions is of great potential benefit to plant operators to reliably meet emission standards. Prototype sensors for spatially resolved leak detection in baghouse filters were presented by [He et al., 2023] (resistance measurement of conductive polymer fibers) and [Li et al., 2020] (optical fiber air pressure sensor). While these authors succeeded in detecting (larger) bag failures based on changes regarding the measurement system, no direct information on the particle emission was gathered.

In recent years, scattered-light based optical particulate matter sensors have gained popularity (e.g. among citizen scientists) to spatially monitor the local air quality regarding particulate matter concentrations (e.g. PM₁₀ or PM_{2.5}) [Kaur & Kelly, 2023; Eilenberg et al., 2020; Badura et al., 2018]. The accuracy and calibration of the sensors regarding monitoring of ambient particle concentrations is a frequent subject of research [Giordano et al., 2021; Asbach et al., 2018]. For example, a known issue during ambient air measurements is hygroscopic growth of particles resulting in higher detected mass concentrations and causing the necessity to correct sensor data or modify the measurement equipment [Chacón-Mateos et al., 2022; Crilley et al., 2020]. The compact size and cheap costs of purchase enable the possibility of use of larger quantities of sensors in technical facilities for spatial emission monitoring [Ostermeyer et al., 2020; Schwarz et al., 2018]. The validation and application of these cheap scattered light based sensors regarding their capability to detect the characteristic emission behavior for pulse-jet cleaned filters and serve as a monitoring (or leak detection) tool for spatial emission monitoring is one of the major topics of this dissertation.

Another current challenge of the process industry in the context of climate change and incentives to lower carbon dioxide emissions as well as rising energy costs is the improvement of energy efficiency of technical processes. Pulse-jet cleaned filters are complex systems where multiple factors (e.g. fan power and consumption of pressurized air for filter regeneration) contribute to the total energy demand for filter operation [Höflinger & Laminger, 2013; Klein et al., 2009]. While guidelines like VDI 3677 give layout instructions and recommendations regarding suitable filter face velocities, energy considerations regarding filter layout and suitable cycle times are not discussed in detail [VDI 3677, 2023]. The evaluation of filter operation in the context of the required power and the resulting particle emission is another focus of this dissertation. Changing filter operation relevant parameters such as regeneration frequency or tank pressure dependent on other process conditions may grant a lower energy demand or lower dust emissions. Identifying suitable operating regions has the potential to set the operation of existing plants and the layout of pulse-jet cleaned filters into perspective with the reduction potential of energy demand and / or particle emissions dependent on the process parameters.

1.2 Research questions

In the context of increasing particle emission standards and a simultaneous drive to lower the energy demand of industrial processes, two main research questions are treated in this dissertation. Due to the high contribution of particle emission hotspots (e.g. leaks) to the total dust emission that can cause exceeding emission limits, spatially resolved online monitoring of the particle emission penetrating individual filter bags could facilitate and accelerate maintenance procedures. For plants operating under suitable (ambient) conditions, low-cost PM-sensors are a potential monitoring tool, leading to the first research question of this thesis.

- **Are low-cost PM-sensors suitable for (local) particle emission monitoring and the identification of particle emission hotspots in baghouse filters?**

Secondly, operation strategies of pulse-jet cleaned filter for the improvement of energy demand and particle emissions are gaining relevance, especially considering typical “rigid” regeneration criteria. Improving the energy efficiency of pulse-jet cleaned filters is the topic of the second research question addressed in this thesis.

- **How can particle emissions from baghouse filter operation be lowered as energy-efficiently as possible and what is the trade-off between energy demand and particle emissions?**

1.3 Structure and Scope

This publication based dissertation deals with the evaluation of scattered-light based low-cost PM-sensors for spatially resolved online emission monitoring of baghouse filters as well as the trade-off between energy consumption and total particle emission for pulse-jet cleaned filters.

The fundamentals of baghouse filter operation are detailed in chapter 2.

Following the theoretical part, the methodology for addressing the research questions, experimental facilities, applied measurement technology and test dust are listed and explained in chapter 3.

The results section is split into three parts (chapter 4, 5 and 6) and is based on several scientific publications. Each subchapter offers a summary of the corresponding publication including the most important results. The individual publications that constitute the core of the research results are provided in the appendix.

- **Potential and limitations of low-cost particulate matter sensors for particle emission measurements for pulse-jet cleaned filters**

In the first part of this dissertation, the suitability of scattered light based “low-cost PM-sensors” for the measurement of the characteristic particle emission behavior of pulse-jet cleaned filters and the identification of emission hotspots is discussed. Building on the preliminary results of [Schwarz et al., 2018], two different low-cost PM-sensors, namely the OPC-N3 of the

manufacturer Alphasense and the SPS30 of the manufacturer Sensirion, were implemented in a filter test rig based on DIN ISO 11057 for evaluation under defined conditions and validation of the measurement technology. In order to evaluate the low-cost PM-sensors under praxis-relevant conditions regarding realistic filter operation after the initial validation in the filter test rig, sensors of the type OPC-N3 from Alphasense were installed in a pilot-plant scale baghouse filter with nine filter bags for spatial online monitoring of particle emissions at each installed filter element. To investigate the detection capabilities under high emission conditions, different types of particle emission hotspots were investigated to demonstrate the potential and limitations of low-cost PM-sensors as a tool for the identification of larger local emission hotspots within a baghouse filter.

- **Characterization of the transient and spatially resolved particle emission behavior of pulse-jet cleaned filters**

Following the demonstration of low-cost PM-sensors as a monitoring tool for leak detection, near ideal emission behavior generated by membrane filter media with sealed seams was investigated in the baghouse filter. Afterwards, different filter media with regular seams were installed in a follow-up investigation to operate the sensors at a higher emission level and investigate run-in effects like filter aging or the impact of increased tank pressures on the spatial emission behavior.

- **Trade-off between energy demand and particle emissions for the operation of pulse-jet cleaned filters**

Finally, an experimental parameter study was performed evaluating filter performance based on the energy demand [Höflinger & Laminger, 2013] and particle emissions for filter operation. Combining energy demand and particle emission enables the construction of an “operation curve” that provides the identification of suitable operating points and cycle times for filter regeneration. Based on the experimental framework, model equations summarized by [Löffler, 1988] were applied and adapted to mathematically describe filter operation and laying the foundation for a “digital twin”.

Finally, the results are discussed in an overarching discussion in chapter 7 and put in an application-orientated context in the outlook in chapter 8.

2 THEORETICAL PART

This chapter offers a brief description of the theoretical basics treated in this dissertation. Fundamentals of particle separation for surface filter media as well as the technical application of baghouse filters and the corresponding operating behavior are explained. The focus of this chapter is put on fabric filters, though the general principles are also valid for rigid surface filters.

2.1 Fundamentals of particle separation for surface filter media

Surface filter media are predominantly used for particle separation in continuous processes that supply higher raw-gas concentrations and large amounts of dust. The formation of a dust cake on the surface of the filter elements requires periodic regeneration that enables long-term continuous and economic operation, which is relevant in many industrial processes [Schmidt, 1998]. The applied filter media typically undergo a surface treatment (e.g. singeing of the upstream side or lamination of a membrane layer onto a fiber support structure) to promote particle separation on the surface of the filter medium [Cirqueira et al., 2017].

The operation of cleanable surface filters consists of different phases that are illustrated in Figure 3. The basic principles of aerosol filtration in fibrous filters also hold true for surface filter media at the initial stages of the filtration process and the clogging phase. Particles carried by a dust-laden gas stream are separated on the collectors within the fiber matrix during the flow through the filter medium based on different mechanisms (diffusion, interception or inertia) according to their size [Brown, 1993]. Mainly during the clogging phase, some particles are not collected and penetrate to the clean gas side [Höflinger et al., 2007]. Bridging and agglomeration of dust structures lead to the formation of a dust cake on the surface of the filter element until the particle separation is completely incurred by the filter cake (surface filtration) [Zhang, 2021].

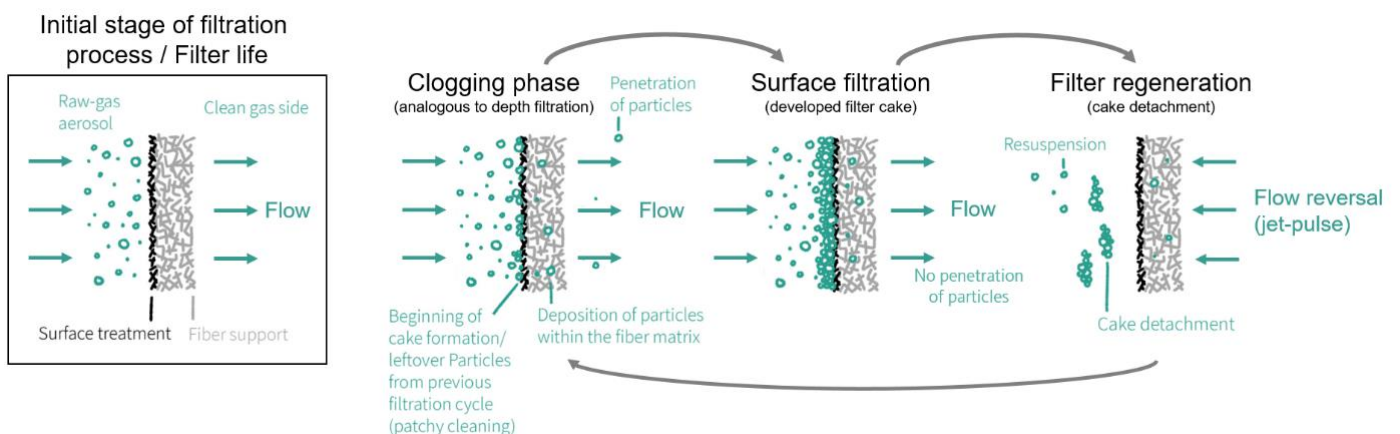


Figure 3 – Overview of the different stages of continuous operation of pulse-jet cleaned filters.

The deliberate cake formation and filter loading is the key aspect of surface filtration. Particle deposition on the surface and subsequent cake buildup further increases the separation efficiency (compared to the bare filter medium) due to a larger collector area. A sufficiently developed dust cake on the filter medium surface completely prevents particle penetration to the clean gas side. The additional flow resistance through the dust cake also leads to a rise in

differential pressure. In order to ensure stable filter operation, the elements have to be regenerated (e.g. via jet-pulse, reverse-air flow, shaking, etc.), removing the dust cake from the filter element. In case of pulse-jet cleaned fabric filters, a burst of pressurized air is injected into the flexible filter element, causing the expansion and rapid deformation of the fabric and subsequent detachment of the dust cake [Klingel, 1983]. Insufficient regeneration due to e.g. low tank pressures or adhesive dust cakes may lead to “patchy cleaning” whereby residue dust cake remains on the filter material. The leftover fragments of dust cake have an effect on filter loading and the differential pressure evolution after regeneration as larger fractions of the total volume flow pass better regenerated areas [Dittler et al., 2002]. Selecting increasingly high tank pressures is known to cause increased dust emissions and may even lead to re-dispersion and entrainment of separated dust in the raw-gas flow and not the desired cake detachment [Leubner & Riebel, 2003].

2.2 Design of baghouse filters

Surface filter media are confectioned into filter elements such as filter bags, envelopes or pleated filter elements (Figure 4). Fabric filter bags are stabilized by a rigid support structure (e.g. support cages) and installed in a filter house separating the clean gas side and the raw-gas side. In processes handling hot gases at higher temperatures where fabric filters are not applicable, ceramic rigid filter elements or filter candles are used.

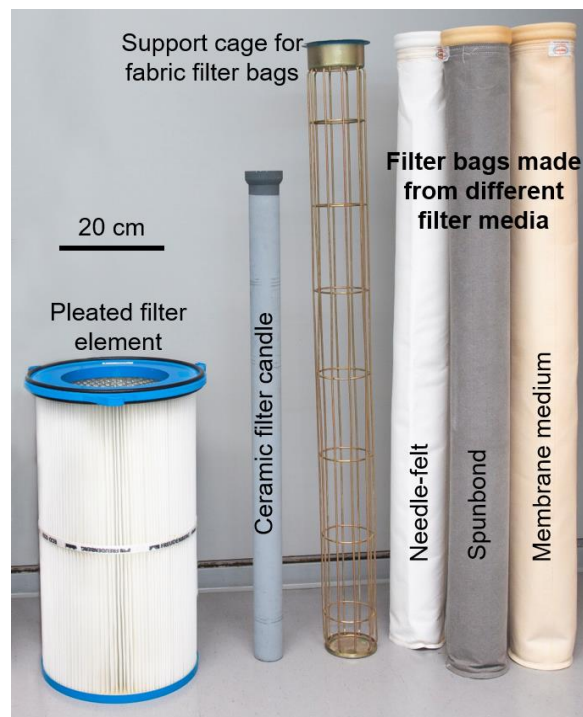


Figure 4 - Overview of different filter elements for surface filtration. The three different filter bags were used in this study and the filter media properties are summarized in Table 4.

Dependent on the raw-gas volume flow, varying number of filter elements are installed in a single baghouse and large scale processes may rely on several baghouses employing thousands of filter elements. While large-scale industrial gas cleaning processes are the prime example for baghouse filter application, smaller scale gas cleaning processes such as extraction systems may also employ cleanable surface filters.

Typical filter face velocities are in the region of 40 – 300 m/h dependent on the application [VDI 3677, 2023]. The filter face velocity selected for filter testing of surface filter media according to DIN ISO 11057 is 120 m/h what composes the higher end of typical filter face velocities [DIN ISO 11057, 2016].

Figure 5 shows a sketch of a typical baghouse filter. A baffle plate can be installed to serve as pre-separator of coarser particles at the inlet of the baghouse. The filter elements are tightly fixed between raw-gas side and clean gas side. During the filtration process, a gas flow passes the filter element from the outside to the inside, whereby the filter element nestles against its support structure. Above the outlet of the filter elements, a blow pipe enables the regeneration by rapid flow-reversal due to the release of pressurized air from a pressure tank. Filter elements or the blow pipes can be equipped with corresponding (venturi-) nozzles to increase regeneration efficiency [Andersen et al., 2016].

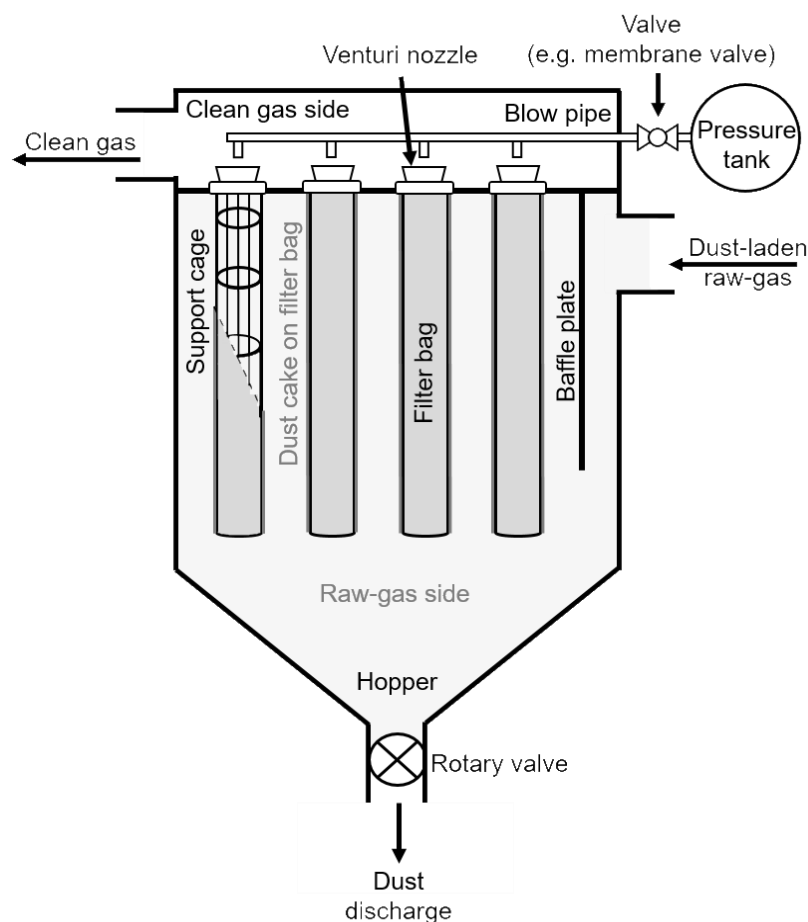


Figure 5 – Schematic sketch of a baghouse filter and several key components.

The layout for efficient regeneration systems has long been subject of research regarding nozzle design, tank pressure for regeneration and electrical valve opening time to control the duration of the pressure pulse [Lu & Tsai, 2003; Sievert & Löffler, 1989]. After successful regeneration, the detached dust cake itself falls into a hopper where it is stored and subsequently discharged (e.g. via rotary valve).

2.3 Operating behavior of pulse-jet cleaned filters

The operating behavior of pulse-jet cleaned filters is cyclically alternating between a filtration phase (clogging and surface filtration) and filter regeneration (e.g. via jet-pulse) as previously shown in Figure 3. There is a distinction between “online” regeneration (blower of the facility is running during the regeneration procedure) and “offline” regeneration (blower of the facility is switched off – no raw-gas flow through the filter house during regeneration). After regeneration, the filtration process continues with renewed loading of the filter elements. Dependent on the size of the baghouse, multiple filter elements (typically a row of elements – row-by-row cleaning strategy) or simply individual filter elements (bag-by-bag cleaning strategy) are regenerated [Kurtz et al., 2016]. The regeneration is typically initiated after exceeding a preset maximum differential pressure (Δp -controlled regeneration) or after passing a certain cycle time (Δt -controlled regeneration) [Hindy, 1986]. A combination of these two operation modes (e.g. Δt -controlled regeneration with differential pressure criteria) is also possible. The consecutive subchapters focus on the impact of the cyclical filter operation (online regeneration) on the differential pressure behavior and the characteristic transient particle emission behavior of pulse-jet cleaned filters.

2.3.1 Differential pressure behavior

Loading of filter elements causes an increase in differential pressure between raw-gas side and clean gas side due to the flow through the growing dust cake on the medium surface. Filter regeneration leads to dust cake detachment and thus causes an abrupt and sharp decrease of the differential pressure due to a decrease in flow resistance of the corresponding filter elements.

The ideal differential pressure behavior for steady-state filter operation (constant raw-gas concentration, constant filter face velocity and complete regeneration of the element) follows a “saw-toothed” pattern as shown in Figure 6. Two distinct cases are typically found in literature. In case of a single filter element, as is the case for filter testing where circular filter samples are regenerated, the complete filter area is regenerated after a jet-pulse (assuming no “patchy-cleaning”). Here, the differential pressure increases linearly with time (assuming no compression of the dust cake) and the differential pressure falls back to the residual differential pressure level of the filter medium after regeneration [Löffler, 1988].

In case of multiple filter elements, only a subset of the total filter area is regenerated. This leads to different loading states of the individual filter elements and creates a spatially and temporally variable flow-profile [Simon et al., 2010]. The differential pressure also decreases to a residual level after regeneration, but the level is not equal to the residual pressure level of the filter medium, as the remaining bags / rows of filter elements all have different loading states. Therefore, the dust cake deposited on these filter elements contributes to the overall differential pressure between raw-gas side and clean gas side.

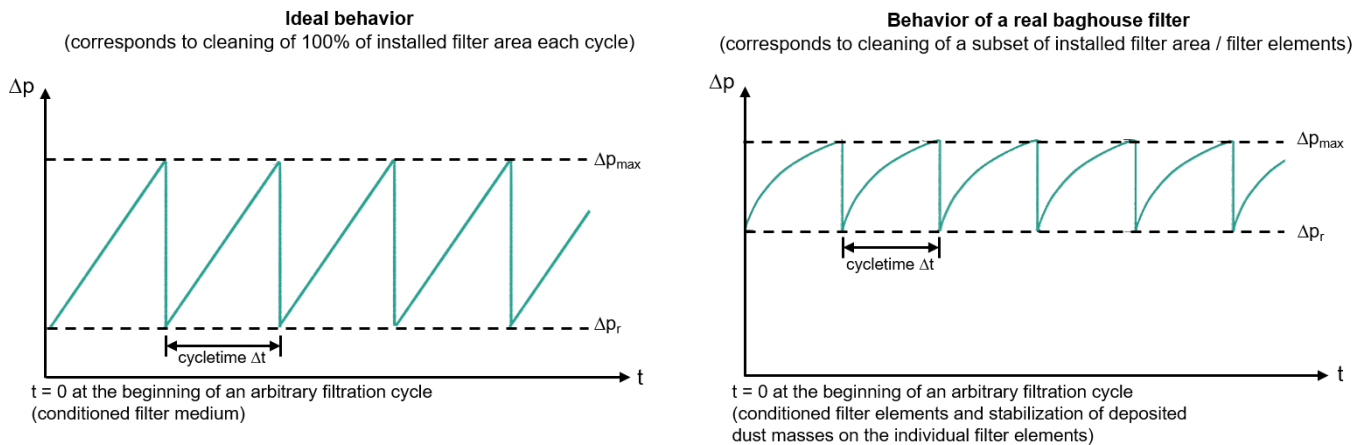


Figure 6 – Differential pressure behavior of a pulse-jet cleaned filter consisting of a single filter element (left: regeneration of complete filter area - e.g. filter testing) or multiple filter elements (right: regeneration of a subset of installed filter elements).

During prolonged filter operation, increasing amounts of particles are deposited within the filter matrix, causing an increase in flow-resistance of the filter medium and an increase in residual differential pressure [Schuberth, 2010; Höflinger et al. 2007]. This behavior typically referred to as filter aging has beneficial effects on the particle emission due to an improved separation efficiency of the filter medium. In filter testing, an artificial aging stage is performed in order to create comparable conditions regarding the life-time of filter samples and exclude run-in effects from the performance analysis [DIN ISO 11057, 2016].

In the large majority of applications, the residual pressure difference increases quickly for the initial filtration cycles and reaches a stable level according to Figure 7, where the residual pressure only gradually increases over multiple months or even years of operation.

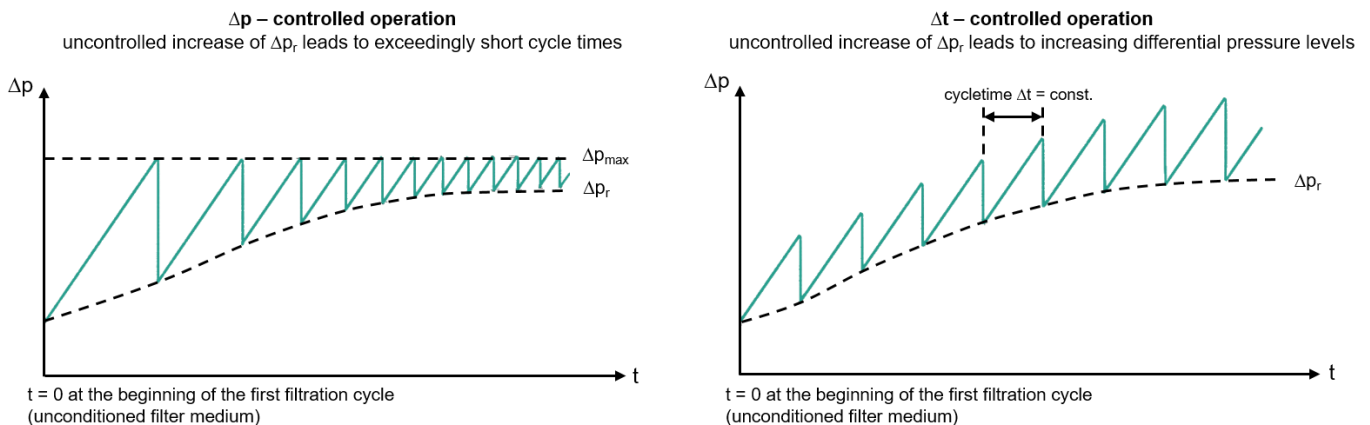


Figure 7 – Consequences of increase in residual pressure difference (rapid increase of residual pressure drop Δp_r) in case of Δp -controlled (left) and of Δt -controlled (right) filter operation.

A sudden and uncontrolled increase of residual differential pressure can lead to unstable filter operation. This is especially relevant for applications, where high concentrations of nanoparticles occur and have to be separated (e.g. thermal spraying, arc welding, metal cutting, etc.) [Khirouni et al., 2020]. In these cases, the filtration of a coarser dust pre-coat can be performed to protect the filter medium from clogging due to excessive deposition of nanoparticles within the fiber matrix [Khirouni et al., 2021; Schiller & Schmid, 2015; Peukert & Wadenpohl, 2001]. Dependent on the regeneration criterion (either Δp -controlled or Δt -controlled operation), the uncontrolled increase of residual differential pressure and unstable

filter operation has different consequences. For Δt -controlled operation, increase of the residual differential pressure leads to an increase in the overall differential pressure level and can drive the blower of the facility to its limits. In case of Δp -controlled operation, the cycle time between filter operation decreases, causing a state of near constant filter regeneration. This behavior leads to increased wear on the filter bag and to increased dust emissions as no sufficient dust-cake can be formed during filter operation and particles can continuously penetrate through to the clean gas side [Kavouras & Krammer, 2005; Leubner & Riebel, 2003].

2.3.2 Particle emission behavior of pulse-jet cleaned filters

The characteristic operating behavior of pulse-jet cleaned filters generates a transient particle emission due to the periodic stages of cake formation on the medium surface and filter regeneration [Löffler, 1988]. Directly after filter regeneration (assuming sufficient filter regeneration and cake detachment), particles may penetrate into the fiber matrix and straight through to the clean-gas side [Binnig et al., 2009]. Other penetration mechanisms, e.g. seepage, have been discussed in the past, however the work of Binnig et al., has proven that particles passing the fiber matrix of the filter element after regeneration (penetration “straight through” the filter medium) is by far the dominating penetration mechanism [Binnig et al., 2009; Leith & Ellenbecker, 1982].

The particle emission increases abruptly after filter regeneration. With increasing formation of the dust cake, the emission decreases until a zero level is reached and no particles penetrate to the clean-gas side. These transient emission peaks mark the characteristic emission behavior of pulse-jet cleaned filters illustrated in Figure 8. Similar to the adjustment of a stable residual differential pressure during the initial filtration cycles, filter aging also impacts particle separation and enhances the separation capability of the filter medium causing a faster decay of particle emission peaks and lower peak heights during the initial filtration cycles [Kurtz et al., 2016; Schuberth, 2010]. The emission penetrating an aged / conditioned filter medium stabilizes accordingly.

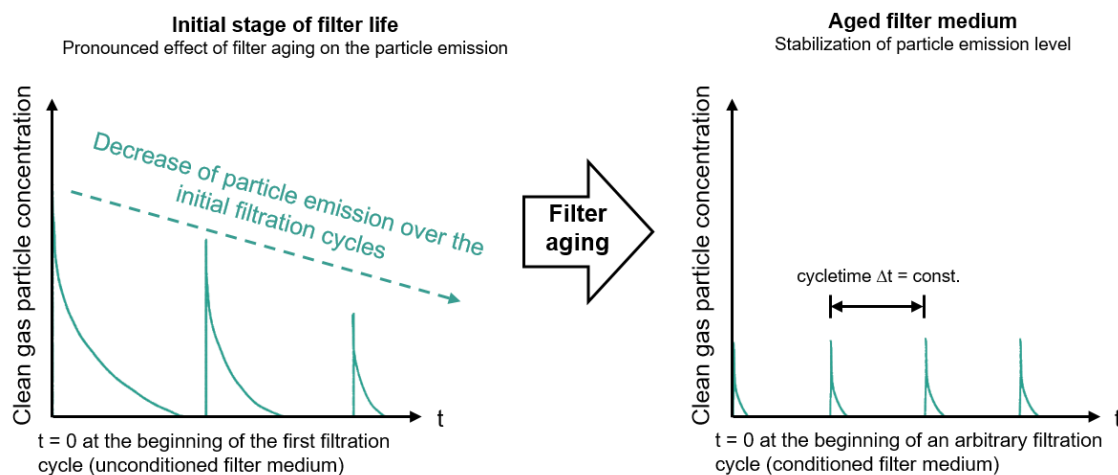


Figure 8 – Characteristic transient particle emission behavior for pulse-jet cleaned filters.

The height and decaying behavior of the emission peak is highly dependent on the filter medium and other process conditions (e.g. raw-gas concentration, filter face velocity, filter age, etc.). Zhang recently showed the transition of the clogging phase into surface filtration based on the decay behavior of the particle emission peaks during the individual phases [Zhang et al., 2021]. The cleaning strategy of pulse-jet cleaned filters also has an impact on the dust emissions.

Investigations have shown that larger tank pressures for filter regeneration typically lead to higher emissions [Kurtz et al., 2016; Klingel, 1983]. The time interval between regenerations directly impacts the amount of emission events in a certain time. Frequent regeneration and cake detachment enables more possibilities for particle penetration through the filter medium [Simon et al., 2014]. Membrane filter media offer high separation efficiencies, where particle penetration may be only possible for several seconds, while needle-felt filter media show higher concentration peaks and a slower decay behavior [Bächler et al., 2024b].

Emission sources other than direct penetration can contribute to the total dust emission for baghouse filters, especially in real-world applications. Starting at the manufacturing process, tailoring of filter elements, e.g. during the sewing process of filter bags, creates small defects that enable particle penetration. [Kurtz, 2018] demonstrated the benefit of sealed seams of filter bags on the particle emission level. [Lacerda et al., 2022] methodically investigated the impact of needle diameter for the sewing process on particle emissions and showed the relationship of increasing particle emission with increasing needle-diameter for filter samples with membrane lamination. The differences in particle emission caused by needles with different diameters was still pronounced after conditioning of the filter sample and a filter aging procedure.

During installation of the filter elements within the baghouse, there is a risk of scratching the medium surface what may be fatal for the separation performance of membrane filter media. In certain applications, sparks or abrasive dusts damage the medium surface. [Bach & Schmidt, 2007] as well as [Li et al., 2022] investigated the emission contribution of small pinhole leaks of varying size, whereby the emission of the pinholes dominated the overall dust emission. The contribution of even small leaks (several parts per million of the installed filter area) may induce emissions larger than caused by particle penetration after filter regeneration [Kurtz et al., 2017]. The constant particle flux penetrating through a leak to the clean gas side leads to a continuous emission signal according to Figure 9.

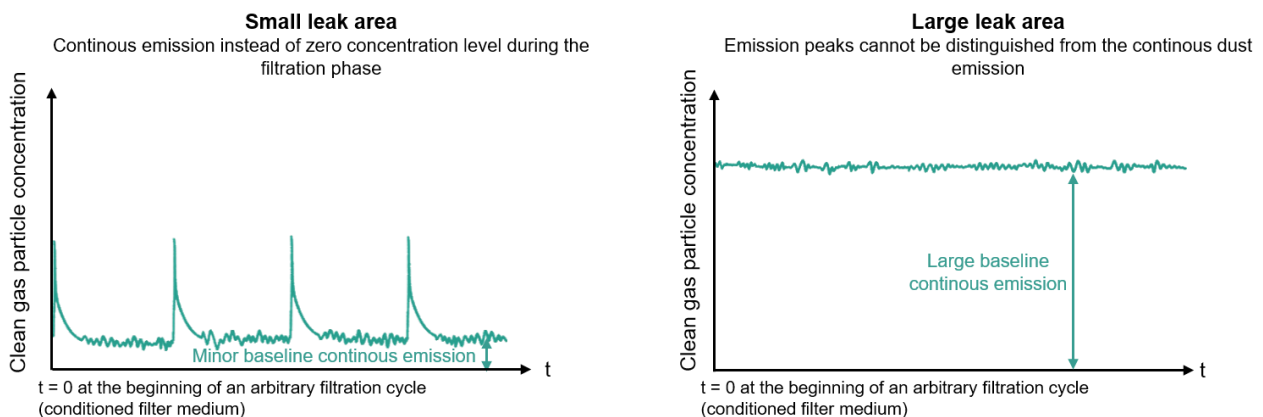


Figure 9 – Particle emission behavior for pulse-jet cleaned filters in case of additional emission contribution of small (e.g. pinhole leak - left) and large (e.g. bag failure - right) leaks between raw-gas side and clean gas side.

The prevention, detection and spatial identification of leaks is one of the most important challenges of the filter industry to reliably meet emission standards. Emission monitoring for pulse-jet cleaned filters is not always mandatory and dependent on plant size. Smaller facilities are often not legally required to continuously monitor and report their dust emission. In case of legally obligated plants, gravimetric measurement is commonly employed which does not offer temporally or spatially resolved information of the emitted particle concentration due to the collection of dust mass on a sample filter in a certain time period. Online measurement technology such as triboelectric sensors enable the detection of increases in dust emission in the clean gas duct [Wiegler, 2016]. In case of larger facilities with multiple baghouses, the

identified conspicuous baghouses can be shut down for troubleshooting and leak elimination. However, the exact identification of the emission source can be a time consuming endeavor. Fluorescent dust for better visual inspection of the baghouse interior or the clean gas side can be of help to identify leaks or damaged filter elements. The accessibility of the filter houses is often limited and due to the high contribution of even small leaks, intact filter elements may be replaced before their eventual end of service life is reached. An exact identification of damaged filter elements has economical and ecological benefits and is a current subject of research [He et al., 2023; Li et al., 2020].

2.4 Particle emission measurement technology

In particle emission measurement and the corresponding guidelines, the determination of gravimetric particle concentrations is required for the vast majority of applications and substances. Exceptions include automotive engine exhausts or processes handling fiber dusts (e.g. asbestos fibers or other biopersistent anorganic fiber dusts) according to TA-Luft where number based limits are established [TA-Luft, 2022; Apicella et al., 2020].

Gravimetric emission monitoring relies on drawing a defined (isokinetic) sample and depositing the total sample dust mass on a pre-conditioned sample filter. Based on mass differences, volume flow and sample time, gravimetric concentrations can be determined [Wiegler, 2016]. Here, larger particles contribute more to the total gravimetric concentration compared to smaller (e.g. submicron or nano-) particles. The most penetrating particle size of pulse-jet cleaned filters is within the submicron size region (approx. of 0.1 – 0.4 μm) so that gravimetric concentrations are respectively low provided the operation conditions (e.g. no leaks) are appropriate [Bächler et al., 2024b; Steiner & Lanzerstorfer, 2023; Schiller & Schmid, 2014; Simon et al., 2014]. For the majority of plants the measurement is not size resolved and offers no direct information on the particle size distribution. Cascade impactors enable size-resolved gravimetric measurements, which are commonly not required by the legislature. The overall low emission levels under suitable operation conditions also result in comparably long measurement times in order to accumulate sufficient amounts of dust on a test filter (no online measurement). This is reflected in current guidelines, where the maximum total gravimetric particle concentration for fabric filters is set at 1-5 mg/m^3 [European Commission, 2023].

Other types of measurement sensors that do not rely on gravimetric sampling are also used in applications where pulse-jet cleaned filters are used for waste-gas treatment. E.g. the measurement of the transmission, respectively extinction or a laser passing the exhaust gas duct may be a suitable online measurement technology for comparably higher dust concentrations. Another example includes triboelectric sensors, where the friction between particles within the aerosol flow and a measurement probe in the gas duct cause the generation of a current due to a charge difference. Triboelectric sensors are commonly used as “filter guards” in order to detect larger bag failures and increased dust emissions for entire baghouses [Wiegler, 2016]. Sensors based on forward- or backward- scattering of light are also an option in the current industrial application [Wiegler, 2016]. The lower detection limit of these devices is typically at larger particle sizes compared to (laboratory) aerosol spectrometers.

In a laboratory environment, measurement technology relying on particle counting better reflects the actual low (fine-) dust emission of filters [Jodeit et al., 1983]. Aerosol spectrometers are an online measurement device and can give temporally resolved information on particle number concentrations and the particle size distribution, what is not possible for conventional gravimetric determination of total dust concentrations. The calculation of a corresponding particle mass concentration can be performed by considering the size distribution and aerosol properties [Kasper et al., 2007]. Of course high precision laboratory particle counters are only rarely used for process monitoring in industrial applications due to high capital costs, the required know-how and the required space for installation and / or sampling lines.

Many studies in literature employed aerosol spectrometers for particle emission measurement of pulse-jet cleaned filters due to the advantage of simultaneous particle concentration and size detection with a high temporal resolution (which is required due to the transient behavior of the dust emission) [Binnig et al., 2007]. Fundamentals on the measurement principle, detection capabilities and potential measurement errors for scattered light based aerosol spectrometers (e.g. coincidence error or border zone error) can be accessed in the corresponding literature (e.g. [Gail & Gommel, 2018; Pletscher et al., 2016; Mölter, 2006; Umhauer 1975]).

In recent years, scattered-light based low-cost PM-sensors have been established as measurement tools for e.g. spatial measurements for ambient air particle concentrations due to their compact size and cheap price. Outside of ambient air measurements, the sensors were used in ventilation applications and show potential to be used in particle emission measurements as well [Ostermeyer et al., 2020; Schwarz et al., 2018]. An advantage compared to devices installed in the clean gas duct (and thus only monitoring the total dust emission) includes the possibility for spatial measurements due to flexible sampling opportunities either due to respective tubing or compact design of the measurement devices themselves. Within the scope of this dissertation, scattered-light based optical particle counters were used as the main aerosol measurement device.

3 MATERIALS AND METHODS

The following chapter gives information on the experimental set-up for the investigation of the (spatial) particle emission and operating behavior of baghouse filters, as well as the employed test dust, filter media and the corresponding scattered-light based particle measurement technology.

The methodical approach for addressing the research questions are displayed in Figure 10 and Figure 11. For the evaluation of the suitability of low-cost PM-sensors for (spatial) particle emission monitoring in pulse-jet cleaned filters, experiments in two different experimental facilities were performed.

Research question: Are low-cost PM-sensors suitable for (local) particle emission monitoring and the identification of particle emission hotspots in baghouse filters?

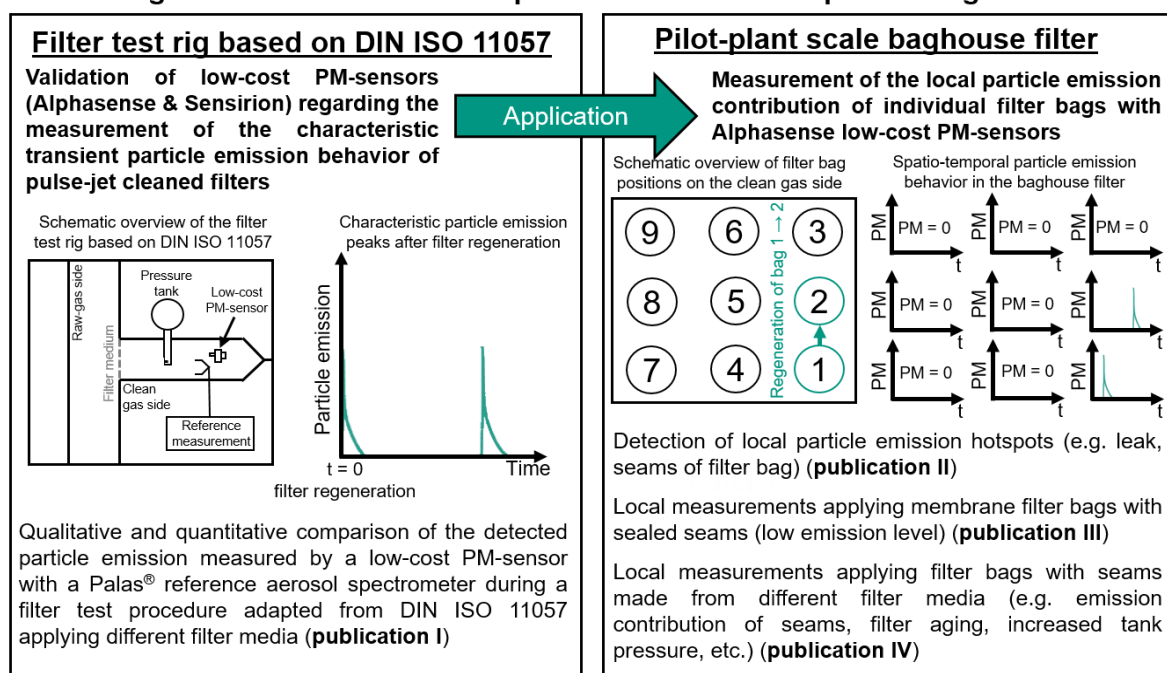


Figure 10 – Experimental methodology for investigations concerning the suitability of low-cost PM-sensors for spatial particle emission monitoring.

Regarding the initial validation of the measurement technology under defined conditions, two different types of low-cost PM-sensors (Alphasense OPC-N3 and Sensirion SPS30) were installed in a filter test rig for the measurement of particle emissions after filter regeneration (publication I). Different filter media were applied following a filter test procedure adapted from DIN ISO 11057 to create different particle emission levels. The detected concentrations were compared to a reference aerosol spectrometer manufactured by Palas®. After a promising validation, the sensors were applied in a pilot-plant scale baghouse filter for local measurements of the particle emission contribution of individual filter bags. Different types of filter bags (e.g. with and without sealed seams) made from different filter media under varying process conditions (publication III and IV) were investigated regarding the corresponding particle emission levels and local emission contributions of particle emission hotspots (publication II).

Addressing the second research question, an evaluation of filter operation regarding energy demand and particle emissions was performed in the pilot-plant scale baghouse filter. Instead of local emission contributions, only the total particle emission measured by the reference aerosol spectrometer was taken into account. Different operating parameters were varied (filter face velocity, raw-gas concentration and tank pressure) following an experimental procedure that included the variation of cycle time between filter regenerations for each set of parameters. This enables the quantification of energy demand for filter operation (consisting of fan power and the consumption of pressurized air according to [Höflinger & Laminger, 2013]) and particle emission for each cycle time and the identification of a power minimum at a corresponding cycle time at the power minimum.

Research question: How can particle emissions from baghouse filter operation be lowered as energy-efficiently as possible and what is the trade-off between energy demand and particle emissions?

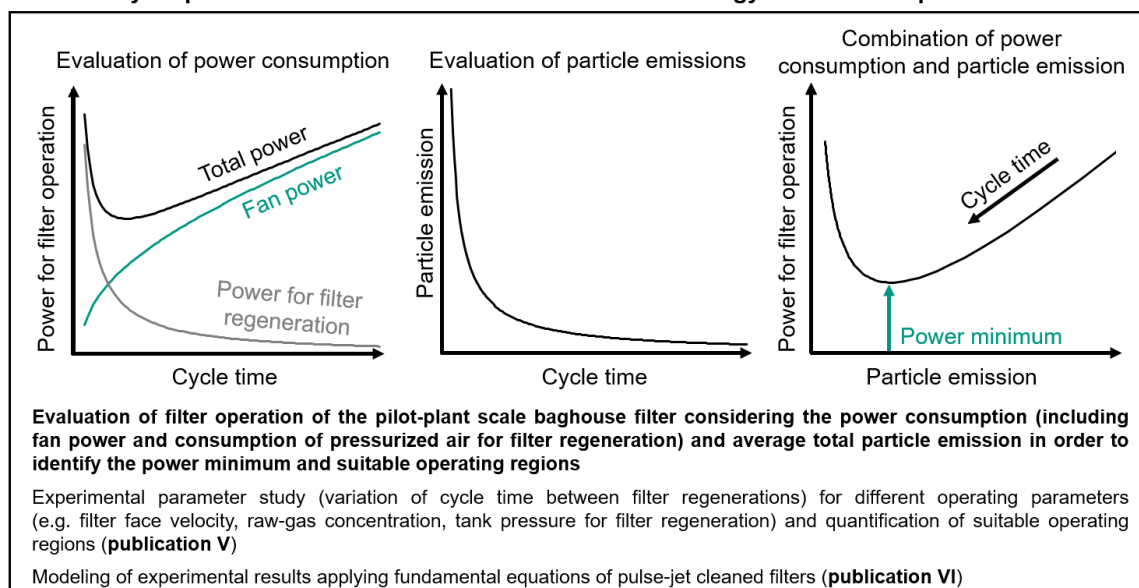


Figure 11 – Methodology for investigations concerning the trade-off between energy demand and particle emissions for pulse-jet cleaned filters.

Combining the experimentally determined energy demand and particle emissions enables the construction of an operating curve that enables the identification of suitable operating regions. Following the experimental parameter study, the dataset served as the foundation for process modeling. Applying fundamental equations of surface filters, the experimentally determined differential pressure is modeled selecting the filter medium resistance as a cycle time dependent fit-parameter. The particle emission is modeled after a hyperbolic trend obtained from the experimental data.

3.1 Filter test rig

The filter test rig and key operating parameters for the initial sensor validation (chapter 4.1 / publication I) is displayed in Figure 12. Modifications from the standard [DIN ISO 11057, 2016] include e.g. the optical particle emission measurement applying the Palas® reference and the low-cost PM-sensors (chapter 3.3). A PM_{2.5} sharp-cut cyclone and an absolute filter on the clean gas side enable additional gravimetric emission measurement for comparison.

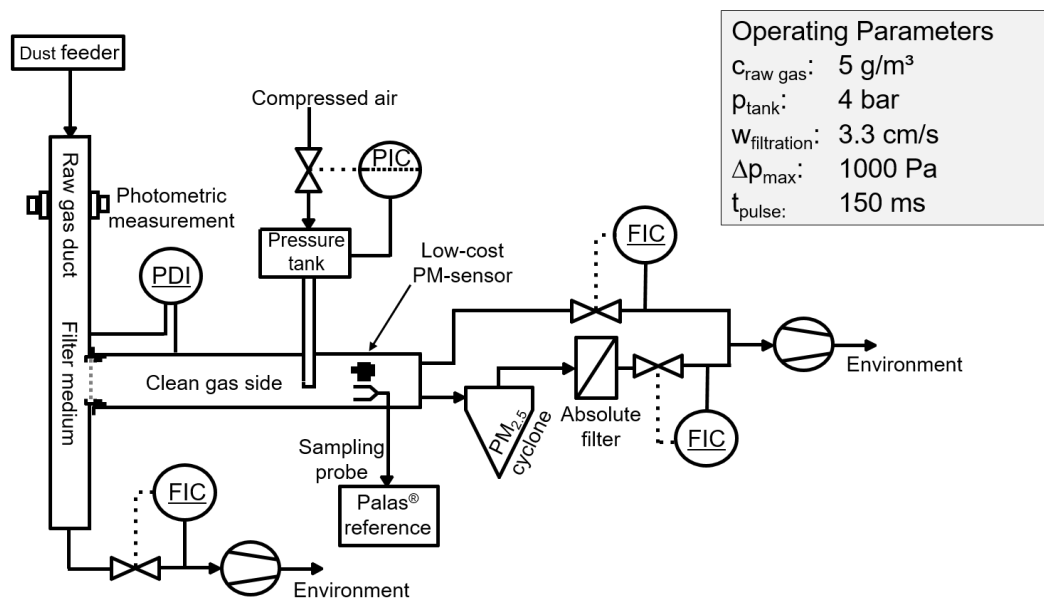


Figure 12 – Modified filter test rig based on DIN ISO 11057. Image adapted from [Bächler et al., 2019a].

The test dust (chapter 3.4) is dispersed into the raw-gas duct, where a photometric measurement monitors the (constant) raw-gas concentration. The filter face velocity was adjusted to 3.3 cm/s as specified in the standard.

Filter tests using low-cost PM-sensors for particle emission monitoring were performed applying an experimental procedure modified from DIN ISO 11057 according to Figure 13.

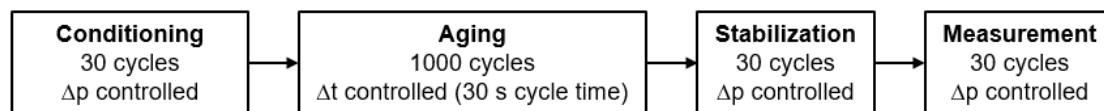


Figure 13 – Experimental procedure of the filtration tests. Image adapted from [Bächler et al., 2019a].

Different regeneration criteria were adjusted depending on the corresponding phase of the filter test. When reaching either the maximum specified differential pressure of 1000 Pa (conditioning, stabilization and measurement) or after passing a time of interval of 30 seconds (filter aging) the circular filter sample (diameter 15 cm) is regenerated with a jet-pulse from the clean gas side (4 bar tank pressure; electrical valve opening time of 150 ms).

The selected filter media are described further in chapter 3.5 and were identical to the filter media used in the pilot plant scale baghouse filter. Further information on sensor installation can be accessed in the corresponding publication I and [Bächler et al., 2019b].

3.2 Pilot-plant scale baghouse filter

The experimental facility where the majority of investigations were performed is a pilot-plant scale baghouse filter with a total of nine filter bags. A flow sheet of the baghouse filter including the surrounding set-up is illustrated in Figure 14.

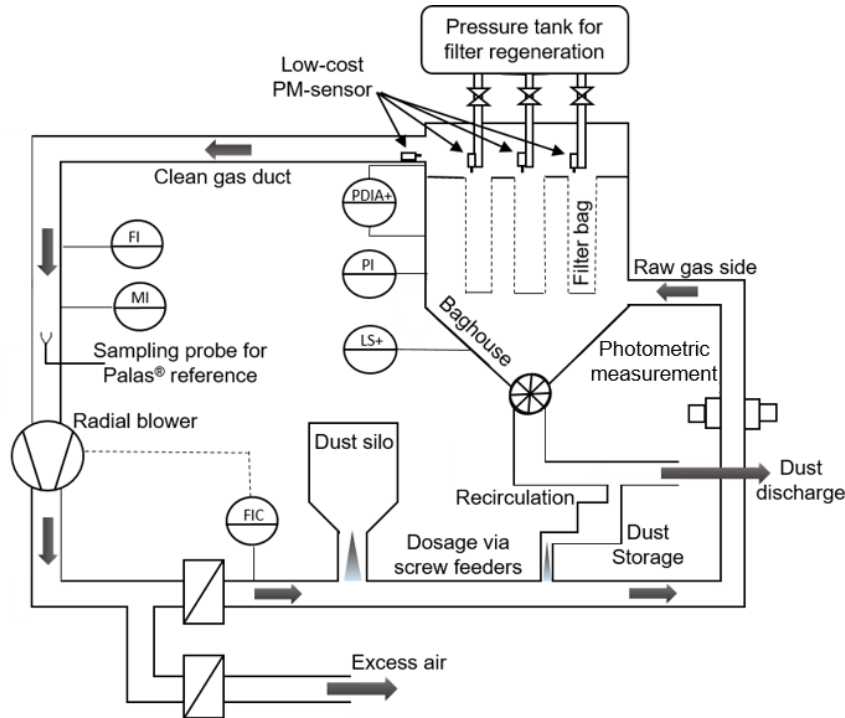


Figure 14 – Flow-sheet of the baghouse filter and the experimental set-up for the investigations presented in publication II-V. Image adapted from [Bächler et al., 2023a].

Each of the nine filter bags has a filter area of 0.46 m^2 (diameter of filter bag 11.7 cm ; length of filter bag 125 cm) so that a total filter area of 4.14 m^2 was installed in the baghouse. Information on different used filter media can be found in chapter 3.5. Each filter element can be regenerated individually during filter operation by a jet-pulse from the corresponding blow pipe. Three pressure tanks control the regeneration pressure (8 bar maximum tank pressure), whereby each pressure tank supplies three blow pipes with pressurized air according to Figure 15.

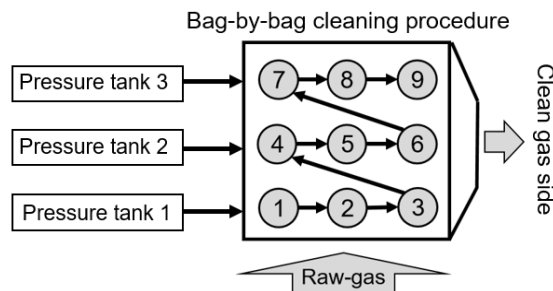


Figure 15 – Bag-by-bag cleaning procedure and pressure tanks enabling the filter regeneration for the corresponding rows (pressure tank 1 supplies bags 1,2 & 3, etc.).

The electrical valve opening time for the filter regeneration was preset at 150 ms and kept constant for all experiments. The regeneration itself was triggered time controlled after a corresponding cycle time. Due to a flexible process control software, multiple cleaning procedures can be adjusted, the most frequently used within this work being a bag-by-bag cleaning procedure where one individual bag is regenerated after a preset cycle time Δt following the sequence shown in Figure 15.

A radial blower creates a circulating volume flow through the testing facility, whereby a flow control enables a constant filter face velocity. The highest filter face velocity adjusted in this work was 3.33 cm/s (corresponds to a volume flow of approx. 500 m³/h). This filter face velocity is based on guidelines for filter testing and is on the upper-end of typical filter-face velocities used in industrial applications. The fan power of the radial blower is limited so that at higher differential pressure levels and corresponding volume flows (e.g. above 2500 Pa at a filter face velocity of 3.33 cm/s), the blower is operated at maximum capacity and the flow throughput slowly decreases. This limitation was only relevant for a few operation scenarios and its effect on the individual results is negligible.

The test dust (compare chapter 3.4) is added at two separate points via screw feeders. New test dust from a silo is added based off the signal at an extinction measurement that monitors the raw-gas concentration (variable rotational speed). The extinction measurement has been calibrated regarding several raw-gas concentration levels specified in the corresponding publications. A recirculation adds separated test dust at a constant rotational speed of the screw-feeder. Dust dosage is set so that the majority of the test dust is recirculated in order to enable stable long-term operation of the testing facility.

Typical operating parameters of the small scale baghouse filter are listed in Table 1.

Table 1 - Operating parameters for the pilot-plant scale baghouse filter.

Parameter	Typical value	Range
Filter face velocity	3.33 cm/s	0 – 4 cm/s
Raw-gas dust concentration	15 g/m ³	0 – 40 g/m ³
Time interval between regenerations (cycle time)	60 s	5 – 200 s
Approx. differential pressure level	2000 Pa	200 – 3000 Pa
Tank pressure for filter regeneration	3 bar	2 – 8 bar
Electrical valve opening time	150 ms	50 – 1000 ms
Temperature	Ambient temperature	0 – 40 °C
Filter media	Variable – dependent on the investigation (refer to chapter 3.5 or the corresponding publication)	
Test dust	Variable - Pural SB was selected in this work (refer to chapter 3.4)	

The particle emission penetrating the filter elements after regeneration is measured applying scattered-light based measurement technology. In the publications dealing with spatial PM-monitoring shown in publication II-IV, low-cost PM-sensors of the model OPC-N3 from Alphasense were fitted at each blow pipe above the outlet of the filter bags for online PM-monitoring according to Figure 16 (in-situ installation of the sensors).

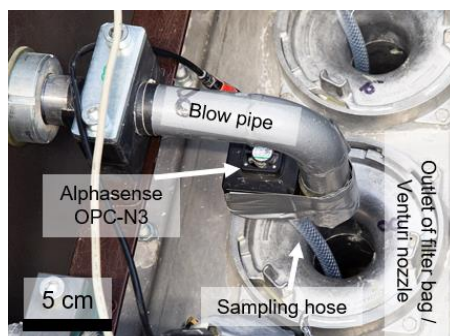


Figure 16 – Image of sensor positioning in the pilot-plant scale baghouse filter. Image adapted from [Bächler et al., 2020].

A sample tube led into the venturi nozzle to measure the particle concentration at each individual filter bag and thus, as close to the source as possible. An additional low-cost PM-sensor was used for the determination of the total particle emission and placed further down the clean gas duct in case of publication IV. A Promo[®]2000 system with a welas[®]2100 sensor of the manufacturer Palas[®] was used as reference aerosol spectrometer (either for local or total particle emission dependent on the investigation).

3.3 Aerosol measurement technology for particle emission measurement

This chapter showcases the different aerosol measurement devices used in this work including differences in their design. Table 2 gives an overview of the specifications of the corresponding measurement devices taken from the datasheet. Two exemplary low-cost PM-sensors manufactured by respectively Sensirion or Alphasense are compared to the highly developed laboratory aerosol spectrometer from Palas[®] used as reference device throughout this work.

Table 2 – Specifications of the aerosol measurement technology.

Manufacturer Device	Alphasense OPC-N3	Sensirion SPS30	Palas [®] Promo [®] 2000 with welas [®] 2100 sensor
Classification	Low-cost sensor	Low-cost sensor	Laboratory aerosol spectrometer
Measurement outputs	PM ₁ , PM _{2.5} , PM ₁₀ ; counting rate; information on sensor status (e.g. sample flow-rate, laser status, etc.)	PM ₁ , PM _{2.5} , PM ₁₀ , size classified number concentrations, “typical particle size”	Total and size resolved number concentrations with PM-conversion
Detectable size range	0.35-40 µm	0.3-10 µm	User selectable: 0.2-10 µm - selected; 0.3-17 µm; 0.6-40 µm
Particle size classification	24 size classes	5 size classes	64 size classes per decade
Maximum particle concentration	2000 µg/m ³ ; 0.84% probability for coincidence at 1000 #/cm ³	1000 µg/m ³ ; 3000 #/cm ³	5 · 10 ⁵ #/cm ³
Approximate cost	400 €	30 €	30.000 €
Dimensions	70 mm · 40 mm · 62 mm	40 mm · 40 mm · 12 mm	245 mm · 100 mm · 80 mm
Temporal resolution	≈ 1 s	≈ 1 s	≈ 1 s
Particle density	User adjustable (Bin-weighting index)	Non-adjustable	User adjustable
Particle refractive index	1.5 (-) Standard setting Non-adjustable	Non-adjustable (calibration with KCl aerosol)	1.59 (-) Standard Setting User adjustable
Temperature range	-10-50 °C	-10-60 °C	10-40 °C (thermodynamic conditions) Heated sensor variants available up to 250 °C

There are several key differences between the measurement devices aside from the obvious difference in acquisition costs. While the Sensirion sensor is a typical “low-cost” device, the Alphasense sensor is a more developed compact scattered-light based sensor that enables more adjustments and a more accurate size resolution.

The Palas[®] device enables even more defined settings regarding the sample aerosol, such as the consideration of particle density and refractive index, which is typically preset and non-adjustable for low-cost PM-sensors. Furthermore, the detectable size range is limited at a lower particle size of down to approx. 200 nm. The maximum particle number concentration is approx. two orders of magnitude higher for the laboratory aerosol spectrometer compared to low-cost PM-sensors that are typically specified regarding mass based concentration limits even though only the counting efficiency / particle number concentration is of technical significance. Key advantage of the low-cost PM-sensors is the compact size, that allows for the application in constricted environments, such as the clean gas side of (pulse-jet cleaned) filters. Limitations regarding the measurement specifications for the industrial application for the low-cost devices include e.g. the temperature range, which is unsuitable for many applications where pulse-jet cleaned filters are used for gas cleaning (e.g. cement production, incineration processes). However here, even the heated variants for the welas[®] sensor rely on corresponding sampling tubes and the whole sensor (including housing and connections) does not withstand extreme temperatures.

Mass based particulate matter (PM) concentrations (in $\mu\text{g}/\text{m}^3$) are typical output values for low-cost PM-sensors. PM_{10} concentrations and $\text{PM}_{2.5}$ concentrations represent the fraction of particles that pass the upper respiratory tract (PM_{10}) or the particle fraction that may penetrate deeper into the bronchial tubes or reach the lungs (respirable dust - $\text{PM}_{2.5}$) [WHO, 2021]. Different sampling apparatuses that serve as pre-separator of coarser particle sizes are used for the gravimetric measurement of PM_{10} and $\text{PM}_{2.5}$ fractions for ambient air quality monitoring, whereby the aerodynamic diameter at 50% separation of the corresponding size corresponds to 10 μm (PM_{10}) or 2.5 μm ($\text{PM}_{2.5}$) respectively [Peters et al., 2001]. The MPPS for pulse-jet cleaned filters is located in the submicron region below a particle size of 2.5 μm and therefore the majority of emitted particles are bound to have a corresponding size. Total dust concentrations and size resolved PM concentrations should therefore yield similar results in the context of particle emissions penetrating surface filters and the $\text{PM}_{2.5}$ concentration was selected as key value for the comparison of the measurement devices in many cases throughout this work.

3.3.1 Reference aerosol spectrometer Promo[®]2000 with welas[®]2100 sensor manufactured by Palas[®]

The laboratory aerosol spectrometer is made up of the Promo[®] device and the welas[®] sensor as illustrated in Figure 17.

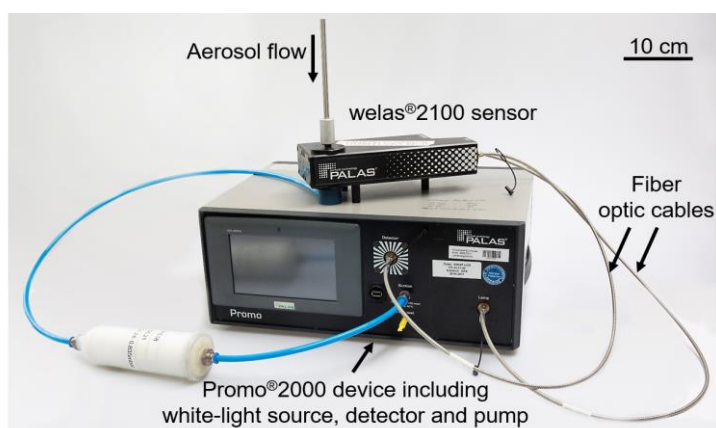


Figure 17 – Image of the Promo[®] system and the welas[®] sensor.

The Promo[®] device serves as monitor and operation control, as well as light source (white light), detector and pump generating the sample flow through the welas[®] sensor. Light source and detector of the Promo[®] device are connected to the welas[®] sensor via fiber optic cables.

Due to the detection of scattered light under a detection angle of 90° from a white-light source, an accurate calibration regarding scattered light intensity and optical particle size can be achieved. Calibration was performed by the manufacturer applying polystyrene aerosol. The measurement volume within the welas[®] sensor is made up in a three-dimensional “t-shape” due to the application of a corresponding aperture, what enables the identification and correction of border-zone errors [Pletscher et al., 2016]. Furthermore, due to the defined measurement volume and device setup, larger particle number concentrations can be detected without the occurrence of coincidence errors compared to the low-cost PM-sensors.

3.3.2 Low-cost PM-sensors

Figure 18 and Figure 19 show photographs of the interior of two exemplary commercially available low-cost PM-sensors of the manufacturers Sensirion and Alphasense. The sensors can be operated e.g. via USB connection and software provided by the manufacturer and are easy to use plug and play devices.

With regards to the Sensirion sensor, the key components such as the laser-diode, detector (scattered light detection angle of 90°) and light trap as well as the flow-path of the aerosol can be clearly identified.

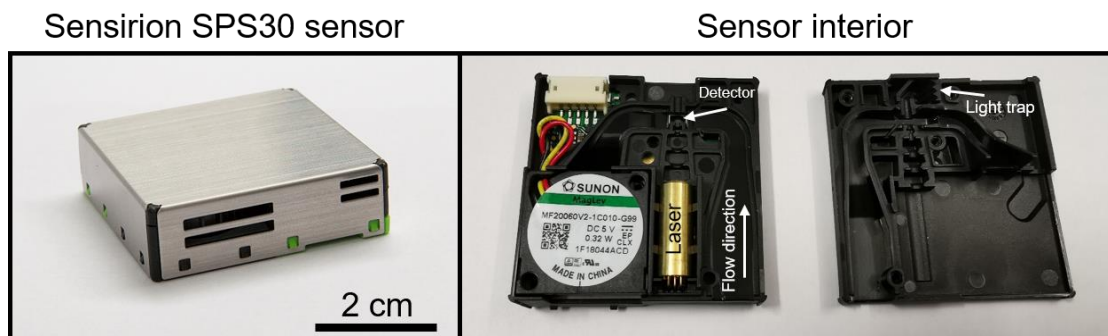


Figure 18 – Images of the SPS30 sensor and the sensor interior.

The wavelength of the laser is 660 nm. The sensor is calibrated against a TSI[®] DustTrak DRX 8533 (particle mass concentration) and TSI[®] OPS 3330 (particle number concentration) applying a KCl aerosol.

The Alphasense sensor is constructed differently, as the aerosol does not follow a constricted path with clearly defined measurement volume and is instead distributed within the total measurement chamber.

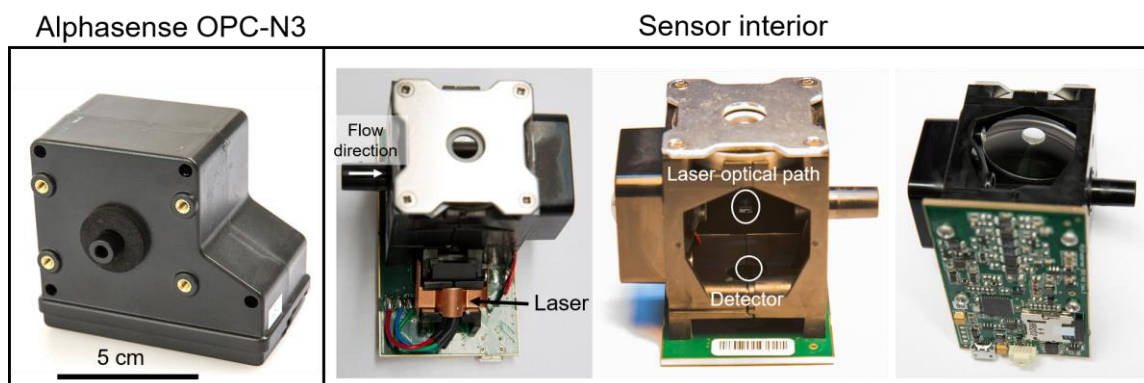


Figure 19 – Images of the OPC-N3 sensor and the sensor interior.

The laser pathway is designed as a “free-jet” whereby the scattered light is detected at a different detection angle ($\approx 135^\circ$) compared to the Sensirion sensor. The laser power is approx. 5-8 mW at a wavelength of 658 nm. The device has been calibrated by the manufacturer using polystyrene latex aerosols containing specific defined particle sizes and compared to a reference OPC (TSI® OPS 3330). The sensor has been designed for applications measuring ambient air. Regarding the implementation in the baghouse filter, a sampling tube with sufficient diameter and negligible pressure drop has been fixed at the sensor inlet. The manufacturer specifies that forced flow through the sensor may impact the measurement result. The performance of the sensor regarding particle emission measurement behavior and accuracy for the complex flow conditions present in the baghouse filter is the topic of many investigations in this work.

Contamination of sensor optics can impact the measurement performance. Due to the transient nature with short dedicated concentration peaks and long periods of (almost) zero concentration during regular filter operation, significant contamination of the optics during the limited time required for the experiments (compared to e.g. 24 h operation in ambient air measurement applications) can be ruled out. The sensors were checked regularly regarding their stability while installed on the clean gas side of the baghouse filter (e.g. detection of a zero concentration level with sufficient dust cake on the filter medium and no additional dust dosage). No further calibration procedures were undergone and the sensors were installed as received “off the shelf”. In case of sensor failure or e.g. after the evaluation of particle emission hotspots (publication II), the corresponding sensors were replaced before starting a new set of experiments.

3.4 Test dust

The aluminum oxide hydroxide powder “Pural SB” of the manufacturer Sasol was selected as test-dust in this work. Several key properties of the dust are summarized in Table 3.

Table 3 – Specifications of the test-dust Pural SB.

Property	Value
Chemical composition	Al O (OH)
Particle solid density	2800 kg/m ³
Bulk density	650 – 850 kg/m ³
Mean particle diameter $x_{50,3}$ from laser diffraction	35 μm
Refractive index	1.64 (-)
Dispersive properties	Non-agglomerating / Free flowing

The test-dust is non-toxic and therefore easy to handle in laboratory environments. The non-agglomerating dispersive properties enable easy dosing / dispersion and cake-detachment during filter operation. The fine-dust fraction of the test dust is comparably low with a mass median diameter of 35 μm . However, the particle penetration through the filter medium is higher compared to more agglomerating dusts [Sobich et al., 2018; Kurtz et al., 2016], as the fine dust fraction is actually available and does not form larger agglomerates that are easier to separate due to the low adhesive and cohesive properties of the dust. The total particle size distribution spans a wide range and has been evaluated with several aerosol measurement devices according to Figure 20 [Bächler et al., 2022a].

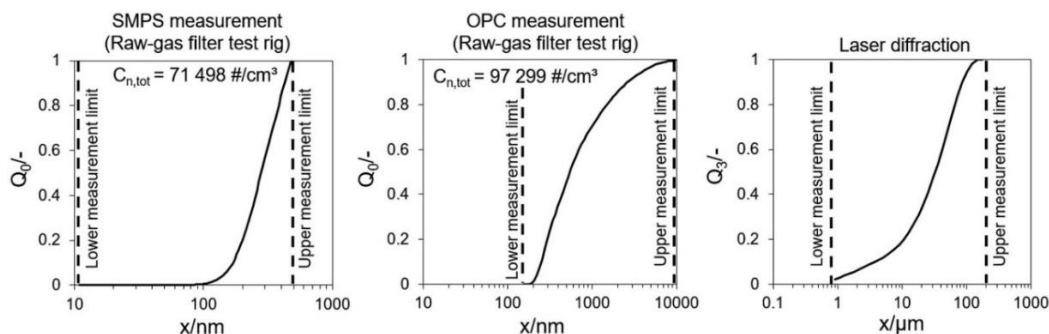


Figure 20 – Cumulative particle size distributions Q_i obtained through application of different aerosol measurement devices. Image taken from [Bächler et al., 2022a].

Applying a mass / volume based evaluation method in the form of laser diffraction (dispersion via Sympatec QUIXEL with water as working fluid - no sonication - and measurement via Sympatec HELOS), the fine dust fraction appears very low. OPC (Promo[®]2000 with welas[®]2100) and SMPS (TSI[®] SMPS 3082 with long DMA and CPC3756) measurements yield more relevant information on the size distribution in the context of filtration and particle penetration. The most penetrating particle size of pulse-jet cleaned filters is located approx. between 0.1 and 0.4 μm so that the test dust covers the relevant region and is suitable for emission measurements. Furthermore, the test dust contains particles up to the lower detection limit of scattered-light based measurement devices, so that the measurement size range for the Palas[®] reference OPC has been selected accordingly (0.2 – 10 μm compare Table 2). The density of the test dust has been considered regarding the determination of mass based particle concentrations of the aerosol measurement technology, if the device offered corresponding setting adjustments (Alphasense and Palas[®] reference).

3.5 Filter media

Filter bags made from different types of filter media were used in the publications in the appendix to generate different particle emission levels based on the separation efficiency of the corresponding media. Table 4 gives an overview on the employed filter media. Note that the designation of the filter media varies depending on the publication so that the filter media are labeled in Table 4 according to the corresponding material or surface treatment. Filter bags confectioned from the corresponding filter media are also shown in Figure 4.

Table 4 – Specifications of the filter media.

Medium	Membrane	Needle-felt	Spunbond
Area weight / g m ⁻²	500	600	240
Thickness / mm	1.9	2	1
Permeability (200 Pa) / l dm ⁻² min ⁻¹	30	70	100
Fiber material	Polyphenylene Sulfide	Polyester	Polyester, Polyamide
Remarks	Heat set, laminated ePTFE membrane	Singed upstream side	Hydro entangled microfilaments

The filter bags were installed and tightly fixed between raw-gas side and clean gas side by the help of the ring sealing (snapping) of the filter element that prevents leaks between raw-gas side and clean gas side. Figure 21 showcases the top part of a filter bag.

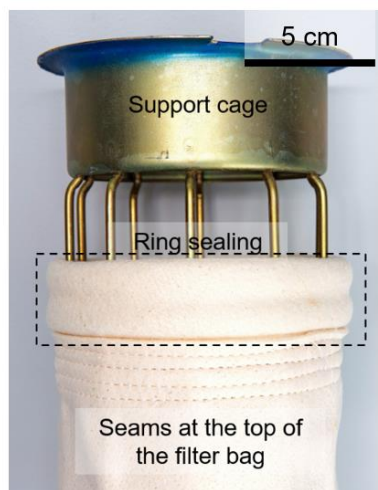


Figure 21 – Top part / outlet of a filter bag. Image adapted from [Bächler et al., 2023a].

4 POTENTIAL AND LIMITATIONS OF LOW-COST PARTICULATE MATTER SENSORS FOR PARTICLE EMISSION MEASUREMENTS FOR PULSE-JET CLEANED FILTERS

The following chapter presents the potential application of low-cost PM-sensors as (spatial) particle emission measurement technology for baghouse filters. The chapter summarizes the key results of two publications from scientific journals. The corresponding publications I and II can be accessed in the appendix.

In chapter 4.1, scattered-light based low-cost PM-sensors are applied in a filter test rig based on DIN ISO 11057 for sensor validation and evaluation of the sensors' capabilities to measure the characteristic transient particle emission behavior of pulse-jet cleaned filters (compare Figure 10).

The potential for online leak detection and the spatial identification of particle emission hotspots is investigated in chapter 4.2 during experiments in the pilot-plant scale baghouse filter (Figure 14).

4.1 Validation of scattered light based low-cost PM-sensors for the detection of the characteristic particle emission behavior in a filter test rig

Results applying the SPS30 low-cost PM-sensor from Sensirion were published in [Bächler et al., 2019a] / publication I. The corresponding publication can be accessed in the appendix. This chapter briefly summarizes the key results and conclusions applying the OPC-N3 low-cost PM-sensor of the manufacturer Alphasense within the identical experimental framework as this sensor is relevant for the further investigations in this thesis. Parts of the results in chapter 4.1 were presented at Filtech 2019 – The Filtration Event (Cologne) [Bächler et al., 2019b].

4.1.1 Extensive summary of publication I

The transient particle emission behavior for pulse-jet cleaned filters poses a measurement challenge for low-cost PM-sensors that are typically applied for ambient air measurements. The sharp increase of particle concentrations (potentially exceeding the specified maximum concentration of the sensor) and the subsequent decay behavior require a fast response time. Investigations led by [Schwarz et al., 2018] showed results of filter emission measurements using an SDS011 low-cost PM-sensor of the manufacturer Nova Fitness compared to the Palas[®] reference system (chapter 3.3.1). While emission peaks were detected by the applied low-cost PM-sensor, the overall curve deviated from the reference, hinting at internal data-smoothing of the low-cost PM-sensor [Schwarz et al., 2018].

Expanding upon the investigation of [Schwarz et al., 2018] and the starting point of research was the application of different types of low-cost PM-sensors in a filter test rig (Figure 12) following a filter test procedure adapted from DIN ISO 11057 (Figure 13). Many different types of low-cost PM-sensors are commercially available on the market. The applied sensor in publication I (SPS30 of the manufacturer Sensirion) was selected based on monitoring capabilities of number based particle concentrations (instead of only mass based PM

concentrations that are the typical output parameter for many other low-cost PM-sensors) and a comprehensive datasheet standing out compared to other manufacturers.

In addition to the SPS30 sensor of the manufacturer Sensirion in publication I, two other sensors were investigated following the same experimental procedure under identical process parameters in the filter test rig [Bächler et al., 2019b]. Namely, the sensor OPC-N3 manufactured by Alphasense was selected for closer evaluation due to its higher number of size classes for a more thorough representation of the particle size distribution (compare Table 2) and the sensor PMS7003 of the manufacturer Plantower (not part of this dissertation) was selected as cheap alternative to the SPS30 sensor applied in publication I. The results of the Alphasense OPC-N3 sensor from the filter test rig are included in this chapter in order to give a complete evaluation of sensor measurement performance, due to its relevance for further investigations in publications II-IV.

The low flow velocities (3.3 cm/s) and the defined conditions within the scope of filter testing enable comprehensive experiments regarding sensor validation. The test procedure included a filter aging stage, increasing the separation efficiency and residual differential pressure of the filter medium sample due to frequent cleaning and deposition of particulate matter in the fiber matrix (Figure 13). Three different filter media with different properties and surface treatments were selected to investigate the effect of filter media properties on the particle emission (Table 4). The focus of this chapter are measurement results after filter aging for a conditioned medium sample (measurement phase according to Figure 13). A decreasing trend of the particle emission was measured over the course of filter aging. Further details on the effect of filter aging and the measurement results of the sensors can be accessed in publication I and [Bächler et al., 2019b].

After filter regeneration (Δp -controlled regeneration at 1000 Pa) and successful cake detachment, particles penetrate the filter medium causing the detection of an emission peak on the clean gas side. As shown for two exemplary filter regenerations in Figure 22, both the low-cost PM-sensor and the Palas[®] reference detect corresponding emission peaks. While there are differences in the exact peak height and decay behavior (e.g. slower decay for the Alphasense sensor and slightly higher peak height), the overall behavior is in good agreement.

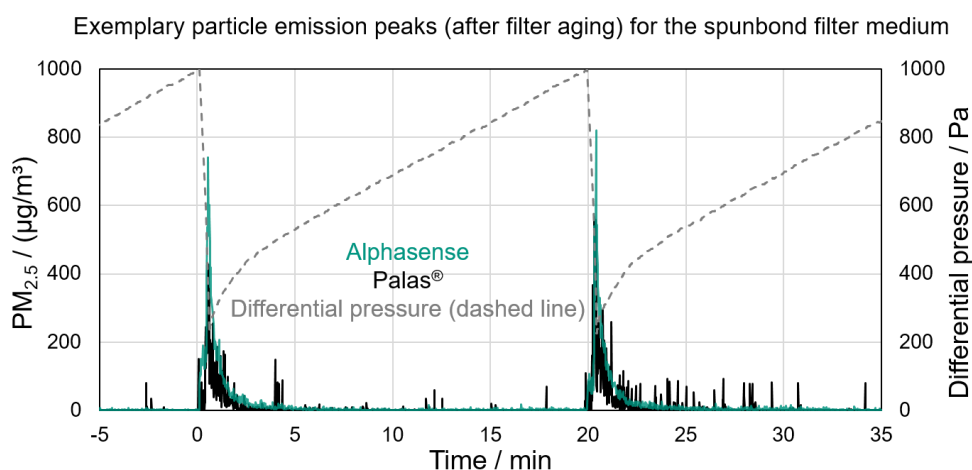


Figure 22 - Comparison of two exemplary particle emission peaks detected by the Alphasense low-cost PM-sensor and the Palas[®] reference for the spunbond filter medium following the filter test procedure detailed in publication I (measurement phase after filter aging). The time axis was shifted to align $t = 0$ at the first filter regeneration.

For a quantitative comparison between reference and low-cost PM-sensor the emitted dust mass per filter area was calculated from the integral of the temporally resolved PM evolution and the

filter face velocity for each individual filtration cycle during the measurement phase. Based on the emitted dust mass per cycle and filter area, three distinct particle emission levels due to application of the three applied filter media were identified as shown in Figure 23. The corresponding labels used in publication I for the different filter media are displayed in Figure 23 for better comparison.

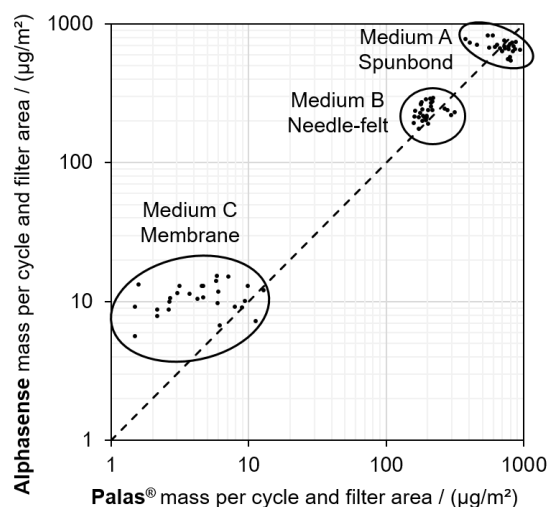


Figure 23 – Comparison of the determined emitted dust mass per cycle and filter area for the Alphasense low-cost PM-sensor and the Palas® reference for all three applied filter media following the filter test procedure detailed in publication I.

As previously discussed, one main advantage of the Alphasense OPC-N3 sensor compared to other low-cost devices is the size classification of the detected particles, that enables the determination of a particle size distribution. The size distributions for the emission penetrating the different filter media were calculated from the internal sensor flow-rate and the number of counting events in the corresponding size classes. A comparison of the size distributions from low-cost PM-sensor data and the Palas® reference for the measurement phase of the filter test procedure is illustrated in Figure 24.

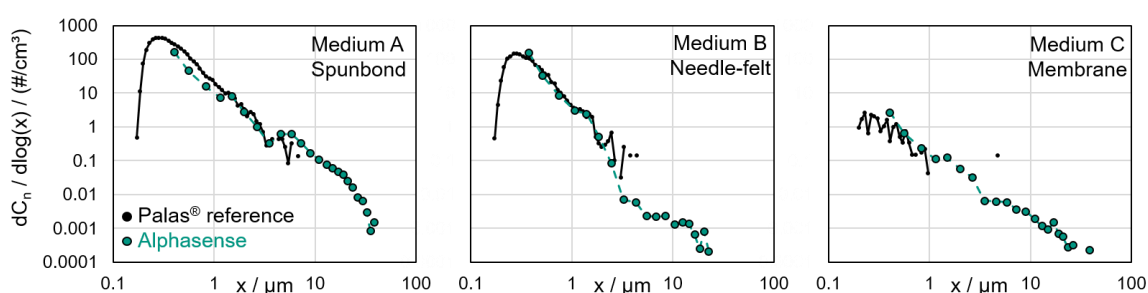


Figure 24 – Comparison of the determined particle size distributions for the Alphasense low-cost PM-sensor and the Palas® reference for all three applied filter media following the filter test procedure detailed in publication I (measurement phase).

The size distributions of the low-cost PM-sensor and the reference are in reasonable agreement. The overall number of size classes is smaller for the low-cost sensor. Considering particle sizes larger than 1 µm, only few individual counting events are registered. The three distinct emission levels according to Figure 23 are also represented by the respective particle size distribution.

The measurements applying the low-cost PM-sensors enabled the detection of qualitative particle emission peaks as well as the quantitative distinction of different particle emission levels compared to the Palas® reference. The same overall conclusions could be drawn for the Sensirion SPS30 shown in publication I / [Bächler et al., 2019a].

4.1.2 Main conclusions of publication I

The experiments in the filter test rig demonstrated the capabilities of low-cost PM-sensors in comparison with a highly developed aerosol spectrometer regarding the measurement of transient particle emission concentrations in the scope of filter testing.

The following key conclusions could be drawn:

- The characteristic particle emission behavior (particle emission peaks after filter regeneration and subsequent zero concentration level) was qualitatively detected by both low-cost PM-sensors (SPS30 from Sensirion and OPC-N3 from Alphasense).
- The Sensirion low-cost PM-sensor generated only limited information on particle size due to the low number of size classes (5 size classes) compared to the reference (64 size classes per decade). The size distribution measured by the Alphasense sensor was in good agreement with the reference measurement.
- In comparison to the Palas[®] reference, quantitative differences regarding the exact PM concentration readings were identified. Before filter aging, the peak concentrations exceeded the maximum particle number concentration specification of the low-cost PM-sensors what may lead to coincidence errors (higher detected peak concentrations of the reference). Even with regards to coincidence-free measurements after filter aging, the determined concentrations of the low-cost sensors deviate from the reference, what may be the case due to different calibration procedures. Additionally, the exact peak shape of the low-cost PM-sensors is different from the Palas[®] reference, hinting at some form of signal smoothing and internal averaging of the registered particle concentrations (especially for the SPS30 sensor).
- Despite these quantitative differences, identical trends regarding particle emission levels of different filter media and particle emission evolution over the course of filter aging could be derived from low-cost PM-sensor data and the Palas[®] reference. Measurements employing an engine exhaust particle sizer (compare [Bächler et al., 2022a]) in another study, also confirmed the different emission levels. Scattered light based devices are suitable for emission monitoring (at least for the applied filter media and test dust) due to the good overlap between the detection range of the instruments and the corresponding particle sizes penetrating the filter media.
- The lowest particle emission level was characterized by low-cost PM-sensors during emission measurements applying the membrane filter medium. Particle emission peaks (with low peak height) were only detected for several seconds. The effect of filter aging was less pronounced for the membrane medium; but still a visible decrease of particle emissions was measured. Due to the unambiguous trend of filter aging, the detected particle concentration on the clean gas side is indeed the result of particle penetration and not e.g. the result of dispersion of dust contaminations on the clean gas side.

The suitable characterization of the particle emissions from surface filters including the measurement of emission peaks, the distinction between different particle emission levels based on sensor data and the effect of filter aging demonstrated the promising potential regarding the application of the compact measurement technology for spatial deployment in pulse-jet cleaned filters.

As a consequence of the elaborate size categorization, as well as the possibilities for adjusting e.g. the particle density for the determination of mass based PM-concentrations and the high amount of additional information regarding data collection and sensor status (e.g. temporally resolved information on sensor flow-rate, laser status), further investigations (publication II-IV) were performed applying the Alphasense OPC-N3 sensor.

4.2 The potential of low-cost PM-sensors for the detection and spatial identification of particle emission hotspots in baghouse filters

The results in this chapter were published in [Bächler et al., 2023a] / publication II. The corresponding publication can be accessed in the appendix. This chapter briefly summarizes the key results and conclusions.

4.2.1 Extensive summary of publication II

Damage to the filter medium can have significant consequences on the total particle emission, as the direct bypass of raw-gas aerosol with high concentration significantly increases the clean gas concentration [Kurtz et al., 2017]. Even small pinhole leaks orders of magnitude lower than the total installed filter area can cause emission increases far above the particle emission caused by regular filter regeneration [Li et al., 2022; Bach & Schmidt, 2007]. This has, aside from negative effects on the environment, economic implications on plant operation, as a temporal shutdown in order to identify the corresponding leaks has to be performed. The exact identification of leaks can be a laborious effort, due to their small potential size and high numbers of filter elements. Triboelectric filter guards can identify an individual filter house as the source of an increased total particle emission [Wiegler, 2016]. Without proper localization of the leak, up to hundreds of filter elements may have to be inspected. Damaged or missing screws or leaks in the plenum plate separating clean gas side and raw-gas side can also be a direct source of continuous particle emissions, increasing the complexity of leak identification [Kurtz, 2018]. Visual identification of larger amounts of dust on the clean gas side can be an indication for leaks. The use of fluorescent dust (predominant particle penetration through the leak) can support the visual identification but is no guarantee for success. The costly alternative to identifying leaks is a wide-scale replacement of filter elements before the end of their service life. Research results from [He et al., 2023] and [Li et al., 2020] present novel prototype sensors for leak identification in baghouse filters, however the developed sensors offer no information on the particle emission contrary to low-cost PM-sensors investigated in this dissertation.

Spatially deployed low-cost PM-sensors have the potential to identify leaks based on the measured local particle concentration. While the large scale application in baghouses equipped with several hundred (or even thousands of) filter elements is economically not feasible (regarding the current generation of available sensors), monitoring a subset of installed filter elements (e.g. within an individual row) could already significantly facilitate maintenance procedures.

In order to investigate the potential for the identification of leaks and other particle emission hotspots applying low-cost PM-sensors, experiments during three different application scenarios were performed according to Figure 25. The raw-gas concentration was set at approx. 5 g/m³ at an average total filter face velocity of 3.3 cm/s and 3 bar tank pressure for filter regeneration during the experiments.

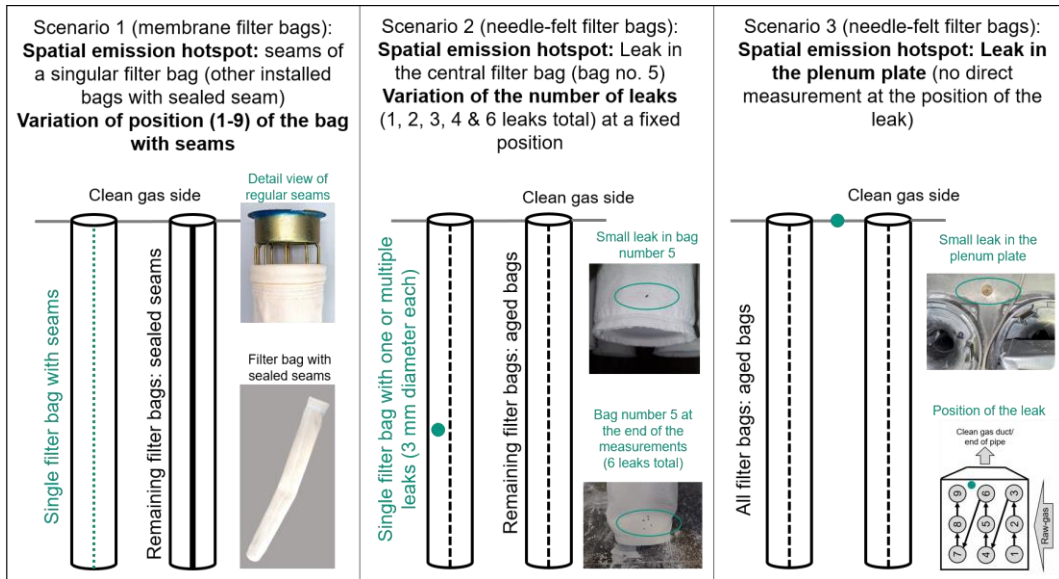


Figure 25 - Overview of the different application scenarios for the detection of a spatial emission hotspot. Image adapted from [Bächler et al., 2023a].

During experiments in scenario 1, the seams of a membrane filter bag (similar to pinhole leaks) are the source of increased particle penetration [Lacerda et al., 2022]. A single factory-new bag was installed at one of the nine positions, while the remaining eight bags were made from the same membrane filter medium but had sealed seams instead. The position of the emission hotspot (factory-new bag with seams) was varied during multiple experimental runs for each position within the baghouse filter. Exemplary results for a single measurement run, where the filter bag with seams was installed at position 1 (compare Figure 15) are presented in Figure 26.

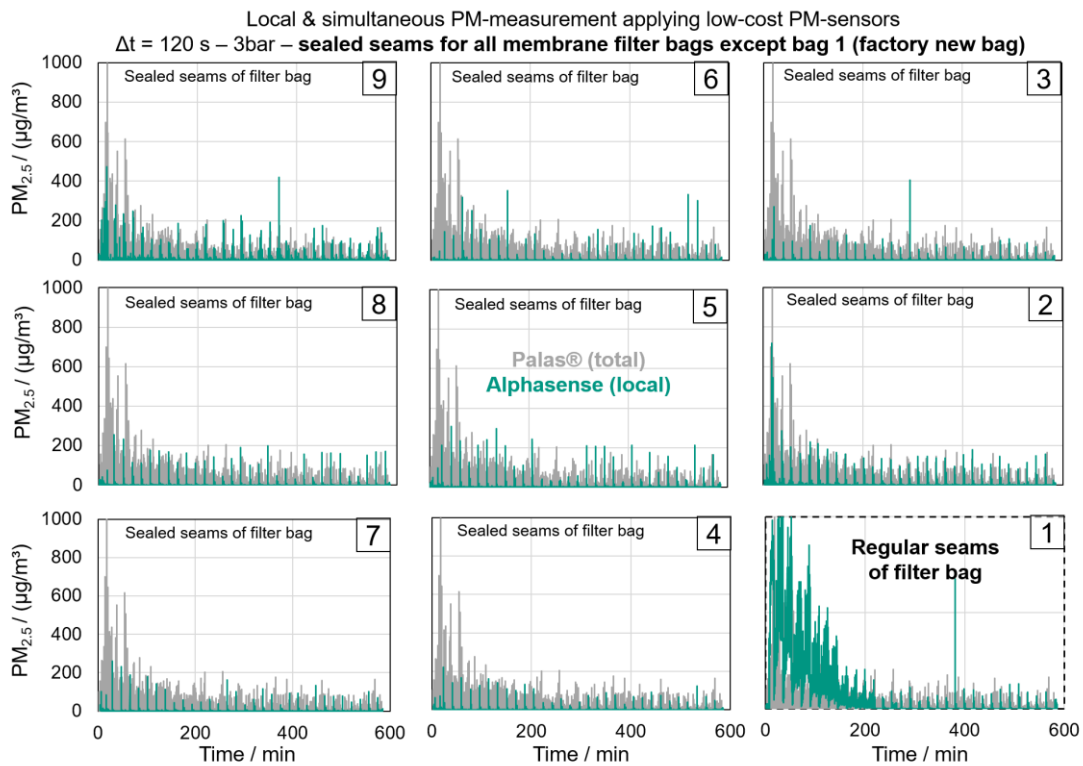


Figure 26 - Spatial PM_{2.5} profile with bag 1 as a temporal emission hotspot due to the seams of the filter bag. Image adapted from [Bächler et al., 2023a].

The particle emission for the filter bags with sealed seams are at a low level (detection of short particle emission peaks only). For the filter bag with regular seams, a decreasing PM concentration is measured over the course of the first 200 minutes of the experiment before reaching a similar particle emission level compared to the remaining bags with sealed seams. This decrease is also reflected by the total particle emission [Palas[®] (total) in Figure 26]. Thus, the source of the particle emission is clearly the factory-new filter bag at position 1 that serves as particle emission hotspot dominating the total dust emission. The concentration decrease is caused by clogging of the seams and filter aging during the initial filtration cycles. Further information on the spatial particle emission behavior during filter aging can be found in chapter 5. Measurement with low-cost PM-sensors enabled the identification of the particle emission hotspot for all nine installment positions (refer to publication II for further information).

In scenario 2, the central filter bag (number 5) served as particle emission hotspot. Over the course of multiple experimental runs, an increasing number of larger leaks (compared to the seams of the filter bag that are similar to “pinhole leaks”) were created by punctuation of the filter bag with a hot needle of 3 mm diameter. The identification of the hotspot was also possible according to the measurement data of the locally installed sensor that measured a high continuous PM₁₀ concentration in each experiment of scenario 2. The reference and another low-cost PM-sensor measuring the total particle emission also detected an increase in the total particle emission due to the emission contribution of the increasing number of leaks. The remaining spatially installed sensors measured a low particle emission level and were unaffected by the particle emission hotspot. Figure 27 shows the average PM concentrations during experimental runs for scenario 2 for all sensors affected by the increased particle emission due to the hotspot.

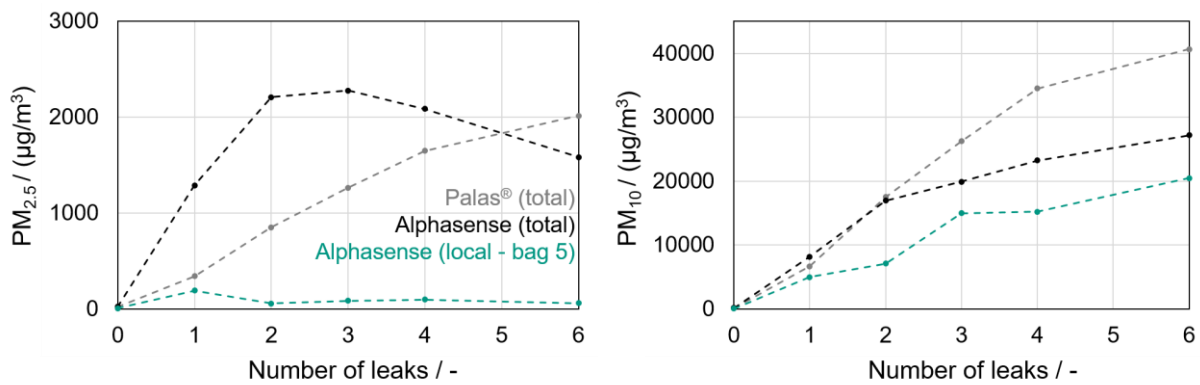


Figure 27 - Optically determined average PM clean gas concentration dependent on the number of leaks (3 mm diameter each). Image adapted from [Bächler et al., 2023a].

All measurement devices registered an increase of the PM₁₀ concentration with increasing number of leaks. After exceeding three leaks total, there are larger deviations between the low-cost PM-sensor and the reference measuring the total particle emission. Nonetheless, the PM₁₀ concentration enables the distinction between different numbers of leaks (respectively leak size). In case of the qualitative PM_{2.5} concentration evolution, the Alphasense sensors and the reference are not in agreement. For the low-cost PM-sensor installed close to the hotspot position, a low particle concentration is detected for each number of leaks. The Alphasense sensor monitoring the total particle concentration shows an increase of the PM_{2.5} concentration for the initial two leaks, however after introducing the 3rd leak and going forward, the PM_{2.5} concentration decreases. Only the Palas[®] reference shows a linear increase of the PM_{2.5} concentration within the scope of the total particle emission.

The observed effect for the low-cost PM-sensors is a clear indication for a coincidence error. If multiple particles pass the measurement volume of the sensor simultaneously, they are detected as a single particle of larger size [Raasch & Umhauer, 1984]. The coincidence error therefore causes a decrease in particle number concentration and an increase in mean particle size. Under these high concentration conditions (up to several g/m^3 raw-gas concentration compared to maximum specified concentrations of $1\text{-}2 \text{ mg}/\text{m}^3$), the low-cost PM-sensor is affected by the coincidence error. Particle sizes exceeding the $\text{PM}_{2.5}$ size fraction are registered accordingly. Thus, the coincidence error causes overall low $\text{PM}_{2.5}$ concentrations in case of the low-cost PM-sensor installed directly at the hotspot and the decrease of $\text{PM}_{2.5}$ concentrations for the low-cost PM-sensor measuring the total emission. The PM_{10} concentration still increases despite the coincidence error due to a shift of the particle size distribution to larger particle diameters.

The assumption is confirmed by the particle size distributions calculated from the counting events registered by the low-cost PM-sensor measuring the total particle emission as shown in Figure 28. While there is reasonable agreement of the particle size distribution between the low-cost PM-sensor and the Palas® reference in case of zero or a single leak, an increasing number of leaks clearly shows a shift towards larger particle sizes and a decrease of counting events in the lower size classes towards the lower end of the detectable size range.

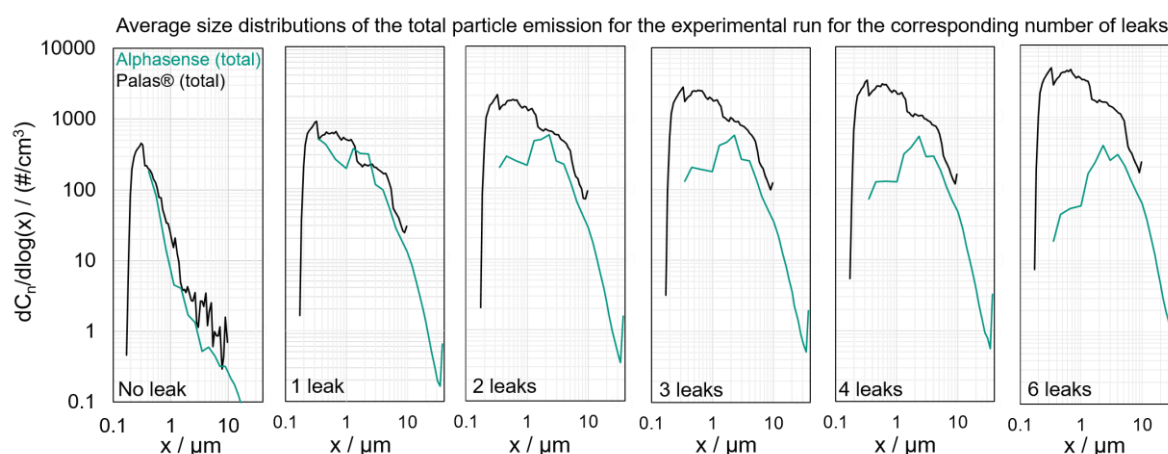


Figure 28 - Comparison of particle size distributions of the total particle emission dependent on the number of leaks for the low-cost PM-sensor and the reference. Image adapted from [Bächler et al., 2023a].

During scenario 3 (leak in the plenum plate), no concentration increase at each local measurement position was registered by the corresponding low-cost PM-sensors. Only the total particle emission strongly increased due to the leak in the plenum plate. Therefore, the filter bags can be ruled out as the source of the emission increase. For spatial identification of emission hotspots, it is important to measure close to the source of increased particle penetration.

4.2.2 Main conclusions of publication II

Exposing the low-cost PM-sensors to higher particle concentrations from emission hotspots pushed the measurement capabilities and detection limits of the low-cost PM-sensors.

The following key conclusions could be drawn:

- The spatial identification of particle emission hotspots (application scenario 1 and 2) was reliably possible based on increased PM_{10} concentration readings of the sensors. Here, different positions of filter elements with regular seams were identified in a field of filter elements with sealed seams (or aged filter bags). Additionally, increasing numbers of holes (3 mm diameter each) in a single filter bag were identified based on sensor data so that the conspicuous filter bag could be quickly replaced in a real application scenario. This demonstrates a similar reliability compared to other online leak measurement devices that are currently subject of research [He et al., 2023; Li et al., 2020].
- Within the scope of the experiments, no increased particle concentrations were registered by low-cost PM-sensors installed at filter elements adjacent to the particle emission hotspot. At the remaining measurement positions, the expected characteristic transient particle emission behavior was measured by the low-cost PM-sensors. In some cases, the regeneration of consecutive filter bags in the cleaning procedure was detected locally. This is no major drawback regarding the unambiguous identification of emission hotspots.
- The leak in the plenum plate (scenario 3 in Figure 25) was only identified with regards to the total concentration. Therefore, the filter elements can be correctly ruled out as the source of the particle emission increase for this application scenario.
- The measurement signal of the sensors exposed to the leaks (application scenario 2) was significantly affected by the coincidence error. The number of counting events in the lower size classes of the low-cost sensor decreases with increasing number of leaks. The mass based PM -concentrations were also affected, as the $PM_{2.5}$ concentration measured by the low-cost PM -sensor started to decrease with an increasing number of leaks despite the definitive uniform increase of the (total) particle emission as shown by the Palas® reference. The PM_{10} concentration detected by the low-cost PM -sensor continued to rise as indicated by the shift in the size distribution. The decrease of particle number concentration with an increase in particle size / mass based concentration is a clear indication for the coincidence error [Raasch & Umhauer, 1984]. Therefore, the $PM_{2.5}$ concentration alone is no clear-cut indication regarding leak detection and supplementary PM_{10} readings can help to indicate measurements affected by coincidence. The clear identification of the coincidence error demonstrates, that the corresponding PM concentrations are indeed determined based on size resolved particle counts (and not e.g. by an assumed correlation between $PM_{2.5}$ and PM_{10} concentration).
- The internal “sample flow rate” logged by the Alphasense sensor has a significant effect on the sensor outputs and may yield inconclusive and erroneous concentration data. Sensor operation under challenging flow conditions has to be characterized on-site to identify potential errors and difficulties regarding sensor operation.

While deviations from highly developed particle counters are somewhat expected due to the constraints of the compact design and economic factors (e.g. calibration and components of low-cost devices), the potential for improved process control through application of spatial particle concentration monitoring based on the qualitative sensor outputs and characterization of particle emission trends was demonstrated. Low-cost PM -sensors can reliably detect leaks and emission hotspots, making them a useful potential monitoring tool for plants around ambient conditions. Further developments regarding long-term stability and temperature resistance are of course necessary before wide-scale industrial application.

5 CHARACTERIZATION OF THE TRANSIENT AND SPATIALLY RESOLVED PARTICLE EMISSION BEHAVIOR OF PULSE-JET CLEANED FILTERS

Due to the sensors' capabilities to measure transient particle emission peaks and overall trends regarding the emission behavior of e.g. different filter media, the sensors were applied for the characterization of the spatial particle emission profile of the pilot-plant scale baghouse filter. The chapter summarizes the key results of two publications from scientific journals. The corresponding publications III and IV can be accessed in the appendix.

In chapter 5.1, investigations under defined conditions at a low particle emission level were performed applying membrane filter bags with sealed seams.

Expanding upon the previous investigation, in chapter 5.2, regular filter bags (no sealed seams) made from different filter media were installed in order to show the impact of e.g. filter aging and variation in tank pressures on the spatial emission behavior.

5.1 Characterization of the spatial particle emission behavior in a pilot-plant scale baghouse filter at a low particle emission level (membrane filter bags with sealed seams)

The results in this chapter were published in [Bächler et al., 2020] / publication III. The corresponding publication can be accessed in the appendix. This chapter briefly summarizes the key results and conclusions.

5.1.1 Extensive summary of publication III

As low-cost PM-sensors have shown to be suitable for the qualitative characterization of the transient particle emission behavior and the investigation of different particle emission levels in a controlled filter test environment, more in-depth experiments in the baghouse filter were performed.

To create suitable operating conditions regarding an "ideal" particle emission behavior, membrane filter bags (compare Table 4) with manually sealed seams applying sealing paste were installed in the baghouse filter (similar to scenario 1 in Figure 25). Thus, particle penetration through the stitching holes of the filter bag can be ruled out [Lacerda et al., 2022]. A Δt -controlled regeneration trigger at a fixed cycle time of 120 seconds should enable the exact allocation of the corresponding regeneration events and the spatial and global / total particle emission at the outlet. The raw-gas concentration was set at 5 g/m³ at a filter face velocity of 3.3 cm/s and 5 bar tank pressure during the experiments.

For the validation of local measurements using low-cost PM-sensors, the Palas[®] reference was also employed for local PM emission measurements (in addition to the previously mentioned measurements of the total emission) by drawing a sample from the corresponding individual filter bag. Figure 29 shows the local particle concentration measured by the Palas[®] reference for one complete filtration cycle (two regenerations of the corresponding filter bag – bag 5).

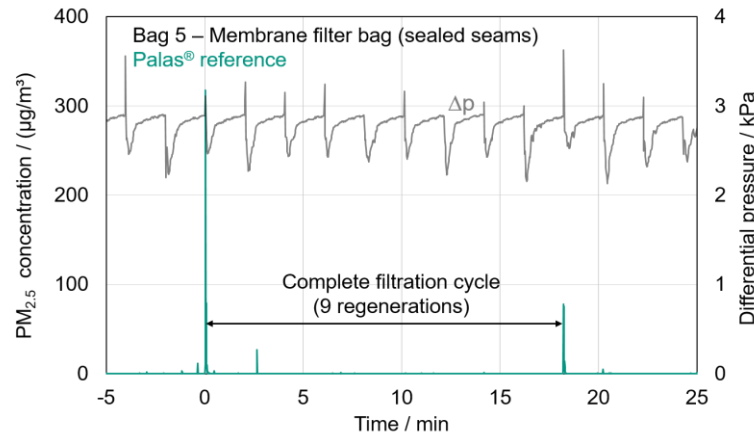


Figure 29 - Time dependent $PM_{2.5}$ concentration detected by the Palas[®] reference at the central filter bag (bag 5) and differential pressure curve. The time axis has been shifted to align $t = 0$ at the first regeneration of the corresponding filter element. Image adapted from [Bächler et al., 2020].

Directly after filter regeneration of the corresponding filter bag, the clean gas concentration increases for several seconds (emission peak), almost immediately declining back to a zero emission level. Due to the high separation efficiency of the membrane layer, almost no particle penetration is possible and a sufficient dust cake is quickly formed on the medium surface. The behavior is in agreement with measurement results for the membrane filter medium shown in the filter test rig presented in publication I. Note that direct comparability with the filter test rig is not possible. Despite an equal average filter face velocity of 3.3 cm/s, the overall flow velocities (e.g. at the outlet of the filter element and therefore close to the measurement location) are higher in the pilot-plant scale baghouse filter. After the regeneration of the consecutive bag in the cleaning procedure, a similar emission peak, albeit with lower peak height, is detected.

The local particle emission behavior measured simultaneously by the grid of low-cost PM-sensors installed on the clean gas side at each filter element according to Figure 16 is in good qualitative agreement with the reference measurement (Figure 29). As an example, the spatially and temporally resolved particle emission measured by each low-cost PM-sensor is illustrated for an experimental run at 8 bar tank pressure in Figure 30. The Palas[®] reference is used as measurement device for the total dust emission as shown in the flow sheet in Figure 14. Results in publication III were obtained at a tank pressure of 5 bar but yield the same qualitative particle emission behavior. The experiments at the higher tank pressure put consecutive results in chapter 5.2 in a better perspective. Pronounced particle emission peaks occur directly after filter regeneration and each locally detected peak (Alphasense local) can be allocated to a corresponding particle emission peak on the clean gas side (Palas[®] total). The height of the particle concentration peaks is in a similar region compared to the reported data in publication III at 5 bar tank pressure (approx. between 100 and 200 $\mu\text{g}/\text{m}^3$).

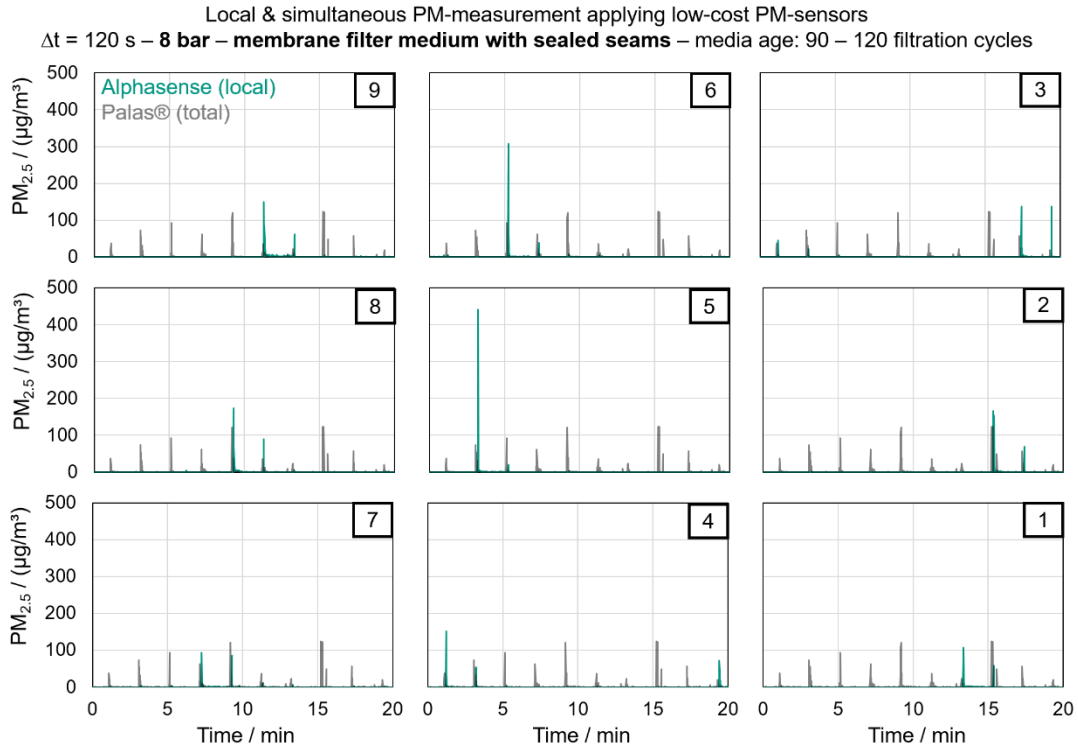


Figure 30 - Spatially resolved $PM_{2.5}$ measurement employing nine low-cost sensors (one at each individual filter bag) and comparison with the detected total emission by the Palas® reference on the clean gas side for several filtration cycles for membrane filter bags with sealed seams at a tank pressure of 8 bar. The number indicates the corresponding filter bag in the baghouse (bag-by-bag cleaning procedure according to Figure 15). The time axis has been shifted to align $t = 0$ during an arbitrary filtration cycle of the measurement run.

Higher tank pressures typically lead to increased dust emissions due to a more thorough cleaning of the filter element. E.g. [Kurtz et al., 2016] report increased particle emissions for higher tank pressures, whereby the difference decreases with increasing filter age and progressing particle deposition within the filter matrix. In case of membrane filter bags with sealed seams, there is no significant difference regarding the corresponding average particle concentrations of the total dust emission for a variation of tank pressures as shown in Figure 31.

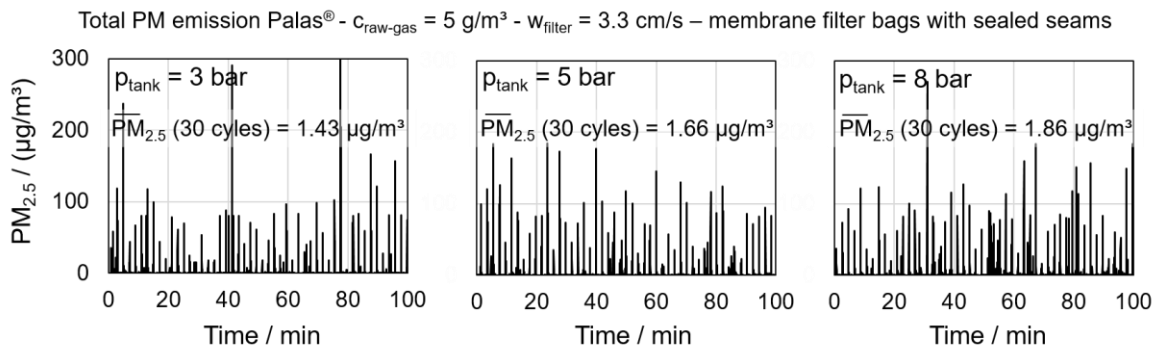


Figure 31 – Total particle emission for several filtration cycles for membrane filter bags with sealed seams at different tank pressures (3 bar, 5 bar and 8 bar) measured by the Palas® reference. The average $PM_{2.5}$ concentration was determined for an entire experimental run consisting of 30 complete filtration cycles.

While there is a slight increase of average $PM_{2.5}$ concentration with increasing tank pressure, the difference is negligible compared to the trends reported in literature. The qualitative particle emission behavior consisting of defined peaks separated by zero concentration levels during

the filtration phase is identical for the different tank pressures. Due to the membrane surface, the separation efficiency of the filter medium is very high. Sealing the seams removes a weak spot of the filter element and the increased tank pressure has a negligible effect on the separation efficiency of the filter element. In that aspect, the membrane surface creates similar conditions compared to filter aging (and clogging / conditioning of the filter material) that also lowers the impact of higher pulse-intensities on particle emissions [Kurtz et al., 2016].

As a comparison to the near ideal particle emission behavior of the membrane filter bag with sealed seams (Figure 29), the particle emission behavior of a spunbond filter bag without sealed seams shows a continuous particle penetration through the stitching holes at a low filter age (factory-new filter bag) and higher peak emissions after filter regeneration (Figure 32).

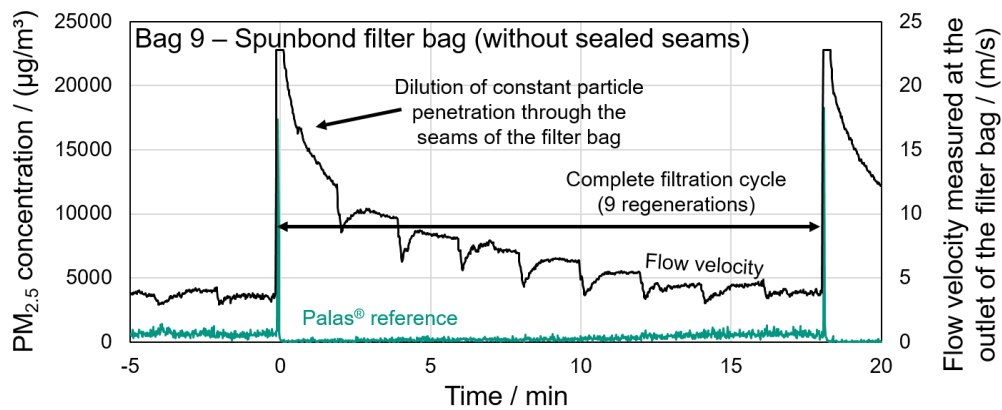


Figure 32 - Reference measurement employing the Palas® system at bag nine with the spunbond medium and flow-velocity measured with a Schmidt® SS 20.250 flow sensor. Image adapted from [Bächler et al., 2020].

The measured particle concentration increases over the course of several filtration cycles what could be caused by a decrease in volume flow through the corresponding filter bag due to the larger flow resistance of the growing dust cake on the medium surface at a constant particle mass flux penetrating through the seams onto the clean gas side. After the regeneration of the corresponding bag, the flow through the bag decreases due to a fast cake formation. After the regeneration of consecutive bags in the cleaning procedure, the volume flow increases over the course of the individual filtration cycle, as the flow resistance through the recently regenerated bag increases and the volume flow splits accordingly. Thus, the source of particle penetration (seams of the filter bag) can be derived from the local PM evolution characteristic.

5.1.2 Main conclusions of publication III

Under the defined low particle emission conditions when applying membrane filter media with sealed seams, the measurement of the spatial particle emission behavior using a grid of low-cost PM-sensors was possible. The measurements were validated using the Palas® reference either for local measurements or for measurements of the total dust emission at the outlet

The following key conclusions could be drawn:

- Particle penetration occurs directly after regeneration at the corresponding filter element. A sharp particle concentration increase (particle emission peak) was detected and clearly allocated to the regeneration event for both, the network of spatially installed low-cost PM-sensors and for an individual filter element applying the reference aerosol spectrometer.
- Particle emission peaks were detected for only a couple of seconds before declining to a zero level for the membrane filter bags (Table 4) with sealed seams. This behavior is qualitatively similar compared to the investigations in the filter test rig (publication I).
- In addition to particle emission peaks that can be clearly allocated to the local filter regeneration, smaller concentration increases below the original peak height after the actual filter regeneration occur at the individual measurement positions. This ostensive concentration increase occurs mainly after the regeneration of the following filter bag within the bag-by-bag cleaning procedure and cannot be clearly allocated to a source. Chapter 7.1.4. offers a more thorough discussion on this systematic concentration peak for consecutive filter bags in the cleaning procedure.
- Applying a different factory-new spunbond filter bag (Table 4) with regular seams (similar to investigations performed in publication II), cause a particle emission hotspot, whereby the individual particle emission peaks cannot be clearly distinguished from the continuous emission of the hotspot within the measurement of the total particle emission.
- Measurements of the particle concentration behavior at the spunbond filter element with regular seams show (in addition to an increased peak height compared to the membrane filter element with sealed seams) a characteristic concentration increase of a continuous particle emission over the course of the filtration cycle. Dilution effects may be the cause of this characteristic concentration behavior (decrease in volume flow through the filter element with proceeding cake formation at a constant penetrating particle mass flux). Measurements increasing the regeneration pressure confirmed the seams as the source of increased particle penetration.
- Peak particle number concentrations detected by the reference aerosol spectrometer are in some cases above the limit of coincidence-free measurement of the low-cost PM-sensor. Combined with the low detection duration of particle concentrations and the complex spatial flow behavior within the baghouse filter, the sensors are operated under challenging conditions. This is reflected in the differences regarding the detected particle size distribution of the low-cost PM-sensor that deviates strongly with regards to the measured number concentration level of the reference.

Summarizing, qualitative agreement between the spatially deployed network of low-cost PM-sensors and the reference aerosol spectrometer was further demonstrated. The spatial detection of characteristic particle emission peaks after the regeneration of the corresponding filter bag is an indication regarding unobstructed filter operation. The measurements exploring the spatially and temporally resolved particle emission behavior of the baghouse filter put further emphasis on the role of the emission contribution of the seams of the filter bag.

5.2 Characterization of the spatial particle emission behavior in a pilot-plant scale baghouse filter applying regular filter bags made from different filter media (without sealed seams)

The results in this chapter were published in [Bächler et al., 2022b] / publication IV. The corresponding publication can be accessed in the appendix. This chapter briefly summarizes the key results and conclusions.

5.2.1 Extensive summary of publication IV

More realistic operating conditions were aimed for after the evaluation of a low (and near ideal) particle emission level enabled by membrane filter bags with sealed seams. Sealing the seams with tape or sealing paste requires additional production effort and is not universally done during the confectioning of filter elements, despite their relevance on particle emissions as shown in publication II and III. Thus, filter bags made from the three different filter media (compare Table 4) without sealed seams were applied in the baghouse filter to cover the common use-case in the industrial application. Results featuring the needle-felt filter medium are an extension of publication IV.

A variety of different operating parameters, their impact on the spatial particle emission behavior and the corresponding performance of low-cost PM-sensors were investigated following an experimental procedure including the variation of cycle time between individual filter regenerations. The exact procedure can be accessed in publication IV and only the key results are presented in this chapter. Experiments consisting of 30 complete filtration cycles each were performed at cycle times of 120 seconds, 90 seconds and finally 60 seconds, whereby this sequence was repeated once to cover different stages of filter age (initial cycles vs. conditioned / aged filter bag). The raw-gas concentration was 5 g/m^3 and the filter face velocity was 3.3 cm/s for all experiments.

The effect of filter aging (especially during the initial filtration cycles) on the spatial particle emission behavior as well as the emission dynamics of particle penetration through the seams is shown in Figure 33 for two different types of filter bags (no sealing of the seams).

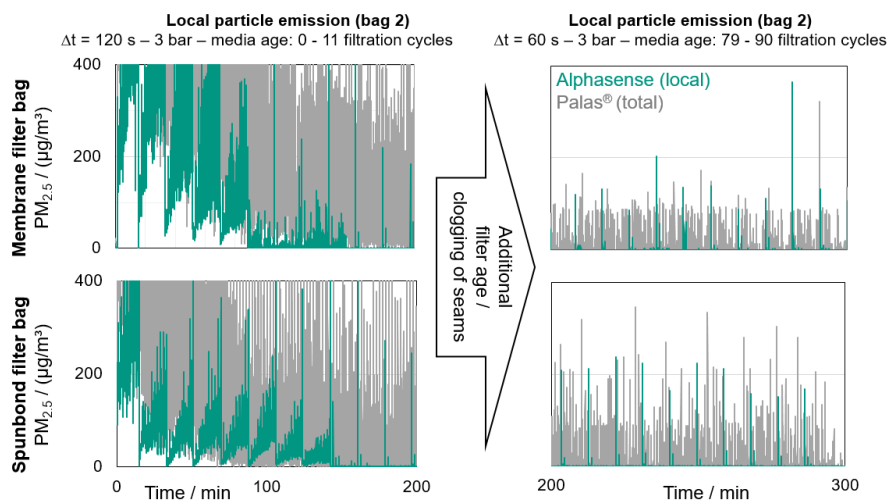


Figure 33 - Detail view of the particle emission of initial filtration cycles of an exemplary filter bag for both filter media and total emission compared to the end of the first measurement procedure. Image adapted from [Bächler et al., 2022b].

During the initial filtration cycles, a continuous particle emission is registered by the low-cost PM-sensors similar to the reference measurements shown in Figure 32. With consecutive cycles, this (continuous) particle emission decreases until reaching the ideal emission behavior where only particle emission peaks directly after filter regeneration are measured on the clean gas side. The total PM_{2.5} emission measured by the Palas® reference shows a qualitatively similar decrease of the particle emission during the initial cycles, serving as validation of the spatial particle emission behavior obtained from low-cost PM-sensor data. This particle emission behavior indicates filter aging and clogging of the seams. As soon as the seams are sufficiently clogged, no particles can penetrate through the stitching holes onto the clean gas side and there is a zero emission during the filtration phase with sufficiently developed dust cake.

Further measurements including a variation of tank pressure for filter regeneration employing the Palas® reference at an individual (aged) filter bag demonstrate the emission dynamics of the seams according to Figure 34.

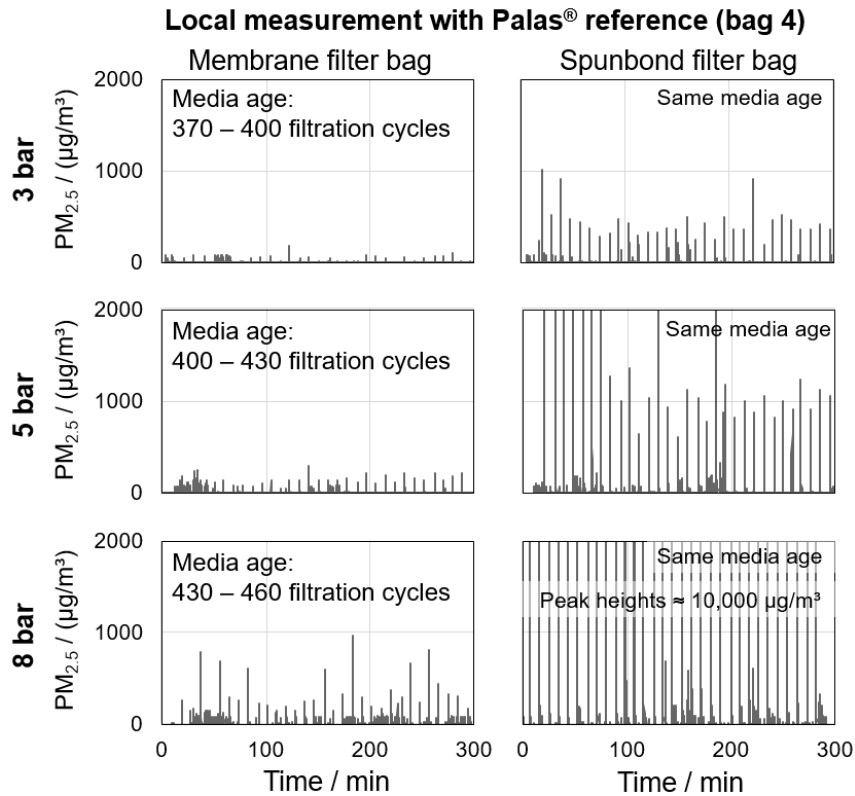


Figure 34 - Local particle emission measurement at an individual filter bag (bag 4) applying the Palas® reference for different tank pressures and two filter media. Image adapted from [Bächler et al., 2022b].

At tank pressures of 3 bar, continuous particle emissions during the filtration phase rarely occur. With increasing tank pressure, the height of the particle emission peaks as well as frequency of temporally occurring continuous emissions increases. As the membrane filter bags (comparably low filter age) from publication III shown in the previous chapter were (almost) completely unaffected by the increase in tank pressure and no significant continuous particle emissions were measured during the filtration phase, the seams of the filter bag are the undisputed source of the increase in dust emission. Increased tank pressures can potentially de-clog the seams, enabling renewed particle penetration through the stitching holes subsequently causing higher emissions.

After sufficient filter aging (at least 90 filtration cycles for each filter bag), the total particle emission measured by a low-cost PM-sensor installed in the clean gas duct and the Palas® reference was compared for the corresponding filter media and the investigated cycle times at a moderate tank pressure of 3 bar according to Figure 35.

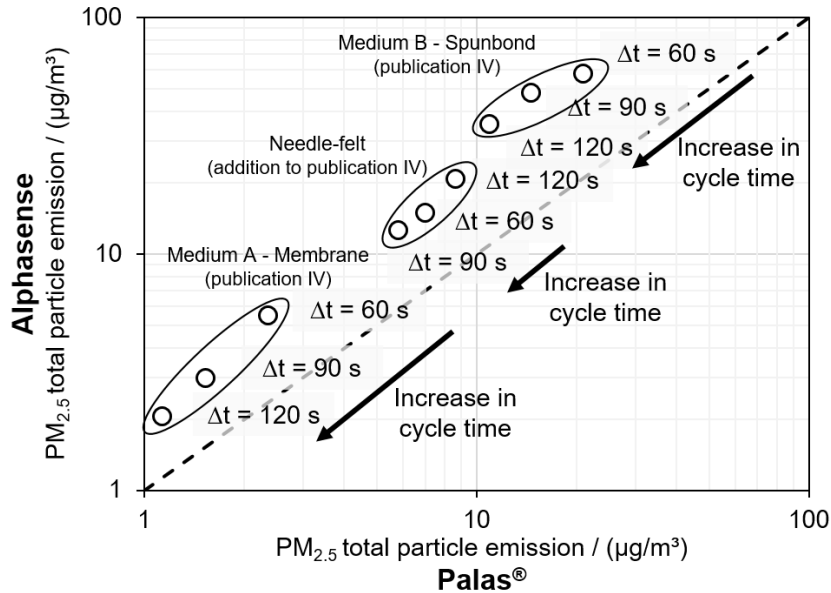


Figure 35 - Comparison of the average clean gas particle concentration of the total emission for both filter media of publication IV and the additional needle-felt filter medium. Image modified from [Bächler et al., 2022b].

The low-cost PM-sensor overestimates the $PM_{2.5}$ concentrations compared to the reference. The order in which the individual data points appear in the scatterplot is identical for the low-cost PM-sensor and the reference aerosol spectrometer. The three distinct filter media can be clearly distinguished regarding the total particle emission, whereby the same relative emission levels are detected compared to the initial investigation of the low-cost PM-sensors in the filter test rig shown in Figure 23. Furthermore, the experimental runs employing different cycle times also follow a trend, whereby the total particle emission is higher for shorter cycle times due to more frequent regenerations and an increased number of particle emission peaks (of similar peak height) in a given time. The only exception is the cycle time of 120 seconds for the needle-felt filter bag. The corresponding measurement run (at a lower filter age compared to the consecutive runs at 90 and 60 seconds cycle time) had more cases of temporally increased particle emissions (e.g. insufficient clogging of the seams). The results regarding the total particle emission underline the accuracy of low-cost PM-sensors regarding the quantitative characterization of different particle emission levels based on cycle time and different filter media. When compared to the detected concentrations of the reference, there are moderate deviations within the same order of magnitude.

A measurement of the local particle emission was performed by simultaneous application of the reference aerosol spectrometer and a low-cost PM-sensor at the same filter bag for direct comparison. The results of the measured PM evolution during 30 filtration cycles of the spunbond filter bag are displayed in Figure 36.

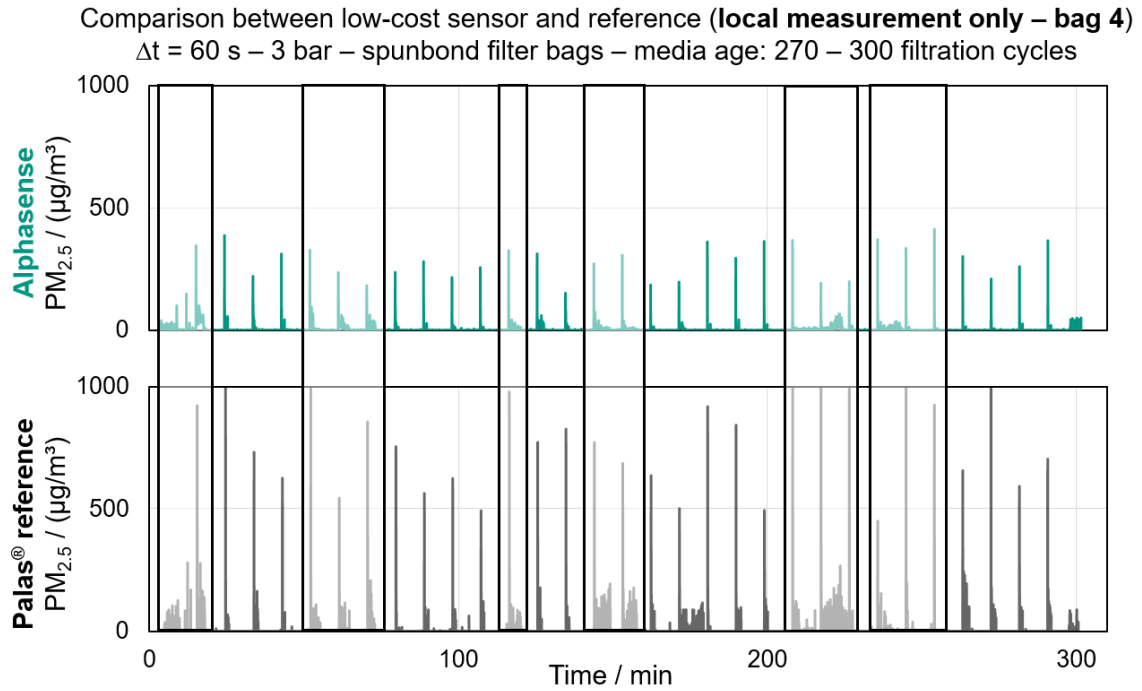


Figure 36 - Direct comparison between the low-cost PM-sensor and the reference at an individual filter bag. Image adapted from [Bächler et al., 2022b].

There are quantitative differences of the determined particle concentrations, as the low-cost PM-sensor detects lower concentration values (peaks and continuous emissions) of the particle emission compared to the Palas® reference when used for local PM measurements. The qualitative PM evolution is in good agreement (compare framed areas in Figure 36) and the differences are moderate and within the same order of magnitude. The respective occurrence of particle emission peaks as well as temporal continuous particle emissions are registered by both devices.

5.2.2 Main conclusions of publication IV

The application of conventional filter elements (without sealed seams) and the variation of several operating parameters yielded further insights on the spatial particle emission behavior of pulse-jet cleaned filters.

The following key conclusions could be drawn:

- The low-cost PM-sensors and the reference aerosol spectrometer detect equivalent trends regarding the varied process parameters. Despite the quantitative differences e.g. for the determined mass based particle concentrations, the sensor signal enables the characterization of the impact of different process parameters on the (spatial) particle emission.
- A direct comparison during a simultaneous measurement of the local particle emission between the reference aerosol spectrometer and a low-cost PM-sensor at an individual filter bag was qualitatively in good agreement. Main differences were e.g. the peak height of the particle emission directly after filter regeneration.

- Different particle emission levels could be identified regarding local (increased peak height of spatially detected emission peaks for the spunbond medium compared to the membrane medium – compare Table 4 / Figure 33) and total particle emission (e.g. regarding average particle concentration – compare Figure 35).
- The experiments applying factory-new filter bags over multiple filtration cycles demonstrated the effect of filter aging in the context of a decrease in spatially detected particle concentrations and the total emission. The local PM behavior corresponded to the previously shown behavior in publication III, where the local concentration increases over the course of an individual filtration cycle. This distinct behavior serves as an indication for filter aging and clogging of the seams of the filter medium. After sufficient filter aging, the qualitative particle emission behavior corresponds to the “ideal behavior”, where particle emission peaks caused by penetration through the filter medium are detected directly after regeneration and quickly decline to a zero level with ongoing cake formation.
- Increases in the measured particle emission (temporally occurring continuous emissions) of the total particle emission frequently coincide with a similar increase in local concentration at individual filter elements. This comparison of local and total particle emission enables the direct allocation of the filter bag serving as the temporal source of the emission.
- Increasing the tank pressure for filter regeneration (here: above 3 bar) causes an increase in particle emission for the filter bags without sealed seams. Locally and temporally occurring particle emission events appear more frequently at increased tank pressures and the peak height of the particle emission peaks increases with increasing tank pressure. This behavior is contrary to the previously discussed particle emission behavior of membrane filter elements with sealed seams. Hence, the reason for this increase in particle emission due to increased tank pressure are presumably the seams of the filter element. The seams of the filter bags clog during filter operation and cake formation. Filter regeneration can clear the previously clogged seams what causes an increased particle penetration through the stitching holes.

These results conclude the online measurements of spatially resolved particle emissions in the pilot-plant scale baghouse filter. Low-cost PM-sensors have demonstrated great potential as compact and cheap monitoring tools in the context of particle emission measurement of pulse-jet cleaned filters provided that the operating conditions are in a suitable range (close to ambient conditions).

6 TRADE-OFF BETWEEN ENERGY DEMAND AND PARTICLE EMISSIONS FOR THE OPERATION OF PULSE-JET CLEANED FILTERS

In addition to particle emission monitoring of baghouse filters, the energy demand of baghouse filter operation is subject to optimization. Many filtration processes are continuously operated without adapting to changes in process conditions, instead following the rigid initially set layout criteria regarding e.g. the regeneration strategy.

The following chapter presents an experimental methodology in order to evaluate filter operation based on power consumption and the total particle emissions within the pilot-plant scale baghouse filter. The corresponding publications V and VI can be accessed in the appendix.

In chapter 6.1, an experimental approach is introduced based on the determination of the power consumption of pulse-jet cleaned filters initially applied by [Höflinger & Laminger, 2013] for the characterization of different filter media under energy-related criteria. Energetically favorable operating points are identified within the framework of an experimental parameter study and put into context with the total particle emission.

In the follow-up chapter 6.2, the experimental data obtained in chapter 6.1 serves as the foundation for a calculation model. The model enables the prediction and calculation of energy demand and particle emission dependent on the input parameters (e.g. filter face velocity, raw-gas concentration, tank pressure, etc.) and demonstrates the potential of a digital twin for the optimization and prediction of baghouse filter operation.

6.1 Experimental parameter study for the evaluation of filter operation regarding energy demand and particle emissions

The results in this chapter were published in [Bächler et al., 2023b] / publication V. The corresponding publication can be accessed in the appendix. This chapter briefly summarizes the key results and conclusions.

6.1.1 Extensive summary of publication V

The energy consumption of baghouse filters is, in most cases, of subsidiary interest for plant operators. Due to the wide application spectrum, including the energy intensive cement industry, the required power for filter operation may amount to only a fraction of the total energy demand. Process stability is of higher interest for operators, as baghouse failure can lead to plant shutdown or can even cause damage to downstream unit operations. Within this mindset, filter operation is rarely optimized and there is a definitive potential to lower the energy demand of pulse-jet cleaned filters. In the context of climate change and the necessity to lower carbon-dioxide emissions, every opportunity for process optimization has to be evaluated.

The boundary conditions for the filtration process (e.g. volume flow, raw-gas dust concentration, particle size distribution and dust properties, temperature, etc.) are often set dependent on the individual process chain. Cleaning intensity (tank pressure, valve opening

time) and cleaning frequency (cycle time) are important factors that can influence the differential pressure level for a certain set of operating parameters for a plant operator [Kurtz et al., 2016]. Higher cleaning intensity and more frequent regenerations can enable lower differential pressure levels at the cost of a higher consumption of pressurized air and higher particle emissions [Kurtz et al., 2016; Simon et al., 2014; Klein et al., 2009].

Publication V introduces an experimental procedure tested in the pilot-plant scale baghouse filter to quantify the total power consumption for pulse-jet cleaned filters based on the fan power and the consumption of pressurized air [Höflinger & Laminger, 2013]. To create an extensive experimental framework, several operating parameters (filter face velocities: 2 cm/s, 2.5 cm/s and 3.3 cm/s; raw-gas concentrations: 15 g/m³ and 30 g/m³; tank pressures: 3 bar and 6 bar) were varied over the course of multiple experimental runs. During each experiment at constant parameters, the cycle time between filter regenerations was varied incrementally (range between 180 down to 10 seconds over the course of an experiment dependent on the operating parameters). This enables the determination of the total power for filter operation and the particle emission for each set of parameters as a function of cycle time.

The experimental methodology is illustrated based on an exemplary results in Figure 37. The fan power was calculated from the determined average differential pressure and the volume flow for each individual cycle time adjusted within an experimental run. An average power for filter regeneration was determined for each cycle time from the volume of the pressure tank and the pressure drop due to jet-pulse cleaning for a corresponding tank pressure. The sum of fan power and the power required for filter regeneration is the total power consumption of filter operation. Similar considerations were made by [Klein et al., 2012] who identified economically beneficial operation regions for pulse-jet cleaned filters.

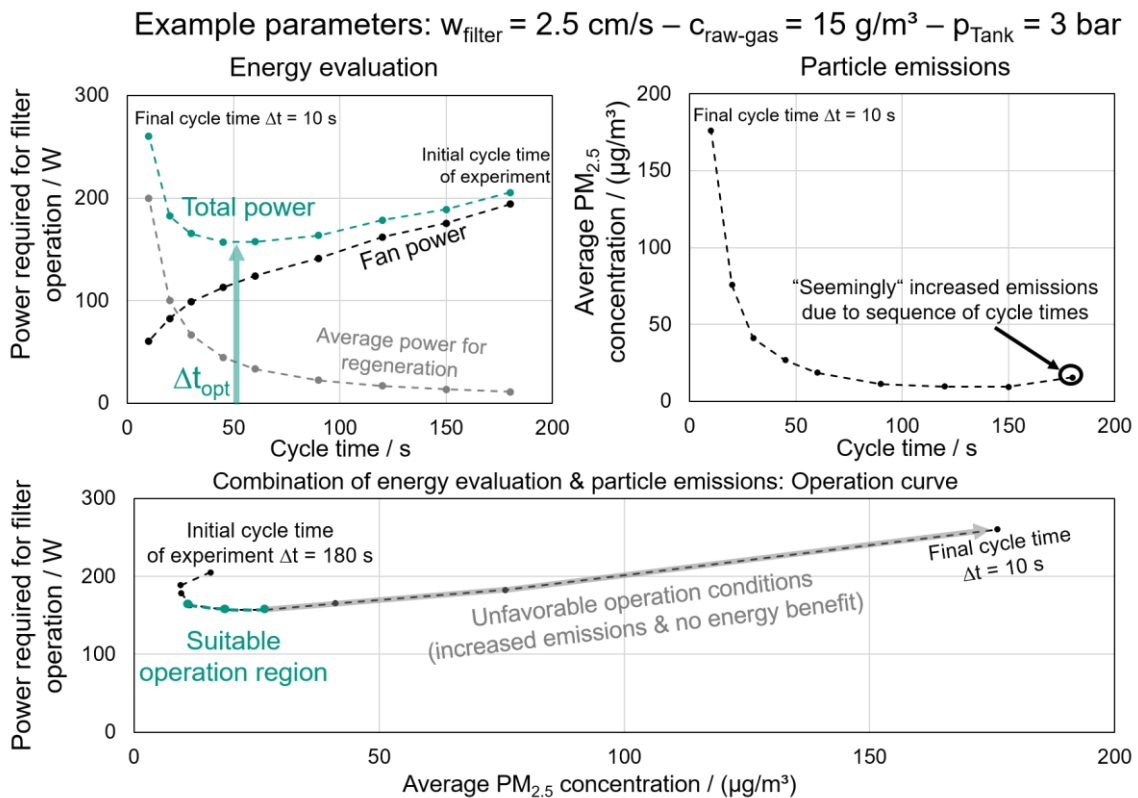


Figure 37 - Evaluation of filter operation based on power consumption and particle emissions for a certain set of parameters ($w_{\text{filter}} = 2.5 \text{ cm s}^{-1}$, $c_{\text{raw-gas}} = 15 \text{ g m}^{-3}$, $p_{\text{Tank}} = 3 \text{ bar}$). Image adapted from [Bächler et al., 2023b].

For very short cycle times (approx. 10 – 30 seconds), the energy consumption for filter regeneration contributes greatly to the total energy consumption due to frequent regenerations. Longer cycle times exceeding approx. 100 seconds cause a higher differential pressure level resulting in higher fan powers that dominate the total power for filter operation. A power minimum can be identified at approx. 45 – 60 seconds for the presented experiment.

In addition to the energy demand, the total particle emission for the corresponding operation points is measured applying the Palas[®] reference aerosol spectrometer (measurement of total emission only – no spatially resolved measurement). The total particle emission as a function of cycle time shows a hyperbolic behavior. For very short cycle times and frequent filter regeneration the particle emission is correspondingly high (compare e.g. Figure 35). Due to the hyperbolic decline, the particle emission reaches a “stable” level for increased cycle times (here: above 90 seconds), where an increase in cycle time leads only to a minor decrease in particle emission. The increase of the particle emission for the highest cycle time of 180 seconds is a measurement artifact caused by the sequence of cycle times within the experimental procedure (more information in publication V).

The combination of particle emission and energy demand (for the corresponding cycle time) enables a comprehensive evaluation of filter operation and the identification of suitable operating regions within the scope of an “operation curve”. Unfavorable operating conditions are located at cycle times shorter than the power minimum as they result in increased particle emissions at no energetic benefit. Increasing the cycle time above the cycle time at the power minimum lowers the particle emission at the cost of additional power input as illustrated in Figure 38 (variation of raw-gas concentration at 3 bar tank pressure and 2 cm/s filter face velocity).

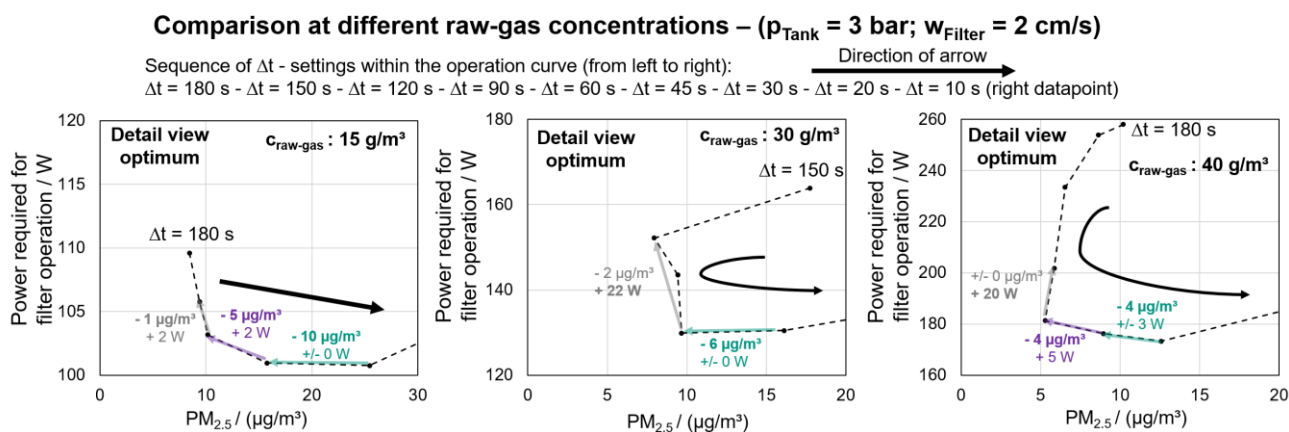


Figure 38 - Detail view of the power minimum of the operation curves at different raw-gas concentrations ($w_{\text{filter}} = 2 \text{ cm s}^{-1}$, $p_{\text{Tank}} = 3 \text{ bar}$). Image adapted from [Bächler et al., 2023b].

A slight increase in cycle time compared to the cycle time at the power minimum can lower particle emissions at negligible energetic drawbacks. Exceeding certain cycle times enables only a minor emission reduction but requires significant additional power input (especially at higher raw-gas concentrations due to a faster increase in fan power).

An evaluation of the power minimum and the corresponding particle emissions for the adjusted operating parameters within the experimental study is summarized in Figure 39. An increase in filter face velocity (respectively raw-gas concentration) causes an increase of the energy consumption for filter operation. The cycle time at the power minimum decreases, as more frequent filter regenerations become feasible to enable a lower differential pressure level.

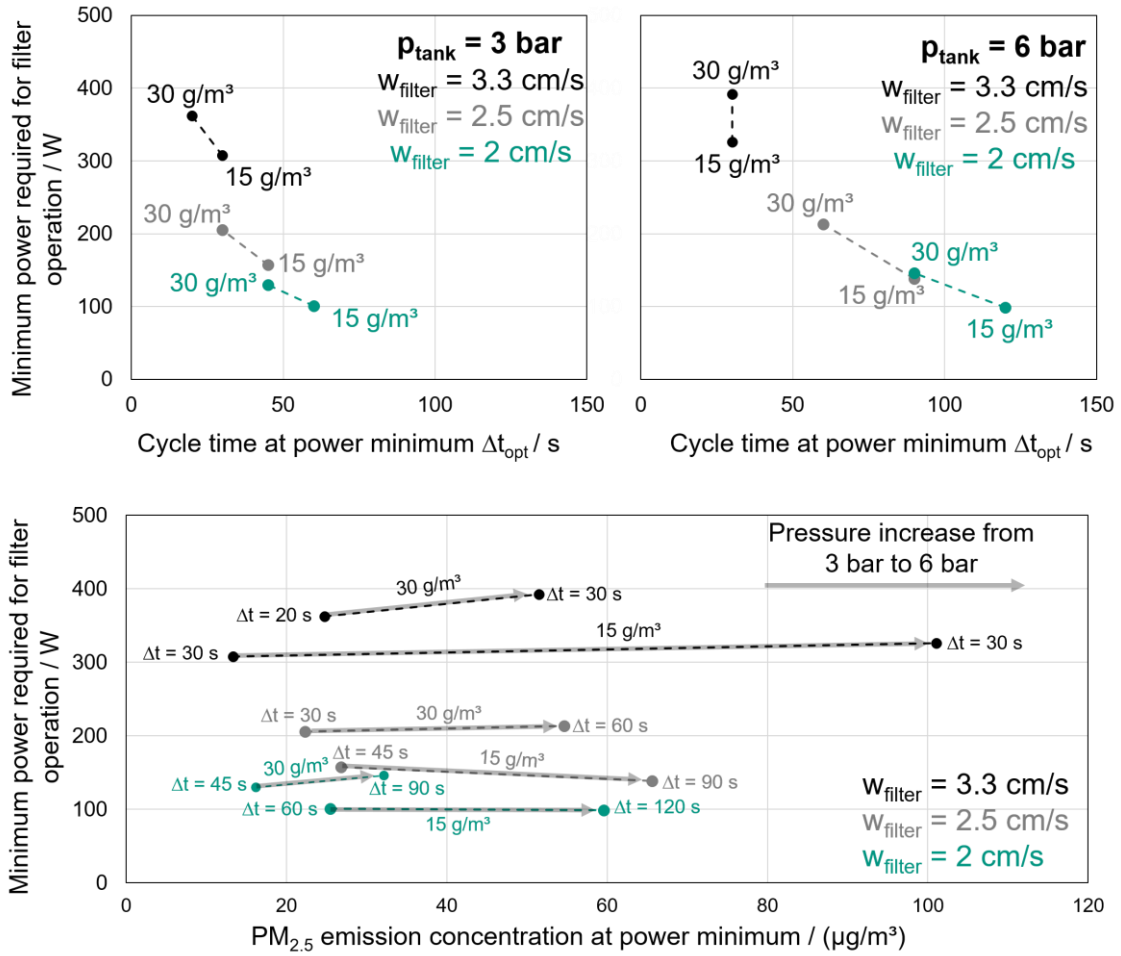


Figure 39 - Comparison of cycle times at minimum power regarding energy demand and particle emissions for two different tank pressures (3 and 6 bar) at varying raw-gas concentrations and filter face velocities. In case of a less pronounced power minimum (multiple datapoints), only a single datapoint is displayed. Image adapted from [Bächler et al., 2023b].

Increasing the tank pressure has major drawbacks on the particle emission (approx. increase by a factor of two when increasing the tank pressure from 3 bar to 6 bar). The cycle time at the power minimum doubles compared to the experiments at 3 bar due to a more efficient cake removal. Note that the power requirement for filter regeneration is higher for increased tank pressures due to a larger pressure drop in the pressure vessel from jet-pulse cleaning and a higher consumption of pressurized air. Thus, the overall total power is on a similar level and increasing the tank pressure offers no real advantage from an energy perspective and major drawbacks regarding particle emissions. Significantly increasing the tank pressure can also cause re-dispersion of the detached dust what can result in a rise of the residual differential pressure and lead to unstable filter operation. This is why approaches to implement demand-orientated tank pressures for jet-pulse cleaning (as described in the VDI 3677 guideline) are only rarely applied [VDI 3677, 2023].

6.1.2 Main conclusions of publication V

The experimental parameter study characterized the trade-off between energy demand and particle emission in the context of pulse-jet cleaned filters.

The following key conclusions could be drawn from the experimental procedure:

- The proposed equations introduced by [Höflinger and Laminger, 2013] can be adapted in the context of baghouse filter operation in order to calculate fan power and an average power representing the consumption of pressurized air for jet-pulse cleaning. This enables the evaluation of the total power for filter operation for different operating conditions. Combining the required power for filter operation and the particle emission enables the construction of an “operation curve” that shows the trade-off between energy demand and particle emissions for pulse-jet cleaned filters.
- A dedicated power minimum can be derived when plotting the total power required for filter operation as a function of cycle time (cleaning frequency). Filter operation is not feasible at too short or exceedingly long cycle times:
 - Exceedingly long cycle times lead to a high differential pressure level and fan power that dominates the total power consumption
 - Too short cycle times lead to an excessive consumption of pressurized air and excessive cleaning of the filter elements, where cake formation is not sufficient and dust may continuously penetrate the filter elements, causing a continuous dust emission (same qualitative behavior compared to filter operation with small leaks). This state of operation is similar to unstable filter operation.
- A suitable cycle time should be selected at (or at cycle times slightly above) the power minimum, as shorter cycle times lead to higher dust emissions and a higher wear on the filter element due to more frequent cleaning at no energy benefit. An increase of the cycle time above the power minimum has the potential to lower dust emissions at only minor energetic drawbacks.
- Regarding particle emissions, longer cycle times are favorable, as longer periods of zero emission due the growing dust cake enable low average particle concentrations on the clean gas side.
- Through the characterization of filter operation considering energy demand and particle emissions, plant operators may evaluate how a certain additional power input can lower particle emissions. There is a point where increasing the cycle time leads to a diminishing decrease in particle emission compared to the additional power input.

The qualitative results from the parameter study are summarized in Table 5 which is taken from the corresponding publication V [Bächler et al., 2023b].

Table 5 - Summary of the results from the experimental parameter study taken from [Bächler et al., 2023b].

Parameter Variation Increase of:	Total power consumption	Cycle time at the power minimum	Particle emission
Raw gas concentration	Increase	Decrease More frequent regeneration	Constant at relevant operation region
Filter face velocity	Increase	Decrease More frequent regeneration	Constant at relevant operation region
Tank pressure	(Almost) constant	Increase Less frequent regeneration	Increase

The main conclusions drawn from the variation of the operating parameters are:

- Increasing the tank pressure beyond certain limits (e.g. approx. 3 bar in case of the pilot-plant scale baghouse filter) is not recommended. While the cycle time at the power minimum increases and the total power does not differ too much between different tank pressures, particle emissions increase significantly for higher tank pressures.
- Lower filter face velocities can significantly lower the overall power consumption and cause a shift of the power minimum to longer cycle times what benefits a lower particle emission. Regarding filter layout, larger filter areas (with sufficient regeneration conditions regarding e.g. cleaning efficiency for jet-pulse cleaning) benefit plant operators in the long run.
- Higher raw-gas concentrations cause a faster cake formation and higher differential pressure levels. Monitoring raw-gas concentration (in addition to differential pressure) can supplement existing operation strategies and indicate a beneficial shift in cycle times.
- While the dust emission was different for the varied parameters (especially when comparing tank pressures for filter regeneration), in the relevant operation region at suitably long cycle times, the differences between the adjusted operating parameters were minor. For the highest filter face velocity, the particle emission was comparably low, what may be caused by dilution effects due to the higher overall volume flow. Thus, pulse-jet cleaned filters are able to generate low particle emission levels, provided the dust cake can be sufficiently developed. The hyperbolic behavior of the dust emission as a function of cycle time is of key importance, as suitable cycle times for a stable and low particle emission level can be identified.

Due to the extensive experimental framework, process modeling was applied in a consecutive step to mathematically describe filter operation based on the corresponding input parameters.

6.2 Modeling of filter operation regarding energy demand and particle emissions

The results in this chapter were published in [Bächler et al., 2024a] / publication VI. The corresponding publication can be accessed in the appendix. This chapter briefly summarizes the key results and conclusions.

6.2.1 Extensive summary of publication VI

Modeling and simulation of processes enables the evaluation of optimization potential dependent on the corresponding input parameters. “Digital twins” enable the comparison of actual processes with models to predict the impact of changing input parameters or alarm plant operators regarding deviations from the expected operating behavior based off of the digital twin.

The extensive experimental framework serves as a foundation for the development of a model to evaluate filter operation based on energy demand and particle emissions. The model equations for the calculation of the differential pressure have been established in the past by e.g. [Leith and Ellenbecker, 1980] and were summarized by [Löffler, 1988]. These equations describe an ideal case of surface filtration. Adapting the equations based on the experimental framework, where some parameters and influences (e.g. baghouse geometry, exact flow conditions, cake properties, regeneration efficiency, etc.) are unknown, and thus not described by the mathematical model, is a form of grey box modeling. The model equations summarized by Löffler were adapted and enhanced by the energy-evaluation introduced by [Höflinger and Laminger, 2013].

Based on the experimental results, empirical fit-functions using the filter medium resistance as a variable fit-parameter were derived. For further information on the exact model approach, refer to publication VI. The selected approach enables a good agreement between the model and the experimental data regarding the determination of the total power required for filter operation as shown for exemplary results in Figure 40. Since the energy consumption due to filter regeneration is based on experimental data, deviations between model and experiment regarding the calculation of fan power have a reduced impact on the determination of the total power especially for the lower end of adjusted cycle times.

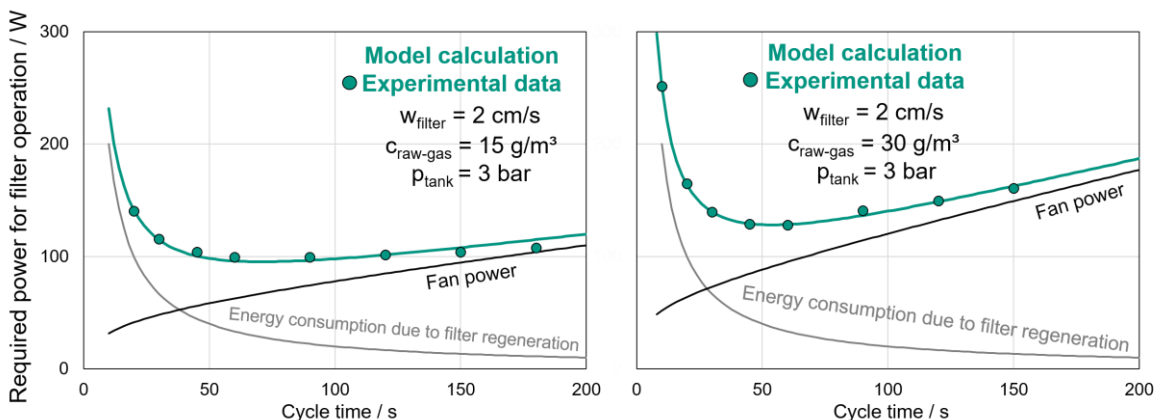


Figure 40 - Comparison of experimental data ($w_{\text{filter}} = 2 \text{ cm s}^{-1}$; $p_{\text{tank}} = 3 \text{ bar}$; $c_{\text{raw-gas}} = 15$ and 30 g m^{-3}) and model calculations regarding the required power for filter operation. Image adapted from [Bächler et al., 2024a].

The particle emission was modeled based on a hyperbolic function including a semi-empirical relation between particle emission, tank pressure and cycle time. Example results for 3 bar tank pressure are displayed in Figure 41. A semi-empirical “emitted dust mass” value was introduced

based on the tank pressure, as well as another empirical coefficient for the individual dataset. The amount of flexible parameters was kept low for emission modeling to maintain general validity of the model at the drawback of larger deviations to the experimental data.

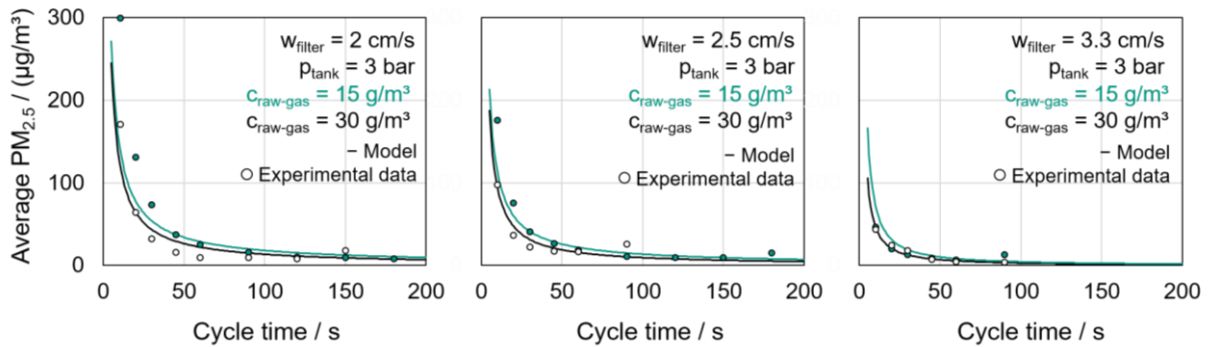


Figure 41 - Modeling of particle emissions for the entire set of experimental parameters based on the determination of the emitted dust mass for 3 bar tank pressure and an individual empirical coefficient for each set of parameters. Image adapted from [Bächler et al., 2024a].

Figure 42 summarizes the experimental and modeling results for the entire dataset. The key conclusions regarding the implications on filter operation from the evaluation of energy demand and particle emissions were already presented in chapter 6.1. (compare e.g. Figure 39 and Table 5). The overall behavior of the operation curve around the power minimum is well reflected by the model and identical conclusions on filter operation can be drawn from the model approach.

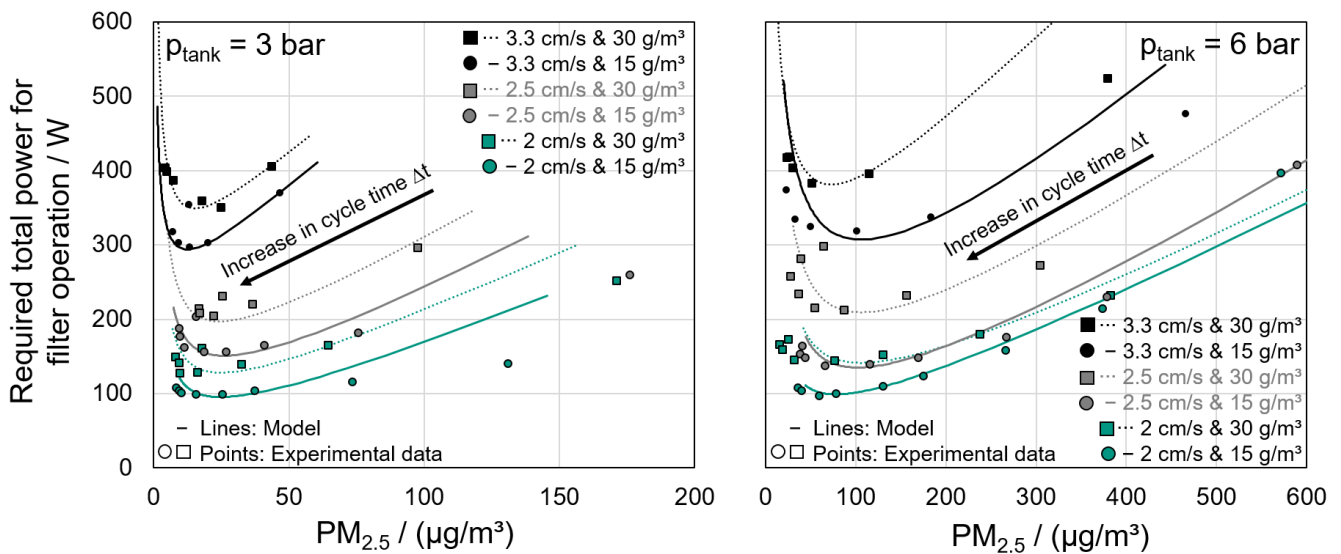


Figure 42 - Modeled operation curves for the complete set of parameters and comparison to experimental data from publication V. Image adapted from [Bächler et al., 2024a].

The accuracy between model and experimental data is reasonably high. Mainly due to the model approach selected for the particle emission some data points (especially for lower cycle times) deviate strongly. However, since the cycle times are far below the power minimum, they are outside of the scope of feasible cycle times considering the actual application. Similar absolute levels regarding the power demand and the particle emission are calculated so that the model equations constitute a “digital twin” of the pilot-plant scale baghouse filter.

6.2.2 Main conclusions of publication VI

Applying model equations extended the investigation presented in chapter 6.1 / publication V.

The following key aspects were shown by process modeling of pulse-jet cleaned filters:

- Adapting the fundamental equations for the calculation of the pressure drop for surface filters summarized by [Löffler, 1988] and introducing the medium resistance as a variable fit parameter enabled very good agreement between experimental data and the model. The model enables the calculation of the transient different pressure behavior for baghouse filters consisting of multiple filter elements.
- Complementing the model with the energy evaluation enables the accurate evaluation of the energy consumption of the pulse-jet cleaned filters. Some drawbacks of the experimental investigation (e.g. run-in effects for the initial cycle time over the course of an experimental run) are neglected by the model.
- The emitted dust mass after filter regeneration is mostly independent of cycle time. This enables semi-empirical modeling that accurately describes the global particle emission behavior as a hyperbolic function of cycle time for certain emission levels. In this investigation, the tank pressures for filter operation is the dominant parameter considering the particle emission level (besides the variation of cycle time).
- Filter regeneration of only a subset of filter elements / installed filter area is mathematically similar to “patchy cleaning” and creates a deviation of the ideal differential pressure behavior [Dittler et al., 2002]. Due to different amounts of deposited dust masses on each filter medium, the volume flow through the corresponding filter bags change accordingly dependent on time and their sequence in the regeneration procedure (identical differential pressure between raw-gas side and clean gas side for all filter elements). The calculated spatio-temporal flow behavior is in agreement with the flow measurements at the outlet of the filter element in publication III and spatial flow measurements reported by [Simon et al., 2010].

The results demonstrate the potential of process modeling and digital twins for the operation of pulse-jet cleaned filters. A small dataset of experimental data suffices to provide a framework for process modeling. The corresponding conclusions regarding suitable cycle times and operation regions drawn from process modeling can benefit plant operators and put current operation strategies into perspective regarding savings- and optimization potential of energy demand and particle emissions. A tight-knit experimental dataset of few adjusted cycle times suffices to feed the model with the required data to predict filter operation at as a function of cycle time.

7 DISCUSSION

This publication based dissertation dealt with the optimization of the operating behavior of pulse-jet cleaned filters regarding spatially resolved online particle emission monitoring and the identification of suitable operating regions taking into account energy demand and the total particle emission. In the following chapter, the results are discussed and evaluated within the context of the two research questions addressed in this thesis (chapter 1.2).

While a certain general applicability of the results is warranted (e.g. derived conclusions from the experimental parameter study, applicability of low-cost PM-sensors, etc.), note that the scope of the investigations was limited. Only results from two commercially available low-cost PM-sensors are reported in this dissertation. With growing technological progress and an ever increasing number of potential sensors on the market, the performance of individual sensors may vary accordingly and a thorough assessment and on-site calibration and testing is required before the application of individual sensor models.

The filter media used in the experiments served as a general representation of currently applied materials. A single test dust was used, that is easy to handle and causes neither significant clogging of the filter element to the point of unstable operation nor problems regarding cake detachment due to the free-flowing and non-agglomerating behavior. The application of the test dust exposed the sensors to higher particle concentrations and emissions compared to more agglomerating dusts. The overall filtration conditions were close to ambient conditions (ambient temperature and pressure, no corrosive gases, no condensation effects, etc.) and are not comparable to many industrial applications. Small scale applications under ambient conditions could profit from spatially resolved emission monitoring using the current generation of low-cost PM-sensors.

7.1 Suitability of low-cost PM-sensors for (local) particle emission monitoring and the identification of particle emission hotspots in baghouse filters

The suitability of low-cost PM-sensors as a potential technology for spatial online particle emission monitoring for baghouse filters is discussed regarding the general measurement behavior of the low-cost devices (including potential measurement errors) as well as the characterization of the spatially resolved particle emission. The discussion is based on publications I – IV.

7.1.1 Quantitative performance of low-cost PM-sensors during filter emission measurements regarding transient particle concentration peaks and potential measurement errors

The measurement of particle emissions for pulse-jet cleaned filters using scattered-light based devices has been prominently performed in literature (e.g. [Kurtz et al., 2016; Binnig et al., 2009]). The measurement range of scattered-light based devices overlaps with the penetration characteristics of the applied filter media. Complimentary measurements applying an engine exhaust particle sizer confirmed the overlap between the measurement range of optical particle counters and filter emissions down into the nanometer region. A fraction of the dust emission (mainly particles with less than 200 nm diameter) remains undetected applying scattered-light

based devices. However, the general particle emission behavior as shown in this dissertation is sufficiently represented by scattered-light based measurements [Bächler et al., 2022a]. When comparing the measured particle concentrations of the reference aerosol spectrometer with low-cost PM-sensor data, quantitative deviations were frequently determined throughout the experiments (publication I – IV).

Particle emission peaks vary strongly in their peak concentration and decay behavior dependent on the filter medium and e.g. the raw-gas concentration. The possible particle concentration region covered in filter emission measurements ranges from the zero concentration level (with a corresponding dust cake) and the peak concentration directly after regeneration (up to several $100 \mu\text{g}/\text{m}^3$ - $1000 \mu\text{g}/\text{m}^3$ or even magnitudes higher for spatial particle emission hotspots). Therefore, the specifications for low-cost PM-sensors are located at the lower concentration end required for the accurate measurement of transient particle emissions occurring in pulse-jet cleaned filters. Ambient particle concentration conditions under which low-cost PM-sensors are typically applied are lower by comparison (compare e.g. [WHO, 2021] recommendation for yearly average $\text{PM}_{2.5}$ concentration of $5 \mu\text{g}/\text{m}^3$) and rarely exceed several $100 \mu\text{g}/\text{m}^3$ (dependent on the measurement location). The main interest during ambient air measurements is the development of global trends and the representation of (average) ambient concentration levels and not concentration peaks decaying over several seconds.

Larger measurement volumes of scattered-light based optical particle counters are beneficial for accurate measurements of lower particle concentrations as is typically the case for ambient air measurements. There is no information of the manufacturers available regarding the design of the sensors (including the size of the measurement volume) so that the current design of low-cost PM-sensors is likely not optimized for the larger concentrations occurring after filter regeneration. This is also reflected by the low-cost PM-sensor specifications, where the maximum number concentration for coincidence-free measurement is approx. two orders of magnitude lower compared to the reference aerosol spectrometer (Table 2). In case of a coincidence error, multiple particles pass the measurement volume of the sensor simultaneously and the signal peaks add up so that the individual particles are detected as a single particle with larger diameter (increase in volume / mass and reduction in number concentration) [Raasch & Umhauer, 1984].

Figure 43 shows the PM evolution for complimentary measurements to investigate the prevalence of coincidence errors for low-cost PM-sensors in an aerosol test chamber (1 m^3 volume, ideally mixed), where test dust is continuously added increasing the particle concentration of the aerosol in the test chamber. After a certain time, dust dosage is stopped and the natural concentration decay is measured. The three used aerosol measurement devices are compared regarding the corresponding PM concentration evolution under more defined conditions to demonstrate the occurrence of the coincidence error.

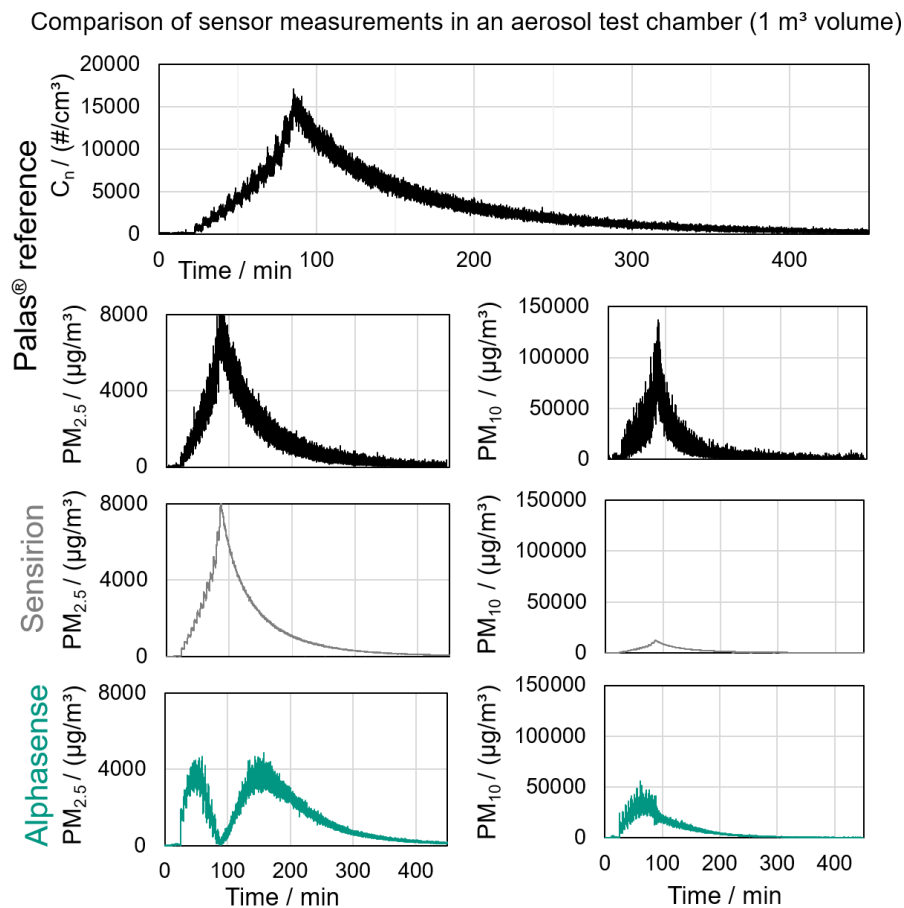


Figure 43 – Measurement behavior of low-cost PM-sensors under exposure to increased particle number concentrations in an aerosol test chamber.

For the reference, dust dosage (concentration increase) and the decay behavior can be clearly identified. Both low-cost PM-sensors underestimate the absolute PM₁₀ concentration but detect an identical qualitative behavior consisting of concentration increase and subsequent decay. The Alphasense sensor registers a less pronounced PM₁₀ concentration peak and deviates with regards to the qualitative PM₁₀ evolution.

For the PM_{2.5} fraction, the two low-cost sensors show a different measurement behavior. While the Sensirion sensor is in good agreement with the Palas[®] reference, the Alphasense sensor is clearly affected by the coincidence error. After approx. 50 minutes time, the PM_{2.5} fraction measured by the Alphasense sensor decreases (while the PM₁₀ concentration continues to increase). The coincidence probability of the sensor specified by the manufacturer is 0.84% at 1000 #/cm³ (no information available regarding higher particle number concentrations). The corresponding particle number concentration of the reference at 50 minutes time is 5000 #/cm³ so that it is likely that the sensor is affected by the coincidence error. During the concentration decay, a subsequent increase of PM_{2.5} concentrations can be observed when undershooting the number concentration of 5000 #/cm³ at about 150 minutes time.

While the impact of the coincidence error was clearly demonstrated within the scope of publication II and particle emission hotspots, the results presented in the remaining publications I, III and IV showed no clear indication of the coincidence error significantly affecting the measurement results. However, it can not be ruled out completely, that the measured concentrations during these experiments are to some degree influenced by the coincidence error.

Internal averaging and smoothing of data can improve the representation of concentration levels with minor fluctuations, where significant transient effects typically do not occur within time periods of several seconds (or, even if they do – they are not relevant regarding the measurement objective due to the evaluation of PM evolutions on a longer time scale). While there is no direct information of the manufacturer regarding internal averaging, the smooth curve of the Sensirion sensor shown in publication I (and by extension Figure 43) compared to the reference data gives reason to assume some form of internal data processing.

Figure 44 shows exemplary particle emission peaks taken from the corresponding investigations in publication I (filter aging) applying the Sensirion sensor, whereby a 20-second moving average was calculated for the reference aerosol spectrometer. The smoother decay behavior of the reference corresponds more closely to the low-cost PM-sensor signal. The peak concentration of the reference is lower in case of averaging the data with a less pronounced peak compared to the raw-data with the time resolution of one second. Internal averaging or signal smoothing cannot be confirmed with absolute certainty and is just a hypothesis; however it would explain the lower peak concentrations detected by the low-cost PM-sensors and the smoother decay behavior. The effect is more pronounced for shorter particle emission peaks (e.g. in the pilot-plant scale baghouse filter during spatial PM monitoring or when applying membrane filter media). Lower peak heights of the low-cost PM-sensors compared to the reference were often observed (in direct comparison or over the scope of comparative measurements) in the corresponding publications (publication I, III and IV). Even though, the Alphasense sensor is likely not affected by internal data-smoothing to the same degree due to larger fluctuations of the temporally resolved PM data. Furthermore, the OPC-N3 offers a moving average PM concentration as an additional data output to the temporally resolved (1 Hz) data.

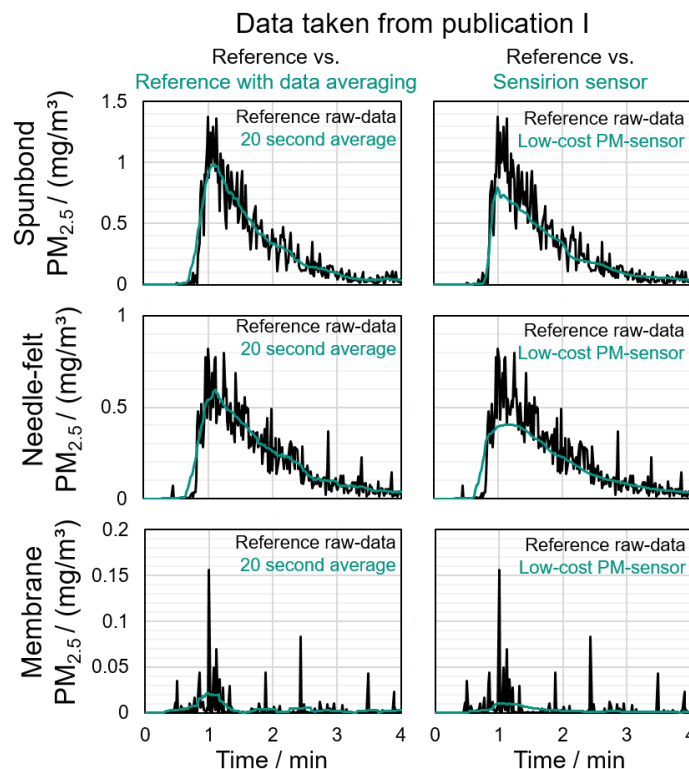


Figure 44 - Impact of a moving average on the decay behavior of particle emission peaks (publication I). The time axis was shifted to align the maximum of the emission peak at 1 minute time.

Another possible measurement error detailed in the supplementary information of publication II occurred regarding the internal sensor sample flow-rate (Alphasense sensor only). Due to deviations within the sensor flow-rate, the counting events are related to a different volume causing larger differences (or even abrupt jumps) in the output particle concentration. The flow-conditions within the pilot-plant scale baghouse filter pose another challenge, as recommended application of the sensors is within constrained screenings that protect the sensor from wind / increased gas flow velocities. Filter regeneration causes a rapid change in flow direction and pressure level on the clean gas side, that may impact the sensors. While filter face velocities are moderate in the region of multiple cm/s, the outlet velocity of the gas flow at a single filter bag ranged up to 20 m/s (compare Figure 32) what may also affect the sensors accuracy. The reference draws a defined sample flow so that errors caused by these variations in flow are unlikely. In the filter test rig (lower absolute flow velocities) particle size distributions were detected with higher accuracy and no significant error regarding particle concentrations based on the sensor flow-rate occurred (Figure 24).

While tests regarding the impact of flow conditions on sensor performance might offer additional insights, these investigations would have exceeded the scope of the experiments and been too much effort considering the high number of potential variables that impact sensor performance in a filtration application.

Two important adjustments for the determination of particle mass concentrations are the refractive index, shape factor and particle density. The only adjusted parameter within the scope of the experiments presented in this thesis was the particle density that has been set according to the test dust solid density of 2800 kg/m³ for the reference aerosol spectrometer *welas*[®]2100 and Alphasense OPC-N3 low-cost PM-sensor. Other settings were left in their default state according to Table 2 (e.g. experiments applying the Sensirion sensor in publication I). The scattered-light detection angle is different for the Alphasense sensor ($\approx 135^\circ$) and the other two measurement devices (90°). The Palas[®] reference employs a “t-shaped” measurement volume to detect and correct for the border-zone error. There is no indication, whether or not the border-zone error is considered within the data processing of low-cost PM-sensors, adding another potential measurement error typical for scattered-light based particle counters that can affect the detected mass based particle concentration [Pletscher et al., 2016]. Therefore, the settings, calibration and sensor design can be a reason for deviations between the reference aerosol spectrometer and low-cost PM-sensors.

Summarizing, the application of low-cost PM-sensors for filter emission measurement pushed the limits of the measurement accuracy due to the transient concentration behavior whose dynamic number concentration range exceeds the sensors’ maximum concentration limits and the spatio-temporal flow conditions in the pilot-plant scale baghouse filter. There were moderate quantitative deviations within the same order of magnitude between the detected particle concentrations of the low-cost PM-sensors and the reference. Reasons for these deviations range from sensor design and calibration to the prevalence of measurement errors. Nonetheless, high quantitative accuracy is not necessarily required in order to gain valuable information on the (spatial) particle emission behavior of pulse-jet cleaned filters and the emission contribution of individual filter elements.

7.1.2 Qualitative assessment of the spatially resolved particle emission measurement applying low-cost PM-sensors

The spatial particle emission behavior for pulse-jet cleaned filters could be characterized via measurements using locally deployed low-cost PM-sensors and was complemented by reference measurements applying a highly developed aerosol spectrometer in a pilot-plant scale baghouse filter. Despite quantitative differences between the low-cost PM-sensors and the reference, identical trends regarding different particle emission levels and the temporally resolved qualitative particle emission behavior could be derived from the different measurement devices.

The distinct phases of a surface filtration process occur within the scope of the total particle emission and also the local particle emission. At the beginning of filter life or the beginning of cake formation after regeneration of an individual filter element, particles penetrate to the clean gas side. This particle penetration causes a steep increase in the total and local particle emission concentration (emission peak). The majority of particles is separated on the surface of the filter element, forming the dust cake. With increasing cake formation, the amount of particles penetrating to the clean gas side decreases and the concentration peak decays until reaching a zero level.

The total dust emission consists of the overlay of the particle emission contribution of all installed filter elements. The local concentrations are affected by the spatio-temporal flow behavior, whereby larger volume flows pass the recently regenerated filter elements. Over the course of a filtration cycle, the volume flow through the recently regenerated element decreases (higher volume flow enables fast cake formation / increase in flow resistance), while the volume flow through the remaining elements increases (slower cake formation / increase in flow resistance) compared to the recently regenerated filter bag (compare Figure 32) [Simon et al., 2010].

Emission sources other than direct penetration also contribute to the total dust emission. Two important aspects are small leaks or the seams of the filter element. Both of which have already been studied in literature. A linear increase of continuous emission with leak area from publication II (Figure 27) is in good agreement with studies by [Bach & Schmidt, 2007] and [Kurtz et al., 2017]. The seams of the filter element as major source for particle penetration have been studied by [Kurtz et al., 2016] and [Lacerda et al., 2022] in similar studies and their relevance is confirmed by spatial PM monitoring (publication IV).

In order to reliably identify spatial PM hotspots applying low-cost PM-sensors, the sample position has to be kept close to the source of particle penetration (e.g. outlet of a filter bag).

The results in this thesis and the corresponding publications present the first local and simultaneous measurements of particle emissions in a pilot-plant scale baghouse filter enabled by the compact design of low-cost PM-sensors.

Due to the high qualitative accuracy of the low-cost PM-sensors compared to the reference aerosol spectrometer, the observed emission behavior is a suitable representation of the spatial particle emission behavior. In addition to the qualitative PM evolution, the investigated (quantitative) particle emission levels were in agreement with trends measured by the reference. The low-cost PM-sensors are therefore applicable for spatial particle emission monitoring and can serve as a reliable tool for leak identification and process control.

7.1.3 Comparison of the local particle emission behavior of the pilot-plant scale baghouse filter with an industrial baghouse filtration process

The investigated measurement results of the local particle emission behavior from the pilot-plant scale baghouse filter can be put into context with industrial field measurements. Investigations of the (nano-) particle emission penetrating individual filter bags made from different filter media of a municipal biomass incineration plant are presented in [Bächler et al., 2024]. The primary objective of these experiments exceeds the scope of this dissertation and the corresponding measurement conditions (raw-gas concentration and aerosol properties, filter face velocity, regeneration conditions, etc.) are not directly comparable to the measurements presented in publication II-V. However, a qualitative comparison of the detected local particle concentration behavior measured at individual filter bags between the industrial process and the pilot-plant scale baghouse filter adds validation context to the results presented in this thesis. Figure 45 shows an exemplary particle emission peak for two different types of filter media in both applications.

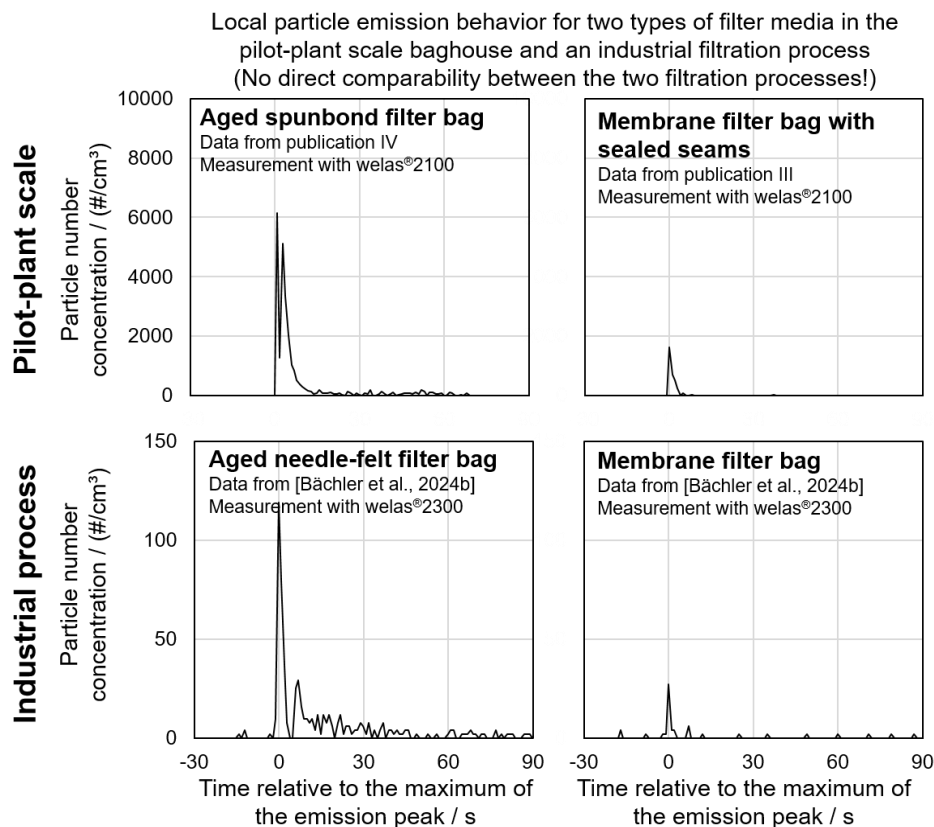


Figure 45 – Particle emission peaks detected at the outlet of an individual filter bag for the pilot plant scale baghouse filter and an industrial filtration process (raw-gas concentration $\approx 60 \text{ mg/m}^3$) [Bächler et al., 2024b]. No direct comparability of the corresponding emission behavior.

The qualitative behavior of the particle emission from the industrial process corresponds well with the observations made in the pilot-plant scale baghouse filter (e.g. Figure 30 and Figure 36). The local particle emission penetrating the filter bag consists of a particle emission peak after filter regeneration that quickly declines to a zero level. The high difference in particle number concentration between pilot-plant scale baghouse filter and industrial baghouse filter is caused by the corresponding size-distribution of Pural SB that overlaps a wider region of the aerosol spectrometers' detectable size range in the pilot-plant scale baghouse filter and the increased raw-gas concentration across this size range. The decay durations are different

depending on the filter element. The membrane filter bags are qualitatively in good agreement and quickly decline to zero over a period of few seconds. The aged spunbond filter bag (pilot-plant scale) and the aged needle-felt filter bag (industrial process) are also qualitatively comparable regarding a longer decay behavior and higher peak emissions.

Another observable effect in the industrial baghouse filter was an increase of the particle emission at an individual filter bag not only after the regeneration of the bag itself, but also after the regeneration of the following rows in the cleaning procedure as shown in Figure 46. Measurements were performed applying a CPC, so that a larger particle number concentration is detected compared to scattered-light based measurements presented in Figure 45 (lower detectable size range). The slow concentration decay in Figure 46 is caused by a comparably low age of the filter medium of 5 months (compared to the aged needle-felt of the industrial baghouse in Figure 45 with a filter age exceeding multiple years of operation).

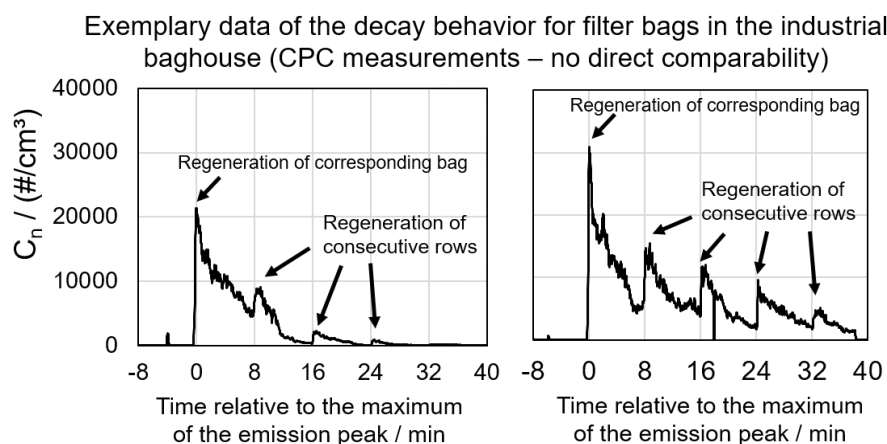


Figure 46 – Particle emission evolution for a recently installed needle-felt filter bag in the industrial baghouse filtration process. Image adapted from [Bächler et al., 2024b].

The original regeneration of the corresponding bag causes the particle concentration increase at $t = 0$. After cycle time increments of 8 minutes, the consecutive rows in the cleaning procedure are regenerated what leads to an additional local concentration increase. This effect was prevalent for a variety of the measurements presented in [Bächler et al., 2024b] and corresponds to the behavior measured in the pilot-plant scale baghouse filter (e.g. Figure 47 or publication III and IV). The origin of this peak is further discussed in the consecutive chapter.

Summarizing, the qualitative relation of the particle emission levels represented by the different filter media (needle-felt vs. membrane medium) in the industrial process are in agreement with the experimental results (spunbond vs. membrane medium) from the filter test rig and the pilot-plant scale baghouse filter presented in this thesis. A qualitatively similar decay behavior was detected for the corresponding filter elements. Additionally, an increase in particle emission caused by the regeneration of adjacent rows of filter elements was also detected in the industrial process, which is in agreement to the measurement results in the pilot-plant scale baghouse filter (compare publication III and IV).

The comparison with the industrial process therefore serves as a validation of the overall particle emission behavior obtained in the pilot-plant scale baghouse filter by both, the low-cost PM-sensors and the reference aerosol spectrometer.

7.1.4 Origin of local particle emissions after the regeneration of consecutive filter bags in the cleaning procedure

One remaining question concerning the local particle emission behavior remains the origin of additional local particle emission peaks that occur at the individual measurement locations after the regeneration of consecutive filter elements of the cleaning procedure. Figure 47 offers additional data, however this effect has been observed during a variety of experiments (e.g. Figure 29) and the industrial process (Figure 46).

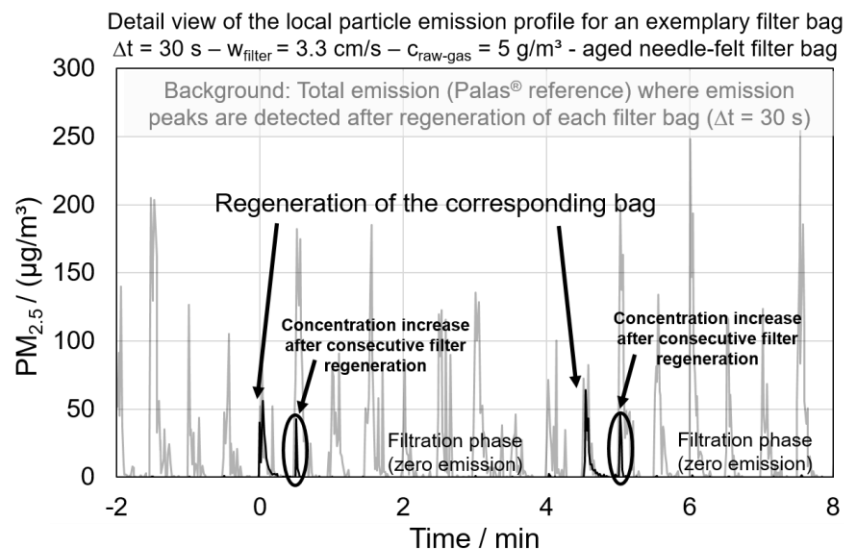


Figure 47 – Exemplary image of the „ideal“ emission behavior for an exemplary filter bag. The time axis has been shifted to align the maximum of the initial emission peak at $t = 0$. Image adapted from the supplementary information of [Bächler et al., 2023a].

The deposited dust mass on each filter element increases continuously after the regeneration of the corresponding element so that this additional peak only occurs for comparably thin filter cakes. The cycle time during the investigations in publication III and IV were sufficiently high (minimum 60 seconds) and clearly exceeded the decay period of the particle emission. Potential sources are discussed below:

- Dust contaminations on the clean gas side may be re-dispersed through vibrations or the jet-pulse and entrained in the gas flow. This entrainment seemingly contributes to particle penetration through the filter medium. Due to the clear systematics regarding the detection of the additional peak after the regeneration of the consecutive filter element within the regeneration procedure, dust contaminations are an unlikely source. For a contaminated clean gas side, the additional increase would not be restricted to only the consecutive bag within the cleaning procedure.
- Measurement artifacts are not the possible source, as the additional peak was detected by both, the reference and low-cost PM-sensors. Note that sampling tubes were led to the outlet of the filter element and the concentration measurement was performed close to the source (no diffuse concentration measurement of the clean gas side).

- The re-dispersion of filter cake (instead of cake detachment) can cause peaks in raw-gas concentration. The re-dispersed dust is quickly entrained in the gas flow and separated on or penetrating through the filter element. This behavior can lead to sharp increases in clean gas concentrations similar to the emission peak. As the flow reversal through the regeneration only occurs for a short time, the effect of a sudden increase in raw-gas concentration should only cause an instantaneous increase with a fast decline back to the original concentration level. Due to the decline to a zero emissions level within the cycle time between regenerations, it can be assumed that the filter cake is sufficiently developed and particles may penetrate only through the recently regenerated filter element to the clean gas side so that concentration increases through re-dispersion do not have the stated effect. Only small leaks (that enable particle penetration below the detection limit of the scattered-light based devices during the filtration phase) and that clog over the course of few filtration cycles could be the reason for a noticeable sudden increase in clean gas-concentration caused by an increase in raw-gas concentration. Thus, this effect cannot be ruled out completely, but is not the most likely source.
- The filter cake (or parts of the filter cake) of the corresponding filter element is in some way influenced and detached through the regeneration of the consecutive filter element in the cleaning procedure. Investigations for the industrial baghouse filtration process have shown that the regeneration of other rows caused the increase in clean gas concentration at an individual filter element (Figure 46). The concentration subsequently decayed in a manner typical for cake formation so that the previously discussed effect of re-dispersion can be ruled out. Therefore, the regeneration of other rows definitely had an impact on the filter cake and the separation characteristics. There are two different reasons that may cause cake detachment.
 - Flow reversal due to jet-pulse cleaning may cause the detachment of segments of the dust cake of neighboring filter elements. This effect is expected to be more relevant, the closer the corresponding regeneration occurs in relation to the filter element. As e.g. the regeneration of the central filter element (bag 5) in the pilot-plant scale baghouse filter does not cause an emission peak for all surrounding elements. Additionally, the furthest possible distance between filter elements within the cleaning procedure shows the corresponding peak at bag number 9 after the regeneration of bag 1 (compare Figure 15). For the municipal biomass incineration plant, there was no clear systematic and rows other than the adjacent row also caused the concentration increase. Thus, it is not necessary a local effect.
 - Vibrations of the filter house that occur during the release of the jet-pulse can cause the detachment of filter cake. If the filter cake is relatively thin and segments of the cake are detached due to vibrations, renewed particle penetration could be possible. Presumably, vibrations are the most likely source of the particle emission peak occurring for the consecutive regeneration. In case of the municipal biomass incineration plant, notable vibrations of the filter house were observed after filter regenerations. For the pilot-plant scale baghouse filter, no extraordinary vibrations were noticed during operation. However, this does not rule out cake detachment due to vibrations as the source of the emission peak.

Confirming the exact source of this minor emission peak (e.g. whether or not it is a consequence direct penetration caused by cake detachment through vibrations, etc.) is difficult and would have exceeded the scope of this work, where the focus was on the suitability of low-cost PM-sensors for spatial emission monitoring. However, due to the extensive reference measurements on a lab and industrial scale, this effect is likely part of the transient particle emission behavior and filter operation and no measurement artifact. The absolute contribution of these secondary peaks is minor and compared to the actual filter regeneration of the corresponding filter element.

7.2 Trade-off between energy-demand and particle emissions for pulse-jet cleaned filters

Publications V and VI introduced methodology to evaluate filter operation based on the energy demand and particle emissions. The implications on filter operation regarding the selection of energy efficient operating points at an adequately low particle emission level are discussed in this chapter.

7.2.1 The combination of energy demand and particle emissions as a guideline for the selection of suitable operating regions for pulse-jet cleaned filters

The “filter operation curve” derived from the energy demand and the particle emission yields a variety of general implications for an efficient filtration process. Selecting appropriate operating parameters (e.g. tank pressure, cycle time, etc.) can have severe effects on power, process stability and particle emissions.

Figure 48 highlights a schematic filter operation curve demonstrating the trade-off between energy demand and particle emissions. The experimental and modeling approach enable the identification of the power minimum and the corresponding cycle time for a certain set of parameters.

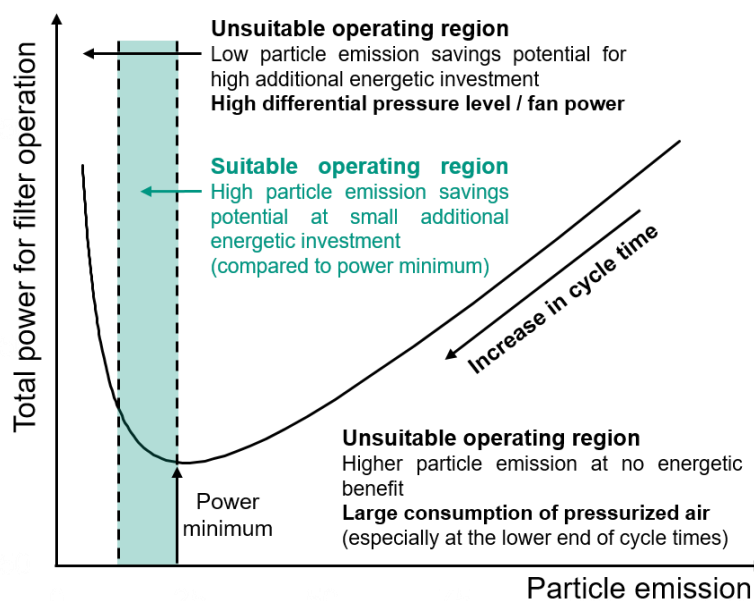


Figure 48 – Schematic operation curve for a pulse-jet cleaned filter.

The increments between energetically favorable cycle times are tightly knit (e.g. differences ranging from 10 – 30 seconds regarding the power minimum between the varied operating parameters of the experiments) and the savings potential between individual cycle times around the power minimum is within the region of several Watt (Figure 39). While this difference in power savings may not seem much, it also implies that slightly increasing the cycle time above the power minimum can prevent particle emissions at a low additional energetic investment. Suitable cycle times for a sustainable filtration process from an energy and emission perspective should be selected at or slightly above the cycle time at the power minimum. In the context of process safety and stable filter operation, a flexible time controlled regeneration trigger is the recommended operation strategy compared to rigid differential pressure controlled

regeneration. A combination of the two strategies, e.g. time controlled regeneration with a differential pressure criterion, can enable the demand-orientated adjustment of cycle time. Further discussing particle emissions, it is important that the cycle time is still sufficiently high to enable proper cake formation. As an example, cycle times longer than the decay period required to reach the zero emission level should be adjusted as a general guideline according to Figure 49.

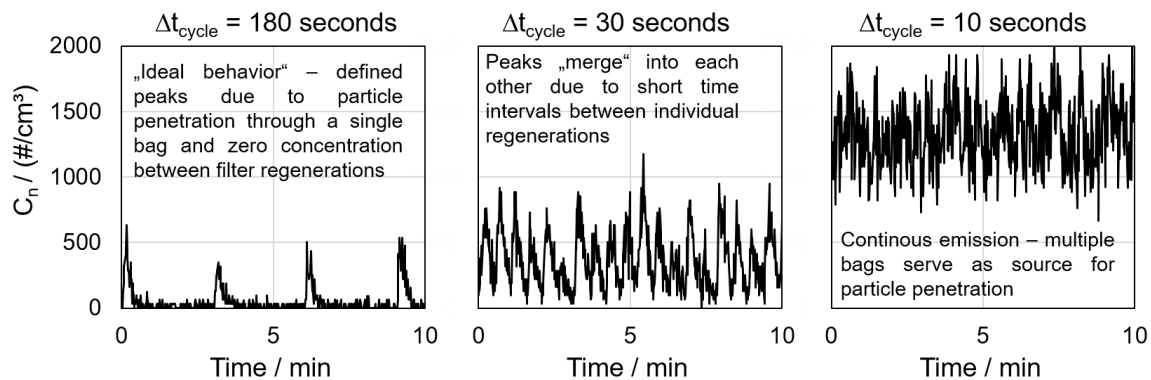


Figure 49 – Emission characteristic for Δt -controlled filter operation. Image adapted from the supplementary information of [Bächler et al., 2023b].

Significantly shorter cycle times cause a state of constant regeneration and excessive consumption of pressurized air, where continuous particle penetration occurs due to incomplete cake formation. This operating behavior is similar to unstable filter operation and also results in increased wear on the filter bag due to the mechanical deformation through the jet-pulse and a higher degree of dust deposition within the filter element (increase in residual differential pressure). Nonetheless, higher dust loads and filter face velocities should be faced with more frequent regenerations (similar to Δp -controlled operation) to operate closer to the power minimum. For filter plants where the number of elements ranges up to multiple hundreds or even thousands of elements, short cycle times where simultaneous particle penetration through multiple rows is possible may have to be accepted.

Exceedingly long cycle times should be avoided as well due to a high differential pressure level and an increase of fan power. However, the consequences of filter operation under these conditions are not as severe, as at least the particle emission level is sufficiently low (or even at the zero level) due to sufficient dust cake and the main risk is the reduction of the process volume flow when reaching the maximum blower capacity. Stopping the regeneration for a certain time duration and observing the trend of the total dust emission can even exploit this particle emission behavior and help in the context of leak identification. If the (total) emission declines to zero, a significant contribution of leaks can be ruled out. The hyperbolic behavior of the particle emission demonstrates that emission levels can be kept very low under the right conditions and help identify cycle times, where a stable sufficiently low emission level is reached.

The developed model demonstrated the potential of data-driven grey-box modeling for pulse-jet cleaned filters. Applications include basic engineering / plant layout and enables the consideration of more application orientated use-cases (e.g. considering economics and real behavior of machinery like fans and compressors) [Ho et al., 2021; Lanzerstrofer et al., 2016; Caputo & Pelagagge, 2004].

The trade-off between energy efficient operation and particle emissions highlights the complexity of efficient and sustainable filtration processes for cleanable filter media. The findings can serve as the basis for operation strategies, process automation and digitalization.

7.3 Summarizing conclusions in the context of the research questions (chapter 1.2.)

The following chapter summarizes the key conclusions of this thesis and gives brief answers to the main research questions of this thesis.

- **Are low-cost PM-sensors suitable for (local) particle emission monitoring and the identification of particle emission hotspots in baghouse filters?**

The suitability of low-cost PM-sensors for local particle emission monitoring was investigated experimentally in a filter test rig for sensor validation and a pilot-plant scale baghouse filter for application-orientated experiments (Figure 10).

In direct comparison to a highly developed reference aerosol spectrometer, measurements applying low-cost PM-sensors show quantitative differences of the detected particle concentration. In most cases, the measured concentrations were in the same order of magnitude. Only measurements under high concentration conditions outside of the sensor specifications (e.g. emission hotspots) demonstrated measurement errors of the low-cost PM-sensors. The qualitative transient particle emission behavior is in good agreement with the reference and follows the expected behavior according to literature. The sensors showed their greatest potential as a qualitative monitoring tool. Changes in particle emission (different filter media, filter aging, emission hotspot, etc.) were reliably quantified based on sensor data so that information on the spatially and temporally resolved particle emission level can be gained. The sensors reliably detected the zero concentration level for sufficiently established dust cakes.

As the sensors were neither intended as certified emission measurement technology, nor directly designed with the concentration dynamics present in pulse-jet cleaned filters in mind, their performance and potential for the improvement of process monitoring and maintenance remains formidable despite the occurrence of measurement errors and limited quantitative accuracy.

- **How can particle emissions from baghouse filter operation be lowered as energy-efficiently as possible and what is the trade-off between energy demand and particle emissions?**

Investigations regarding the energy-efficiency of pulse-jet cleaned filters and the impact of varying operating parameters were performed in a pilot-plant scale baghouse filter. The experimental results served as the foundation for process modeling in a follow-up investigation (Figure 11). Both investigations yielded the same general conclusions on the operating behavior of pulse-jet cleaned filters in the context of energy demand and particle emissions.

A power minimum for filter operation can be identified at a certain cycle time based on the fan power and the consumption of pressurized air for jet-pulse cleaning. An increase of raw-gas concentration or filter face velocity causes a shift of the power minimum to shorter cycle times. Increasing the tank pressure for filter regeneration can cause significantly increased particle emissions while offering no significant benefit considering the total power for filter operation. A suitable cycle time should be selected at (or slightly above) the power minimum. Increasing the cycle time above the power minimum leads to lower particle emissions at the trade-off of higher energy input. The particle emission decreases hyperbolically with increasing cycle time, so that for exceedingly long cycle times a “stable emission level” is reached and only minor reductions of the particle emission level are achieved at the drawback of significant increase of total power.

8 OUTLOOK

This work demonstrated the potential of compact and cheap low-cost PM-sensors as a monitoring tool for the detection of spatially resolved particle emissions. Many existing processes under suitable conditions could greatly profit from application of low-cost PM-sensors. As the low-cost devices are not certified for the measurements of particle emissions regarding statutory limits, they can either complement existing emission measurements or enable cheap particle emission monitoring at a low acquisition cost for filter systems that are not legally obligated to monitor their particle emission (e.g. worker protection, small scale baghouses, etc.). An example application are extraction systems equipped with pulse-jet cleaned filters, where particle emission monitoring is not mandatory. The implementation of low-cost PM-sensors can provide valuable information on the particle emission level and indicate the necessity for maintenance procedures in case of small leaks. Manufacturers for filter media (e.g. according to DIN ISO 11057) could implement low-cost PM-sensors as cheap alternative to costly aerosol spectrometers for the online characterization of particle emissions during filter testing (as an extension to gravimetric measurements). While the possibility for leak identification and online process monitoring offers promising benefits for plant operators, several drawbacks of the sensors could be identified and prevent the current state of the measurement technology from wide-spread application and unfolding their full potential.

First and foremost, process conditions within many industrial applications are harsher compared to laboratory environments so that the current generation of sensors is not suitable for many industrial processes (e.g. temperatures above 100°C, corrosive gases, etc.). Further technological progress regarding sensor development (e.g. the use of temperature resistant materials, changes in sensor design like cooling or sampling options, etc.) could result in more resilient sensors that can be applied under more challenging conditions. Another potential possibility would be drawing a sample flow out of the baghouse within a measurement chamber, where the conditions are suitable for low-cost PM-sensors and measurement is possible. However, aerosol conditioning and a variety of sampling periphery would be required, what is a detriment compared to the easy to use plug and play nature of the measurement devices.

The sheer number of filter elements in an industrial process can make the wide-spread application of low-cost PM-sensors a difficult economic case. Instead of monitoring individual filter elements, monitoring a subset of installed filter elements or individual rows would be an option. Limiting the amount of filter bags that are replaced during plant shutdown / maintenance by directly identifying damaged or conspicuous elements and preventing premature exchange of filter elements before the end of their service life offers economic advantages (for suitable sensors with sufficiently long lifetimes). Another drawback is sensor stability regarding dust contamination and continuous stable measurement signals. As could be observed e.g. in the context of leak detection, measurement errors due to coincidence or other factors (e.g. internal sensor flowrate) can have larger effects on the data output. Therefore, sensors can at best serve as a monitoring tool and are not suitable for implementation in process control loops.

Taking into account the trade-off between energy demand and particle emissions, can put filter operation of existing plants into perspective regarding suitable operating points and improve the layout of energy efficient low emission filtration processes. The implementation of the evaluation of the energy demand for pulse-jet cleaned filters within engineering standards (e.g. VDI 3677 or DIN ISO 11057 / VDI 3926 as proposed by [Höflinger & Laminger, 2013]) can complement the layout of baghouses and the characterization of filter media.

The application of process modeling and digital twins is expected to gain further relevance and enhances the experimental results. While the overall applicability of the operation curve should be transferrable outside of the experimental laboratory context, results may vary for other test dusts, filter media and filter geometries (e.g. cleanable pleated filters). While data-driven process modeling enables an accurate mathematical description of the dataset, extrapolation to other process conditions can show the stability and reliability of the derived models. Therefore, expanding on the current investigations (e.g. different dusts or filter media) or implementing operating strategies in (industrial) processes / different filter systems (e.g. pleated filters) based on the evaluation of energy demand and particle emissions would enhance the currently explored set of parameters.

The two aspects of spatially resolved online process monitoring and energy efficient operation of pulse-jet cleaned filters within the current trend towards digitalization in the process industry were investigated in this work. Pulse-jet cleaned filters will remain a key technology to provide low emission levels and protect the environment from dust emissions due to their high reliability and separation efficiency. With rising requirements on filter efficiency due to stricter statutory limits (e.g. according to WGC BREF [European Commission, 2023]), improved (spatial) online process monitoring and the development of energy- and emission based operating strategies can contribute to the optimization of baghouse filter operation.

REFERENCES

Note that the reference section only lists references within the main body of the dissertation. Each publication within the appendices also contains a corresponding section with more specific references.

- [Apicella et al., 2020] Apicella, B., Mancaruso, E., Russo, C., Tregrossi, A., Oliano, M., M., Ciajolo, A., Vaglieco, B., M., (2020). Effect of after-treatment systems on particulate matter emissions in diesel engine exhaust. *Experimental Thermal and Fluid Science*, 116, 110107, <https://doi.org/10.1016/j.expthermflusci.2020.110107>
- [Andersen et al., 2016] Andersen, B., O., Nielsen, N., F., Walther, J., H., (2016). Numerical and experimental study of pulse-jet cleaning in fabric filters. *Powder Technology*, 291, 284-298, <https://doi.org/10.1016/j.powtec.2015.12.028>
- [Asbach et al., 2018] Asbach, C., Hellack, B., Schumacher, S., Bässler, M., Spreitzer, M., Pohl, T., Weber, K., Monz, C., Bieder, S., Schultze, T., Todea, A., M., (2018). Anwendungsmöglichkeiten und Grenzen kostengünstiger Feinstaubsensoren. *Gefahrstoffe, Reinhaltung der Luft*, 78 (6), 242-250
- [Bach & Schmidt, 2007] Bach, B., Schmidt, E., (2007). Influence of leaks in surface filters on particulate emissions. *Journal of hazardous materials*, 143 (3), 673 – 676, <https://doi.org/10.1016/j.jhazmat.2007.01.093>
- [Bächler et al., 2024a] Bächler, P., Meyer, J., Dittler, A., (2024). Operating Behavior of Pulse Jet-Cleaned Filters Regarding Energy Demand and Particle Emissions – Part 2: Modeling. *Chemical Engineering & Technology*, 47 (4), 722-731, <https://doi.org/10.1002/ceat.202300409>
- [Bächler et al., 2024b] Bächler, P., Meyer, J., Ligotski, R., Krug, P., Dittler, A., (2024). Measurement of transient nanoparticle emissions of a municipal biomass incineration plant equipped with pulse-jet cleaned filters. *Process Safety and Environmental Protection*, 184, 601-614, <https://doi.org/10.1016/j.psep.2024.02.013>
- [Bächler et al., 2023a] Bächler, P., Meyer, J., Dittler, A., (2023). Spatially Resolved Online Leak Detection in a Baghouse Filter Applying Low-Cost PM-Sensors . *Chemie Ingenieur Technik*, 95 (1-2), 178-188, <https://doi.org/10.1002/cite.202200116>
- [Bächler et al., 2023b] Bächler, P., Meyer, J., Dittler, A., (2023). Operating Behavior of Pulse Jet-Cleaned Filters Regarding Energy Demand and Particle Emissions – Part 1: Experimental Parameter Study. *Chemical Engineering & Technology*, 46 (8), 1689 – 1697, <https://doi.org/10.1002/ceat.202300080>
- [Bächler et al., 2022a] Bächler, P., Meyer, J., Dittler, A., (2022). Measurement of transient nanoparticle emissions of pulse-jet cleaned filters applying an engine exhaust particle sizer. *Aerosol Science & Technology*, 56 (4), 394 – 402, <https://doi.org/10.1080/02786826.2022.2027335>
- [Bächler et al., 2022b] Bächler, P., Löschner, V., Meyer, J., Dittler, A., (2022). Process integrated monitoring of spatially resolved particle emissions of a baghouse filter using a network of low-cost PM-sensors. *Process Safety and Environmental Protection*, 160, 411 – 423, <https://doi.org/10.1016/j.psep.2022.02.005>
- [Bächler et al., 2020] Bächler, P., Szabadi, J., Meyer, J., Dittler, A., (2020). Simultaneous measurement of spatially resolved particle emissions in a pilot plant scale baghouse filter applying distributed low-cost particulate matter sensors. *Journal of Aerosol Science*, 150, 105644, <https://doi.org/10.1016/j.jaerosci.2020.105644>
- [Bächler et al., 2019a] Bächler, P., Meyer, J., Dittler, A., (2019). Characterization of the emission behavior of pulse-jet cleaned filters using a low-cost particulate matter sensor. *Gefahrstoffe – Reinhaltung der Luft*, 79 (11-12), 443-450, <https://doi.org/10.37544/0949-8036-2019-11-12-49>
- [Bächler et al., 2019b] Bächler, P., Meyer, J., Dittler, A., (2019). Investigation of low-cost PM-sensors regarding the suitability for emission measurement for pulse-jet cleaned filters. *Conference paper at FILTECH 2019 – The Filtration Event (Cologne)*
- [Badura et al., 2018] Badura, M., Batog, P., Drzeniecka-Osiadacz, A., Modzel, P., (2018). Evaluation of Low-Cost Sensors for Ambient PM_{2.5} Monitoring. *Journal of Sensors*, 2018, 5096540, <https://doi.org/10.1155/2018/5096540>
- [Binnig et al., 2009] Binnig, J., Meyer, J., Kasper, G., (2009). Origin and mechanisms of dust emission from pulse-jet cleaned filter media. *Powder Technology*, 189 (1), 108 – 114, <https://doi.org/10.1016/j.powtec.2008.06.012>
- [Binnig et al., 2007] Binnig, J., Meyer, J., Kasper, G., (2007). Calibration of an optical particle counter to provide PM_{2.5} mass for well-defined particle materials. *Journal of Aerosol Science*, 38 (3), 325-332, <https://doi.org/10.1016/j.jaerosci.2006.12.001>
- [Brown, 1993] Brown, R., C., *Air Filtration – an integrative approach to the theory and applications of fibrous filters*. Pergamon Press – Oxford, New York, Seoul, Tokyo 1993
- [Caputo & Pelagagge, 2004] Caputo, A., C., Pelagagge, P., M., (2004). Baghouse system design based on economic optimization. *Environmental Progress*, 19 (4), 238-245, <https://doi.org/10.1002/ep.670190410>

- [Chacón-Mateos et al., 2022] Chacón-Mateos, M., Laquai, B., Vogt, U., Stubendrauch, C., (2022). Evaluation of a low-cost dryer for a low-cost optical particle counter. *Atmospheric Measurement Techniques*, 15 (24), 7395-7410, <https://doi.org/10.5194/amt-15-7395-2022>
- [Cirqueira et al., 2017] Cirqueira, S., S., R., Tanabe, E., H., Aguiar, M., L., (2017). Evaluation of operating conditions during the pulse jet cleaning filtration using different surface treated fibrous filters. *Process Safety and Environmental Protection*, 105, 69-78, <https://doi.org/10.1016/j.psep.2016.10.010>
- [Cora & Hung, 2002] Cora, M. G., Hung, Y.-T., (2002). Controlling industrial particulate emissions: A practical overview of baghouse technology. *Environmental Quality Management*, 11 (4), 53 – 64, <https://doi.org/10.1002/tqem.10041>
- [Crilley et al., 2020] Crilley, L., R., Singh, A., Kramer, L., J., Shaw, M., D., Alam, M., S., Apte, J., S., Bloss, W., J., Hildebrandt Ruiz, L., Fu, P., Fu, W., Gani, S., Gatari, M., Ilyinskaya, E., Lewis, A., C., Ng'ang'a, D., Sun, Y., Whitty, R., C., W., Yue, S., Young, S., Pope, F., D., (2020). Effect of aerosol composition on the performance of low-cost optical particle counter correction factors. *Atmospheric Measurement Techniques*, 13 (3), 1181-1193, <https://doi.org/10.5194/amt-13-1181-2020>
- [DIN ISO 11057, 2016] DIN ISO 11057:2012-05 (2016), Air quality – Test method for filtration characterization of cleanable filter media (ISO 11057:2011)
- [Dittler et al., 2002] Dittler, A., Ferer, M., V., Mathur, P., Djuranovic, P., Kasper, G., Smith, D., H., (2002). Patchy cleaning of rigid gas filters – transient regeneration phenomena comparison of modelling to experiment. *Powder Technology*, 124 (1-2), 55-66, [https://doi.org/10.1016/S0032-5910\(01\)00481-8](https://doi.org/10.1016/S0032-5910(01)00481-8)
- [Eilenberg et al., 2020] Eilenberg, S., R., Subramanian, R., Malings, C., Haurlyiuk, A., Presto, A., A., Robinson, A., L., (2020). Using a network of lower-cost monitors to identify the influence of modifiable factors driving spatial patterns in fine particulate matter concentrations in an urban environment, *Journal of Exposure Science & Environmental Epidemiology*, 30, 949-961, <https://doi.org/10.1038/s41370-020-0255-x>
- [European Commission, 2023] European Commission, Joint Research Centre, Daginnus, K., Marty, T., Trotta, N. V., Brinkmann, T., Whitfield, A., Roudier, S., (2023). Best available techniques (BAT) reference document for common waste gas management and treatment systems in the chemical sector – Industrial Emissions Directive 2010/75/EU (integrated pollution prevention and control). Publications Office of the European Union, <https://doi.org/10.2760/220326>
- [Gail & Gommel, 2018] Gail, L., Gommel, U., (2018). *Reinraumtechnik*. Springer Vieweg, Wiesbaden 2018, <https://doi.org/10.1007/978-3-662-54915-5>
- [Giordano et al., 2021] Giordano, M., R., Malings, C., Pandis, S., N., Presto, A., A., McNeill, V., F., Westervelt, D., M., Beekmann, M., Subramanian, R., (2021). From low-cost sensors to high-quality data: A summary of challenges and best practices for effectively calibrating low-cost particulate matter mass sensors, *Journal of Aerosol Science*, 158, 105833, <https://doi.org/10.1016/j.jaerosci.2021.105833>
- [He et al., 2023] He, W., Guo, Y., Shen, R., Feng, D., Zhou, X., Liu, J., (2023). In-situ leakage detection of single bag filter in baghouse based on the resistance change of conductive polymer fibers. *Journal of Applied Polymer Science*, 140 (39), e54453, <https://doi.org/10.1002/app.54453>
- [Hindy, 1986] Hindy, K., T., (1967). Influence of selected fixed parameters on pulse-jet fabric filter operation. *Atmospheric Environment*, 20 (8), 1517 – 1521, [https://doi.org/10.1016/0004-6981\(86\)90240-4](https://doi.org/10.1016/0004-6981(86)90240-4)
- [Ho et al., 2021] Ho, C.-L., Tang, Y.-C., Chiu, W.-C., (2021). The Optimal Performance of the Energy Efficiency of a Pulse Dust Collection System towards Sustainability. *Applied Sciences*, 11 (22), 10941, <https://doi.org/10.3390/app112210941>
- [Höflinger & Laminger, 2013] Höflinger, W., Laminger, T., (2013). Standard test procedure to characterise different filter media under energy consideration. *Energy & Sustainability*, 176, 3 – 13, <https://doi.org/10.2495/ESUS130121>
- [Höflinger et al., 2007] Höflinger, W., Rud, H., Mauschitz, G., (2007). Estimation of the particle penetration and the dust holding capacity of different surface-treated needle felts. *Separation and Purification Technology*, 58 (2), 256-261, <https://doi.org/10.1016/j.seppur.2007.03.021>
- [Huang et al., 2015] Huang, X.-L., Badawy, A., M., Arambewela, M., Adkins, R., Tolaymat, T., Mineral phases and metals in baghouse dust from secondary aluminum production. *Chemosphere*, 134, 250, 30, <https://doi.org/10.1016/j.powtec.2015.06.056>
- [Jodeit et al., 1983] Jodeit, H., Löffler, F., Umhauer, H., (1983). Eine schnelle Methode zur Bestimmung der Abscheideeigenschaften von Faserfiltern. *Chemie Ingenieur Technik*, 55 (7), 551-553, <https://doi.org/10.1002/cite.330550709>
- [Kasper et al., 2007] Kasper, G., Binnig, J., Meyer, J., (2007). Particulate emissions from filter-based gas cleaning devices and their characterization according to PM 2.5 criteria. *Filtration*, 7 (1), 49-54

- [Kaur & Kelly, 2023] Kaur, K., Kelly, K., (2023). Performance evaluation of the Alphasense OPC-N3 and Plantower PMS5003 sensor in measuring dust events in the Salt Lake Valley, Utah. *Atmospheric Measurement Techniques*, 16 (10), 2455-270, <https://doi.org/10.5194/amt-16-2455-2023>
- [Kavouras & Krammer, 2005] Kavouras, A., Krammer, G., (2005) A model analysis on the reasons for unstable operation of jet-pulsed filters. *Powder Technology*, 154 (1), 24-32, <https://doi.org/10.1016/j.powtec.2005.03.016>
- [Khirouni et al., 2021] Khirouni, N., Charvet, A., Drisket, C., Ginestet, A., Thomas, D., Bémer, D., (2021). Precoating for improving the cleaning of filter media clogged with metallic nanoparticles. *Process Safety and Environmental Protection*, 147, 311-319, <https://doi.org/10.1016/j.psep.2020.09.045>
- [Khirouni et al., 2020] Khirouni, N., Charvet, A., Thomas, D., Bémer, D., (2020). Regeneration of dust filters challenged with metallic nanoparticles: Influence of atmospheric aging. *Process Safety and Environmental Protection*, 138, 1-8, <https://doi.org/10.1016/j.psep.2020.02.040>
- [Klein et al., 2012] Klein, G.-M., Schrooten, T., Neuhaus, T., (2012). Reduction of Energy Demand for Industrial Dedusting Plants. *Chemie Ingenieur Technik*, 84 (7), 1121-1129, <https://doi.org/10.1002/cite.201100251>
- [Klein et al., 2009] Klein, G.-M., T. Schrooten, T., Neuhaus, T., Kräbs, R., (2009) Energieeffiziente Jet-Pulse-Entstaubungsanlagen. *Gefahrstoffe – Reinhaltung der Luft*, 2009, 5
- [Klingel, 1983] Klingel, R., (1983). Untersuchung der Partikelabscheidung aus Gasen an einem Schlauchfilter mit Druckstoßfabreinigung, VDI-Fortschritts-Berichte, Reihe 3: Verfahrenstechnik, Nr. 76, Düsseldorf: VDI-Verlag.
- [Kurtz, 2018] Kurtz, O., (2018). Ursachen für Emissionen in Filteranlagen. Dissertation Karlsruher Institut für Technologie, Verlag Dr. Hut, Reihe Verfahrenstechnik
- [Kurtz et al., 2017] Kurtz, O., Meyer, J., Kasper, G., (2017). The contribution of small leaks in a baghouse filter to dust emission in the PM_{2.5} range – A system approach. *Particuology*, 30, 40-52, <https://doi.org/10.1016/j.partic.2016.08.001>
- [Kurtz et al., 2016] Kurtz, O., Meyer, J., Kasper, G., (2016). Influence of Filter Operating Parameters on Fine Dust Emissions from Pulse-Cleaned Filter Bags. *Chemical Engineering & Technology*, 39 (3), 435-443. <https://doi.org/10.1002/ceat.201500340>
- [Lacerda et al., 2022] Lacerda, C., R., Bächler, P., Schwarz, A., D., Sartim, R., Aguiar, M., L., Dittler, A., (2022). Impact of Seams on the Operating Behavior of Surface Filters Regarding Particle Emissions. *Chemical Engineering & Technology*, 45 (7), 1354 – 1362, <https://doi.org/10.1002/ceat.202200132>
- [Leith & Ellenbecker, 1982] Leith, D., Ellenbecker, M., J., (1982). Dust emission characteristics of pulse-jet-cleaned fabric filters. *Aerosol Science and Technology*, 1 (4), 401 – 408, <https://doi.org/10.1080/02786828208958604>
- [Leith and Ellenbecker, 1980] Leith, D., Ellenbecker, M., J., (1980). Theory for pressure drop in a pulse-jet cleaned fabric filter. *Atmospheric Environment*, 14 (7), 845-852, [https://doi.org/10.1016/0004-6981\(80\)90141-9](https://doi.org/10.1016/0004-6981(80)90141-9)
- [Leubner & Riebel, 2003] Leubner, H., Riebel, U., (2003). Empirische Untersuchungen zum instabilen Filterbetrieb. *Chemie Ingenieur Technik*, 75 (1-2), 82-86, <https://doi.org/10.1002/cite.200390027>
- [Li et al., 2022] Li, J., Wu, Q., Huang, Y., Sun, Z., Li, J., Wu, D., (2022). Particulate matters filtration by filter medium with pin holes: modeling and experimental verification. *Process Safety and Environmental Protection*, 158, 282-290, <https://doi.org/10.1016/j.psep.2021.12.012>
- [Li et al., 2020] Li, J., Lu, X., Wang, W., F., (2020). Leak monitoring and localization in baghouse filtration system using a distributed optical fiber dynamic air pressure sensor. *Optical Fiber Technology*, 57, 102218, <https://doi.org/10.1016/j.yofte.2020.102218>
- [Litchwark et al., 2015] Litchwark, J., O., Winchester, J., Nijdam, J., J., (2015). Design of pulse-jet systems for milk powder baghouses. *Powder Technology*, 284, 379 – 386, <https://doi.org/10.1016/j.powtec.2015.06.056>
- [Löffler, 1988] Löffler, F., *Staubabscheiden*. Georg Thieme Verlag Stuttgart - New York 1988
- [Lu & Tsai, 2003] Lu, H.-C., Tsai, C.-J., (2003). Influence of Different Cleaning Conditions on Cleaning Performance of Pilot-Scale Pulse-Jet Baghouse. *Journal of Environmental Engineering*, 129 (9), [https://doi.org/10.1061/\(ASCE\)0733-9372\(2003\)129:9\(811\)](https://doi.org/10.1061/(ASCE)0733-9372(2003)129:9(811))
- [Mauschitz et al., 2018] Mauschitz, G., Secklehner, A., Hagn, S., (2018). The DeCONOX process - An example of advanced exhaust gas cleaning technology in the Austrian cement industry. *Cement International*, 16 (2), 34-53
- [Möller, 2006] Möller, L., (2006). Bestimmung der Anzahlverteilung von Tracerpartikeln. Conference paper at Fachtagung "Lasermethoden in der Strömungsmesstechnik (Braunschweig)

- [Ostermeyer et al., 2020] Ostermeyer, G., P., Kwade, A., Sandgaard, M., Carsten, S., Otto, J., Brandt, S., Finke, B., Gramstat, S., Stebner, F., Drescher, T., (2020). Measurement of Dynamic Signature of Brake Emissions on a Pin-On-Disc Tribotester with Low-Cost Particulate Sensors. Conference paper at EuroBrake 2020 – EB2020-EBS-029 (Barcelona), <https://doi.org/10.46720/EB2020-EBS-029>
- [Peukert, 2022] Peukert, W., (2022). „Grüne“ Partikeltechnik?. *Chemie Ingenieur Technik*, 95 (1-2), 1-8, <https://doi.org/10.1002/cite.202200159>
- [Peukert & Wadenpohl, 2001] Peukert, W., Wadenpohl, C., (2001). Industrial separation of fine particles with difficult dust properties. *Powder Technology*, 118 (1-2), 136-148, [https://doi.org/10.1016/S0032-5910\(01\)00304-7](https://doi.org/10.1016/S0032-5910(01)00304-7)
- [Peters et al., 2001] Peters, T., M., Vanderpool, R., W., Wiener, R., W., (2001). Design and Calibration of the EPA PM_{2.5} well impactor ninety-six (WINS). *Aerosol Science & Technology*, 34 (5), 389 – 397, <https://doi.org/10.1080/02786820120352>
- [Pletscher et al., 2016] Pletscher, K., Weiß, M., Mölter, L., (2016). Simultaneous Determination of PM Fractions, Particle Number and Particle Size Distribution in High Time Resolution Applying One and the Same Optical Measurement Technique. *Gefahrstoffe – Reinhaltung der Luft*, 76 (11/12), 425-436
- [Raasch & Umhauer, 1984] Raasch, J., Umhauer, H., (1984). Errors in the Determination of Particle Size Distributions Caused by coincidences in optical particle counters. *Particle & Particle Systems Characterization*, 1 (1-4), <https://doi.org/10.1002/ppsc.19840010109>
- [Schiller & Schmid, 2015] Schiller, S., Schmid, H.-J., (2015). Highly efficient filtration of ultrafine dust in baghouse filters using precoat materials. *Powder Technology*, 279, 96 – 105, <https://doi.org/10.1016/j.powtec.2015.03.048>
- [Schiller & Schmid, 2014] Schiller, S., Schmid, H.-J., (2015). Ultrafine Dust Filtration Using Precoat Materials Considering the Influence of Filter Media. *Chemical Engineering and Technology*, 37 (6), 1009-1020, <https://doi.org/10.1002/ceat.201300856>
- [Schmidt, 2003] Schmidt, E., (2003). Gasreinigung. *Chemie Ingenieur Technik*, 75 (10), 1468-1471, <https://doi.org/10.1002/cite.200303282>
- [Schmidt, 1998] Schmidt, E., (1998). Abscheidung von Partikeln aus Gasen mit Oberflächenfiltern. *Fortschritt-Berichte der VDI-Zeitschriften, Reihe 3 (546)*. Düsseldorf: VDI Verlag
- [Schott et al. 2022] Schott, F., Baumbach, G., Straub, D., Thorwarth, H., Vogt, U., (2022). Novel metal mesh filter equipped with pulse-jet regeneration for small-scale biomass boilers. *Biomass and Bioenergy*, 163, 106520, <https://doi.org/10.1016/j.biombioe.2022.106520>
- [Sobich et al., 2018] Sobich, S., Meyer, J., Dittler, A., Kasper, G., (2018). Baghouse filtration: A praxis-relevant media parameter to determine an emissions level of a pulse-jet cleanable filter. Conference paper at FILTECH 2018 – The Filtration Event (Cologne)
- [Schuberth, 2010] Schuberth, J., (2010). Untersuchung des Alterungsvorganges von abreinigbaren Staubfiltermedien bei zeitgesteuerter Abreinigung. Dissertation TU Wien, reposiTUM. <https://resolver.obvsg.at/urn:nbn:at:at:ubtuw:1-45722>
- [Schwarz et al., 2022] Schwarz, A., D., Meyer, J., Dittler, A., (2022). Penetration of Water-Soluble Material through Gas-Cleaning Filters. *Membranes*, 12 (8), 776, <https://doi.org/10.3390/membranes12080776>
- [Schwarz et al., 2018] Schwarz, A., D., Meyer, J., Dittler, A., (2018). Opportunities for low-cost particulate matter sensors in filter emission measurements. *Chemical Engineering & Technology*, 41 (9), 1826-1832, <https://doi.org/10.1002/ceat.201800209>
- [Simon et al., 2014] Simon, X., Bémer, D., Chazelet, S., Thomas, D., (2014). Downstream particle puffs emitted during pulse-jet cleaning of a baghouse wood dust collector: Influence of operating conditions and filter surface treatment. *Powder Technology*, 261, 61 – 70, <https://doi.org/10.1016/j.powtec.2014.04.028>
- [Simon et al., 2010] Simon, X., Bémer, D., Chazelet, S., Thomas, D., Régnier, R., (2010). Consequences of high transitory airflows generated by segmented pulse-jet cleaning of dust collector filter bags. *Powder Technology*, 201 (1), 37-48, <https://doi.org/10.1016/j.powtec.2010.02.036>
- [Sievert & Löffler, 1989] Sievert, J., Löffler, F., (1989). Fabric cleaning in pulse-jet filters. *Chemical Engineering and Process Intensification*, 26 (2), 179-183, [https://doi.org/10.1016/0255-2701\(89\)90010-X](https://doi.org/10.1016/0255-2701(89)90010-X)
- [Stabile et al., 2020] Stabile, L., Scungio, M., Frattolillo, A., Buonanno, G., (2020). Effects of the flue gas treatment of incinerator plants on sub-micron particle concentrations at the stack. *Waste Management*, 101, 9 – 17, <https://doi.org/10.1016/j.wasman.2019.09.038>

[Steiner & Lanzerstorfer, 2023] Steiner, D., Lanzerstorfer, C., (2023). Particulate emissions from biomass power plants: a practical review and measurement uncertainty issues. *Clean Technologies and Environmental Policy*. <https://doi.org/10.1007/s10098-023-02645-6>

[VDI 3677, 2023] VDI 3677 Blatt 1:2023-05 (2023), Filtering Separators – Surface Filters (VDI 3677:2010-11)

[WHO, 2021] WHO global air quality guidelines. Particulate matter (PM_{2.5} and PM₁₀), ozone, nitrogen dioxide, sulfur dioxide and carbon monoxide. Geneva: World Health Organization 2021

[Wiegleb, 2016] Wiegleb, G., (2016). *Gasesstechnik in Theorie und Praxis*. Springer Vieweg, Wiesbaden 2016, <https://doi.org/10.1007/978-3-658-10687-4>

[Wilanowicz et al., 2013] Wilanowicz, J., Grabowski, W., Andrzejczak, M., Chromiec, A., (2013). Assessment of the suitability of baghouse dusts from a dust extractor as fillers for hot-mix asphalt. *Procedia Engineering*, 57, 1269 – 1277, <https://doi.org/10.1016/j.proeng.2013.04.160>

[TA-Luft, 2022] Federal Ministry for the Environment, Nature Conservation, Nuclear Safety and Consumer Protection: Technical Instructions on Air Quality Control – TA Luft). GMBI (2002), Heft 25-29, 511– 560 https://www.verwaltungsvorschriften-im-internet.de/bsvwvbund_18082021_IGI25025005.htm, accessed on 02/19/2024

[Zhang, 2021] Zhang, Q., (2021). Online Particle Measurement in Clean Gas at the Beginning of Cake-forming Dust Separation with Needled Felts in the Gas Cleaning. *Chemie Ingenieur Technik*, 94 (4), 572-584, <https://doi.org/10.1002/cite.202100053>

List of Tables

Table 1 - Operating parameters for the pilot-plant scale baghouse filter	19
Table 2 – Specifications of the aerosol measurement technology.....	20
Table 3 – Specifications of the test-dust Pural SB.	24
Table 4 – Specifications of the filter media.....	25
Table 5 - Summary of the results from the experimental parameter study taken from [Bächler et al., 2023b]......	50

List of Figures

Figure 1 – Historical evolution of statutory limits for the dust mass concentration of particle emissions as a function of exhaust gas volume flow. Image adapted from [Schmidt, 2003].	1
Figure 2 – Concept of a baghouse filter as a “black box” with only rudimentary process monitoring and control.	2
Figure 3 – Overview of the different stages of continuous operation of pulse-jet cleaned filters.	6
Figure 4 - Overview of different filter elements for surface filtration. The three different filter bags were used in this study and the filter media properties are summarized in Table 4.	7
Figure 5 – Schematic sketch of a baghouse filter and several key components.	8
Figure 6 – Differential pressure behavior of a pulse-jet cleaned filter consisting of a single filter element (left: regeneration of complete filter area - e.g. filter testing) or multiple filter elements (right: regeneration of a subset of installed filter elements).	10
Figure 7 – Consequences of increase in residual pressure difference (rapid increase of residual pressure drop Δp_r) in case of Δp -controlled (left) and of Δt -controlled (right) filter operation.	10
Figure 8 – Characteristic transient particle emission behavior for pulse-jet cleaned filters.	11
Figure 9 – Particle emission behavior for pulse-jet cleaned filters in case of additional emission contribution of small (e.g. pinhole leak - left) and large (e.g. bag failure - right) leaks between raw-gas side and clean gas side.	12
Figure 10 – Experimental methodology for investigations concerning the suitability of low-cost PM-sensors for spatial particle emission monitoring.	15
Figure 11 – Methodology for investigations concerning the trade-off between energy demand and particle emissions for pulse-jet cleaned filters.	16
Figure 12 – Modified filter test rig based on DIN ISO 11057. Image adapted from [Bächler et al., 2019a].	17
Figure 13 – Experimental procedure of the filtration tests. Image adapted from [Bächler et al., 2019a].	17
Figure 14 – Flow-sheet of the baghouse filter and the experimental set-up for the investigations presented in publication II-V. Image adapted from [Bächler et al., 2023a].	18
Figure 15 – Bag-by-bag cleaning procedure and pressure tanks enabling the filter regeneration for the corresponding rows (pressure tank 1 supplies bags 1,2 & 3, etc.).	18
Figure 16 – Image of sensor positioning in the pilot-plant scale baghouse filter. Image adapted from [Bächler et al., 2020].	19
Figure 17 – Image of the Promo® system and the welas® sensor.	21
Figure 18 – Images of the SPS30 sensor and the sensor interior.	22
Figure 19 – Images of the OPC-N3 sensor and the sensor interior.	23

Figure 20 – Cumulative particle size distributions Q_i obtained through application of different aerosol measurement devices. Image taken from [Bächler et al., 2022a].	24
Figure 21 – Top part / outlet of a filter bag. Image adapted from [Bächler et al., 2023a].	25
Figure 22 - Comparison of two exemplary particle emission peaks detected by the Alphasense low-cost PM-sensor and the Palas® reference for the spunbond filter medium following the filter test procedure detailed in publication I (measurement phase after filter aging). The time axis was shifted to align $t = 0$ at the first filter regeneration.	27
Figure 23 – Comparison of the determined emitted dust mass per cycle and filter area for the Alphasense low-cost PM-sensor and the Palas® reference for all three applied filter media following the filter test procedure detailed in publication I.	28
Figure 24 – Comparison of the determined particle size distributions for the Alphasense low-cost PM-sensor and the Palas® reference for all three applied filter media following the filter test procedure detailed in publication I (measurement phase).	28
Figure 25 - Overview of the different application scenarios for the detection of a spatial emission hotspot. Image adapted from [Bächler et al., 2023a].	31
Figure 26 - Spatial $PM_{2.5}$ profile with bag 1 as a temporal emission hotspot due to the seams of the filter bag. Image adapted from [Bächler et al., 2023a].	31
Figure 27 - Optically determined average PM clean gas concentration dependent on the number of leaks (3 mm diameter each). Image adapted from [Bächler et al., 2023a].	32
Figure 28 - Comparison of particle size distributions of the total particle emission dependent on the number of leaks for the low-cost PM-sensor and the reference. Image adapted from [Bächler et al., 2023a].	33
Figure 29 - Time dependent $PM_{2.5}$ concentration detected by the Palas® reference at the central filter bag (bag 5) and differential pressure curve. The time axis has been shifted to align $t = 0$ at the first regeneration of the corresponding filter element. Image adapted from [Bächler et al., 2020].	36
Figure 30 - Spatially resolved $PM_{2.5}$ measurement employing nine low-cost sensors (one at each individual filter bag) and comparison with the detected total emission by the Palas® reference on the clean gas side for several filtration cycles for membrane filter bags with sealed seams at a tank pressure of 8 bar. The number indicates the corresponding filter bag in the baghouse (bag-by-bag cleaning procedure according to Figure 15). The time axis has been shifted to align $t = 0$ during an arbitrary filtration cycle of the measurement run.	37
Figure 31 – Total particle emission for several filtration cycles for membrane filter bags with sealed seams at different tank pressures (3 bar, 5 bar and 8 bar) measured by the Palas® reference. The average $PM_{2.5}$ concentration was determined for an entire experimental run consisting of 30 complete filtration cycles.	37
Figure 32 - Reference measurement employing the Palas® system at bag nine with the spunbond medium and flow-velocity measured with a Schmidt® SS 20.250 flow sensor. Image adapted from [Bächler et al., 2020].	38
Figure 33 - Detail view of the particle emission of initial filtration cycles of an exemplary filter bag for both filter media and total emission compared to the end of the first measurement procedure. Image adapted from [Bächler et al., 2022b].	40

Figure 34 - Local particle emission measurement at an individual filter bag (bag 4) applying the Palas® reference for different tank pressures and two filter media. Image adapted from [Bächler et al., 2022b].	41
Figure 35 - Comparison of the average clean gas particle concentration of the total emission for both filter media of publication IV and the additional needle-felt filter medium. Image modified from [Bächler et al., 2022b].	42
Figure 36 - Direct comparison between the low-cost PM-sensor and the reference at an individual filter bag. Image adapted from [Bächler et al., 2022b].	43
Figure 37 - Evaluation of filter operation based on power consumption and particle emissions for a certain set of parameters ($w_{\text{filter}} = 2.5 \text{ cm s}^{-1}$, $c_{\text{raw-gas}} = 15 \text{ g m}^{-3}$, $p_{\text{Tank}} = 3 \text{ bar}$). Image adapted from [Bächler et al., 2023b].	46
Figure 38 - Detail view of the power minimum of the operation curves at different raw-gas concentrations ($w_{\text{filter}} = 2 \text{ cm s}^{-1}$, $p_{\text{Tank}} = 3 \text{ bar}$). Image adapted from [Bächler et al., 2023b].	47
Figure 39 - Comparison of cycle times at minimum power regarding energy demand and particle emissions for two different tank pressures (3 and 6 bar) at varying raw-gas concentrations and filter face velocities. In case of a less pronounced power minimum (multiple datapoints), only a single datapoint is displayed. Image adapted from [Bächler et al., 2023b].	48
Figure 40 - Comparison of experimental data ($w_{\text{filter}} = 2 \text{ cm s}^{-1}$; $p_{\text{tank}} = 3 \text{ bar}$; $c_{\text{raw-gas}} = 15 \text{ and } 30 \text{ g m}^{-3}$) and model calculations regarding the required power for filter operation. Image adapted from [Bächler et al., 2024a].	51
Figure 41 - Modeling of particle emissions for the entire set of experimental parameters based on the determination of the emitted dust mass for 3 bar tank pressure and an individual empirical coefficient for each set of parameters. Image adapted from [Bächler et al., 2024a].	52
Figure 42 - Modeled operation curves for the complete set of parameters and comparison to experimental data from publication V. Image adapted from [Bächler et al., 2024a].	52
Figure 43 – Measurement behavior of low-cost PM-sensors under exposure to increased particle number concentrations in an aerosol test chamber.	56
Figure 44 - Impact of a moving average on the decay behavior of particle emission peaks (publication I). The time axis was shifted to align the maximum of the emission peak at 1 minute time.	57
Figure 45 – Particle emission peaks detected at the outlet of an individual filter bag for the pilot plant scale baghouse filter and an industrial filtration process (raw-gas concentration $\approx 60 \text{ mg/m}^3$) [Bächler et al., 2024b]. No direct comparability of the corresponding emission behavior.	60
Figure 46 – Particle emission evolution for a recently installed needle-felt filter bag in the industrial baghouse filtration process. Image adapted from [Bächler et al., 2024b].	61
Figure 47 – Exemplary image of the „ideal“ emission behavior for an exemplary filter bag. The time axis has been shifted to align the maximum of the initial emission peak at $t = 0$. Image adapted from the supplementary information of [Bächler et al., 2023a].	62
Figure 48 – Schematic operation curve for a pulse-jet cleaned filter.	64
Figure 49 – Emission characteristic for Δt -controlled filter operation. Image adapted from the supplementary information of [Bächler et al., 2023b].	65

APPENDIX

The following chapter includes the publications and the supplementary information for the corresponding articles. The publications are listed based on their appearance within this publication based dissertation.

Publication I

Title: Characterization of the emission behavior of pulse-jet cleaned filters using a low-cost particulate matter sensor

Authors: Peter Bächler, Jörg Meyer, Achim Dittler

Journal: Gefahrstoffe – Reinhaltung der Luft

Year of Publication: 2019

Volume and Issue: 79 (11-12)

Page Numbers: 443 – 450

Reference: [Bächler et al., 2019a]

Abstract:

The reduction of fine dust emissions with pulse-jet cleaned filters plays an important role in industrial gas cleaning to meet emission standards and protect the environment. The dust emission of technical facilities is typically measured “end of pipe”, so that no information about the local emission contribution of individual filter elements exists. Cheap and compact low-cost PM-sensors, which have been prominently applied for immission monitoring of fine dust concentrations in recent years have the potential for emission measurement of filters to improve process monitoring. This publication discusses the suitability of a low-cost PM-sensor, the model SPS30 from the manufacturer Sensirion, in terms of the potential for particle emission measurement of surface filters in a filter test rig based on DIN ISO11057. A Promo[®] 2000 in combination with a welas[®] 2100 sensor serves as the optical reference device for the evaluation of the detected PM_{2.5} concentration and particle size distribution of the emission measured by the low-cost sensor. The Sensirion sensor shows qualitatively similar results of the detected PM_{2.5} emission as the low-cost sensor SDS011 from the manufacturer Nova Fitness, which was investigated by Schwarz et al. in a former study. The typical emission peak after jet-pulse cleaning of the filter, due to the penetration of particles through the filter medium, is detected during Δp -controlled operation. The particle size distribution calculated from the size resolved number concentrations of the low-cost sensor yields a distinct distribution for three different employed filter media and qualitatively fits the size distribution detected by the Palas[®] reference. The emission of these three different types of filter media can be distinguished clearly by the measured PM_{2.5} concentration and the emitted mass per cycle and filter area, demonstrating the potential for PM emission monitoring by the low-cost PM-sensor. During the period of Δt -controlled filter aging, a decreasing emission, caused by an increasing amount of stored particles in the filter medium, is detected. Due to the reduced particle emission after filter aging, the specified maximum concentration of the low-cost sensor is not exceeded so that coincidence is unlikely to affect the measurement results of the sensor for all but the very first stage of filter life.

Characterization of the emission behavior of pulse-jet cleaned filters using a low-cost particulate matter sensor

P. Bächler, J. Meyer, A. Dittler

ABSTRACT The reduction of fine dust emissions with pulse-jet cleaned filters plays an important role in industrial gas cleaning to meet emission standards and protect the environment. The dust emission of technical facilities is typically measured "end of pipe", so that no information about the local emission contribution of individual filter elements exists. Cheap and compact low-cost sensors for the detection of particulate matter (PM) concentrations, which have been prominently applied for immission monitoring in recent years have the potential for emission measurement of filters to improve process monitoring. This publication discusses the suitability of a low-cost PM-sensor, the model SPS30 from the manufacturer Sensirion, in terms of the potential for particle emission measurement of surface filters in a filter test rig based on DIN ISO 11057. A Promo® 2000 in combination with a Welas® 2100 sensor serves as the optical reference device for the evaluation of the detected $PM_{2.5}$ concentration and particle size distribution of the emission measured by the low-cost sensor. The Sensirion sensor shows qualitatively similar results of the detected $PM_{2.5}$ emission as the low-cost sensor SDS011 from the manufacturer Nova Fitness, which was investigated by Schwarz et al. in a former study. The typical emission peak after jet-pulse cleaning of the filter, due to the penetration of particles through the filter medium, is detected during Δp -controlled operation. The particle size distribution calculated from the size resolved number concentrations of the low-cost sensor yields a distinct distribution for three different employed filter media and qualitatively fits the size distribution detected by the Palas® reference. The emission of these three different types of filter media can be distinguished clearly by the measured $PM_{2.5}$ concentration and the emitted mass per cycle and filter area, demonstrating the potential for PM emission monitoring by the low-cost PM-sensor. During the period of Δt -controlled filter aging, a decreasing emission, caused by an increasing amount of stored particles in the filter medium, is detected. Due to the reduced particle emission after filter aging, the specified maximum concentration of the low-cost sensor is not exceeded so that coincidence is unlikely to affect the measurement results of the sensor for all but the very first stage of filter life.

Charakterisierung der Emission von druckstoßgereinigten Oberflächenfiltern mit einem Low-Cost-Feinstaubsensor

ZUSAMMENFASSUNG Die Minderung von Feinstaubemissionen durch den Einsatz von druckstoßgereinigten Oberflächenfiltern im Rahmen von industrieller Gasreinigung spielt eine wichtige Rolle bei der Einhaltung von Emissionsgrenzwerten und dem Schutz der Umwelt. Bisher erfolgt die Messung von Staubemissionen von technischen Anlagen häufig nur am Kamin, sodass keine Informationen über den lokalen Emissionsbeitrag einzelner Filterelemente vorhanden sind. Kompakte und kostengünstige Feinstaubsensoren, die in den letzten Jahren vermehrt zur Messung von Partikelimmissionen eingesetzt wurden, haben das Potenzial zur Erfassung der Partikelemission in Filteranlagen und der Verbesserung der Prozessüberwachung. In dieser Veröffentlichung wird die Eignung eines kostengünstigen Feinstaubensors, dem SPS30 des Herstellers Sensirion, zur Emissionsmessung von Partikeln bei der Oberflächenfiltration in einem Filterprüfstand, angelehnt an die Norm DIN ISO 11057, diskutiert. Ein Promo® 2000 in Kombination mit einem Welas® 2100 Sensor des Herstellers Palas® wurde als optische Referenz zur Bewertung des Low-Cost-Sensors eingesetzt. Der SPS30 liefert qualitativ ähnliche Ergebnisse wie der SDS011 des Herstellers Nova Fitness, welcher bereits von Schwarz et al. untersucht wurde. Der charakteristische Emissionspeak nach der Abreinigung eines Filtermediums durch die Penetration von Partikeln durch das Filtermedium wird während des differenzdruckgesteuerten Betriebs detektiert. Die Partikelgrößenverteilung, welche anhand der detektierten größenselektiven Anzahlkonzentrationen des Low-Cost-Sensors berechnet wurde, lässt deutliche Unterschiede zwischen drei unterschiedlichen Filtermedien erkennen und zeigt eine qualitative Übereinstimmung mit der Palas®-Referenz. Die Emission der verschiedenen Filtermedien kann anhand der gemessenen $PM_{2.5}$ -Konzentrationen und der Masse pro Zyklus und Filterfläche klar unterschieden werden, was das Potenzial für eine PM-Emissionsüberwachung mittels Low-Cost-Sensoren aufzeigt. Während der zeitgesteuerten Alterungsphase des Filtermediums wird eine sinkende Emission, bedingt durch eine zunehmende Menge an eingelagerten Partikeln im Filtermedium, detektiert. Aufgrund der gesunkenen Emission nach der Alterungsphase des Filtermediums wird die spezifizizierte Maximalkonzentration des Low-Cost-Sensors eingehalten, sodass die Messergebnisse nach einer kurzen Einlaufphase nicht durch Koinzidenz beeinflusst werden.

1 Introduction

In the context of environmental pollution control, facilities are legally obligated to measure their emission of pollutants into the environment. Bundes-Immissionsschutzgesetz (BImSchg) sets the legal framework for emission monitoring of facilities where a high risk for pollution exists [1]. TA Luft sets limits regarding different species of pollutants, restricting dust emissions to a maximum concentration of 20 mg/m³ [2]. Surface filtration plays an important role in industrial gas cleaning, where high raw-gas concentrations of dust have to be removed from dust-laden gas flows. Particles are collected at the surface of a filter medium and form a filter cake with a high separation efficiency. With increasing thickness of the filter cake during operation, the pressure difference between the raw and the clean gas side rises. To enable stable and economic operation, filters are periodically regenerated via a jet pulse from the clean gas side after reaching a preset differential pressure or after a specified time (Δp - or Δt -controlled operation). The removal of the dust cake causes the typical emission behavior of surface filters, where particles mainly penetrate the filter medium right after cleaning, and an emission peak occurs until a sufficient dust cake is formed again [3; 4].



In industrial applications, the filters are typically arranged as filter bags inside one or multiple filter houses, depending on the raw-gas volume flow. Particulate matter (PM) emissions of industrial facilities are mainly monitored at the end of the pipe. Smaller scale apparatuses that are not legally obligated to measure their PM emission often do not have any form of emission monitoring. PM emissions can either be measured gravimetrically by extracting a sample flow through a probe or via other methods, like laser extinction or triboelectrical measurement [5]. As only one set of measurement equipment monitors the emission of the entire system, the local emission behavior of individual filter bags remains unknown. Improved process monitoring due to local measurement could enable a more efficient operating behavior of filter houses regarding their energy demand and emissions and facilitate maintenance procedures. Leakages are a common occur-

rence in filter houses and contribute greatly to the emissions. Conventional methods of leakage detection include analysis with fluorescent dust to detect damaged filter bags. This trouble shooting is time consuming and even unsuitable for some applications, thus operators would benefit greatly from online measurement techniques to detect leaks [4].

A potential online-measurement technology for emission detection in surface filters are low-cost PM sensors based on single particle light scattering. These cheap and compact devices were originally established for online PM monitoring of smaller devices (e. g. air conditioning). A recent application of these sensors is immission measurement at indoor and outdoor areas to monitor particle concentrations and the respective fine dust fractions like PM₁₀ or PM_{2.5} with high temporal and spatial resolution [6 to 10]. Their compact design also allows for an application inside baghouse filters to investigate the local emission behavior of individual filter elements. Problems like interferences due to changes in temperature or humidity, long term stability and inter-sensor variability between different sensors of the same model are known from their application in immission measurement [6; 8; 10]. In comparison to changing outdoor environments due to seasons and the weather, steady state processes in many cases do not show high fluctuations regarding process parameters, so that the risk of inaccuracies due to changing measurement conditions is reduced. This means that low-cost sensors could be suited especially for emission monitoring with an according on-site calibration.

Schwarz et al. showed the qualitative behavior of the PM concentration measured by the sensor SDS011 from Nova Fitness during surface filtration [11]. This study expands on the qualitative assessments, employing another low-cost sensor, the SPS30 from the manufacturer Sensirion. The detected particle concentrations are compared to a state-of-the-art advanced optical particle counter from Palas® as reference device. The emission behavior of three different filter media, measured by the low-cost sensor and the reference system is shown using a filter test rig based on DIN ISO 11057.

Table 1. Sensor information [12; 13].

Device	SPS30	Promo® 2000 with Welas® 2100 Promo® 2000 not shown in picture
	 1 cm	 5 cm
Manufacturer	Sensirion	Palas®
Measurements	Mass based concentration: PM ₁ , PM _{2.5} , PM ₄ , PM ₁₀ ; Number based concentration*: PM _{0.5} , PM ₁ , PM _{2.5} , PM ₄ , PM ₁₀ ; *typical particle size *(Values are in fact PN _x number concentrations)	Mass and number based total concentration and size distributions with size resolved PM conversion
Detectable size range	0.3 to 10 µm	0.2 to 10 µm; 0.3 to 17 µm; 0.6 to 40 µm (user selectable)
Size categorization	5 bins	64 bins per decade
Maximum concentration	Mass based: 1 mg/m ³ Number based: 3000 #/cm ³	5 · 10 ⁵ #/cm ³
Approximate cost	30 €	> 30.000 €
Length x Width x Height	40 mm x 40 mm x 12 mm	245 mm x 100 mm x 80 mm
Response time	≈ 1 s	≈ 1 s

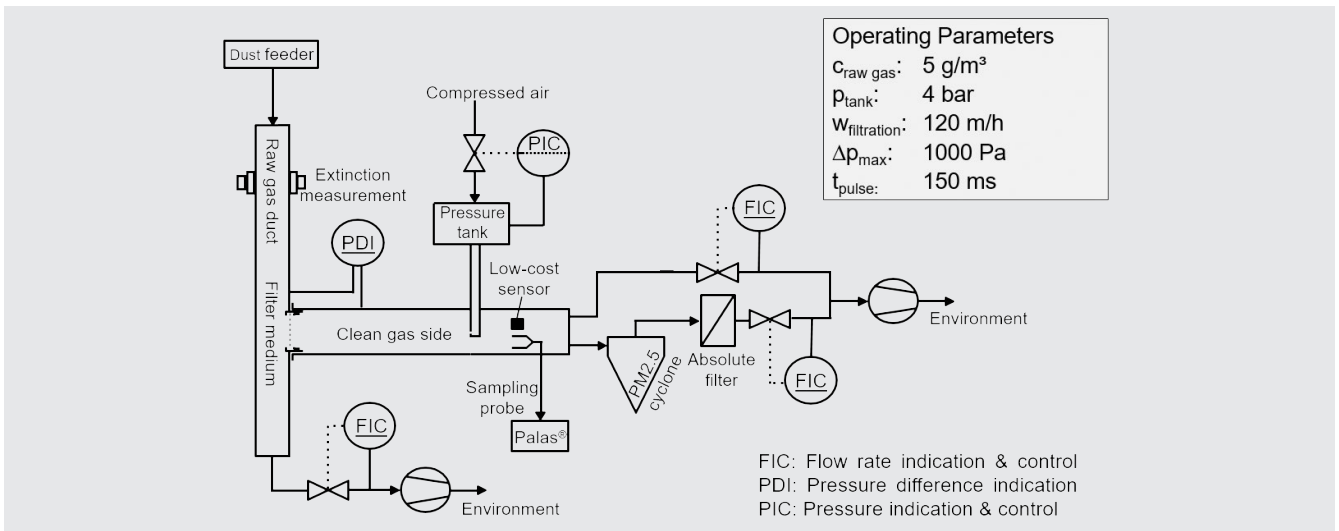


Figure 1. Modified test rig based on DIN ISO 11057.

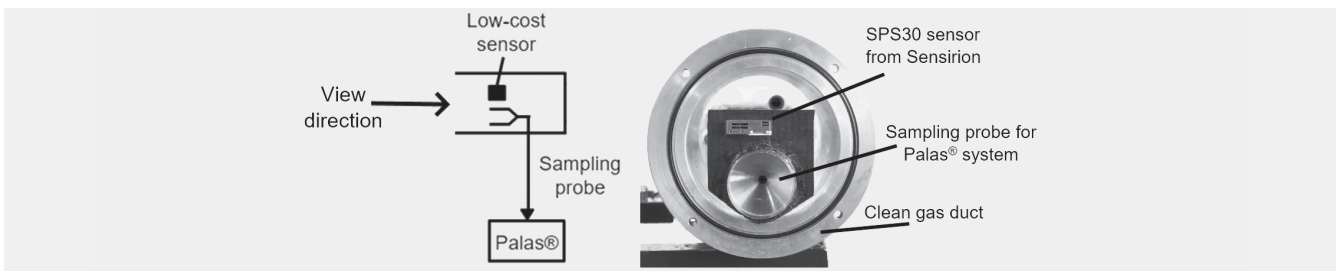


Figure 2. Arrangement of the sampling probe for the Palas® reference and the Sensirion sensor on the clean gas side.

2 Experimental set-up, procedures and materials

2.1 Measurement technology

Wide varieties of low-cost PM-sensors from different manufacturers are commercially available. The measurement principle is based on optical light scattering of single particles passing through a defined sampling volume. Many of the sensors do not offer comprehensive information in their datasheet. The SPS30 from Sensirion has a detailed datasheet compared to other available low-cost sensors, and in addition to the typical PM-weighted mass concentrations, it can output size resolved number based particle concentrations [12]. The specifications taken from the datasheet of the low-cost sensor and the optical reference, consisting of a Promo® 2000 with a Welas® 2100 sensor from the manufacturer Palas®, are listed in **table 1**.

Regarding the low-cost sensor specification in the context of surface filtration, the most penetrating particle size of surface filters is commonly found around a particle diameter of 0.1 to 1 μm, which overlaps the detectable size range of the low-cost sensor [4]. There are two values given for the maximum concentration of the Sensirion sensor. On the one hand, a maximum mass concentration of 1 mg/m³ and on the other hand a maximum number concentration of 3 000 #/cm³ [12]. Only the number concentration is relevant for particle measurement, since high number concentrations lead to multiple particles simultaneously passing through the optical measurement volume so that they are detected as a single, bigger particle (coincidence error) [14]. The maximum concentration is expected to be exceeded in surface fil-

tration under certain conditions, depending on filter medium design, operating conditions, media age and dust properties.

The reason why the Palas® system was selected as the optical reference for the experiments is given by the high maximum concentration and the accurate size categorization. The selected measurement range for the Palas® system was 0.2 to 10 μm to be close to the specifications of the low-cost sensor and the most penetrating particle size of surface filters.

The Sensirion sensor is known to be calibrated against a TSI DustTrak™ DRX Aerosol Monitor 8533 and the PM_{2.5} concentration is verified against a defined potassium chloride aerosol [12]. This calibration results in differences compared to the Palas® reference, where different particle densities, refractive indices and form factors can be considered in the configuration of the instrument software, depending on the measured aerosol [13].

2.2 Filter test rig

The general layout of the filter test rig is based on ISO11057 [15]. The optical emission measurement via the Palas® reference and the low-cost sensors are added as extensions to the norm (**figure 1**).

A dust feeder disperses the test dust into the raw gas duct, where an extinction measurement monitors a constant raw gas concentration. The volume flow to the clean gas side is adjusted to a filtration velocity of 120 m/h. The dust is collected at the surface of the filter medium, so that a dust cake is formed and the differential pressure between raw and clean gas side increases. When reaching a preset maximum value of 1 000 Pa, a jet pulse

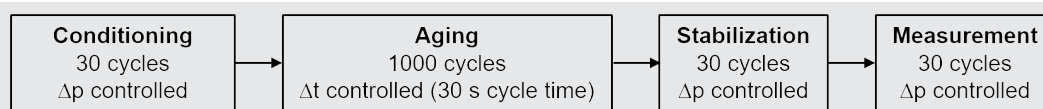


Figure 3. Experimental procedure of the filtration tests.

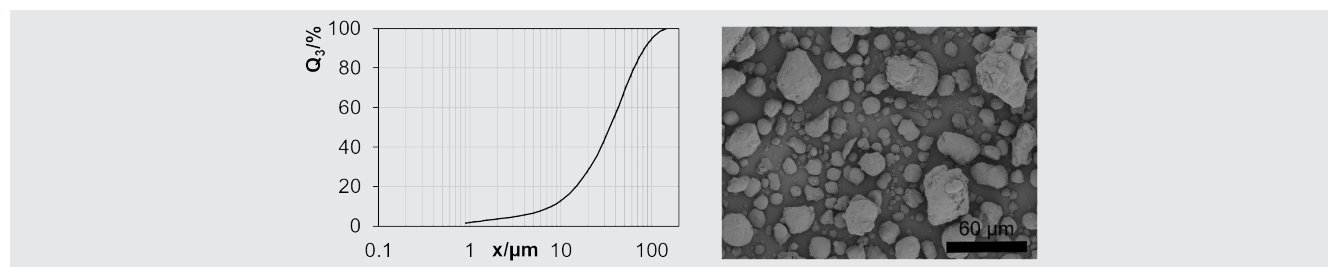


Figure 4. Particle size distribution (cumulative, mass based) from PURAL SB® measured via laser diffraction and SEM image of the selected test dust PURAL SB®.

from the pressure tank (tank pressure of 4 bar) is released to enable dust cake removal from the filter surface (pulse length of 150 ms). The low-cost sensor and a sampling probe for the Palas® system are located at the end of the clean gas side (figure 2). A $PM_{2.5}$ sharp cut cyclone in combination with a glass fiber filter serves as an additional gravimetric comparison for the measurement of the $PM_{2.5}$ emissions.

The experimental procedure has been adapted from the filter test procedure in DIN ISO11057. A filter test consists of four different stages (figure 3). The first phase, consisting of 30 filtration cycles, is the conditioning phase, where an unstable operation with high fluctuations in terms of residual pressure and cycle time are possible. Afterwards, a Δt -controlled filter aging step causes the storage of particles inside the filter medium to emulate conditions of the filter medium similar to real operation. Afterwards, a stabilization phase and a measurement phase, each consisting of 30 Δp -controlled cycles, are performed. The cycle times for the filter aging step and number of cycles for the stabilization have been slightly altered compared to the standard [15].

The low-cost sensor was placed inside a holder above the sampling probe for the Palas® system on the clean gas side as displayed in figure 2. The influence of the holder on the flow-conditions on the clean gas side is expected to be negligible, due to the low flow velocity and low MPPS particle size of the emissions found on the clean gas side.

2.3 Test dust

The selected test dust was PURAL® SB from the manufacturer Sasol. PURAL SB® is nontoxic and easy to handle. The density of PURAL SB is 2 800 kg/m³ and was included in the configuration of the Palas® system for the determination of mass concentrations.

The index of refraction of the test dust was provided by the manufacturer and is about 1.64 (-). Since it was not possible to adjust the index of refraction to exactly this value and no dust specific calibration of the Palas® reference was performed, the index of refraction in the configuration of the Promo® 2000 was left at the default setting of 1.59 (-). The Sensirion sensor does not allow a configuration regarding dust specific properties and the default values are used in this study.

The fine dust fraction of PURAL SB® is rather low (figure 4), but the dust is non-agglomerating and shows a high penetration

of smaller particles through the filter medium. This leads to rather high emissions with peak concentrations potentially exceeding the specifications of the low-cost sensor at 3 000 #/cm³, so that there is a possibility of coincidence during measurement. Due to the non-agglomerating behavior and the low adhesive and cohesive properties of the dust, there is a reduced risk for contamination of the optics of the low-cost sensors. Sticky and agglomerating test dusts might limit the suitability for emission measurement and reduce the life time of the sensors.

2.4 Filter media

Three different filter media were selected for the experiments to evaluate the low-cost sensors' capability of measuring different emission levels. The specifications of the media are listed in table 2. Medium A and medium B share a similar permeability despite a much higher area weight of medium B. The key difference between these two media and filter medium C consists of an ePTFE layer laminated to the upstream side of medium C, which causes a lower permeability, a higher dust separation efficiency and a lower dust penetration into the depth of the medium.

3 Results and discussion

In the following section, only the results for the particle size distributions as well as the $PM_{2.5}$ and number concentrations will be discussed in detail, since only the $PM_{2.5}$ values of the Sensirion sensor are calibrated against a TSI DustTrak™ reference. The main part of this study consists of a comparison between the low-cost sensor and the Palas® system in terms of the measured $PM_{2.5}$ concentrations and particle size distributions. First, the suitability of the sensor regarding PM-emission monitoring during the Δp -controlled conditioning and measurement phase are discussed. Afterwards, the development of the filter emission during the Δt -controlled filter aging procedure is shown.

3.1 Evaluation of valid measurement regions regarding filter conditioning and measurement phase

The conditioning phase consists of 30 regenerations of a new sample of filter medium. After each regeneration, a temporary increase in mass and number based particle concentration is detected by both optical devices. The filtration cycles during condi-

Table 2. Specifications of employed filter media. PES: polyester, PA: polyamide, PE: polyethylene, PPS: polyphenylene sulfide, ePTFE: expanded polytetrafluorethylene.

Medium	Area weight/ gm ⁻²	Thickness/ mm	Permeability (200 Pa)/ ldm ² min ⁻¹	Fiber material & remarks
A	240	1	100	PES, PA, hydro entangled microfilaments
B	600	2	70	PE, singed upstream side
C	500	1.9	30	PPS (heat set) with laminated ePTFE membrane

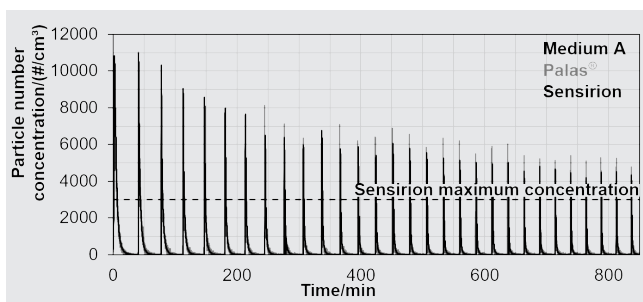


Figure 5. Number concentration for the Palas® reference (grey) and the low-cost sensor (black) for medium A in comparison with the maximum number concentration of the low-cost sensor (dashed line) during the 30 cycles of the conditioning phase.

tioning are usually part of an unstable operation, where the cycle times and residual pressure after a regeneration may change and scatter significantly. Additionally, the PM emission of a filter is at its highest during these first cycles. With an ongoing number of regenerations, PM emission, cycle times and residual pressure adjust to a stable level with lower fluctuations [2; 4].

The detected particle number concentration of the Palas® reference (total concentration) and the Sensirion sensor (PM₁₀ number concentration) during filter conditioning of medium A (highest emissions of all 3 filter media) are displayed in **figure 5**. The high number concentrations exceed the specified maximum number concentration of the low-cost sensor (3000 #/cm³), even though the peak particle number concentrations decrease over the course of the 30 filtration cycles of filter conditioning.

The detected number concentration of the Sensirion sensor is below the Palas® reference, which has a specified maximum number concentration of 50 000 #/cm³ and thus, is suitable for higher dust concentrations. The accuracy of the detected PM emission of the low-cost sensor is probably affected by coincidence when exceeding the specified concentration range. Due to the consecutive aging steps after the conditioning phase, the peak number concentrations decrease further, so that the specified maximum concentration of the sensor is only rarely exceeded during the subsequent measurement phase (**figure 6**). This allows for an in-depth evaluation of the measurement phase, where the reliability of the data generated by the low-cost sensor is unlikely to be affected by coincidence.

3.2 Evaluation of the PM emission and particle size distribution during the measurement phase

Before filter aging and stabilization during the conditioning phase, peak concentrations of far above 3 000 #/cm³ occurred af-

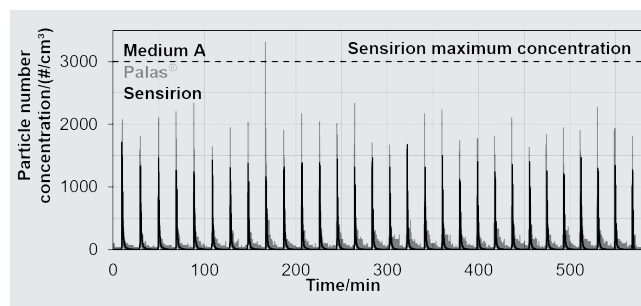


Figure 6. Number concentration for the Palas® reference (grey) and the low-cost sensor (black) for medium A in comparison with the maximum number concentration of the low-cost sensor during the 30 cycles of the measurement phase.

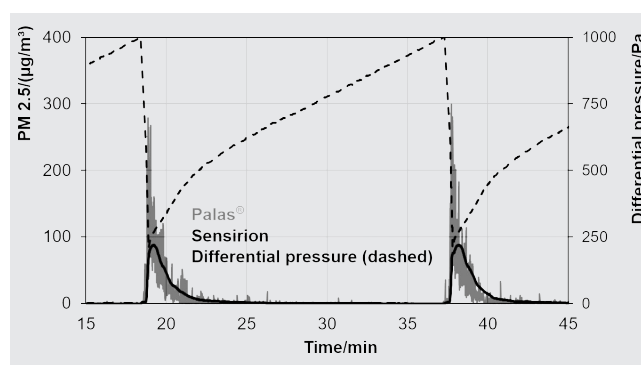


Figure 7. First two emission peaks from the measurement phase of the low-cost sensor (black) and the Palas® reference (grey) for medium B.

ter the regeneration of the filter medium and exceeded the maximum specified concentration of the low-cost sensor. After the filter aging step, the peak PM_{2.5} concentrations decreased to a level where the low-cost sensor and the Palas® reference detect concentrations within the specified concentration range of the low-cost sensor, particularly during the measurement phase. The typical PM emission of a surface filter consists of an emission peak detected as an increase in PM_{2.5} mass concentration after the jet pulse due to particles penetrating the filter medium until a new dust cake is formed. This behavior is clearly visible both for the low-cost sensor and the Palas® system. The result corresponds to the findings shown by Schwarz et al. for the SDS011 sensor from Nova Fitness, where a similar qualitative correlation was presented [11]. As an example, the first two emission peaks of the measurement phase of medium B are displayed in **figure 7**.

The detected peak PM_{2.5} concentration of the Sensirion sensor is lower compared to the Palas® system, which shows a higher amount of hissing due to a higher sensibility of the Welas® 2100 sensor. The curve of the Sensirion sensor appears smoother and it is unknown, if the internal data processing of the sensor performs some form of time averaging (same nominal time resolution of both measurement devices).

For a quantitative evaluation assuming a constant filtration flow rate, the mass per cycle and filter area can be calculated for both measurement devices to generate one single value for each emission peak that is easy to compare. The time dependent PM-curve is integrated numerically and multiplied with the constant filtration velocity:

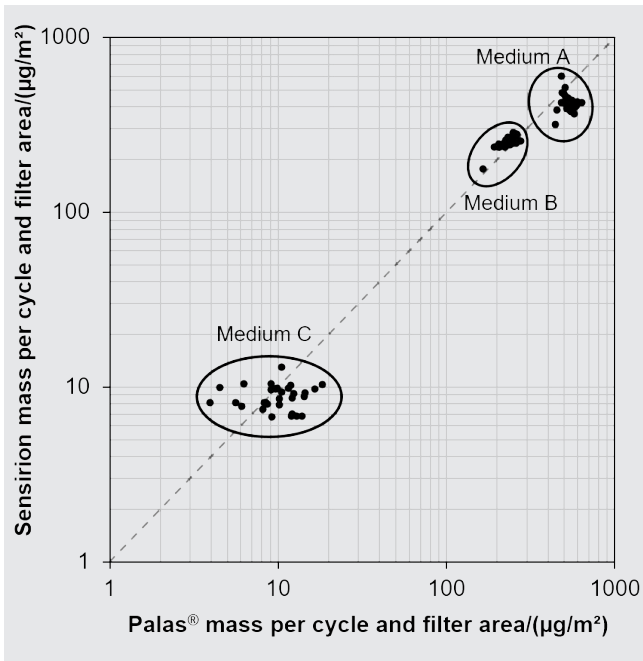


Figure 8. Scatterplot of mass per cycle and filter area calculated from the PM-curve of the optical measurement devices for all filter media.

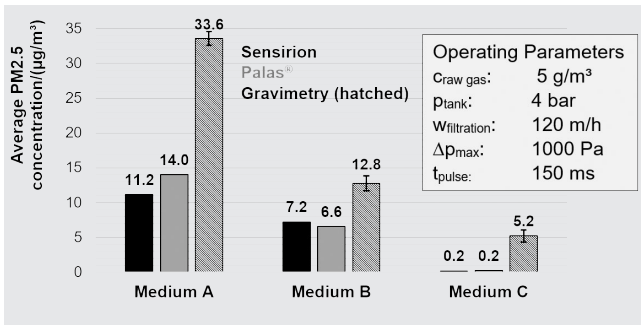


Figure 9. Average PM_{2.5} concentration for the 30 filtration cycles of the measurement phase for the optical and gravimetric PM_{2.5} measurement.

$$PM_{2.5} \text{ mass per cycle and filter area} = \int_{t_{0,i}}^{t_{0,i}+t_{\text{cycle}}} c_{m,PM_{2.5}}(t) \cdot \frac{\dot{V}}{A_{\text{filter}}} dt$$

$$= w_{\text{filtration}} \cdot \int_{t_{0,i}}^{t_{0,i}+t_{\text{cycle}}} c_{m,PM_{2.5}}(t) dt$$

In figure 8, the results for the calculated mass per cycle and filter area for the Sensorion sensor are plotted versus the values of the Palas® reference for each filtration cycle. The three filter media all show distinct emission levels, with medium A and B having similar PM_{2.5} emission levels while the PM_{2.5} emission of medium C is orders of magnitude lower due to the membrane layer.

The three emission levels can also be recognized via the average PM_{2.5} concentrations during the measurement phase. The average concentrations detected by the optical devices were determined for the three measurement phases and compared to the gravimetric measurement with the PM_{2.5} sharp cut cyclone (figure 9). Only the density of the test dust (2 800 kg/m³) was taken into account regarding the configuration of the Palas® system, so that spherical particles with a refractive index of 1.59 (-) were assumed for the evaluation. Without a dust specific calibration, the gravimetric measurement is not expected to match the optical results. The determination of gravimetric mass concentrations is especially difficult when considering low mass differences due to small particles in the PM_{2.5} fraction.

However, the different emission levels of the three filter media can be clearly distinguished via the average concentrations. The average concentration determined by the optical devices within one medium are similar, even though different calibrations of the optical devices are deployed by the manufacturers. Deviations exist for the gravimetrically determined values, which are always higher compared to the optical measurement. Qualitatively, the gravimetric concentrations also verify the three distinct emission levels of the filter media.

The mass differences measured for the gravimetric PM_{2.5} determination were sufficiently above the precision of measurements of the deployed balance. The respective mass differences did, however, not exceed several 100 µg and can be easily influenced by bigger particles that bypass the sampling of the optical devices, smaller particles below the detectable size range of the

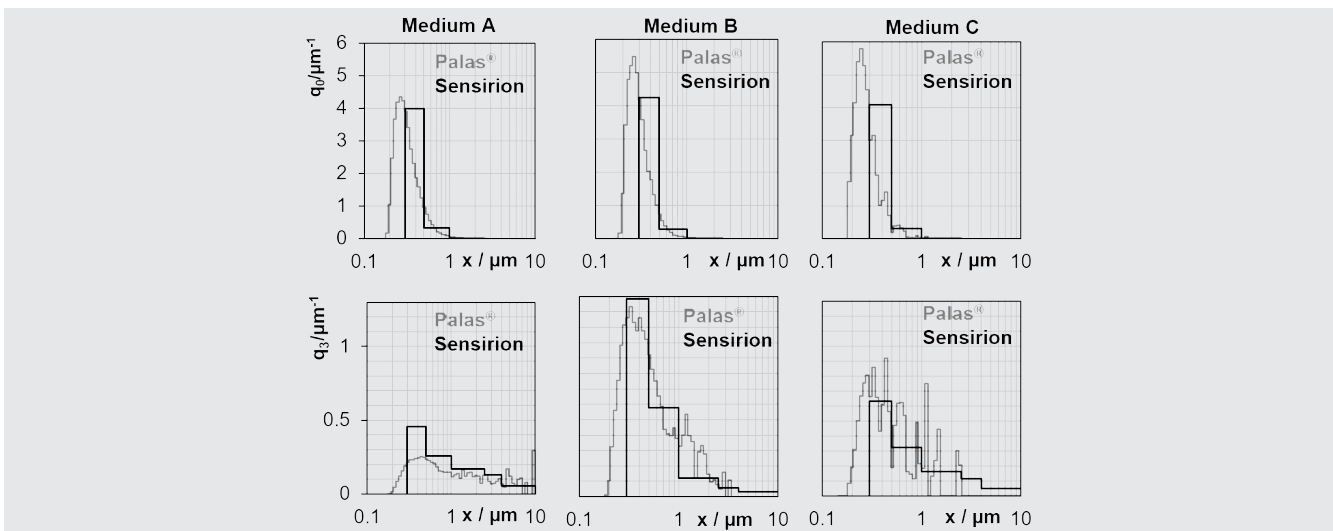


Figure 10. Particle size distribution for the Palas® system (grey) and the low-cost sensor (black) for all three filter media (top: number based; bottom: mass based).

optical devices or external influences (e. g. handling of the sample).

In addition to the PM data, the low-cost sensor also yields size resolved number concentrations, so that the calculation of particle size distributions is possible and there is a potential for size-resolved information from the low-cost sensor. The calculated particle size distributions from the number concentrations detected by the low-cost sensor and the measured distribution from the Palas® systems are displayed in **figure 10**. All filter media show a distinct size distribution based on the data of the Palas® reference. The particle number distribution of the low-cost sensor appears similar for all three filter media, where the highest amount of particles is correctly detected in the size bin closest to the most penetrating particle size (0.3 to 0.5 µm). Regarding the volume distribution, the size distribution of the low-cost sensor qualitatively fits the distributions detected by the Palas® system, which has a more accurate size categorization compared to the mere 5 size bins of the Sensirion sensor.

In addition to the number concentrations that allow for a calculation of particle size distributions, one of the output values of the Sensirion sensor is a “typical particle size” (**Figure 11**). The typical particle size changes over the course of the filtration cycle and shows a behavior similar to the PM_{2.5} concentration (peak increase after regeneration) for medium A and medium B.

The average typical particle size across the entire filter test for medium B is lower than for medium A. Though the membrane medium has the lowest emission, the average typical particle size is the highest of all three filter media. The values for the typical particle size remain inside the MPPS region of surface filters for all three filter media, however it cannot be clearly assigned to the most penetrating particle size determined by the Palas® system (figure 10). As there exists no information how this typical particle size is determined, the significance of the value is inconclusive.

3.3 Characterization of the PM emission during the Δt-controlled filter aging procedure

The filter aging step consists of 1 000 regeneration pulses with a cycle time of 30 s (figure 3). The aim of the artificial filter aging is to create conditions of the filter medium closer to the real application. During filter aging, the formation of a complete dust cake is not possible due to short cycle times, so that a constant emission flux of particles that penetrate the filter medium can be detected on the clean gas side. Particles are stored inside the filter medium, similar to depth filtration, so that the residual pressure drop increases over the course of the filter aging procedure. The stored particles have an additional effect, as they improve the separation efficiency and thus lower the emission concentration. This typical behavior of a decreasing particle emission during filter aging is detected by both optical measurement devices and displayed in **figure 12** (one minute averaged values).

Differences regarding the residual pressure drop and the emission between the employed filter media exist. The membrane medium has the lowest emission and the highest residual pressure drop, corresponding to its low permeability. The three emission levels (figure 8 and figure 9) can also be identified according to the PM_{2.5} concentrations during the filter aging step.

Another indication for filter aging can be demonstrated by comparing the PM emission peaks before and after filter aging and stabilization. In **Figure 13**, the 29th emission peak of the

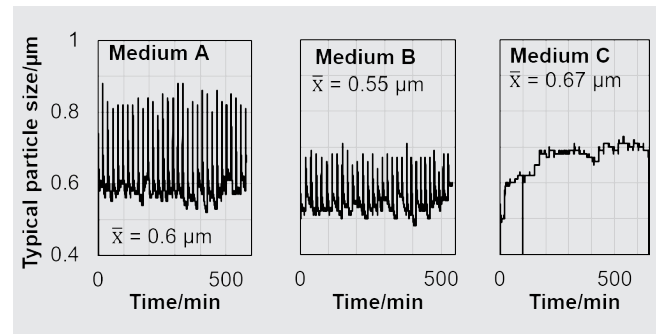


Figure 11. Typical particle size determined by the Sensirion sensor.

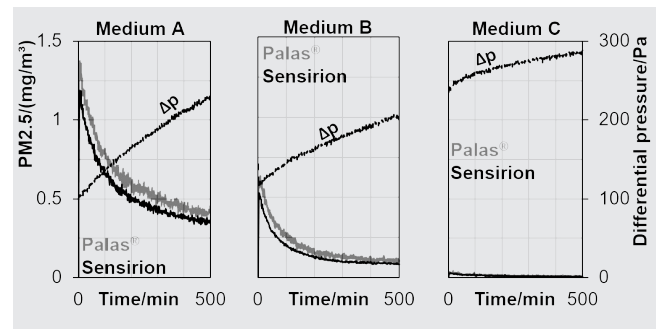


Figure 12. PM_{2.5} concentrations and residual pressure drop (one minute averaged values) during the filter aging procedure for the low-cost sensor (black) and the Palas® system (grey) for all filter media.

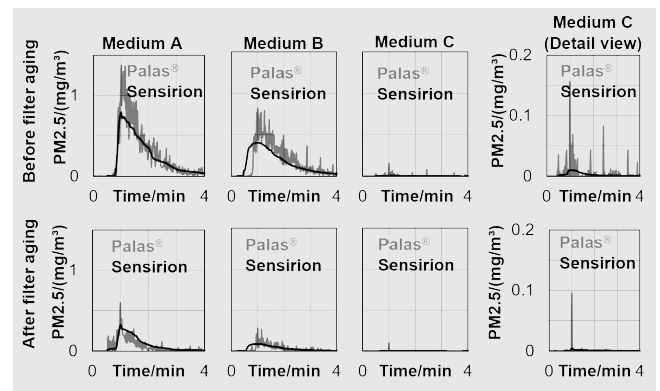


Figure 13. 29th emission peak of the conditioning phase (before filter aging) and first peak of the measurement phase (after filter aging) for the Palas® reference (grey) and the low-cost sensor (black) for all three media.

conditioning phase is compared to the first peak of the measurement phase, after filter aging. The 29th peak of conditioning is selected for comparison instead of the 30th peak, because the pump switches off after performing the last regeneration of the corresponding phase and thus the emission peak of the last cycle is not fully representative. The time axis is shifted to align the maximum of the corresponding emission peak at 1 minute time for better comparability between the individual peaks.

4 Summary and outlook

The low-cost PM-sensor SPS30 from the manufacturer Sensirion was evaluated regarding its suitability for PM emission monitoring during filter tests based on DIN ISO11057. A Palas®

system consisting of a Palas Promo® 2000 in combination with a Welas® 2100 sensor served as the optical reference device for the filter tests.

The characteristic PM emission behavior of surface filters consisting of a PM emission peak after pulse-jet regeneration was qualitatively shown by the low-cost sensor and the reference. In addition to the qualitative detection of the emission peak, three distinct emission levels of the three employed filter media can be clearly identified by the mass per cycle and filter area and the average mass concentration during the measurement phase of the experiments.

The calculated particle size distributions of the low-cost sensor show a distinct volume distribution for each filter medium and qualitatively fit the detected size distributions detected by the Palas® reference. The “typical particle size” that is determined by the low-cost sensor yields inconclusive results, where the generated data cannot be confirmed by the reference measurement. The accuracy of the sensor is limited due to the small number of size bins for size categorization compared to the Palas® reference. Different low-cost sensors with a more accurate size resolution might be able to provide better results with regards to the determination of particle size distributions of the emission.

Effects of filter aging can be demonstrated during the Δt -controlled operation, where the emission and peak concentrations decreased due to the storage of an increasing amount of particles inside the filter medium. Filter aging caused a lower particle emission for all filter media, so that the detected peak concentrations remained largely inside the specified maximum concentration and coincidence errors during measurement are unlikely.

According to the results of two different low-cost sensors in another publication, the SPS30 should also be able to detect different emissions from a damaged and a non-damaged membrane filter medium in the test rig, as the increase in particle concentration due to membrane damage is much higher than the differences of the employed filter media [16].

The next step in research after the application of the low-cost measurement technology under defined conditions in a filter test rig will be the application in a small scale pilot baghouse. Each of a total of nine filter bags will be equipped with a low-cost sensor to study the emission behavior of individual filter bags to investigate the potential for local online emission monitoring with regards to an optimized emission based operation strategy, predictive maintenance and the detection of damaged filter media and leakages. Long term stability problems and experimental conditions (e. g. dust properties, temperature, particle concentration) could limit the suitability of the low-cost sensor for the industrial application.

Literature

- [1] Bundesministerium für Justiz und Verbraucherschutz: Gesetz zum Schutz vor schädlichen Umwelteinwirkungen durch Luftverunreinigungen, Geräusche, Erschütterungen und ähnliche Vorgänge (Bundes-Immissionsschutzgesetz – BImSchG). <https://www.gesetze-im-internet.de/bimsg/index.html> (Accessed on November 1, 2019)
- [2] Bundesministerium für Umwelt, Naturschutz und Reaktorsicherheit: Erste Allgemeine Verwaltungsvorschrift zum Bundesimmissionsschutzgesetz (Technische Anleitung zur Reinhaltung der Luft – TA Luft). GMBI. (2002) Nr. 25-29, S. 511-560
- [3] Löffler, F.: Staubabscheiden. Stuttgart: Georg Thieme 1988
- [4] Kurtz, O.: Ursachen für Emissionen in Mehrfilteranlagen, Dissertation Karlsruhe Institut für Technologie 2018
- [5] Wiegleb, G.: Gasmestechnik in Theorie und Praxis. Wiesbaden: Springer Vieweg 2016
- [6] Asbach, C.; Hellack, B.; Schumacher, S.; Bässler, M.; Spreitzer, M.; Pohl, T. et al.: Anwendungsmöglichkeiten und Grenzen kostengünstiger Feinstaubsensoren. Gefahrstoffe – Reinhalt. Luft 78 (2018) Nr. 6, S. 242-250.
- [7] Budde, M.; Schwarz, A. D.; Müller, T.; Laquai, B.; Streibl, N.; Schindler, G. et al.: Potential and Limitations of the Low-Cost SDS011 Particle Sensor for Monitoring Urban Air Quality. Proscience Dust 2018 (2018) Nr. 5, S. 6-12.
- [8] Crilley, L. R.; Shaw, M.; Pound, R.; Kramer, L. J.; Price, R.; Young, S. et al.: Evaluation of a low-cost optical particle counter (Alphasense OPC-N2) for ambient air monitoring. Atmos. Meas. Tech. (2017) Nr. 11, S. 709-720.
- [9] Kelly, K. E.; Whitaker, J.; Petty, A.; Widmer, C.; Dybwad, A.; Sleeth, D. et al.: Ambient and laboratory evaluation of a low-cost particulate matter sensor. Environ. Pollut. (2016) Nr. 221, S. 491-500.
- [10] Messungen mit dem Feinstaubsensor SDS011 – Ein Vergleich mit einem eignungsgeprüften Feinstaubanalysator. Hrsg.: LUBW Landesamt für Umwelt, Messungen und Naturschutz, Karlsruhe 2017.
- [11] Schwarz, A. D.; Meyer, J.; Dittler, A.: Opportunities for low-cost particulate matter sensors in filter emission measurements. Chem. Eng. Technol. 41 (2018), Nr. 9, S.1826-1832.
- [12] <https://www.sensirion.com/de/umweltsensoren/feinstaubsensoren-pm25/> (Accessed on October 30, 2019)
- [13] <https://www.palas.de/product/promo2000> (Accessed on October 25, 2019)
- [14] Gail, L.; Gommel, L.: Reinraumtechnik. 4. Aufl. Berlin: Springer 2018.
- [15] DIN ISO 11057: Emissionen aus stationären Quellen – Prüfverfahren für die Charakterisierung des Filtrationsverhaltens abreinigbarer Filtermedien. Berlin: Beuth 2012.
- [16] Bächler, P.; Meyer, J.; Dittler, A.: Investigation of low-cost PM-sensors regarding the suitability for emission measurement for pulse-jet cleaned filters. Vortrag Filtech 2019, Cologne October 2019.

ACKNOWLEDGEMENTS

We acknowledge the financial support and close cooperation of Filterkonsortium at KIT. Filterkonsortium at KIT unites leading companies in the fields of fiber and media production, assembly, plant engineering and measurement technology with the research activities of the working group Gas-Particle-Systems of the Institute of Mechanical Process Engineering and Mechanics (MVM). The members of Filterkonsortium at KIT are as follows:

BWFTec GmbH & Co. KG.
 ESTA Apparatebau GmbH & Co. KG
 Evonik Fibres GmbH
 Freudenberg Filtration Technologies SE & Co. KG
 Junker-Filter GmbH
 KAYSER FILTERTECH GmbH
 MANN+HUMMEL GmbH
 PALAS GmbH
 Sick AG

We acknowledge the collaboration of *Bora Bulut* for his help in conducting the experiments.

**Peter Bächler, M.Sc.,
 Dr.-Ing. Jörg Meyer,
 Prof. Dr.-Ing. habil. Achim Dittler,**
 Institute of Mechanical Process Engineering and Mechanics, Gas-Particle-Systems, Karlsruhe Institute of Technology, Karlsruhe, Germany.

Publication II

Title: Spatially Resolved Online Leak Detection in a Baghouse Filter Applying Low-Cost PM-Sensors

Authors: Peter Bächler, Jörg Meyer, Achim Dittler

Journal: Chemie Ingenieur Technik

Year of Publication: 2022

Volume and Issue: 95 (1-2)

Page Numbers: 178-188

Reference: [Bächler et al., 2023a]


Abstract:

Conventional particle emission measurement technology only takes into account the total emission and does not offer spatial resolution. Extensive troubleshooting is required in order to identify potential emission hotspots (e.g., small leaks) that contribute strongly to dust emissions. A network of inexpensive low-cost PM-sensors was used in a small-scale baghouse filter for spatial online particle emission monitoring. Different types of emission hotspots were investigated. Spatial PM monitoring enabled the reliable identification of the position of the hotspot as well as estimation of leak size.

Spatially Resolved Online Leak Detection in a Baghouse Filter Applying Low-Cost PM-Sensors

Peter Bächler*, Jörg Meyer, and Achim Dittler

DOI: 10.1002/cite.202200116

 This is an open access article under the terms of the Creative Commons Attribution License, which permits use, distribution and reproduction in any medium, provided the original work is properly cited.



Supporting Information
available online

Dedicated to Prof. Dr.-Ing. Joachim Werther on the occasion of his 80th birthday

Conventional particle emission measurement technology only takes into account the total emission and does not offer spatial resolution. Extensive troubleshooting is required in order to identify potential emission hotspots (e.g., small leaks) that contribute strongly to dust emissions. A network of inexpensive low-cost PM-sensors was used in a small-scale baghouse filter for spatial online particle emission monitoring. Different types of emission hotspots were investigated. Spatial PM monitoring enabled the reliable identification of the position of the hotspot as well as estimation of leak size.

Keywords: Baghouse filter, Emission monitoring, Filtration, Leak detection, Low-cost PM-sensor

Received: June 27, 2022; *revised:* October 04, 2022; *accepted:* November 10, 2022


1 Introduction

Modern filter media applied for particle separation in industrial pulse-jet cleaned filters (baghouse filters) can provide very low particle emission levels and enable sufficient protection of the environment and downstream unit operations from dust emissions [1]. During filter operation, dust is separated at the surface of the filter medium what leads to the formation of a dust cake with high separation efficiency. The dust cake is periodically removed (e.g., via jet pulse) in order to lower the differential pressure between raw-gas side and clean gas side to grant economic long-term operation [2, 3]. After jet-pulse cleaning, a particle emission peak can be detected on the clean gas side (or locally at the corresponding filter element), as particles can briefly penetrate the unprotected previously regenerated filter medium [4]. Penetration mechanisms through filter media other than direct penetration (e.g., seepage) have also been proposed in the past [5] but play a subsidiary role. Dependent on the age and the surface properties of the filter medium as well as the raw gas-concentration and other operating parameters, the particle emission peak only occurs over several minutes or even seconds and rapidly decreases to a zero level [6]. Baghouse filters remain one of the state-of-the-art methods for industrial dust removal, but the operation and maintenance of the filters is not without individual challenges depending on process parameters, type of dust and gas composition [7].

Problems regarding stable filter operation occur, if the cycle time between individual cleaning events approaches

zero (Δp -controlled operation) or the differential pressure vastly exceeds the desired operation window (Δt -controlled operation) [8, 9]. These effects can be caused by an increase of residual pressure drop over the course of long-term filter operation. Especially nanoparticles can lead to clogging and significant aging of the filter medium, so that e.g., filtration of a pre-coat consisting of coarser particles may be necessary [10–12].

In the industrial application, the ideal emission behavior (emission peak after filter regeneration only) is seldom the case. Here, leaks of the filter bag (e.g., due to mechanical stress on the bag after many years of operation, pinhole leaks caused by sparks, abrasive dusts, particle penetration through the seams etc.) or the plenum plate (incorrectly installed filter elements, missing or damaged screws, etc.) can greatly contribute to the over-all dust emission [13–15]. Bach and Schmidt [16] investigated the contribution of small pinhole leaks in a filter test rig and Kurtz et al. [17] investigated the contribution of leaks in a small-scale baghouse filter. Both studies showed the dominating role of even small leaks (several ppm of installed filter area) on the total dust emission. Exceeding emission limits is one of the main reasons for shutdown of the plant or individual filter

Peter Bächler  <https://orcid.org/0000-0001-9172-5880>, Dr.-Ing. Jörg Meyer, Prof. Dr.-Ing. habil. Achim Dittler (peter.baechler@kit.edu)

Institute of Mechanical Process Engineering and Mechanics, Straße am Forum 8, 76137 Karlsruhe, Germany.

houses. The reliable detection of leaks is one of the most important challenges of the filtration industry [18].

Conventional monitoring systems for dust emissions are, e.g., gravimetric measurement or triboelectric sensors [19]. Gravimetric measurement requires averaging intervals in order to determine the total mass-based dust emission, offering no online information on the current emission. Triboelectric sensors offer a temporally resolved emission signal for the total dust emission on the clean gas side. However, even if a high continuous emission, hinting at a leak, is detected the origin of the emission hotspot remains unknown. In order to identify the position of a leak, a common method is the application of fluorescent dust, so that regions of increased particle penetration may be visually identified during a plant shutdown.

A cost-efficient and spatially applicable online monitoring tool could greatly help plant operators to identify local emission hotspots within the filter house. Li et al. employed an optical sensor, which could reliably detect a highly damaged filter bag (several cm² leak area) [20]. As previously stated, the range of potential damage on a filter bag is wide, as even small defects can cause a high emission contribution.

In previous studies, the potential of cheap, scattered-light-based low-cost PM-sensors has been investigated regarding their ability to correctly monitor the emission behavior of pulse-jet cleaned filters [6, 21, 22]. The sensors could reliably detect the PM-emission peak at the corresponding, previously regenerated, filter bag and showed qualitative agreement with a highly developed laboratory optical particle counter. Different (spatial) emission levels based on different filter media were investigated in a filter test rig and in a small-scale baghouse filter.

In this study, the suitability of the identification and localization of particle emission hotspots via low-cost PM-sensors is performed in a small-scale baghouse filter. On the one hand, spatial identification of a filter bag with open seams (whereby the seams enable high particle penetration during the initial filtration cycles) is investigated. Additionally, the impact of an increasing number of small leaks of several mm in diameter in a single filter bag on the measurement and detection capabilities of low-cost PM-sensors is shown.

2 Material and Methods

2.1 Objective of the Investigations

Previous investigations regarding spatial particle emission monitoring for pulse-jet cleaned filters mainly dealt with the overall characterization of the (spatial) emission behavior and validating the suitability of the low-cost PM-sensors for filtration applications. The characteristic emission behavior and distinct particle emission levels based on particle penetration through different filter media were identified in a filter test rig under defined conditions [21]. Additional investigations were performed in a small-scale baghouse fil-

ter with 9 filter bags under more praxis-relevant operation conditions. Ideal emission behavior (detection of a particle emission peak after filter regeneration of the corresponding filter bag only) was correctly detected by spatially deployed low-cost PM-sensors for membrane filter bags with sealed seams (low emission level, no emission contribution of the seams, etc.) [22]. The emission behavior for regular bags is different especially during the initial filtration cycles and for higher tank pressures for filter regeneration, as particles can penetrate the seams of the filter medium [6]. Clogging of the seams causes a decrease in particle emission and spatial particle emission peaks are detected at the corresponding filter bag after jet-pulse cleaning. Different particle emission levels could also be distinguished in the small-scale baghouse filter due to the measurement with low-cost PM-sensors. The local and total qualitative emission behavior corresponded well to reference measurements employing a highly developed laboratory optical particle counter.

One of the most prominent potential applications for spatial particle emission monitoring is the detection and identification of emission hotspots, as leaks may contribute greatly to the dust emission of pulse-jet cleaned filters, even exceeding the emission contribution of all installed filter elements that are in sound conditions [17, 18]. The objective of the presented measurements was the local identification and evaluation of the emission contribution of spatial particle emission hotspots. Different application scenarios were investigated according to Fig. 1.

In the first measurement campaign (scenario 1), all filter bags were made from medium A and the seams of all but one factory-new filter bag were sealed applying a sealing paste. This creates an emission dynamic, whereby one filter bag with the regular non-sealed seams contributes greatly to the overall dust emission, as particles can easily penetrate the seams of the filter bag during the initial filtration cycles [6, 14]. After several cycles, the seams are (mostly) clogged and the emission behavior approaches ideal behavior (detection of particle emission peak after filter regeneration only). This case represents a moderate fluctuating temporal emission hotspot. The position of the corresponding bag with non-sealed seams was varied in order to investigate the potential of the sensors to localize the particle emission hotspot within the baghouse filter. A similar experiment was shown in a previous publication for one filter position only [22].

In the second measurement campaign (scenario 2), filter bags made from medium B were installed. After previous measurement campaigns, consisting of approx. 400 filtration cycles, the emission behavior was close to ideal operation due to filter aging and clogging of the seams. Afterwards, the central filter bag (bag number 5) was pierced with a hot cannula of 3 mm diameter, creating a small leak. After 30 Δt -controlled overall filtration cycles for each filter bag, an additional hole was added (repetition of procedure up to six small leaks; exception for the case of four holes, where two additional holes were added). This scenario enables the detection of a strong spatial emission hotspot.

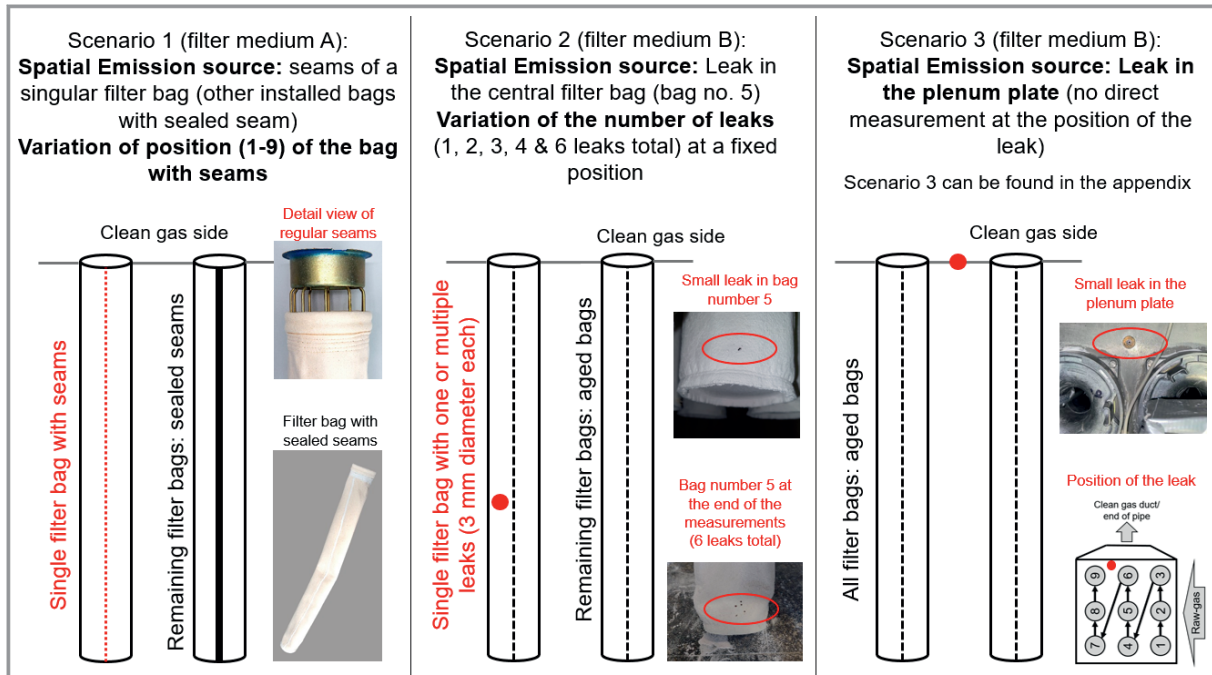


Figure 1. Overview of the different application scenarios for the detection of a spatial emission hotspot (scenario 3 in the appendix).

In addition to the implementation of leaks in the filter medium, a screw with a defined leak diameter of 4.2 mm was installed in the plenum plate without direct measurement in order to check, if a spatial emission hotspot further away from the sampling ducts of the spatially deployed low-cost PM-sensors could be identified (scenario 3, Supporting Information, SI).

2.2 Small-Scale Baghouse Filter

In Fig. 2, a schematic overview of the testing facility including the employed operating parameters is displayed. A radial blower creates a circulating air flow through the testing facility. Dust is dispersed into the raw gas at two separate points. Dust from a silo enables a steady supply of new dust and separated dust is recirculated back into the system in

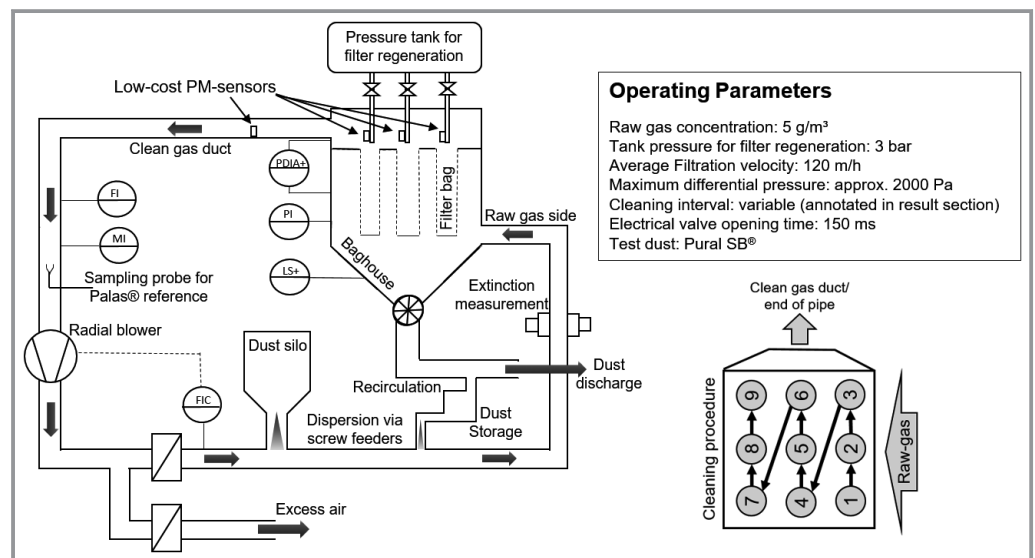


Figure 2. Schematic overview of the experimental facility including the small-scale baghouse filter (figure modified from [6, 22, 23]).

order to grant economic long-term operation. The raw-gas concentration is monitored at an extinction measurement, which has been calibrated to a mass-based raw-gas concentration of approx. 5 g m^{-3} .

The central element of the experimental facility is a small-scale baghouse with a total of nine filter bags (installed filter area of 4.14 m^2). The differential pressure between raw-gas side and clean-gas side is monitored and each filter bag can be regenerated individually by a jet pulse from the clean-gas side. During regeneration, the dust cake is detached from the filter surface and drops into the hopper. The employed cleaning strategy was a bag-by-bag cleaning algorithm. The cycle time between the individual filter regenerations varies between experiments and was kept above 30 s to grant stable operating conditions. The exact cycle time for the corresponding experiment is annotated in the figure.

Particle emission monitoring is performed locally via the application of low-cost PM-sensors (spatial PM monitoring) and further down the line at the outlet of the filter house in order to monitor the total emission both with a low-cost PM-sensor and a highly developed laboratory aerosol spectrometer (cf. Sect. 2.2).

The employed test dust was Pural SB[®]. It is a free-flowing test dust with a mass median diameter of approx. $45 \mu\text{m}$. Nonetheless, there are significant amounts of submicron particles within the test dust [23]. Due to its non-agglomerating behavior, the dust tends to cause high emissions in filter tests [24].

2.3 Aerosol Measurement Technology

Emission measurements were performed employing two different types of optical particle counter. On the one hand,

low-cost PM-sensors of the model OPC-N3 by the manufacturer Alphasense were mounted at the blast pipe of each individual filter bag. Each sensor is equipped with a sampling hose in order to measure the emission close to the source at the outlet of the filter bag. Another low-cost PM-sensor was placed at the outlet of the filter house in order to monitor the total dust emission (Fig. 3).

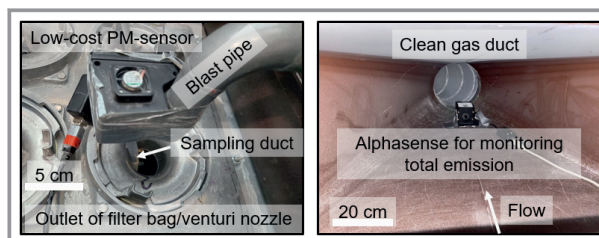


Figure 3. Photograph of the positioning of low-cost PM-sensors at the individual filter bag and for monitoring of the total dust emission on the clean gas side.

As reference, a highly developed laboratory aerosol spectrometer (Promo[®] 2000 with welas[®]2100 sensor) of the manufacturer Palas[®] was also installed on the clean gas side (cf. Fig. 1). Several key specifications of the two different devices are summarized in Tab. 1.

The low-cost sensors were not calibrated against the reference. The index of refraction of the test dust was not considered in the configuration of the measurement devices (standard setting). The density of the test dust was adjusted in the configuration of the Palas[®] system and via adjustment of the “bin weighting index” of the Alphasense sensor. While the Palas[®] system has an implemented coincidence correction and takes into account border-zone errors, there is no information available whether or not the Alphasense sensor internally corrects potential measurement errors [27].

Table 1. Overview of sensor specifications [25, 26].

Device	OPC-N3	Promo [®] 2000 with Welas [®] 2100
Manufacturer	Alphasense	Palas [®]
Measurements	Mass-based concentration: PM_{10} , $\text{PM}_{2.5}$, PM_{10} ; Count rate and size resolved particle counts	Mass and number based total concentration, size distributions, size resolved PM_x conversion
Maximum concentration	$2000 \mu\text{g m}^{-3}$; coincidence probability of 0.84 at $1000 \# \text{ cm}^{-3}$	$500\,000 \# \text{ cm}^{-3}$
Detectable size range	0.35–40 μm	0.2–10 μm ; 0.3–17 μm ; 0.6–40 μm (user selectable)
Size categorization	24 bins	64 bins per decade
Approximate cost (including required cables & connectors)	≈ 400 €	> 30 000 €
Length x Width x Height	75 mm x 45 mm x 63.5 mm	245 mm x 100 mm x 80 mm (Welas [®] sensor only)
Response time	≈ 1 s	≈ 1 s
Volume flow	5.5 L min^{-1} ; 280 mL min^{-1} (sample)	5 L min^{-1}
Configuration	$\rho_{\text{particle}} = 2800 \text{ kg m}^{-3}$; $n_{\text{aerosol}} = 1.5$; spherical particles	$\rho_{\text{particle}} = 2800 \text{ kg m}^{-3}$; $n_{\text{aerosol}} = 1.59$; spherical particles

2.4 Filter Media and Methodology for the Detection of Particle Emission Hotspots

Tab. 2 lists the employed filter media. Note that the emission contribution of the filter media plays a subordinate role when compared to the investigated emission hotspots in the different test scenarios.

Filter medium A (scenario 1) is a membrane filter medium (high separation efficiency). Sealing the seams of the filter bag enables test conditions with ideal emission behavior. A filter bag without sealed seams shows increased continuous particle emissions during the initial filtration cycles, as particles can penetrate the seams of the filter bag. For the investigations (Fig. 1), the seams of all but one filter bag were sealed. The filter bag without sealed seams was a factory-new bag for each run and filter position. The bags with sealed seams have not been aged prior to the investigations. Due to the high separation efficiency of the membrane, significant filter aging effects due to agglomeration of particles within the filter matrix are not expected over the course of the experiments.

Filter medium B (scenario 2 & 3) is a typical polyester needle-felt. The filter bags have been aged prior to the investigation (400+ filtration cycles each). Since the experiments in scenario 2 and 3 focus on leak detection, the emission contribution of the intact bags is negligible compared to the strong emission hotspots and further filter aging does not impact the results.

3 Results

The following section presents the experimental results from scenario 1 and scenario 2 (see Fig. 1). Note that scenario 3 can be found in the SI.

3.1 Localization of a Temporal Emission Hotspot (Seams of a Single Filter Bag) – Scenario 1

During the initial filtration cycles of a factory new bag (or filter medium), increased particle penetration is possible, as the deposition of particles within the filter matrix over time increases the separation efficiency. This effect is commonly referred to as filter aging and is accounted for in test procedures for the characterization of filter media [28]. In order to create temporal particle emission hotspots, this behavior was exploited as the seams of all but one filter bag were sealed. The sealed bags enable the ideal emission behavior with defined peaks after each regeneration, whereas the bag with the regular seam is subject to increased particle penetration during the ini-

tial filtration cycles. Fig. 4 shows the temporal and spatial particle emission profile of the measurement where bag number one was the factory-new bag without sealed seams.

The particle emission contribution of the filter bag with open seams dominates the total particle emission. After several cleaning cycles, both the total emission (Palas® – total) and the local emission at the filter bag with regular seams decrease, indicating clogging of the seams. As the pressure for filter regeneration was kept at a moderate level of 3 bar, ideal emission behavior with defined peaks after jet-pulse cleaning and zero emission during the filtration phase is reached and maintained during the experiment.

A summary of the experimental results repeating the procedure for each filter position is shown in Tab. 3 with regards to the average PM concentrations during the experiments. Note that concentrations are subject to fluctuating flow conditions within the baghouse, as larger volume flows occur at the recently regenerated bag [22, 29]. Nonetheless, the values are suitable for a semi-quantitative comparison of different (spatial) emission levels.

Table 2. Specifications of employed filter media

Medium	Area weight [g m ⁻³]	Thickness [mm]	Permeability (200 Pa) [L dm ⁻² min ⁻¹]	Fiber material & remarks
A (membrane)	500	1.9	30	PPS (heat set) with laminated ePTFE membrane
B (needle-felt)	600	2	70	PE, singed upstream side

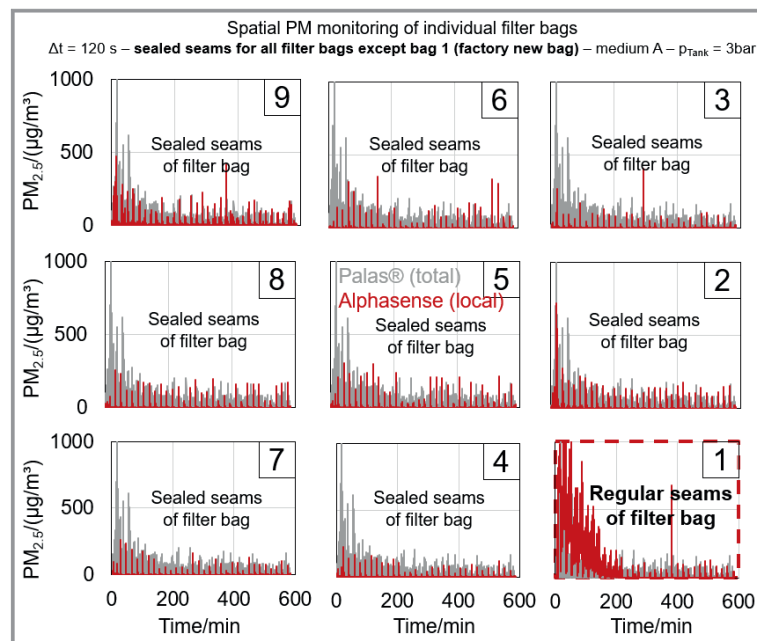


Figure 4. Spatial PM_{2.5} profile with bag 1 as a temporal emission hotspot due to the seams of the filter bag.

Table 3. Summary of measurements regarding the spatial identification of a temporal emission hotspot ($\Delta t = 120$ s, filter medium A, $p_{\text{tank}} = 3$ bar).

Local measurement bag no.		Bag with regular seams ^{a)}									All bags with sealed seams
		9	8	7	6	5	4	3	2	1	
1	Avg. PM _{2.5} [$\mu\text{g m}^{-3}$]	0.3	0.4	0.3	0.5	0.4	0.4	0.3	0.4	72.8	0.3
	Avg. PM ₁₀ [$\mu\text{g m}^{-3}$]	3.7	5.0	3.8	4.3	3.3	4.0	2.2	3.0	860.3	4.0
2	Avg. PM _{2.5} [$\mu\text{g m}^{-3}$]	0.3	0.3	0.3	0.5	0.3	0.3	0.4	82.0	0.8	0.3
	Avg. PM ₁₀ [$\mu\text{g m}^{-3}$]	7.5	7.5	6.2	9.0	5.3	6.5	5.2	416.4	13.0	8.4
3	Avg. PM _{2.5} [$\mu\text{g m}^{-3}$]	1.2	1.7	2.1	0.3	0.3	0.8	121.4	1.2	0.3	1.5
	Avg. PM ₁₀ [$\mu\text{g m}^{-3}$]	10.8	13.3	14.8	3.7	3.4	7.3	815.1	12.0	2.7	11.0
4	Avg. PM _{2.5} [$\mu\text{g m}^{-3}$]	0.3	0.3	0.3	0.4	1.4	149.3	0.2	0.4	0.2	0.3
	Avg. PM ₁₀ [$\mu\text{g m}^{-3}$]	2.2	2.5	2.6	3.4	11.1	1812.9	1.6	3.6	2.6	2.5
5	Avg. PM _{2.5} [$\mu\text{g m}^{-3}$]	0.2	0.4	0.2	1.4	20.9	0.3	0.4	0.4	0.4	0.5
	Avg. PM ₁₀ [$\mu\text{g m}^{-3}$]	1.7	3.7	1.9	13.8	117.2	2.8	3.1	3.2	2.8	5.9
6	Avg. PM _{2.5} [$\mu\text{g m}^{-3}$]	0.2	0.2	0.2	18.1	0.1	0.2	0.5	0.3	0.2	0.2
	Avg. PM ₁₀ [$\mu\text{g m}^{-3}$]	1.5	1.4	1.2	184.3	0.7	1.2	6.9	2.2	3.5	3.2
7	Avg. PM _{2.5} [$\mu\text{g m}^{-3}$]	0.9	0.6	25.1	0.3	0.4	0.5	0.2	0.2	0.3	0.4
	Avg. PM ₁₀ [$\mu\text{g m}^{-3}$]	9.8	9.0	509.2	3.6	3.1	5.3	1.7	1.4	2.0	2.6
8	Avg. PM _{2.5} [$\mu\text{g m}^{-3}$]	0.6	28.2	1.3	0.4	0.4	0.5	0.3	0.3	0.4	0.3
	Avg. PM ₁₀ [$\mu\text{g m}^{-3}$]	6.9	705.4	15.2	3.8	5.0	4.9	2.7	2.5	2.3	5.2
9	Avg. PM _{2.5} [$\mu\text{g m}^{-3}$]	308.3	0.4	0.3	1.4	1.9	2.7	1.3	0.9	0.7	0.4
	Avg. PM ₁₀ [$\mu\text{g m}^{-3}$]	8530.0	9.0	4.4	24.9	40.5	62.9	23.1	13.7	10.3	6.4
Total emission (Palas [®])	Avg. PM _{2.5} [$\mu\text{g m}^{-3}$]	78.0	49.9	24.8	21.9	n.a.	9.0	10.6	12.9	5.9	1.4
	Avg. PM ₁₀ [$\mu\text{g m}^{-3}$]	1055.1	688.3	313.6	281.4	n. a.	127.5	133.4	162.4	75.5	16.8

a) all other bags with sealed seams.

The single bag with regular seams can be easily identified due to the increased PM concentrations at each position (compare the diagonal of the table). The average PM concentrations are subject to long averaging intervals (30 filtration cycles for each bag with $\Delta t = 2$ min), where the highest emissions occur during the initial cycles, where constant particle penetration through the seams is possible. Therefore, the absolute concentration peaks and the concentrations during these corresponding cycles are significantly higher compared to the average of the total experimental duration displayed in Tab. 3. At all other measurement positions with bags with sealed seams, the resulting PM concentrations are lower and almost at a zero level. The concentrations are similar to the concentrations obtained during a previous reference measurement, where all bags had sealed seams and correspond to ideal emission behavior (right column of the diagram).

An exception is bag number nine, where consistently higher concentrations are detected compared to the other bags. This is also in agreement with the measurement where bag 9 was exchanged with a factory-new bag with regular seams, as

the measured concentrations exceed the concentrations from the other positions by a large margin. Nonetheless, the concentrations at bag 9 remain lower than the concentrations of the respective bag with regular seams. A concise explanation for this outlier is difficult, as a direct comparison between the total and local concentrations is not possible and it remains unclear if the emission were indeed higher at this measurement position, e.g., due to faulty installation of the bag. Another possibility is a systematic error of the sensor itself, however sensor 9 did not show notable differences during the reference measurement (all bags with sealed seam) and in consecutive measurement campaigns.

There is no direct correlation between the total concentration measured by the Palas[®] reference and the average concentrations measured by the low-cost sensors. Thus, an estimation of the intensity of the total PM emission from the local measurement is not possible and the sensor may merely serve as a qualitative monitoring tool. However, the spatial identification of the temporal emission source was very reliable for each measurement position.

Another experiment can be found in the SI, where an entire row of filter bags (position 4, 5 and 6) was exchanged with factory new bags. The corresponding row could also be reliably identified as the main contribution to the total emission with the help of low-cost PM-sensors.

3.2.1 Localization of a Strong Continuous Emission Hotspot (Leak in a Single Filter Bag) – Scenario 2

While the seams of the filter bag mainly serve as a temporal origin for dust emissions during the initial filtration cycles, their impact on the total dust emission is comparably small when related to the total lifetime of the filter bag. Leaks may cause sudden significant increase in dust emissions and are one of the major reasons for the shutdown of filter houses.

In scenario 2, the filter bag at position made from filter medium B was pierced with a cannula of 3 mm diameter in order to create an increasing number of leaks over multiple experimental runs ($\Delta t = 30$ s). Fig. 5 displays the spatial $PM_{2.5}$ emission profile for the initial experiment (one leak).

Similar to the experiments shown in Sect. 3.1, the position of the damaged filter bag can be easily identified from the measured PM data. The constant particle flux through the leak is indicated via the total concentration measured by the Palas® reference in the background of Fig. 5. The surrounding filter bags mostly show the ideal emission behavior, where distinct emission peaks are detected after jet-pulse cleaning. A preceding measurement before creating the leaks can be found in the SI and also shows the ideal emission behavior for all measurement positions.

When increasing the number of leaks, the bypass flow penetrating to the clean gas side without filtration also increases, resulting in higher clean gas concentrations. When comparing the measurements with one leak and six leaks regarding the PM concentrations at the damaged filter bag, a measurement error of the low-cost PM-sensor can be observed (Fig. 6). The same error likely occurs during minute 100–150 of the experiment with one leak.

Even though the leak area increases, the measured $PM_{2.5}$ concentration of the low-cost sensor at the emission hotspot decreases, seemingly giving an indication of a zero-emission level. The PM_{10} concentration shows the actual correct trend of increasing concentration with increasing leak area/bypass flow. This correlation (high PM_{10} and low $PM_{2.5}$ at high concentration conditions and no change in raw gas particle size distribution) is a clear indication for a coincidence error, where multiple particles pass the measure-

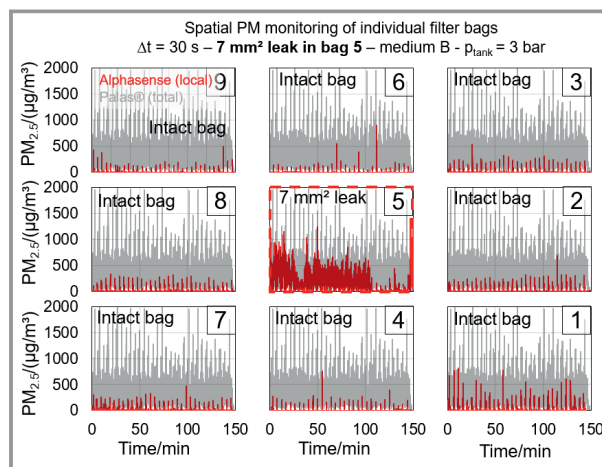


Figure 5. Spatial $PM_{2.5}$ profile with bag 5 as a strong continuous emission hotspot due a leak of 3 mm diameter.

ment volume of the low-cost PM-sensor simultaneously. A more in-depth explanation of the coincidence error, referencing the relevant standards, can be, e.g., found in the book by Gail and Gommel [30]. When a particle passes the measurement volume of an optical particle counter, light is scattered at the single particle. The scattered light causes a signal peak at the detector of the sensor. Based on the peak height, particles are classified into the respective optical size class. The number of counting events in a certain time duration related to the measurement volume yields the particle number concentration. The determined particle size, particle density, shape factor and index of refraction, enable the calculation of particle mass concentrations from the previously determined particle number concentration. Based on their size, they contribute to the corresponding mass-based PM concentrations (e.g., $PM_{2.5}$ or PM_{10}). When multiple

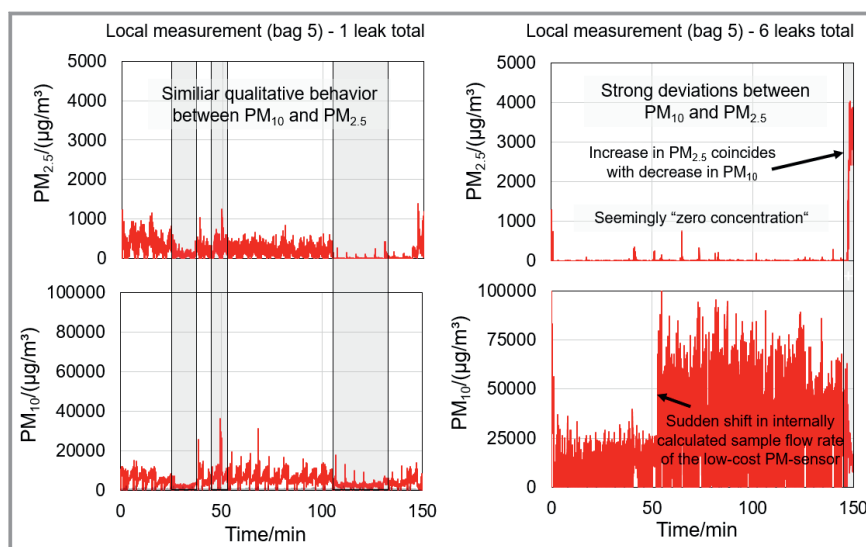


Figure 6. Comparison of the measured local dust emissions for one and six leaks regarding $PM_{2.5}$ and PM_{10} concentrations.

particles pass the measurement volume simultaneously, the signal peak is overestimated, and the individual counting events cannot be distinguished. Thus, the number of counting events is lower, but the determined particle size is higher than in reality [27, 30–32]. If this wrongly allocated diameter exceeds the $PM_{2.5}$ size class and is instead classified as a PM_{10} relevant particle, the $PM_{2.5}$ concentration decreases while the PM_{10} concentration further increases. The decrease of detected particles in the smaller size fraction can also be derived from the particle size distribution (cf. Fig. 9). In general, coincidence-free measurement is limited by a maximum count-rate that depends, e.g., on the size of the measurement volume. Highly developed aerosol spectrometers (or optical particle counters) may employ a coincidence correction, as is the case for the Palas® reference [25]. It is unknown, whether or not the employed low-cost sensor utilizes similar methods.

At the end of the experiment and the end of dust dosage (no emission bypass through the leak), the PM_{10} concentration decreases, which is linked to an increase in $PM_{2.5}$ concentration. The number of particles passing the measurement volume decreases, so that the impact of the coincidence error is lower and counting events can be correctly distinguished and particles are allocated to the correct $PM_{2.5}$ relevant size classes.

The measurement error puts the quantitative accuracy of the low-cost sensor into question, however qualitative or semi-quantitative information regarding the size of the leak and its position may still be gained. Fig. 7 shows the spatial PM_{10} profile for the case of six leaks total, as the $PM_{2.5}$ reading of the sensor is greatly affected by coincidence effects.

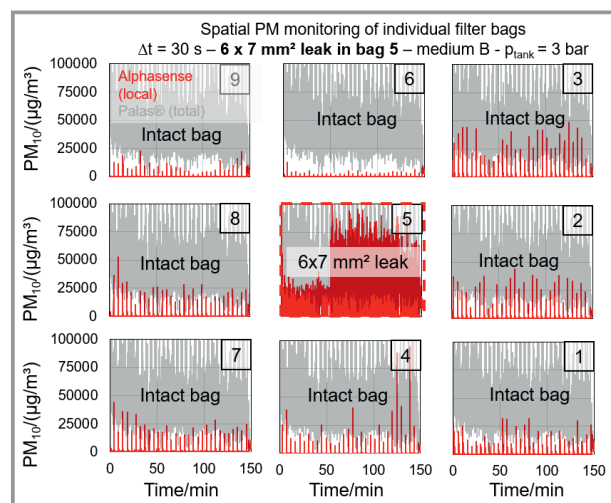


Figure 7. Spatial PM_{10} profile with bag 5 as a strong continuous emission hotspot due to six leaks of 3 mm diameter each.

The dust emission has increased considerably (average of $2000 \mu\text{g m}^{-3}$ $PM_{2.5}$ and $40\,000 \mu\text{g m}^{-3}$ PM_{10} – cf. Palas® reference in Fig. 6), greatly exceeding the manufacturer specifications of the sensor (see Tab. 1). However, even for this

case, a clear identification of the damaged bag is possible and all other low-cost PM-sensors show the expected ideal behavior. The sharp increase of the particle concentration at about 50 min time at position 5 is caused by a sudden shift in the internally determined sensor flow rate. A decrease in flow rate causes higher concentrations, as the counting events are related to a smaller volume for the determination of particle number concentration and the respective PM values. A more in-depth discussion of this measurement artifact (sample flow rate) can be found in the SI. The findings further demonstrate the limitations of the sensors, which are not suitable for accurate concentration readings under these conditions.

Despite the resident measurement artifacts, a reliable identification of the strong emission hotspot could be achieved by operating a network of low-cost PM-sensors within the baghouse filter. There is a clear potential for improved process monitoring applying low-cost PM-sensors as a cheap monitoring tool in order to identify the origin of dust emissions and qualitative trends regarding the emission level. The investigations in scenario 3 in the appendix show that measurement close to the hotspot is crucial for a successful identification. The leak in the plenum plate could not be allocated via the sensor data from the positions at the individual filter bags. Nonetheless, the low-cost PM-sensor monitoring the total dust emission correctly detected the concentration increase, offering an indication on the required maintenance and showing that the filter bags are intact and not the origin of the increased emission.

3.2.2 Impact of Leak Diameter on the Detection Capabilities of the Low-Cost PM Sensors – Scenario 2

While the position of the leak at bag number 5 could be reliably identified, coincidence effects were observed in the form of an increasing PM_{10} concentration and a decreasing $PM_{2.5}$ concentration at the PM emission hotspot. Presumably, multiple particles pass the measurement volume simultaneously under high concentration conditions, causing the detection of a lower particle number concentration with a larger overall particle size as the individual counting events can no longer be distinguished. Fig. 8 shows the average concentrations of the total dust emission as determined by the Palas® reference and the low-cost sensor further down the clean gas duct (Fig. 3), as well as the local concentration measured by the low-cost PM-sensor positioned at the emission hotspot (bag 5).

The Palas® reference shows the correct behavior reported in literature, whereby the dust concentration increases linearly with leak area [16, 17]. The deviation to perfect linear behavior (especially visible for the change from four to six leaks total) originates from smaller fluctuations regarding the dust dosage and the possibility of particle deposition and bridging of the leaks during the experiment (see Fig. 1 where part of the circular 3 mm leak is blocked by particles).

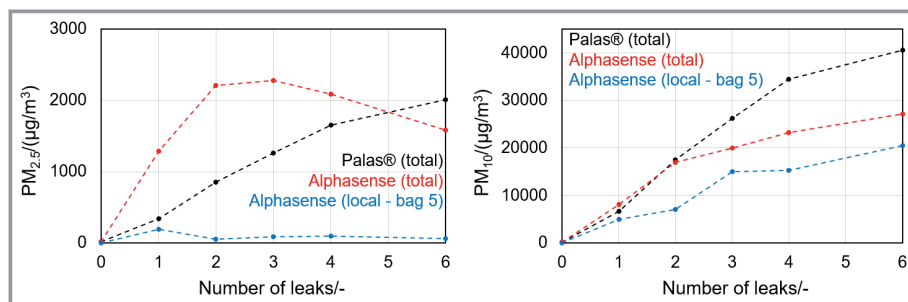


Figure 8. Optically determined average PM clean gas concentration dependent on the number of leaks (3 mm diameter each).

The average number concentration detected by the Palas® reference during the experiment with six leaks was approx. 4000 cm^{-3} (maximum peak at approx. $25\,000\text{ # cm}^{-3}$) so that a coincidence error of the reference is unlikely [25].

The Alphasense sensor also measuring the total concentration in the clean gas duct shows a linear increase for the first two leaks. Afterwards, the slope of the average PM_{10} concentration curve decreases. The effect on $PM_{2.5}$ concentration is more pronounced by the larger amount of particles penetrating to the clean gas side. Adding a third leak results in a seemingly constant $PM_{2.5}$ concentration and adding even further leaks causes the discussed drop in $PM_{2.5}$ concentration that is linked to the coincidence error.

The locally determined concentrations (blue curve) also show the previously discussed coincidence effect. While there is an increase in $PM_{2.5}$ concentration from none to one leak, the $PM_{2.5}$ concentration does not increase further and an increase in concentration is only notable via the increase of detected PM_{10} relevant particles.

The particle size distributions of the total dust emission (Fig. 9) further confirm the measurement error. For the case of zero leaks, the size distributions are in relatively good agreement. With increasing number of leaks, the amount of particles classified in the smaller size classes decreases for the low-cost PM-sensor (see, e.g., drop in the smallest size

class). The number of counting events of bigger particles increases respectively (e.g., increase of $10\text{ }\mu\text{m}$ particles). The correct trend of a uniform increase of counting events across all size classes is monitored by the Palas® reference.

Even though the measurements of the low-cost PM-sensors are strongly affected by the coincidence error, semi quantitative information regarding leak size can be gained. A decrease in $PM_{2.5}$ readings linked to an increase in PM_{10} concentrations is an indication for high particle concentrations, exceeding the maximum counting rate. While the low-cost PM-sensor did not correctly measure the linear increase of clean gas concentration with increase in leak diameter, a further increase in PM_{10} concentrations was recorded so that the overall emission level caused by the different numbers of leaks can be distinguished.

4 Summary and Outlook

Experiments regarding the identification of spatial particle emission hotspots were performed in a small-scale bag-house filter by operating a network of low-cost PM-sensors for emission monitoring of each individual filter bag. The experiments were divided into three scenarios.

In the first scenario, one of the nine filter bags made from a membrane filter medium with sealed seams was exchanged with a factory-new bag with regular seams. As the seams enable particle penetration during the initial filtration cycles before clogging, the exchanged filter bag serves as a temporal emission hotspot. Increased concentrations were measured by the low-cost PM-sensor positioned at the

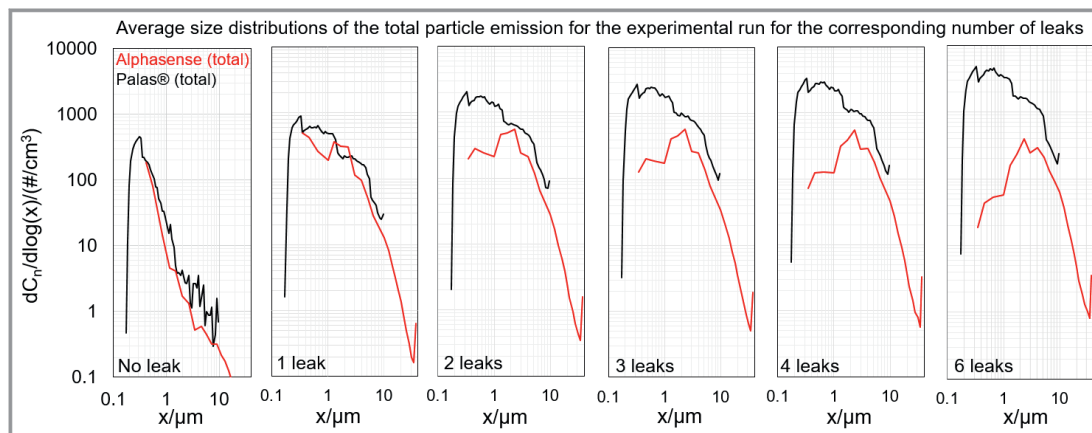


Figure 9. Comparison of particle size distributions of the total particle emission dependent on the number of leaks for the low-cost PM-sensor and the reference.

emission hotspot for each measurement run. The concentrations measured at all other bags followed an ideal behavior where a distinct particle emission peak is detected for a short duration after filter regeneration. The investigations demonstrate the possibility of spatial identification of an emission hotspot by implementing a network of low-cost PM-sensors.

In the second scenario, an increasing number of defined leaks (3 mm diameter each) were introduced in a single filter bag made from a standard needle-felt. The spatial identification of the damaged bag was possible for each case, however, increased concentrations due to higher numbers of leaks/a higher leak area led to coincidence errors for the low-cost PM-sensor. Here, the number of counting events in the PM_{2.5} relevant size classes was very small, as multiple smaller particles passing the measurement volume of the sensor simultaneously were presumably detected as fewer and larger particles, where the detected particle size exceeded the PM_{2.5} fraction and was only accounted for in the PM₁₀ relevant size fractions. Even though the measurements of the low-cost PM-sensors are heavily influenced by the coincidence error, an increasing PM₁₀ concentration was detected with increasing numbers of leaks, enabling the estimation of leak size. The concentrations detected by low-cost PM-sensors have to be evaluated carefully and both, PM_{2.5} and PM₁₀ signals have to be considered in order to give accurate interpretations on the current particle emission level (especially in the case of higher concentration regions where coincidence errors become relevant).

In the third and final scenario, a leak was introduced into the plenum plate of the filter house without direct monitoring of the emission source. The sensors positioned at the filter bag measured an ideal emission behavior. The increase of the particle emission was only detected by sensors monitoring the total dust emission. Thus, positioning close to the source is important when employing low-cost PM-sensors for emission monitoring.

The experiments in the small-scale baghouse filter showed the possibilities of reliable identification of leaks as well as the potential for the estimation of leak sizes when correctly interpreting sensor data. Coincidence errors for higher particle concentrations and quantitative deviations to state-of-the-art optical particle counters limit the quantitative accuracy and reliability of the sensors. Further technical limitations are long term stability and the use of the sensors in demanding filtration applications (corrosive gases, higher temperatures). Nonetheless, leak detection poses one of the most prominent potential applications when implementing low-cost PM-sensors in technical facilities for (spatial) PM monitoring. Suitable sensors could greatly improve process monitoring of filter houses and the operation and maintenance procedures by identifying damaged filter elements.

Supporting Information

Supporting Information for this article can be found under DOI: <https://doi.org/10.1002/cite.202200116>.

We acknowledge the financial support and close cooperation of Filterkonsortium at KIT. Filterkonsortium at KIT unites leading companies in the fields of fiber and media production, assembly, plant engineering and measurement technology with the research activities of the research group Gas-Particle-Systems of the Institute of Mechanical Process Engineering and Mechanics (MVM). The members of Filterkonsortium at KIT are as follows: BWF Tec GmbH & Co. KG, ESTA Apparatebau GmbH & Co. KG, Evonik Fibres GmbH, Freudenberg Filtration Technologies SE & Co. KG, Junker-Filter GmbH, MANN+HUMMEL GmbH, PALAS GmbH, Sick AG.

We acknowledge the collaboration of Enes Malik Akdas and Daniel Arnaud Sokoundjou Fotsing for their help in conducting the experiments.

We acknowledge that part of the materials (Sect. 3.1) have been first presented in FiltCon 2021 conference, USA organized by the American Filtration and Separations Society. Parts of this work were presented at FILTECH 2022. Open access funding enabled and organized by Projekt DEAL.

Symbols used

C_n	[# cm ⁻³]	particle number concentration
n_{aerosol}	[-]	index of refraction
r_{particle}	[kg m ⁻³]	particle density
x	[μm]	particle diameter

Abbreviations

PM	particulate matter
PM _x	weighted mass based particulate matter concentration whereby the x refers to the corresponding size fraction

References

- [1] H. J. Imminger, P. Krug, *Cleanable filter media go close to zero emission*, Filtech, Cologne, October 2019.
- [2] F. Löffler, *Staubabscheiden*, Georg Thieme, Stuttgart 1988.
- [3] E. Schmidt, *Fortschr.-Ber. VDI-Z.* 1998, Reihe 3, Nr. 546.
- [4] J. Binnig, J. Meyer, G. Kasper, *Powder Technol.* 2009, 189 (1), 108–114. DOI: <https://doi.org/10.1016/j.powtec.2008.06.012>
- [5] D. Leith, M. J. Ellenbecker, *Aerosol Sci. Technol.* 1982, 1 (4), 401–408. DOI: <https://doi.org/10.1080/02786828208958604>

- [6] P. Bächler, V. Löschner, J. Meyer, A. Dittler, *Process. Saf. Environ. Prot.* **2022**, *160*, 411–423. DOI: <https://doi.org/10.1016/j.psep.2022.02.005>
- [7] VDI 3677 Blatt 1, *Filtering Separators – Surface Filters*, Beuth Verlag, Berlin **2010**.
- [8] P. Spanring, N. A. Nowak, T. Laminger, G. Mauschwitz, *Investigation of regeneration stability of pulse-jet regenerated filter media under laboratory test conditions*, Filtec, Cologne, October **2019**.
- [9] H. Leubner, U. Riebel, *Chem. Ing. Tech.* **2003**, *75* (12), 82–86. DOI: <https://doi.org/10.1002/cite.200390027>
- [10] S. Schiller, H. J. Schmid, *Powder Technol.* **2015**, *279*, 96–105. DOI: <https://doi.org/10.1016/j.powtec.2015.03.048>
- [11] H. Leubner, *Die simultane Abscheidung von Stäuben und sauren Gasen (HCl, SO₂) aus Abgasströmen durch Precoatfiltration bei 150–300°C*, Ph. D. Thesis, BTU Cottbus-Senftenberg **2004**.
- [12] N. Khirouni, A. Charvet, D. Thomas, D. Bémer, *Process. Saf. Environ. Prot.* **2020**, *138*, 1–8. DOI: <https://doi.org/10.1016/j.psep.2020.02.040>
- [13] G. Mouret, D. Thomas, S. Chazelet, J. C. Appert-Collin, D. Bémer, *J. Aerosol. Sci.* **2009**, *40* (9), 762–775. DOI: <https://doi.org/10.1016/j.jaerosci.2009.04.010>
- [14] C. R. de Lacerda, P. Bächler, A. D. Schwarz, R. Sartim, M. L. Aguiar, A. Dittler, Impact of Seams on the Operating Behavior of Surface Filters Regarding Particle Emissions, *Chem. Eng. Technol.* **2022**, *45* (7), 1354–1362. DOI: <https://doi.org/10.1002/ceat.202200132>
- [15] J. Li, Q. Wu, Y. Huang, Z. Sun, J. Li, D. Wu, *Process Saf. Environ. Prot.* **2022**, *158*, 282–290. DOI: <https://doi.org/10.1016/j.psep.2021.12.012>
- [16] B. Bach, E. Schmidt, *J. Hazard. Mater.* **2007**, *143* (3), 673–676. DOI: <https://doi.org/10.1016/j.jhazmat.2007.01.093>
- [17] O. Kurtz, J. Meyer, G. Kasper, *Particuology* **2017**, *30*, 40–52. DOI: <https://doi.org/10.1016/j.partic.2016.08.001>
- [18] O. Kurtz, *Ursachen für Emissionen in Mehrfilteranlagen*, Ph. D. Thesis, Karlsruhe Institute of Technology **2017**.
- [19] G. Wiegleb, *Gasmestechnik in Theorie und Praxis*, Springer Vieweg, Wiesbaden **2016**. DOI: <https://doi.org/10.1007/978-3-658-10687-4>
- [20] J. Li, X. Lu, W. F. Wang, *Opt. Fiber Technol.* **2020**, *57*, 102218. DOI: <https://doi.org/10.1016/j.yofte.2020.102218>
- [21] P. Bächler, J. Meyer, A. Dittler, *Gefahrst. Reinhalt. Luft.* **2019**, *79* (11–12), 443–450. DOI: <https://doi.org/10.37544/0949-8036-2019-11-12-49>
- [22] P. Bächler, J. Szabadi, J. Meyer, A. Dittler, *J. Aerosol. Sci.* **2020**, *150*, 105644. DOI: <https://doi.org/10.1016/j.jaerosci.2020.105644>
- [23] P. Bächler, J. Meyer, A. Dittler, *Aerosol Sci. Technol.* **2022**, *56* (4), 394–402. DOI: <https://doi.org/10.1080/02786826.2022.2027335>
- [24] S. Sobich, J. Meyer, A. Dittler, G. Kasper, *Baghouse filtration: a praxis relevant media parameter to determine an emissions level of a pulse-jet cleanable filter*, Filtech, Cologne, March **2018**.
- [25] www.palas.de/product/aerosolsensorwelas2100 (Accessed on May 13, 2022)
- [26] www.alphasense.com/wp-content/uploads/2019/03/OPC-N3.pdf (Accessed on May 13, 2022)
- [27] L. Mölter, *Bestimmung der Anzahlverteilung von Tracerpartikeln*, Fachtagung Lasermethoden in der Strömungsmesstechnik, Braunschweig, September **2006**.
- [28] DIN ISO 11057, *Air quality – Test method for filtration characterization of cleanable filter media*, Beuth Verlag, Berlin **2011**.
- [29] X. Simon, D. Bémer, S. Chazelet, D. Thomas, R. Régnoer, *Powder Technol.* **2010**, *201* (1), 37–48. DOI: <https://doi.org/10.1016/j.powtec.2010.02.036>
- [30] L. Gail, U. Gommel, *Reinraumtechnik*, Springer Vieweg, Wiesbaden **2018**. DOI: <https://doi.org/10.1007/978-3-662-54915-5>
- [31] J. Raasch, H. Umhauer, *Fortschr.-Ber. VDI-Z.* **1984**, Reihe 3, Nr. 95.
- [32] B. Sachweg, H. Umhauer, F. Ebert, H. Büttner, R. Friehmelt, *J. Aerosol. Sci.* **1998**, *29* (9), 1075–1086. DOI: [https://doi.org/10.1016/S0021-8502\(98\)80004-9](https://doi.org/10.1016/S0021-8502(98)80004-9)

Supporting Information

Spatially resolved online leak detection in a baghouse filter applying low-cost PM-sensors

M.Sc. Peter Bächler*, Dr.-Ing. Jörg Meyer and Prof. Dr.-Ing. habil. Achim Dittler

DOI: 10.1002/cite.202200116

Correspondence: Peter Bächler (peter.baechler@kit.edu), Straße am Forum 8, 76137 Karlsruhe, Germany

The supporting information section offers additional context to the experiments, explanations regarding the frequently mentioned “ideal” emission behavior for pulse-jet cleaned filters and comments from the author regarding measurements with low-cost PM-sensors in the baghouse filtration application regarding measurement artifacts.

Identification of filter bags with regular seams and their impact on the total dust emission (additional information for scenario 1)

Following the procedure described in scenario 1, a similar experiment has been performed at a later stage. Here, an entire row of filter bags (bag 4, 5 & 6) made from filter medium B has been exchanged with factory-new filter bags. The rest of the bags (bag 1,2,3,7,8 & 9) have been aged prior to the experiment so that the emission contribution of the seams of the filter bags was negligible.

Figure S1 shows the result of the experiment, where the factory-new filter bags can be easily identified due to the high continuous emissions detected at the corresponding filter positions.

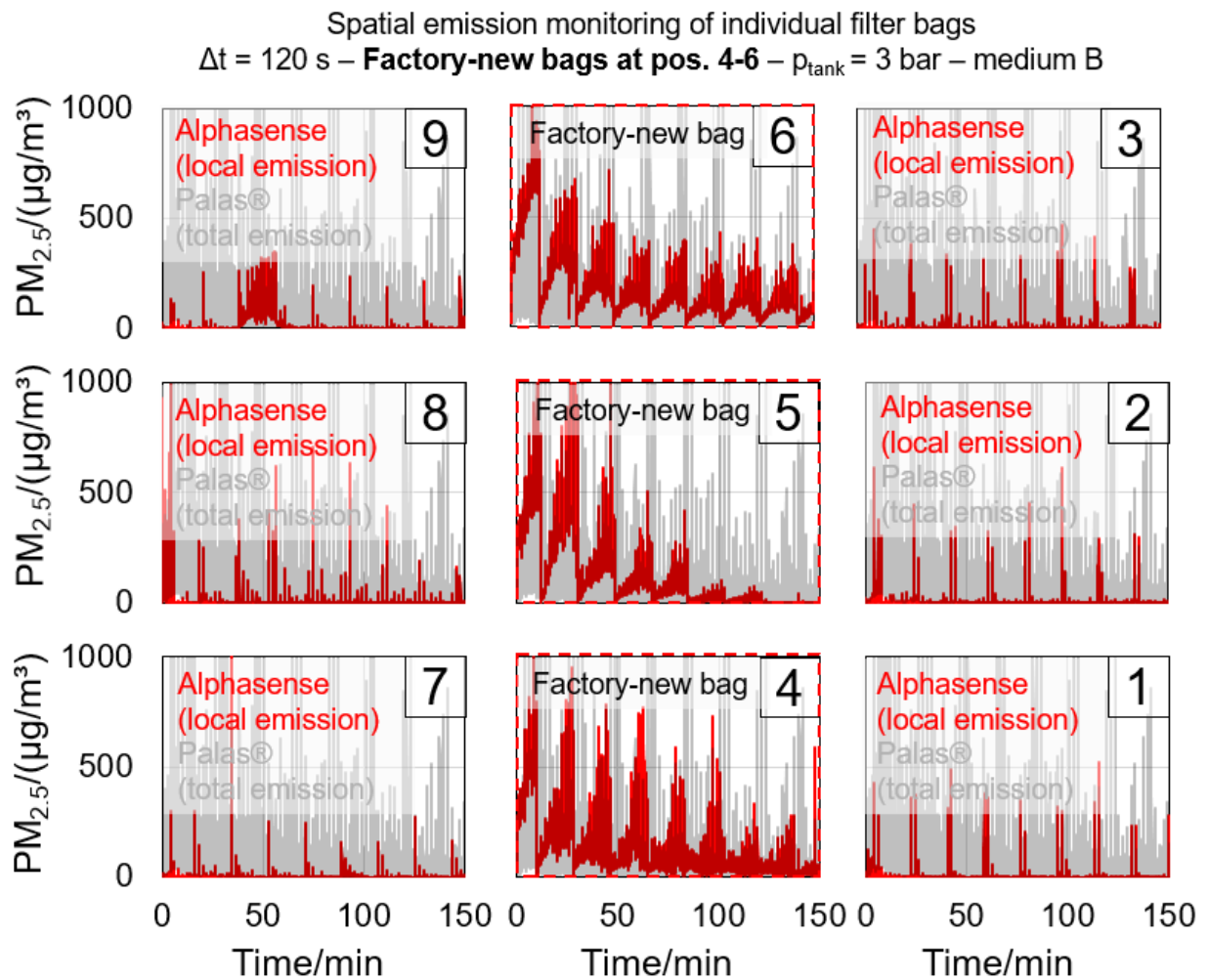


Figure S1. Spatial $\text{PM}_{2.5}$ profile with bags 4, 5 & 6 as temporal emission hotspots due to the seams of the filter bag.

The bags show the typical behavior of factory-new bags that has been discussed in previous publications [6, 22]. Due to clogging of the seams, the emission gradually decreases over the initial filtration cycles until ideal emission behavior is reached and emissions are only detected for a short time duration after the cleaning pulse. Between cleaning events, the emission decreases to a zero level. One small exception is bag number 9, where at about minute 50, continuous emissions arise. This behavior was observed before and likely occurs due to renewed continuous particle penetration through the seams of the bag or smaller defects that eventually clog over time.

In this case, multiple bags are emission hotspots and are the main contributors to the total dust emission. The total emission measured by the Palas® reference is shown in figure S2.

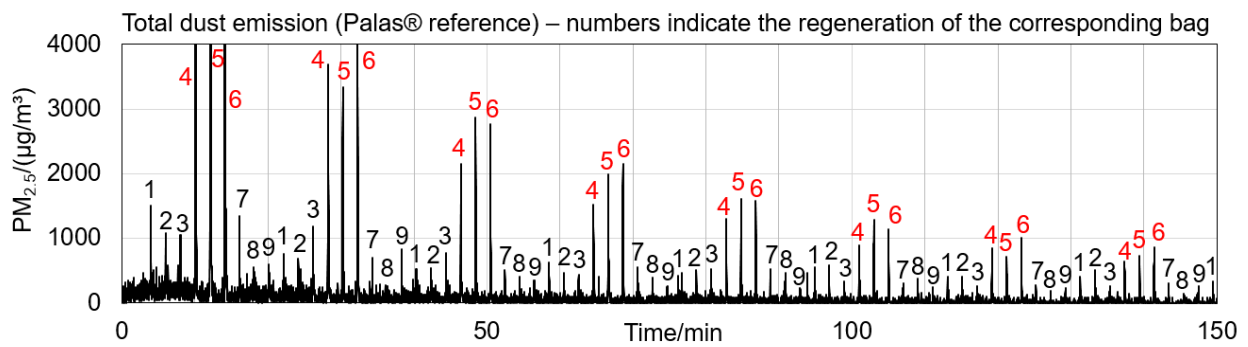


Figure S2. Total dust emission for the experiment with bags 4, 5 & 6 serving as temporal emission hotspots due to the seams of the filter bag.

The qualitative trend of a decreasing continuous emission is similar to the local measurement at the factory-new bags. Additionally, the peaks after the regeneration of the factory-new bags are a lot higher during the initial cycles compared to the other filter elements. However, the peak height quickly decreases and the peaks are practically indistinguishable from the rest of the filter elements at the end of the experiment with further filter aging.

This measurement complements the observations in chapter 3.1 of the publication, as again, multiple noticeable filter bags were clearly identified based on local PM monitoring. Their impact on the total dust emission was validated by referring to the total emission where continuous emissions are detected and the peak heights of the exchanged bags are higher compared to the aged filter bags.

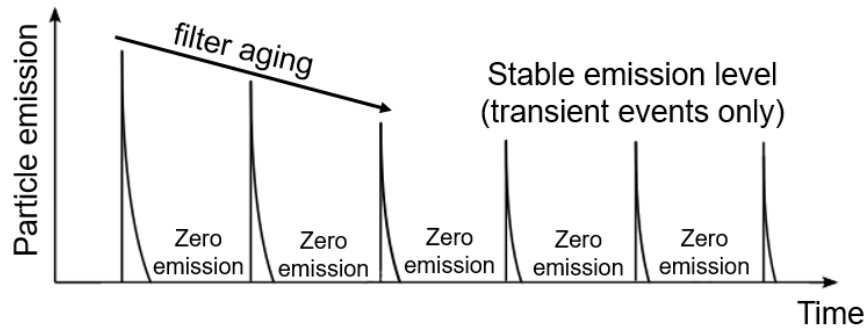
“Ideal emission behavior” for medium B before introducing the leaks

Since the publication often refers to “ideal” emission behavior, this behavior is further explained here via an example from typical measurement data.

After sufficient cake-build up, baghouse filters enable near perfect particle separation. Particle emissions may only reach the clean gas side via bypass through leaks or other small defects (e.g. seams of the filter bag). These smaller defects typically results in a baseline particle emission. As the small-scale baghouse filter is relatively easy to maintain regarding the size and the number of filter elements, leak-free operation can typically be guaranteed and no baseline emission is measured.

After filter regeneration, particles may briefly penetrate the filter medium, resulting in the distinct “emission peak” that is characteristic for baghouse filters. A picture commonly found in literature is displayed in figure S3.

Ideal behavior: Emission peak after filter regeneration



Real behavior: Emission peak and baseline emission

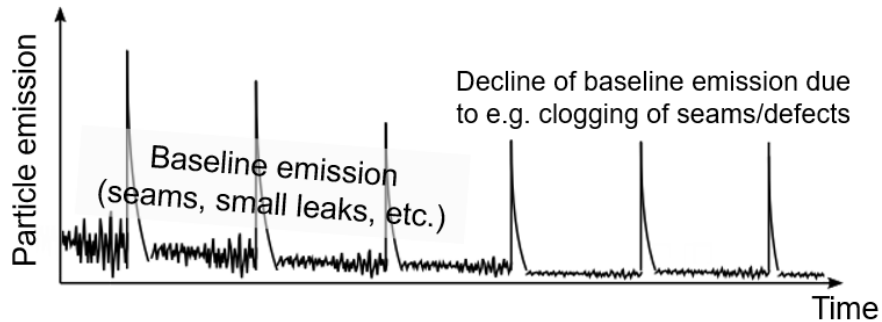


Figure S3. Typical emission behavior for pulse-jet cleaned filters

The height, length and shape of the peak greatly depend on the type of dust, the raw-gas concentration, the flow velocity at the sample position and the filter medium. For membrane filter media, very short timespans of only several seconds regarding the duration of the peak have been shown in a previous publication [22]. In filter test rigs, the emission is typically detected over a longer decay period of the peak of up to several minutes [21] due to the lower flow velocity of 0.033 m/s (compared to approx. 5.7 m/s flow velocity in the clean gas duct of the baghouse filter in this publication). This ideal emission behavior can be characterized qualitatively by low-cost PM-sensors what can be observed throughout the publication for filter bags that are not impacted by the emission hotspot.

However, to give another indication for the "ideal behavior" as it can be spatially measured by low-cost PM-sensors, an example run for medium B before introducing the leaks is shown in figure S4.

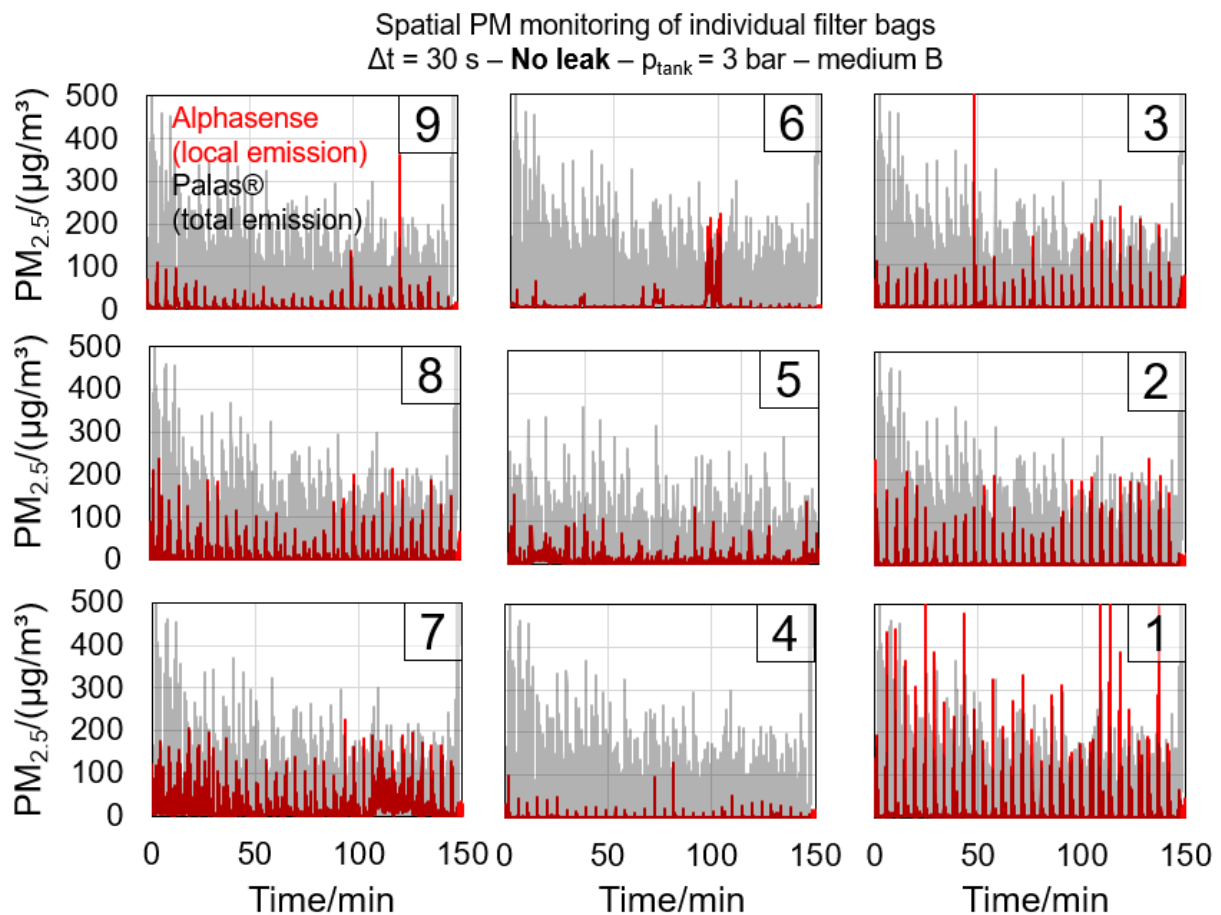


Figure S4. Spatial $\text{PM}_{2.5}$ profile for an experiment with filter medium B before introducing the leaks.

Due to the temporal resolution (1 value / second) and the overall measurement period of 150 minutes), ideal behavior may not be visible at first glance. However, several filter bags (e.g. bag 1 – 4 & 9) clearly follow the trend of ideal behavior described above as indicated by the defined peaks. Some bags (e.g. bag 7 & 8) show continuous emissions during the initial cycles. This trend is often observed and in-line with the total concentration. During the initial cycles, stabilization of the process conditions and deposited dust mass on the filter bags takes place, what may lead to higher emissions. Bag 6 only monitors very small peaks that are almost indistinguishable from zero emission except for two cases of increased continuous emissions at around 100 minute time, what may once again be caused by particle penetration through the seams. The sensors mainly serve as a qualitative monitoring tool, though it has been shown in previous publications that different emission levels based on different filter media can be distinguished from local PM measurements [6, 22]. In these publications, longer cycle times of at least 60 seconds better enabled ideal emission behavior and an easier distinction of the individual peaks, compared to shorter cycle times, where continuous emissions appear more frequently. A cycle time of 30 seconds was selected in the test runs with the leak to lower the time duration for experiments consisting of 30 full filtration cycles and prevent damage to the testing facility due to increased dust exposure by particle bypass from the respective leaks.

Figure S5 shows a detail view of bag number 3 from figure S4.

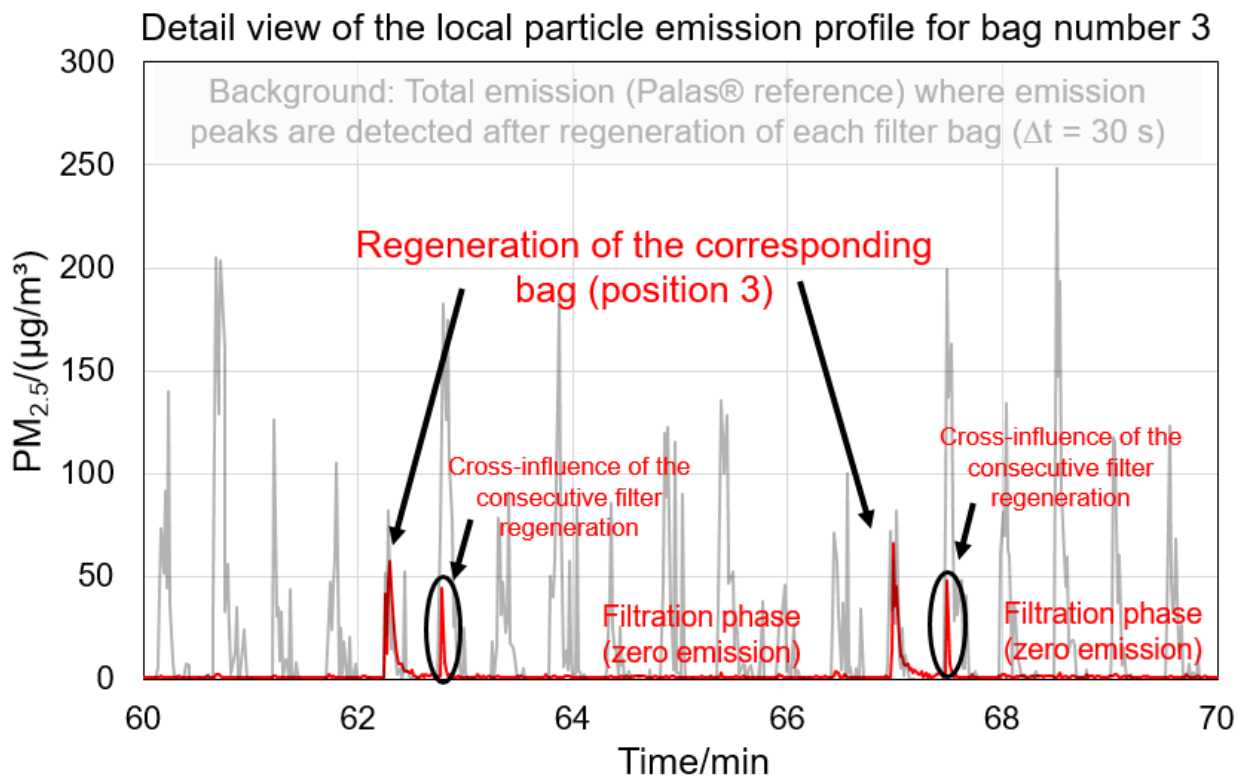


Figure S5. Detail view of filter bag number 3 regarding local and total dust emission

Ideal emission behavior can be clearly observed. The duration of the local peak is approx. 10 – 20 seconds until the drop to zero level. Note that the cycle time for this experiment was very low at only 30 seconds so that the filtration phase is quite short. Experiments with longer cycle times can be found in sources [6] & [22]. The peaks in the background, indicating the total emission, always decrease to a zero level in between filter regenerations. The local emission qualitatively corresponds to this behavior. One commonly observed measurement artifact is the detection of peaks other than the peak directly after the regeneration of the corresponding filter bag. The most pronounced secondary peak is typically the peak of the consecutive bag in the cleaning strategy.

Summarizing, low-cost PM-sensors may characterize the expected ideal emission behavior sufficiently well on a qualitative basis but cross-influence from the regeneration other filter bags cannot be avoided completely. These measurement artifacts caused by the sampling often have a lower peak height and/or duration and play only a subordinate role.

Impact of internal “sample flow rate” on calculated PM emissions (additional information for scenario 2)

As a final remark on the results obtained when measuring particle concentrations with low-cost PM-sensors, especially regarding measurements of the sensor OPC-N3 from Alphasense, the sensor internal “sample flow-rate” has to be mentioned. In addition to PM concentrations and counting events, the sensor supplies data on several other key parameters during operation (e.g. “laser status” as an indication of correct sensor operation, temperature, relative humidity, sample flow-rate). This is quite rare in comparison to other commercially available sensors that mostly yield mass based PM concentrations without further context. Note, that the manufacturer gives advice on how to best operate the sensor under ambient conditions (e.g. regarding sampling tubes, sensor housing, orientation etc.), which are different from our application in the filter house. Nonetheless, our

installation approach proved to be practical and pragmatic regarding the (geometrical) restrictions of our testing facility and the sensors have been installed in a variety of previous investigations in this manner (compare figure 3 of the article) [6, 22].

As shown in figure 7 of the manuscript, sharp drops or increases in PM concentrations may occur. These drops may be linked to a change in the internally logged sensor flow-rate as shown in Figure S6.

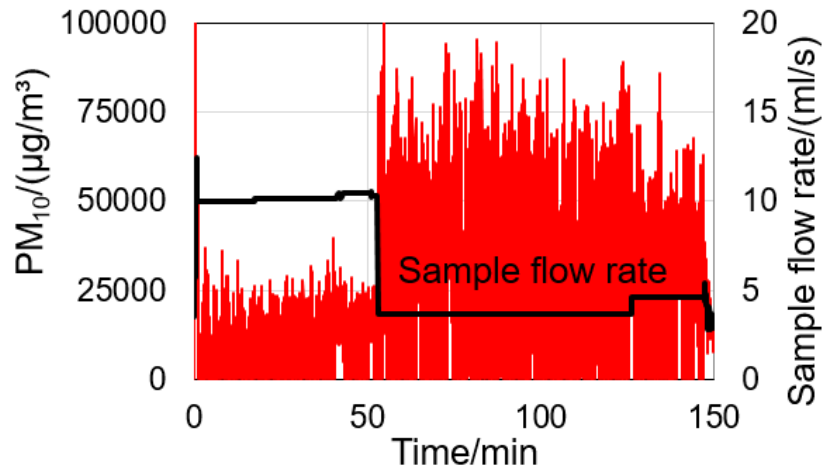


Figure S6. Sensor flow-rate for sensor 5 in figure 7 of the manuscript

Shortly after 50 minutes time, the sample flow-rate drops significantly from about 10 ml/s to approx. 4.5 ml/s. The specified sample flow-rate from the datasheet is 4.67 ml/s. The drop in sample flow-rate leads to an increase in PM₁₀ concentration. According to the manufacturer, the flow-rate is determined via a time of flight method. The sensor itself is operated with a small ventilator with a variable volume flow (respectively rotary speed) (total flow rate of 5.5 l/min according to the datasheet). It is not clearly specified in the manual of the sensor how the flow-rate is considered in internal data processing and the determination of mass based PM concentrations. According to these measurements, a direct impact is likely. An increase in concentration with a decrease in flow-rate is plausible, if a determined (constant) mass flow of particulate matter is related to a smaller volume.

Figure S7 shows the development of the sensor sample flow-rate during the “ideal emission behavior” for sensor 3 in figure S4.

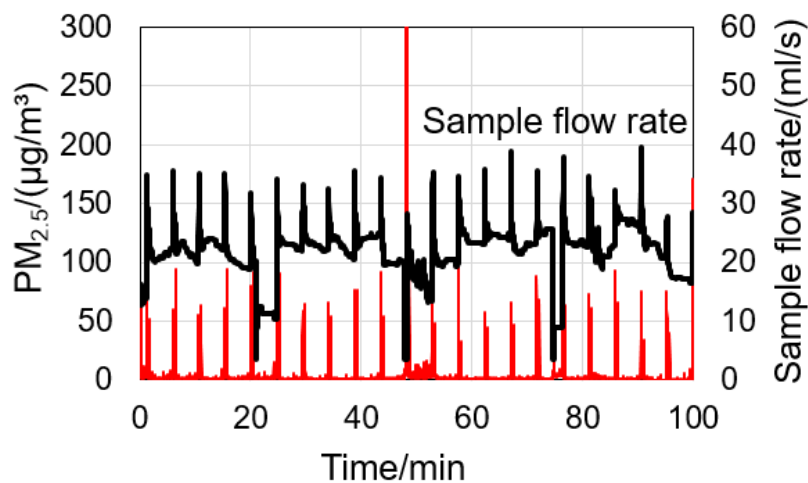


Figure S7. Sensor flow-rate for sensor 3 in figure S4

The sensor flow-rate is not constant during filter operation. Distinct changes in flow-rate are linked to the detected emission peaks and regenerations of other filter bags so that the profile of the sample flow rate in some cases corresponds qualitatively to the velocity profile within the baghouse [22]. It could

very well be that the sensor's internal determination of the sample flow-rate is influenced directly after the cleaning pulse as a larger fraction of emitted particles penetrates the filter element. Other experiments with longer cycle times have shown that the sample-flow rate remains constant during the filtration phase when no particles penetrate the filter medium.

A correction of the sample-flow rate (e.g. by implementing a correction factor that relates the currently determined sample flow-rate to the specified standard flow-rate) may improve the quantitative accuracy of the sensor. No such correction has been done in the publication, as the findings stand on their own and can be derived from the uncorrected raw-data. Nonetheless, the exact sensor behavior is certainly important when considering the implementation in technical facilities and offers a more in-depth interpretation of measured data.

Localization of a strong continuous emission hotspot (leak in the plenum plate) – scenario 3

As a third scenario, the detection of a leak of in the plenum plate was investigated. No low-cost PM-sensor was positioned directly at this emission hotspot. Figure S8 shows the spatial PM₁₀ emission profile for the measurement as well as a detail view of the total particle concentrations detected by the Palas® reference and the low-cost PM-sensor positioned at the outlet of the filter house.

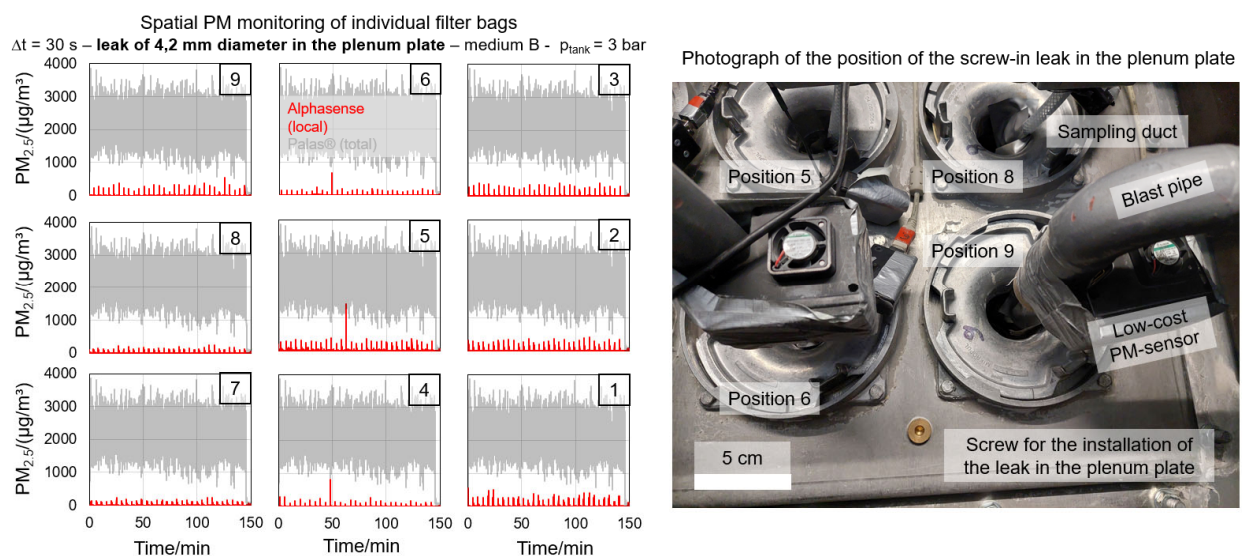


Figure S8. Spatial PM_{2.5} profile with a leak of 4.2 mm diameter in the plenum plate as a strong continuous emission hotspot.

The increase in particle concentration is only monitored by the measurement devices located at the outlet of the filter house. While the Palas® reference detects average PM_x concentrations of 2036 µg/m³ (PM_{2.5}) and 40 909 µg/m³ (PM₁₀), the low-cost PM-sensor at the outlet detects average concentrations of 1662 µg/m³ (PM_{2.5}) and 16 652 µg/m³ (PM₁₀). While this is a high quantitative difference, the low-cost PM-sensor could still detect the concentration increase and may serve a similar function like a triboelectric sensor for monitoring of the total concentration. The investigations shows the importance of correct positioning and sampling when employing a grid of low-cost PM-sensors for emission monitoring. The sensors have to be positioned close to the emission hotspot in order to monitor the increase in particle concentration and offer information on the spatial origin of the dust emission.

Publication III

Title: Simultaneous measurement of spatially resolved particle emissions in a pilot plant scale baghouse filter applying distributed low-cost particulate matter sensors

Authors: Peter Bächler, Julia Szabadi-Fuchs, Jörg Meyer, Achim Dittler

Journal: Journal of Aerosol Science

Year of Publication: 2020

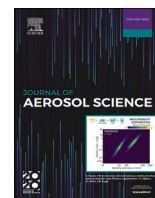
Volume and Issue: 150

Page Numbers: 105644

Reference: [Bächler et al., 2020]

Abstract:

Baghouse filters are widely applied in industrial gas cleaning, for example in waste incineration plants and the cement industry, to meet particle emission standards and for product recovery. The global particle emission of pulse-jet cleaned surface filters is typically monitored end of pipe (e.g. in the stack). Since the particulate matter emission of baghouse filters originates often from leaks and incorrectly installed or damaged filter bags, operators would greatly profit from online measurement technology that monitors the emission contribution of individual filter bags or at least a subset of all installed filter elements to the total emission. Low-cost particulate matter sensors can be deployed inside filter houses in larger quantities due to their compact design and low asset cost compared to conventional aerosol measurement technology. The ability of several low-cost sensors to detect the characteristic PM emission behavior of surface filters has been shown in previous investigations in a filter test rig. This study shows first results regarding the emission contribution of individual filter bags of a pilot plant scale baghouse filter employing distributed low-cost sensors of the model OPC-N3 from the manufacturer Alphasense. A Promo[®] 2000 aerosol spectrometer with a welas[®] 2100 sensor serves as reference regarding the particulate matter concentration detected by the low-cost sensors and as end of pipe measurement equipment to monitor the global emission. The selected filter medium was a membrane filter medium with sealed seams to provide low emission levels and defined conditions on the clean gas side. The employed low-cost sensors detect an emission peak right after cleaning of the corresponding filter bag only. The global emission measured in the clean gas duct consists of the overlay of the individual emission peaks detected locally at the corresponding filter bags. By exchanging one filter bag with a filter bag made from a non-membrane filter medium without sealed seams, an increase of the total continuous emission can be detected, both end of pipe in the clean gas duct and locally via the low-cost particulate matter sensor. This demonstrates the applicability of the measurement technology for the detection and identification of leaks and damaged filter bags that serve as emission hotspots in baghouse filters.



Simultaneous measurement of spatially resolved particle emissions in a pilot plant scale baghouse filter applying distributed low-cost particulate matter sensors

P. Bächler^{*}, J. Szabadi, J. Meyer, A. Dittler

Institute of Mechanical Process Engineering and Mechanics, Karlsruhe Institute of Technology, Straße Am Forum 8, 76131, Karlsruhe, Germany

ARTICLE INFO

Keywords:

Low-cost PM-sensors
Emission measurement
Dust separation
Surface filtration
Baghouse filtration
Smart filter

ABSTRACT

Baghouse filters are widely applied in industrial gas cleaning, for example in waste incineration plants and the cement industry, to meet particle emission standards and for product recovery. The global particle emission of pulse-jet cleaned surface filters is typically monitored end of pipe (e.g. in the stack). Since the particulate matter emission of baghouse filters originates often from leaks and incorrectly installed or damaged filter bags, operators would greatly profit from online measurement technology that monitors the emission contribution of individual filter bags or at least a subset of all installed filter elements to the total emission. Low-cost particulate matter sensors can be deployed inside filter houses in larger quantities due to their compact design and low asset cost compared to conventional aerosol measurement technology. The ability of several low-cost sensors to detect the characteristic PM emission behavior of surface filters has been shown in previous investigations in a filter test rig. This study shows first results regarding the emission contribution of individual filter bags of a pilot plant scale baghouse filter employing distributed low-cost sensors of the model OPC-N3 from the manufacturer Alphasense. A Promo® 2000 aerosol spectrometer with a welas® 2100 sensor serves as reference regarding the particulate matter concentration detected by the low-cost sensors and as end of pipe measurement equipment to monitor the global emission. The selected filter medium was a membrane filter medium with sealed seams to provide low emission levels and defined conditions on the clean gas side. The employed low-cost sensors detect an emission peak right after cleaning of the corresponding filter bag only. The global emission measured in the clean gas duct consists of the overlay of the individual emission peaks detected locally at the corresponding filter bags. By exchanging one filter bag with a filter bag made from a non-membrane filter medium without sealed seams, an increase of the total continuous emission can be detected, both end of pipe in the clean gas duct and locally via the low-cost particulate matter sensor. This demonstrates the applicability of the measurement technology for the detection and identification of leaks and damaged filter bags that serve as emission hotspots in baghouse filters.

1. Introduction

Pulse-jet cleaned surface filters remain state of the art technology for industrial gas cleaning, where particle mass concentrations in

^{*} Corresponding author.

E-mail address: peter.baechler@kit.edu (P. Bächler).

<https://doi.org/10.1016/j.jaerosci.2020.105644>

Received 29 April 2020; Received in revised form 15 July 2020; Accepted 4 August 2020

Available online 14 August 2020

0021-8502/© 2020 The Authors. Published by Elsevier Ltd. This is an open access article under the CC BY-NC-ND license

(<http://creativecommons.org/licenses/by-nc-nd/4.0/>).

the region of multiple grams per cubic meter have to be separated from dust-laden gas streams in order to fulfill emission standards. The key advantage of surface filters is the continuous operation, where a dust cake with a high separation efficiency is formed by collecting particles on the surface of a filter medium. The formation of the filter cake increases the differential pressure between the raw-gas side and the clean gas side. Thus, the cake has to be removed periodically, e.g. by a jet-pulse from the clean gas side, after a specified time has passed (Δt -controlled operation) or a maximum differential pressure is reached (Δp -controlled operation). The filter medium is often confectioned in the form of a filter bag and multiple filter bags are arranged inside a filter house dependent on the volume flow of the dust-laden gas.

Continuously tightening emission standards for technical facilities as well as the inclusion of particle size resolved immission limits in the form of $PM_{2.5}$ and PM_{10} mass concentrations put high demands on plant operators. An optimal operating strategy for surface filters would combine low emissions with a low energy consumption. In this context, the operation and emission behavior of baghouse filters is still subject of research. Here, filter tests are typically performed inside standardized test rigs [e.g. Binnig et al., 2009; Bach & Schmidt, 2007; Höflinger and Laminger, 2013; Sobich et al., 2018], that do not necessarily represent the operating conditions of industrial baghouse filters.

The usual end of pipe particle emission that can be detected in the clean gas duct of filter houses consists of a continuous baseline emission in addition to emission peaks after jet-pulse cleaning of the filter bags. The origins of the continuous emission are for example leaks or defects of filter bags and the plenum plate, incorrectly installed filter bags and the seams of the filter bag (Kurtz et al., 2017). Process conditions, especially the intensity of the cleaning pulse and the interval between cleaning pulses, can also play a role. Insufficiently short cleaning intervals may not grant enough time for cake buildup of the previously cleaned bag, so that the dust emission detected in the clean gas duct originates from multiple bags. This emission behavior is not reflected in filter tests, where mainly the emission of particle penetration through the filter medium itself contributes to the emission (Binnig et al., 2009).

Simon et al. studied the complex flow conditions inside a pilot filter unit and discussed the impact of newly regenerated filter bags on the total particle emission (Simon et al., 2010). Kurtz et al. showed the high impact of leaks on the global emission detected at the end of the pipe of baghouse filters (Kurtz et al., 2017). Similar investigations were led by Bach et al. who studied the influence of pinhole leakages in a filter test rig (Bach & Schmidt, 2007).

Due to the dominating role of leaks on the total particle emission, new methods for an easy on-line detection that help identify different emission levels within the baghouse can greatly help plant operators. Conventional methods for the detection of leaks include triboelectrical measurements and the use of fluorescent dust, both of which have drawbacks. Triboelectrical sensors enable on-line measurement of the global dust concentration on the clean gas side. Due to their size and comparably high cost, triboelectrical sensors are difficult to implement on multiple measurement points within the baghouse, thus offering no local information about the location of emission hotspots. The identification of leaks via fluorescent dust requires a temporary shutdown of the filter house and considerable troubleshooting concerning the location of the source of the PM emission (e.g. leaks, damaged filter media or plenum plate,

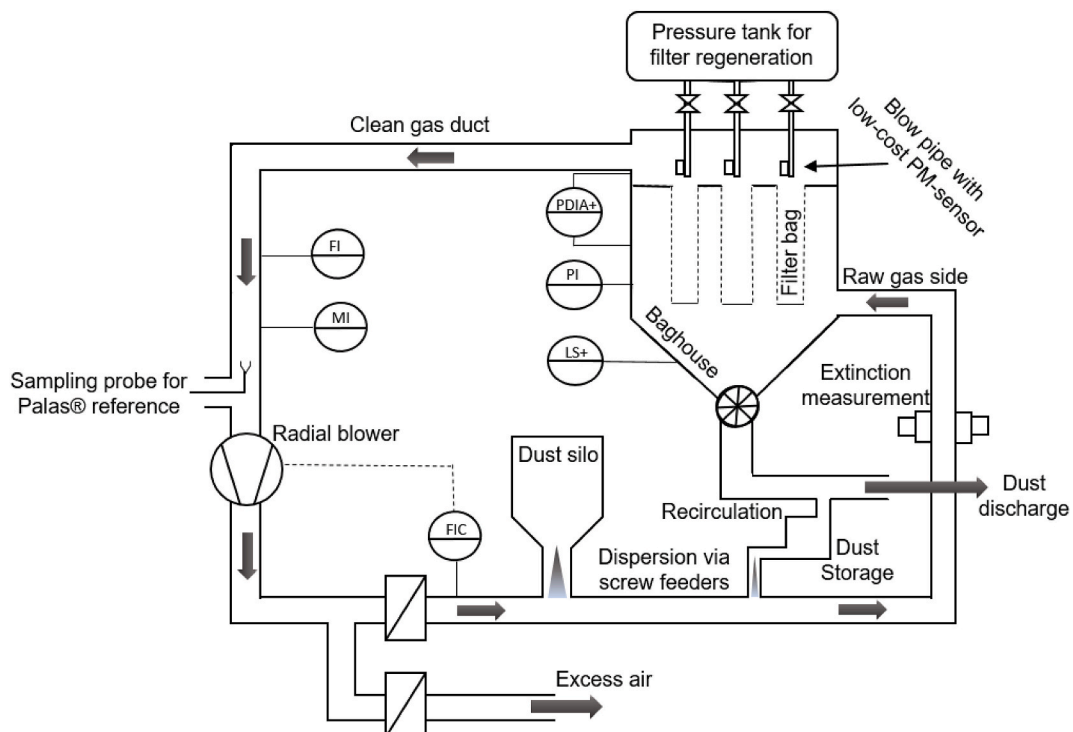


Fig. 1. Flow sheet of the pilot plant scale baghouse with nine filter bags.

incorrect installation of bags, etc.).

With increasing popularity of low-cost sensors for the determination of local particulate matter concentrations with respect to immission measurement, cheap and compact measurement technology is available that could potentially be used inside filter houses to detect local dust emissions of individual filter bags (Schwarz et al., 2018). Many publications exist that investigate sensor performance for the immission application, e.g indoor and outdoor air quality, detailing challenges regarding sensor accuracy, inter-sensor variability and impact of measurement conditions (e.g. relative humidity) [e.g. Asbach et al., 2018; Badura et al., 2019; Budde et al., 2018; Crilley et al., 2020; Feenstra et al., 2019; Karagulian et al., 2019; Kelly et al., 2016; Zou et al., 2020].

In previous publications, the suitability of low-cost sensors to characterize the typical emission behavior of surface filters have been investigated in a filter test rig. The characteristic emission peak after jet-pulse cleaning of the filter medium could be detected by the low-cost sensors. Additionally, different emission levels from different filter media could be identified from PM measurements using low-cost sensors (Bächler et al., 2019a, 2019b; Schwarz et al., 2018).

This publication presents first results regarding the local particle emission contribution of individual filter bags in a pilot plant scale baghouse employing spatially distributed low-cost sensors for simultaneous measurement of the local PM concentration with high temporal resolution.

2. Experimental set-up, procedures and materials

2.1. Pilot plant scale baghouse

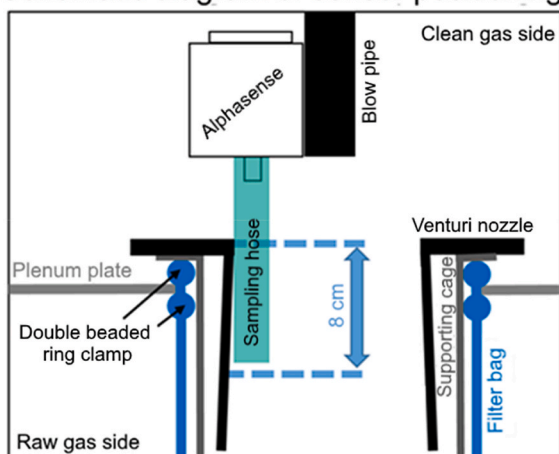
A pilot plant scale baghouse filter serves as the testing facility for the experiments. The corresponding schematic set-up is shown in Fig. 1. Contrary to typical filter test rigs, where circular filter coupons are investigated, the filter medium is confectioned as filter bags similar to the industrial application.

A total of nine filter bags (diameter 11.7 cm; length: 125 cm) are installed inside the baghouse. The bags are fixed on the plenum plate via MikroPul Venturi bayonet fittings and double beaded ring clamps, thus separating the raw and clean gas side of the testing facility. Each of the nine bags can be cleaned individually by a jet pulse from a blow pipe that is connected to a pressure tank. A radial blower recirculates the air flow through the testing facility. The air flow is adjusted to set an overall filter face velocity of approximately 120 m/h. Dust is fed in the raw gas duct via dosage from screw feeders at two different locations. A storage silo ensures that a sufficient amount of test dust is available. Additionally, collected dust is mostly recirculated to enable a more economic test operation. The dust dosage is controlled by an extinction measurement, which is calibrated to a gravimetric raw dust concentration of 5 g/m^3 . To determine the global particle emission in the clean gas duct, a Promo® 2000 aerosol spectrometer in combination with a welas® 2100 sensor from the manufacturer Palas® (<https://www.palas.de/prod>) draws a sample flow via an isokinetic probe in the downflow pipe of the clean gas.

The local PM emissions of the nine individual filter bags are measured via nine low-cost PM-sensors of the model OPC-N3 from the manufacturer Alphasense (<http://www.alphasense.com>), which are described in detail in the following chapter. One sensor is attached to each blow pipe for filter regeneration according to Fig. 2. A small hose is attached to the sensor outlet to be able to draw a sample closer to the outlet of the venturi nozzle of the individual bag and avoid lateral interferences and dispersion effects on the clean gas side. The sampling hose is fixed on the inside of the venturi nozzle.

In addition to emission measurement, other process parameters like the differential pressure between raw-and clean gas side, the signal of the extinction measurement, the total volume flow, temperature and the pressure inside the pressure tanks for filter regeneration are monitored by an independent process control system. The employed process parameters are summarized in Fig. 3. To

Schematic diagram of sensor positioning



Photograph of sensor at filter bag number 8

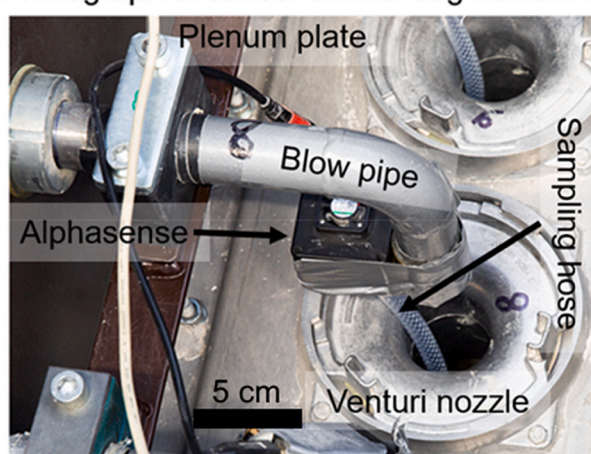


Fig. 2. Schematic diagram and photograph of sensor positioning.

be able to easily allocate filter regeneration events to the corresponding emission data, a Δt -controlled operation with a bag-by-bag cleaning rhythm (Fig. 3 - left) was selected for the experiments. The cleaning interval was set to 120 s to enable sufficient cake build up between the different filter regenerations, thus avoiding emission contribution of multiple bags due to insufficient cake build up. The differential pressure range during steady state operation was between 2 and 3 kPa. Before starting the experiments, a leakage test using fluorescent dust was performed to ensure that no significant leaks on the plenum plate exist and that the filter bags have been installed correctly.

2.2. Aerosol measurement technology

A Promo® 2000 aerosol spectrometer in combination with a welas® 2100 sensor from the manufacturer Palas® serves as the reference instrument, due to its high maximum concentration and accurate size categorization (<https://www.palas.de/prod>). As state of the art aerosol measurement technology, the Promo® 2000 corrects for coincidence and border zone errors. Particles that pass the measurement volume are assigned to a certain optical particle size dependent on intensity of the light that is scattered by particles. Based on the measured particle number and particle size, PM_x concentrations are subsequently calculated assuming spherical shape, a given particle density and index of refraction of the particle. The Palas® reference has been deployed both for the emission measurement of the clean gas via the extraction of a sample flow with an isokinetic probe and to investigate the local emission of an individual filter bag after regeneration to compare to PM measurements of distributed low-cost sensors.

To simultaneously investigate the local emission behavior of all filter bags of the pilot plant scale baghouse, nine low-cost PM sensors were spatially deployed. From a variety of commercially available sensors, the sensor OPC-N3 from the manufacturer Alphasense has been selected for the investigation (<http://www.alphasense.com>). In a previous publication, the low-cost PM -sensor SPS30 from the manufacturer Sensirion has been investigated regarding its performance for the characterization of the emission behavior of surface filters in a test rig according to ISO11057 (Bächler et al., 2019a). The Alphasense sensor showed similar results to the Sensirion sensor regarding the identification of different emission levels (Bächler et al., 2019b). Yet, the advantage of the Alphasense sensor compared over other low-cost PM -sensors is the improved size categorization of detected particles. In addition to PM_x -weighted mass concentrations, the sensor classifies particle counts in one of 24 size intervals across its measurement range. Additionally, the maximum concentration of the sensor is comparatively high at a specified mass concentration of $2000 \mu\text{g}/\text{m}^3$. A maximum number concentration is not stated; however, a coincidence probability of 0.84% can be expected at a particle number concentration of 10^3 \#/cm^3 according to the manufacturer (<https://www.palas.de/prod>).

The low-cost sensor allows for the consideration of aerosol properties through a coefficient called “bin-weighting index”. In its default setting, the bin weighting index is set at 1.65 (–) corresponding to a particle density of $1650 \text{ kg}/\text{m}^3$. A higher bin-weighting index thus causes a higher particle mass concentration due to an increased particle mass from the individual counting event (Crilley et al., 2020). The index of refraction of the dust, applied by the sensor, is 1.5 (–). As only the bin-weighting can be changed, only the particle density of the aerosol can be considered in the configuration of the Alphasense sensor.

Table 1 summarizes several key specifications of the two optical particle counters applied. The selected measurement range for the Palas® system was $0.2\text{--}10 \mu\text{m}$ to be close to the most penetrating particle size of surface filters and to obtain the most accurate $PM_{2.5}$ mass concentration (Binnig et al., 2009; Kurtz et al., 2017). The Alphasense sensor has by default a wider measurement range, due to its focus on immission measurement and the requirement to detect larger particles present in outdoor aerosols (e.g. pollen) (<https://www.palas.de/prod>). A low response time is crucial for emission measurement including a clear detection of the emission peak. The sensors have not been calibrated against each other or against the reference particle counter.

In the result section, the main value for characterization of the emission will be $PM_{2.5}$, as it has high relevance regarding human health and international immission law (German National Academy of Sciences, 2019). Furthermore, the $PM_{2.5}$ mass concentration is not as easily influenced by singular bigger particles compared to PM_{10} .

2.3. Test dust

The employed test dust was PURAL® SB from the manufacturer Sasol. It has a solid density of $2800 \text{ kg}/\text{m}^3$, a mass median diameter $x_{50,3}$ of $45 \mu\text{m}$ and an index of refraction of 1.64 (–) according to the manufacturer. The dust is non agglomerating and has good

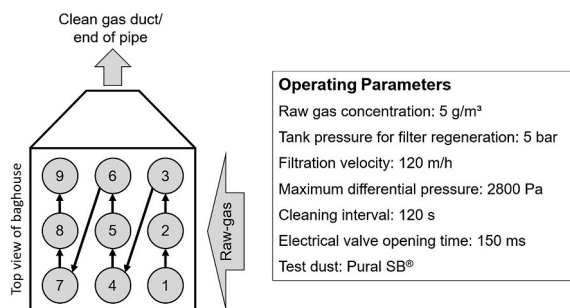


Fig. 3. Bag by bag cleaning rhythm and summary of operating parameters.

Table 1List of several key sensor specifications (<https://www.palاس.de/prod>; <http://www.alphasense.com>).

Device	OPC-N3	Promo® 2000 with welas® 2100
Manufacturer	Alphasense	Palas®
Measurements	Mass based concentration PM ₁ , PM _{2.5} , PM ₁₀ Count rate and size resolved particle counts	Mass and number based total concentration and size distributions with size resolved PM conversion
Detectable size range	0.35–40 µm	0.2–10 µm; 0.3–17 µm; 0.6–40 µm (user selectable)
Size categorization	24 bins	64 bins per decade
Maximum concentration	Mass based: 2000 µg/m ³ 0.84% coincidence probability at 1000 #/cm ³	5 · 10 ⁵ #/cm ³
Approximate cost (including required cables & connectors)	400 €	>30.000 €
Length x Width x Height	75 mm × 45 mm x 63.5 mm	245 mm × 100 mm x 80 mm (welاس® sensor only)
Response time	≈ 1 s	≈ 1 s
Configuration	ρ _{particle} = 2800 kg/m ³ n _{aerosol} = 1.5 (-) Spherical particles	ρ _{particle} = 2800 kg/m ³ n _{aerosol} = 1.59 (-) Spherical particles

dispersion properties, therefore the emission of the test dust in filter tests is higher compared to agglomerating dusts (Kurtz et al., 2017). The density of the test dust has been considered in the configuration of both, the low-cost sensors and the Palas® reference.

2.4. Filter media

The selected filter medium for the investigation is a polyphenylene sulfide medium with an ePTFE membrane layer laminated on the upstream side (area weight: 500 g m⁻²; air permeability (200 Pa): 30 l dm⁻² min⁻¹). This medium was also investigated in a previous publication and showed a lower emission compared to two filter media without a membrane (Bächler et al., 2019a). The filter medium was not aged significantly, however due to the membrane layer the storage of particles inside the medium is relatively low, so that filter aging has a reduced effect. A main source of emissions in baghouses are the seams of the filter medium (Kurtz et al., 2017). To provide a low emission level and defined conditions for the first evaluation of spatial emission measurement, the seams of the employed filter medium have been sealed with sealing compound. Fig. 4 shows SEM images of the filter medium before and after sealing the seams. The membrane layer can be clearly distinguished from the area around the seams, where regular fibers are visible.

3. Results and discussion

3.1. Reference measurement of emissions from individual filter bags using a Palas® Promo® 2000 aerosol spectrometer with welas® 2100 sensor

As a first step, measurements employing the Palas® reference system have been performed at each individual filter bag in order to evaluate the performance of the low-cost sensors afterwards. The data for each filter bag had to be taken from an individual experiment, as parallel deployment of multiple welas® 2100 sensors is not possible from an economic point of view, due to the comparatively high cost of the measurement instrument compared to low-cost PM-sensors. The whole Palas® system was located outside of

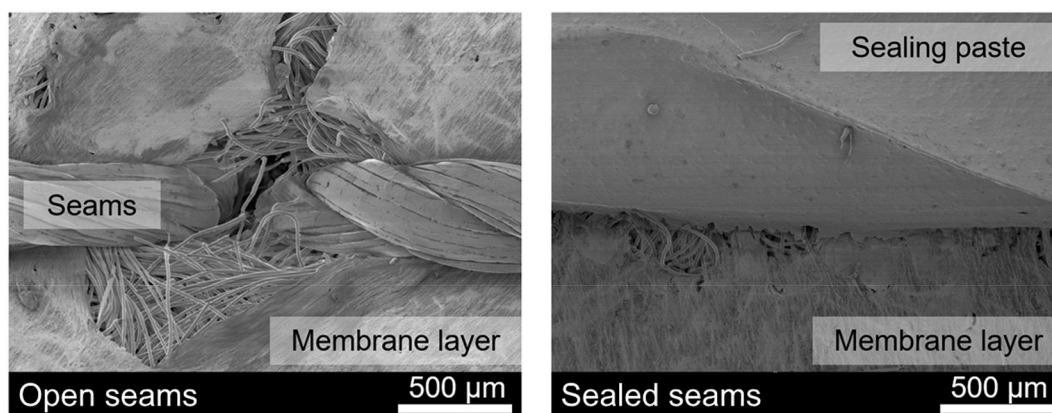


Fig. 4. SEM images of the membrane filter medium with open (left) and with sealed (right) seams.

the filter house, while the inlet tube for the welas® 2100 sensor was connected to the interior of the clean gas side of the baghouse. A sampling hose was then led from the inlet tube to the respective filter bag to measure the local PM emission similarly to the deployment of the low-cost sensor (see appendix for detailed figure of setup).

The time dependent PM-series of a complete filtration cycle (consisting of a time controlled regeneration series of all of the nine filter bags individually) is shown for the central filter bag (bag 5) in Fig. 5. The differential pressure curve serves as an indication for the cleaning pulses for a single bag occurring every 120 s. After each jet pulse, the differential pressure decreases rapidly due to the detachment of the filter cake.

The results show a single distinct PM_{2.5} emission peak with high intensity during each complete filtration cycle (one filter regeneration of each bag). This emission peak can be allocated to the jet-pulse cleaning of the corresponding filter bag. The dust cake that is formed on the surface of the filter medium during operation has a high separation efficiency. Cake removal via jet pulse enables particle penetration through the filter medium at the respective measurement position, what causes the characteristic PM emission peak in surface filtration (Binnig et al., 2009). Almost no continuous emission flux between the respective peaks is detected mainly due to the sealing of the seams of the filter bag (Kurtz et al., 2017). Hence, the emission behavior is similar to the ideal emission behavior typical for filter coupon test rigs (Bächler et al., 2019a). The measurement is slightly influenced by the consecutive regeneration of the next filter bag, however the intensity of this peak is much lower compared to the actual cleaning. Other runs at different filter bags show qualitatively similar results, where the emission peaks with the highest intensity can be clearly designated to the regeneration of the corresponding filter bag and regenerations of the adjacent filter bags are detected with lower intensity, if at all.

This low emission level should create unproblematic conditions regarding sensor lifetime, as during the filtration phase, almost no contamination of the sensor optics can occur. More realistic testing conditions at a higher emission level, where filter bags with open seams are employed might be a challenge for the lifetime of low-cost PM-sensors.

For better assessment of sensor accuracy during the cleaning event, the particle number concentration detected by the Palas® reference during individual measurements at each single filter bag is shown in Fig. 6.

Note that a direct comparison between each measurement is not possible, as the reference could only be employed at a single bag, nonetheless the data gives an overview of the approximate number concentration after cleaning. As the number concentration right after cleaning often exceeds the concentration limit of 1000 #/cm³ of the Alphasense sensor, a coincidence free measurement with the low-cost sensor at all times is unlikely.

3.2. Results of simultaneous local emission measurement at individual filter bags

For the simultaneous measurement of the local PM_{2.5} concentration on the clean gas side of the baghouse, one Alphasense sensor has been installed at each of the nine filter bags according to Fig. 2. The Palas® reference has been set up for measurement of the global PM emission downstream on the clean gas side (Fig. 1).

Fig. 7 shows the time resolved local PM_{2.5} concentration measured simultaneously by the low-cost sensors at each filter bag compared to the global end of pipe emission detected on the clean gas side by the Palas® reference.

The detected PM emission contribution of the individual filter bag is qualitatively similar to the reference measurement discussed in the previous chapter (Fig. 6). Every low-cost sensor detects a clearly assignable emission peak after the regeneration of the corresponding filter bag. Local differences between the individual filter bags exist. When comparing the PM_{2.5} concentrations of all low-cost sensors with the reference measurement at the end of the pipe, the emission peaks detected by the low-cost sensors at each individual filter bag correspond predominantly to an emission peak detected by the Palas® reference further down the clean gas duct. The global emission consists qualitatively of the overlay of the individual PM measurements of the low-cost sensors.

Differences regarding peak intensity and the overall detected particulate matter concentration between the two measurement devices are to be expected (e.g. different detectable size ranges) (Asbach et al., 2018; Bächler et al., 2019b). Additionally, the concentration detected at the filter bag as an emission hotspot can deviate from the concentration detected in the downflow pipe due to several reasons. Firstly, dilution effects due to a higher cross section of the downflow pipe on the clean gas side could lower the detected concentration compared to the emission hotspot. Though the majority of the total volume flow passes the newly regenerated bag, the emitted particle mass gets further diluted by the volume flow through the other eight filter bags, lowering the concentration of

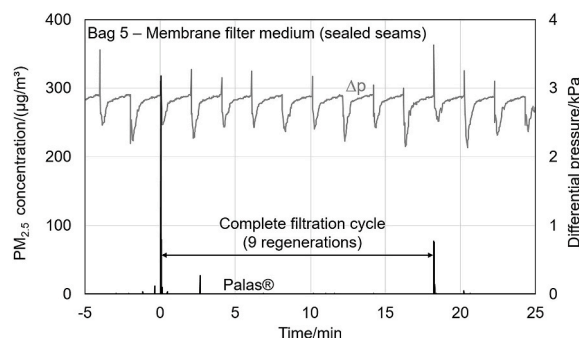


Fig. 5. Time dependent PM_{2.5} concentration detected by the Palas® reference at the central filter bag (bag 5) and differential pressure curve.

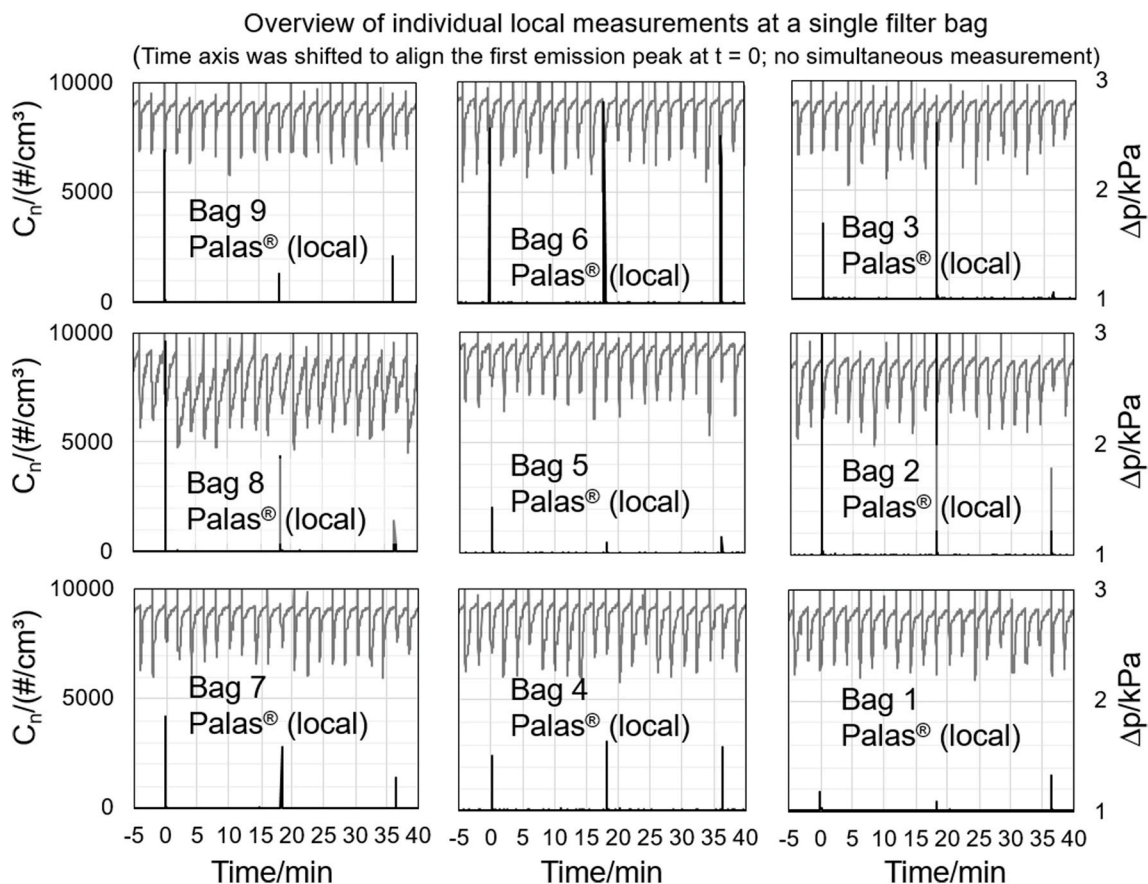


Fig. 6. Overview of time dependent particle number concentrations detected by the Palas® reference at each filter bag (no simultaneous measurement) and differential pressure curve.

the emitted particle mass. Secondly, spatial inhomogeneity of the particle concentration inside the filter bag could cause differences between the actual emitted particle mass that affects the global PM emission and the resident concentration that is detected at the sampling position of the sensor.

Finally, signal smoothing (unspecified for the low-cost sensor) and the response time regarding swift concentration variations in the case of a cleaning event affect the output signal peak height.

For further evaluation of the individual PM emission peaks, Fig. 8 displays a comparison between the peak detected locally at the recently cleaned filter bag with the emission peak detected at the end of the pipe by the Palas® reference.

Note that the overall emission level is low due to the high separation efficiency of the membrane filter medium and the sealed seams. Thus, the emission itself only occurs over a time period of several seconds, where the peak intensity is often defined by only one or two datapoints, making an in depth quantitative evaluation difficult. Additionally, the measuring conditions at the end of the pipe and the local measurement are different (e.g. different volume flow/dilution of emitted particle mass), so that for a better quantification of the PM emission, not the concentration but the emitted dust mass would have to be considered.

Furthermore, as these results describe the very first stages of filter life, fluctuations between individual cleaning events regarding peak intensity are to be expected. Coincidence errors caused by high particle number concentrations after jet-pulse cleaning could potentially affect the measurement result of the low-cost sensors, as was shown by the particle number concentrations detected by the Palas® reference in Fig. 6. Another factor that has to be considered regarding sensor accuracy is the flow through the sensor. The pressure pulse and the varying flow conditions on the clean gas side influence the sensor's sampling flow and could potentially affect the detected PM concentrations. To be able to create more defined measurement conditions, a sensor housing will be employed in future investigations to be able to draw a defined volume flow and improve sensor accuracy.

Summarizing, the low-cost sensors can qualitatively characterize the spatial PM emission behavior of baghouse filters under the applied defined conditions (sealed seams, low emission level). This demonstrates the potential for improved process monitoring by the application of distributed sensors. Deviations to the steady state PM emission behavior could be detected and alarm plant operators. The following chapter presents results regarding the identification of a local emission hotspot.

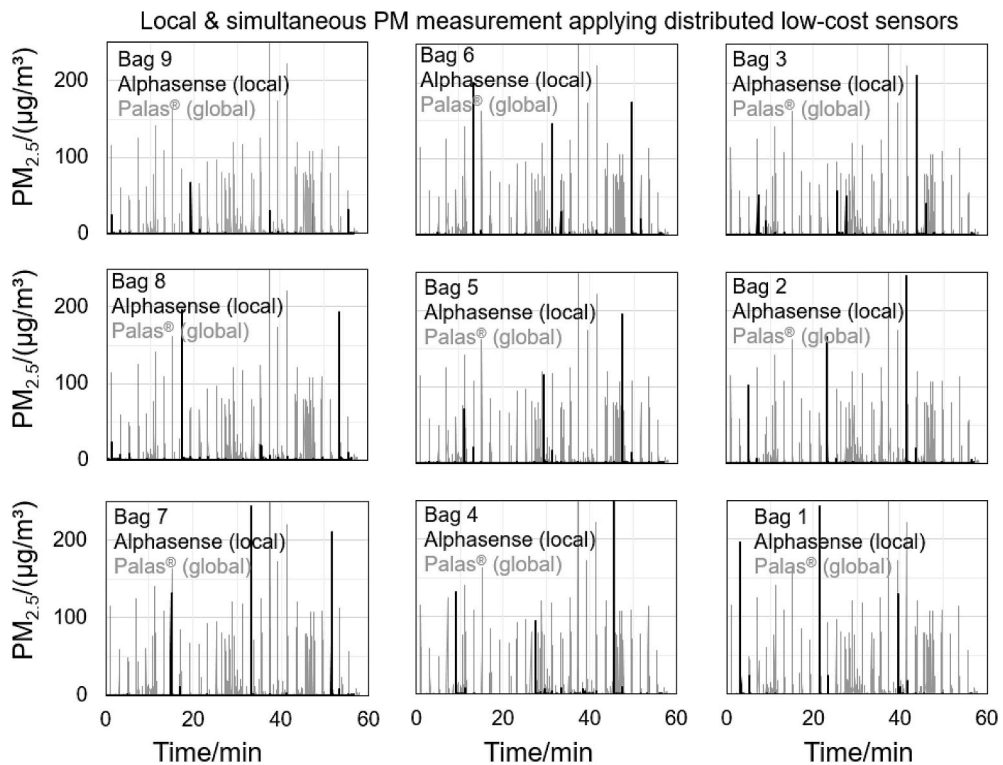


Fig. 7. Simultaneous PM_{2.5} measurement employing nine low-cost sensors (one at each individual filter bag) and comparison with the detected global emission by the Palas® reference on the clean gas side. All bags made from membrane medium with sealed seams.

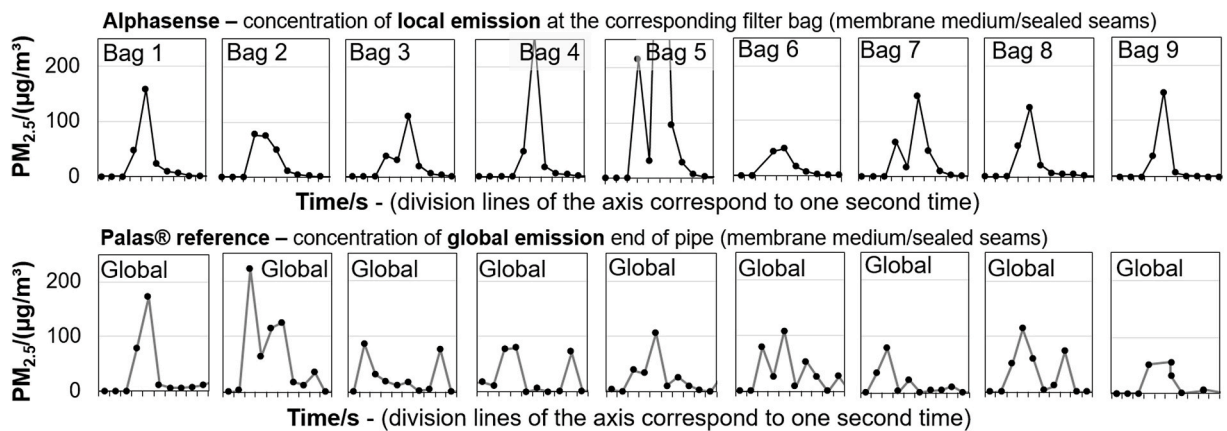


Fig. 8. PM Emission peak of recently cleaned filter bag detected by a locally deployed Alphasense sensor and the Palas® reference measuring the global emission (Time axis always represents the 10 s time period where the corresponding PM emission peak is detected).

3.3. Impact of a different filter media on local and global PM emission level

To investigate the contribution of locally increased emission levels, one of the bags made from the membrane medium with sealed seams has been exchanged by a filter bag made from a non membrane medium (area weight of 240 g m⁻²; no membrane; air permeability at 200 Pa of 100 l dm⁻² min⁻¹) and with open seams. The emission of the replacement filter bag is expected to be higher, as the seams contribute to the emission and the efficiency of the more open base felt is not boosted by a membrane layer. The filter medium has been evaluated in a filter test rig and showed a higher emission level compared to the membrane filter medium (Bächler et al., 2019a).

The time resolved PM_{2.5} measurements are shown in Fig. 9. The regular filter bag has been installed at position nine for this experiment. The Palas® reference detects a strong increase in the continuous particle emission in the clean gas duct.

The difference in particle emissions from the two different types of filter bags can be clearly identified in the local $PM_{2.5}$ concentration measured by the low-cost sensors. While the sealed membrane medium only shows an emission peak directly after jet pulse cleaning of the corresponding filter bag, the particle emission of the exchanged bag is vastly different. Instead of clearly assignable emission peaks, a permanent particle emission flux is detected. This steady flux coming from bag number nine does not influence the measurements at adjacent filter bags, which still show an ideal emission behavior.

For the validation of the spatially resolved data, reference measurements employing the Palas® system have been performed at filter bag number nine and the adjacent bag number six in two consecutive test runs (Fig. 10).

The reference measurement qualitatively validates the spatially resolved data. While the PM emission of the membrane medium with sealed seams only consists of the peaks right after cleaning of bag 6, the PM emission of the non-membrane medium without sealed seams at bag nine has a permanent PM emission and emission peaks with high intensity after jet-pulse cleaning. The peak concentrations detected by the Palas® reference at these two bags are higher compared to the PM emission detected by the low-cost sensors, exceeding the maximum mass concentration specified in the datasheet of the low-cost sensor (Fig. 10) (<http://www.alpha-sense.com>). This is another indication, that the measurements of the low-cost sensors could potentially be affected by coincidence errors or signal smoothing, limiting their potential for quantitative information. The permanent emission is increasing over the course of each complete filtration cycle and decreases after the PM emission peak due to jet-pulse cleaning. The global emission presented in Fig. 9 does not show the same trend and does not change significantly over time. This could potentially be an indication that the seams are not clogged by the dust cake and serve as a constant PM emission source. A possible explanation for the rising continuous particle emission detected at filter bag number nine can be given by evaluation of the flow conditions inside the baghouse.

Several Schmidt® SS.20.250 flow sensors have been employed to determine the local flow-velocity at the outlet of each filter bag (see appendix for detailed figure of setup).

A qualitatively similar velocity profile was obtained at all nine measurement locations. Due to the limited space available on the clean gas side not all flow sensors could be installed exactly the same way, so that slight variations are to be expected. Fig. 11 shows the flow velocity for filter bag number nine measured with the flow sensor and the PM emission of the non-membrane medium without membrane and sealed seams.

Directly after regeneration, the velocity through the filter bag increases, as the flow resistance of the filter bag is lowered due to the removal of the dust cake. With increasing thickness of the dust cake during operation, the volume flow through the filter bag, respectively the flow velocity, decreases at the newly regenerated bag. The regeneration of consecutive filter bags abruptly decreases the flow of the other bags, as a higher fraction of the total flow passes the newly regenerated bag. Over the course of the cake formation of the regenerated bag, the flow through all other bags increases slightly. The results correspond to the findings of Simon et al., who investigated the flow through individual filter bags. They already demonstrated that the flow through recently cleaned bags is higher

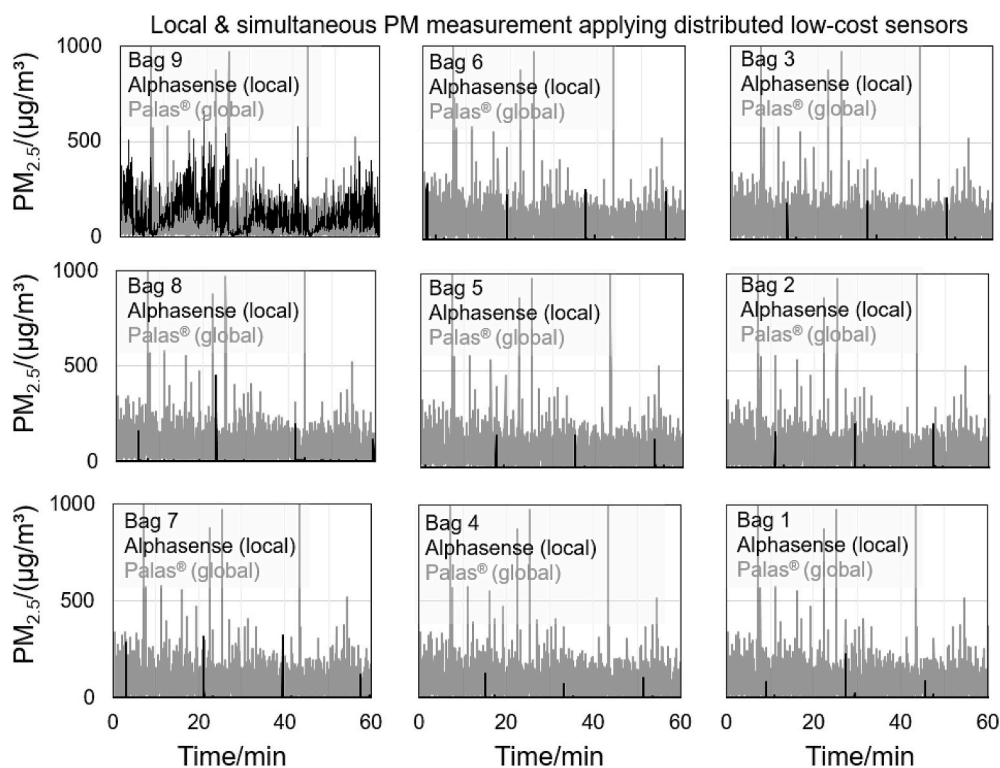


Fig. 9. Simultaneous $PM_{2.5}$ measurement employing nine low-cost sensors (one at each individual filter bag) and comparison with the detected global emission by the Palas® reference on the clean gas side. Bags 1–8: membrane medium. Bag 9: non-membrane medium with open seams.

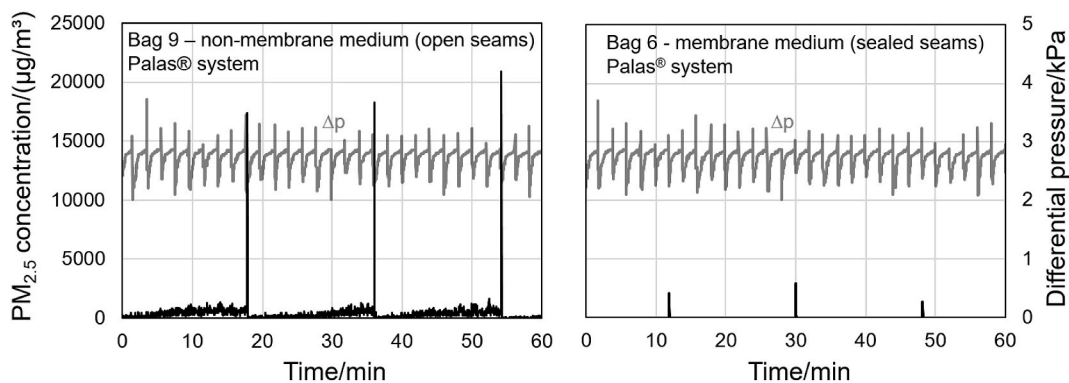


Fig. 10. Reference measurement employing the Palas® system at bag nine with the non-membrane medium and bag six with the filter bag made from a membrane medium with sealed seams.

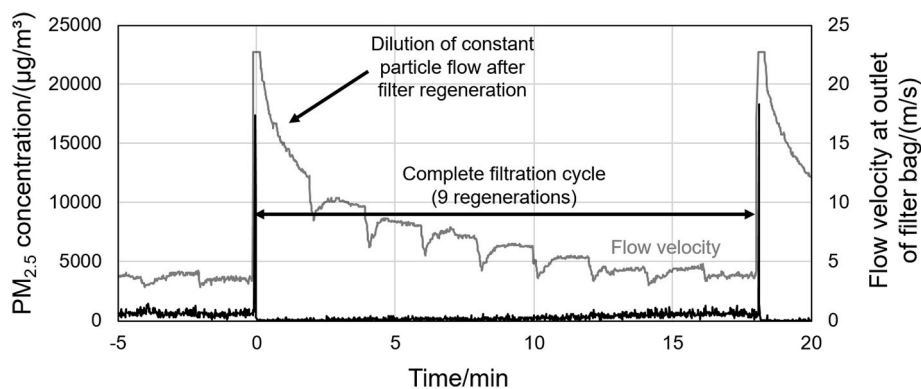


Fig. 11. Reference measurement employing the Palas® system at bag nine with the non-membrane medium and flow-velocity measured with a Schmidt® SS 20.250 flow sensor.

compared to clogged bags with an established dust cake (Simon et al., 2010). The absolute velocities right after jet-pulse cleaning are likely to be influenced by the pressure pulse and the sensor reaches its maximum value.

Since the passage of particles through the seams is likely not significantly affected by the cake formation on the filter medium, as shown by the permanent PM emission in Fig. 8, dilution effects can explain the rising particle concentration detected by the Palas® reference. Assuming a constant particle flow through the seams of the filter bag, a high total flow through the bag after jet pulse cleaning dilutes the local particle concentration at the outlet of the filter bag. With increasing cake thickness the flow through the medium decreases, thus the local concentration of the continuous PM emission is higher by comparison.

In addition to different particle concentration levels, the local particle size distribution is also affected by the exchanged filter bag (Fig. 12). The size distribution for the low-cost sensors has been calculated from the sampling flow rate, time interval and the number of particles for the corresponding size interval.

The number concentration varies and is about an order of magnitude lower for bag number six, where bigger particles with a diameter higher than $1\ \mu\text{m}$ are only rarely detected (single counting events) due to the membrane and sealing of the seams. The highest number of particles is detected close to the most penetrating particle size of surface filters at about $0.3\ \mu\text{m}$. The respective size distributions of reference and low-cost sensor deviate, which can be attributed to sensor limitations (e.g. sampling conditions, coincidence effects, etc.). Due to the limited use of the detected particle size distributions, cheaper PM sensors with limited sizing might also be suitable for simple PM monitoring (Bächler et al., 2019a). Improved sampling conditions might improve the potential for size resolved information and will be investigated further.

The results demonstrate potential applications for the implementation of spatially resolved particle emission level measurements. The emission hotspot can be easily identified by the $\text{PM}_{2.5}$ concentration measured by one of the low-cost sensors. This could potentially help operators detect damaged filter media or leaks. It remains to be seen how well the qualitative information of the low-cost PM-sensors follows similar trends in comparison to the reference measurements for different process conditions and emission levels.

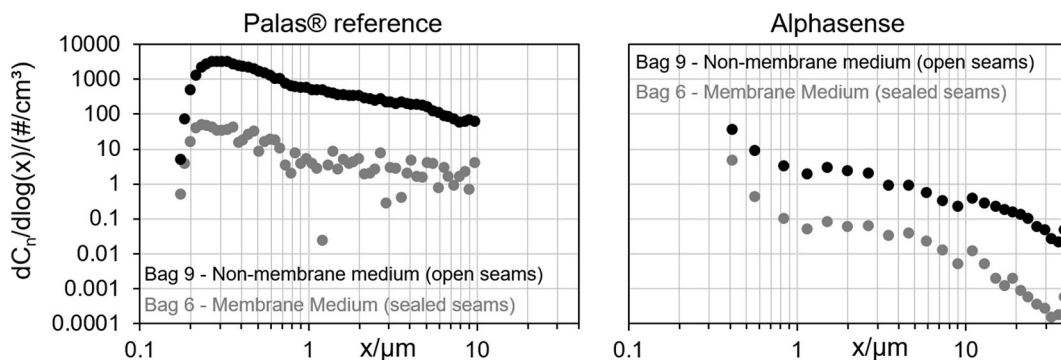


Fig. 12. Particle size distributions detected by the Palas® system and the low cost sensor at bag nine with the non-membrane medium and bag 6 with the filter bag made from a membrane medium with sealed seams.

4. Summary and outlook

The local PM emission contributions of individual bags to the overall PM emission of a pilot plant scale baghouse filter was evaluated under defined conditions by equipping each filter bag with a low-cost PM-sensor. Contrary to typical emission measurement, where only a global emission in the clean gas duct is evaluated, the novel approach of utilizing distributed sensors in baghouse filters allows for the detection of spatially resolved PM-emission data with high temporal resolution.

The baghouse filter was equipped with nine filter bags that were made from an e-PTFE laminated needle felt and all seams were sealed to provide a low emission level on the clean gas side. The filter regeneration was time-controlled with intervals set at 120 s to enable a sufficient cake formation after each cleaning pulse to lower potential interferences and dispersion effects. The selected low-cost PM-sensor for this investigation was the sensor OPC-N3 from the manufacturer Alphasense.

A reference measurement employing a Palas® Promo® 2000 in combination with a welas® 2100 sensor showed clear emission peaks after the regeneration of each filter bag when measuring in the collector line of the clean gas, and a distinct single peak associated with the respective regeneration pulse when measuring at the exit of a single bag. A permanent emission flux typical for baghouses at real conditions was prevented due to sealing of the seams of the filter bag, and regenerations of adjacent bags were either not detected or had small peak heights compared to peaks caused by the regeneration of the corresponding bag.

One low-cost sensor was mounted above the outlet of the venturi nozzle of each filter bag, thus enabling the simultaneous measurement of the spatial particulate matter concentration during operation of the baghouse filter. The detected PM-emission was qualitatively similar to results of the reference measurement (distinct PM emission peaks after jet-pulse cleaning).

Differences in the local emission levels were provided by exchanging one of the filter bags with membrane layer and sealed seams with a filter bag without membrane and with open seams. A constant emission flux and a higher emission level with less pronounced emission peaks was detected at the measurement position of the exchanged bag. The detected particle emission level of the original bags was not affected by the exchanged bag, and pronounced emission peaks, which can be assigned to the regeneration of the respective filter bag, were still detected. This demonstrates the potential for the detection of damaged filter media or filter media with different properties in real applications, provided the emission level on the clean gas side is low enough.

In further investigations, the applicability of the low-cost sensors under different conditions (e.g. different filter media, tank pressures, cleaning intervals, raw-gas concentrations) will be tested. The applied process parameters in this study aimed to generate a low emission level with clearly assignable events (e.g. filter regenerations). Additionally, the local particle size distribution of the emission will be evaluated to potentially gain further information on filter aging, leaks and damaged filter media from the size distribution.

Further challenges regarding the industrial application of low-cost PM-sensors include the lifetime and functionality of these sensors under real process conditions over a larger period of time. Exposure to increased temperatures, corrosive gases, or higher dust concentrations that might cause soiling of sensor optics are limitations to the current state of technology of low-cost PM-sensors. This study showed first results of spatial and simultaneous PM emission monitoring in a baghouse filter and the potential to characterize the local emission behavior at a low emission level applying highly efficient membrane filter media with sealed seams as well as to show potential for further applications regarding identification of different emission levels on the clean gas side.

The goal of this research is to transfer the conclusions from spatially resolved measurements to optimization strategies to improve the operating behavior of baghouse filters regarding energy demand and their particle emission, as well as employing aspects of digitalization like predictive maintenance and online process monitoring.

Declaration of competing interest

The authors declare that they have no known competing financial interests or personal relationships that could have appeared to influence the work reported in this paper.

Acknowledgements

We acknowledge the financial support and close cooperation of Filterkonsortium at KIT. Filterkonsortium at KIT unites leading companies in the fields of fiber and media production, assembly, plant engineering and measurement technology with the research activities of the working group Gas-Particle-Systems of the Institute of Mechanical Process Engineering and Mechanics (MVM). The members of Filterkonsortium at KIT are as follows: BWF Tec GmbH & Co. KG, ESTA Apparatebau GmbH & Co. KG, Evonik Fibres GmbH, Freudenberg Filtration Technologies SE & Co. KG, Junker-Filter GmbH, KAYSER FILTERTECH GmbH, MANN + HUMMEL GmbH, PALAS GmbH, Sick AG.

We acknowledge the collaboration of Grigor Vrhovac for his help in conducting the experiments.

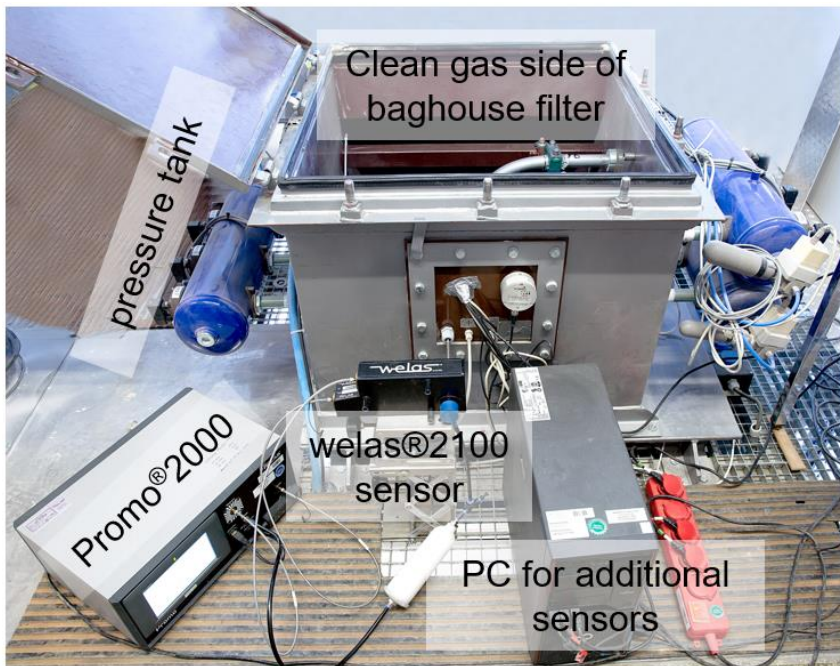
Appendix A. Supplementary Figures

Supplementary figures to this article can be found online at <https://doi.org/10.1016/j.jaerosci.2020.105644>.

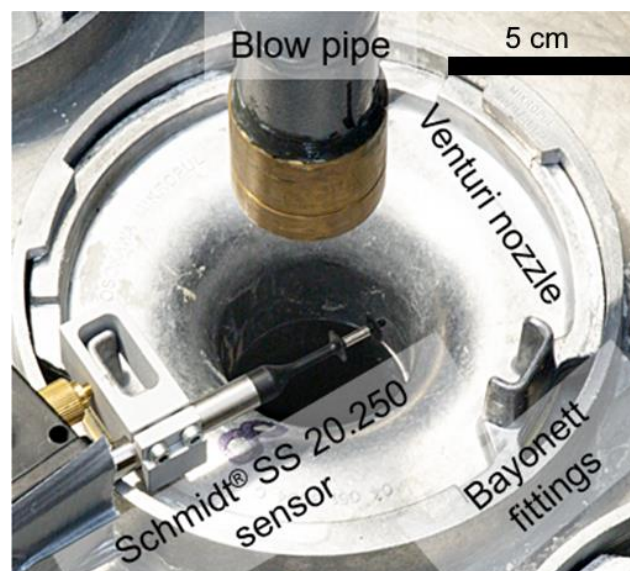
References

- Asbach, C., Hellack, B., Schumacher, S., Bässler, M., Spreitzer, M., Pohl, T., Weber, K., Monz, C., Bieder, S., Schultze, T., & Todea, A. M. (2018). Anwendungsmöglichkeiten und Grenzen kostengünstiger Feinstaubsensoren. *Gefahrstoffe Reinhaltung der Luft*, 78(6), 242–250.
- Bächler, P., Meyer, J., & Dittler, A. (2019a). Characterization of the emission behavior of pulse-jet cleaned filters using a low-cost particulate matter sensor. *Gefahrstoffe Reinhaltung der Luft*, 79(11–12), 443–450.
- Bächler, P., Meyer, J., & Dittler, A. (2019b). Investigation of low-cost PM-sensors regarding the suitability for emission measurement for pulse-jet cleaned filters. In *Conference paper at FILTECH 2019 – the filtration event (Cologne)*.
- Bach, B., & Schmidt, E. (2007). Influence of leaks in surface filters on particulate emissions. *Journal of Hazardous Materials*, 143(3), 673–676. <https://doi.org/10.1016/j.jhazmat.2007.01.093>.
- Badura, M., Batog, P., Drzeniecka-Osiadacz, A., & Modzel, P. (2019). Regression methods in the calibration of low-cost sensors for ambient particulate matter measurements. *SN Applied Sciences*, 1(622). <https://doi.org/10.1007/s42452-019-0630-1>.
- Binnig, J., Meyer, J., & Kasper, G. (2009). Origin and mechanisms of dust emission pulse-jet cleaning filter media. *Powder Technology*, 189(1), 108–114. <https://doi.org/10.1016/j.powtec.2008.06.012>.
- Budde, M., Schwarz, A. D., Müller, T., Laquai, B., Streibl, N., Schindler, G., et al. (2018). Potential and limitations of the low-cost SDS011 particle sensor for monitoring urban air quality. *Proscience Dust*, 2018(5), 6–12.
- Cirilley, L. R., Singh, A., Kramer, L. J., Shaw, M. D., Alam, M. S., Apte, J. S., et al. (2020). Effect of aerosol composition on the performance of low-cost optical particle counter correction factors. *Atmospheric Measurement Techniques*, 13, 1181–1193. <https://doi.org/10.5194/amt-13-1181-2020>.
- Feenstra, B., Papapostolou, V., Hasheminassab, S., Zhang, H., Boghossian, B., Cocker, D., et al. (2019). Performance evaluation of twelve low-cost PM_{2.5} sensors at an ambient air monitoring site. *Atmospheric Environment*, 216, 116946. <https://doi.org/10.1016/j.atmosenv.2019.116946>.
- German National Academy of Sciences Leopoldina. (2019). Clean air. Nitrogen oxides and particulate matter in ambient air: Basic principles and recommendations. Halle (Saale) https://www.leopoldina.org/uploads/tx_leopublication/2019_Leo_Stellungnahme_Saubere_Luft_en_web_05.pdf.
- Höflinger, W., & Laminger, T. (2013). Standard test procedure to characterize different filter media under energy consideration. *Energy and Sustainability*, 176, 3–13. <https://doi.org/10.2495/ESUS130121>.
- Karagulian, F., Barbiere, F., Kotsev, A., Spinelle, L., Gerboles, M., Lagler, F., et al. (2019). Review of the performance of low-cost sensors for air quality monitoring. *Atmosphere*, 10(9), 506. <https://doi.org/10.3390/atmos10090506>.
- Kelly, K., Whitaker, J., Petty, A., Widmer, C., Dybwad, A., et al. (2016). Ambient and laboratory evaluation of a low-cost particulate matter sensor. *Environmental Pollution*, 221, 491–500. <https://doi.org/10.1016/j.envpol.2016.12.039>.
- Kurtz, O., Meyer, J., & Kasper, G. (2017). The contribution of small leaks in a baghouse filter to dust emission in the PM_{2.5} range – a system approach. *Particuology*, 30, 40–52. <https://doi.org/10.1016/j.partic.2016.08.001>.
- Schwarz, A. D., Meyer, J., & Dittler, A. (2018). Opportunities for low-cost particulate matter sensors in filter emission measurements. *Chemical Engineering & Technology*, 41(9), 1826–1832. <https://doi.org/10.1002/ceat.201800209>.
- Simon, X., Bémer, D., Chazelet, S., Thomas, D., & Régnier, R. (2010). Consequences of high transitory airflows generated by segmented pulse-jet cleaning of dust collector filter bags. *Powder Technology*, 201(1), 37–48. <https://doi.org/10.1016/j.powtec.2010.02.036>.
- Sobich, S., Meyer, J., & Kasper, G. (2018). Baghouse filtration: A praxis-relevant media parameter to determine an emissions level of a pulse-jet cleanable filter. In *Conference paper at FILTECH 2018 – the filtration event (Cologne)*.
- Zou, Y., Young, M., Chen, J., Liu, J., May, A., & Clark, J. D. (2020). Examining the functional range of commercially available low-cost airborne particle sensors and consequences for monitoring of indoor air quality in residences. *Indoor Air*, 30(2), 213–234. <https://doi.org/10.1111/ina.12621>. <http://www.alphasense.com/index.php/products/optical-particle-counter/> accessed on 03/20/2020. <https://www.palasd.com/product/promo2000> accessed on 03/20/2020.

1. Supplementary Information



Appendix 1 – Setup of reference measurement employing the Palas® system at individual filter bags on the clean gas side of the filter



Appendix 2 – Photograph of one Schmidt® SS 20.250 sensor installed at the outlet of the venturi nozzle

Publication IV

Title: Process integrated monitoring of spatially resolved particle emissions of a baghouse filter using a network of low-cost PM-sensors

Authors: Peter Bächler, Vanessa Löschner, Jörg Meyer, Achim Dittler

Journal: Process Safety and Environmental Protection

Year of Publication: 2022

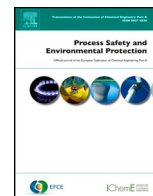
Volume and Issue: 160

Page Numbers: 411-423

Reference: [Bächler et al., 2022b]

Abstract:

In industrial applications of baghouse filters, emission sources other than direct penetration contribute greatly to the overall outlet dust emission. Spatio-temporal process monitoring could enable the detection of local particle emission hotspots and facilitate maintenance procedures by offering new insights regarding the emission behavior of baghouse filters. This publication shows the spatial emission behavior measured by low-cost sensors in a small scale baghouse filter with nine filter bags. After initial cleaning cycles, which cause clogging of the seams and a decrease of the particle emission level, the emission behavior corresponds to ideal filter operation. However, seemingly random continuous particle emissions are temporarily measured at individual filter bags within the baghouse. Via spatial monitoring and comparison with the total dust emission of the process, measured by a state-of-the-art precision laboratory optical particle counter, these events can be allocated to a corresponding filter bag, which serves as the source of temporary increase in dust emission. An increase in tank pressure shows a rise of the intensity and frequency of temporarily occurring continuous emissions. This behavior can be directly linked to a release of particles from previously clogged seams, thus enabling renewed particle penetration through the stitching holes of the seams.



Process integrated monitoring of spatially resolved particle emissions of a baghouse filter using a network of low-cost PM-sensors

Bächler P.^{*}, Löschner V., Meyer J., Dittler A.

Institute of Mechanical Process Engineering and Mechanics, Karlsruhe Institute of Technology, Straße am Forum 8, 76131 Karlsruhe, Germany

ARTICLE INFO

Article history:

Received 19 July 2021

Received in revised form 21 January 2022

Accepted 3 February 2022

Available online 10 February 2022

Keywords:

Baghouse filter
Surface filtration
Low-cost PM-sensor
Process monitoring
Leak detection
Dust separation
Emission control

ABSTRACT

In industrial applications of baghouse filters, emission sources other than direct penetration contribute greatly to the overall outlet dust emission. Spatio-temporal process monitoring could enable the detection of local particle emission hotspots and facilitate maintenance procedures by offering new insights regarding the emission behavior of baghouse filters. This publication shows the spatial emission behavior measured by low-cost sensors in a small scale baghouse filter with nine filter bags. After initial cleaning cycles, which cause clogging of the seams and a decrease of the particle emission level, the emission behavior corresponds to ideal filter operation. However, seemingly random continuous particle emissions are temporarily measured at individual filter bags within the baghouse. Via spatial monitoring and comparison with the total dust emission of the process, measured by a state-of-the-art precision laboratory optical particle counter, these events can be allocated to a corresponding filter bag, which serves as the source of temporary increase in dust emission. An increase in tank pressure shows a rise of the intensity and frequency of temporarily occurring continuous emissions. This behavior can be directly linked to a release of particles from previously clogged seams, thus enabling renewed particle penetration through the stitching holes of the seams.

© 2022 Institution of Chemical Engineers. Published by Elsevier Ltd. All rights reserved.

1. Introduction

In filtration applications, pulse jet cleaned surface filters are applied to separate particles from dust-laden gas streams in order to meet legal limits and protect the environment and human health from dust emissions. Additionally, process efficiency can be increased by recovering particulate products, or downstream unit operations after the filter may rely on particle free air, e.g. catalysts could be deactivated due to dust contamination (Klein et al., 2009; Mauschitz et al., 2018; Schmidt, 1998). The filters are often confectioned in the form of filter bags and arranged in filter houses in varying numbers dependent on the raw gas volume flow.

Abbreviations: BImSchG – Federal Immission Control Act (Germany); C_n – particle number concentration; PA – polyamide; PES – polyester; PM – particulate matter; PPS – polyphenylene sulfide; ePTFE – expanded polytetrafluoroethylene; n – index of refraction; Δp_{\max} – maximum differential pressure; Δt – time interval between individual filter regenerations; $w_{\text{filtration}}$ – filter face velocity; x – particle diameter; $x_{50,3}$ – mass median particle diameter; ρ_{solid} – solid density; SEM – scanning electron microscope

^{*} Corresponding author.

E-mail addresses: peter.baechler@kit.edu (B. P.), vanessa.joeschner@kit.edu (L. V.), joerg.meyer@kit.edu (M. J.), achim.dittler@kit.edu (D. A.).

<https://doi.org/10.1016/j.psep.2022.02.005>

0957-5820/© 2022 Institution of Chemical Engineers. Published by Elsevier Ltd. All rights reserved.

So far, process monitoring of filter houses is limited. Legislative rules often only demand emission monitoring in the stack and not all deployed filters are legally required to monitor their particle emission continuously (BImSchG, 2019). Especially smaller scale filters for e.g. ventilation systems, are not required to monitor their dust emission. The outlet of filter houses can be equipped with triboelectrical sensors to enable online measurement of the overall PM evolution of the filter house (Wiegler, 2016). Nonetheless, the baghouse is practically a black box, without any information about local events or significant spatial emission hotspots.

During filter operation, particles are separated at the surface of a filter medium, forming a dust cake and increasing the differential pressure between raw gas side and clean gas side. The filter cake grants a very high separation efficiency, therefore, assuming ideal operation, the particle emission drops to a zero level. To enable economic operation, the filters are periodically regenerated, e.g. by a pressure pulse from the clean gas side, to remove the dust cake (Löfler, 1988). After cake removal, particles can penetrate the filter medium, causing a particle emission peak, until a sufficiently thick dust cake is formed again (Binnig et al., 2009).

The theoretical basis for the general layout of baghouse filters ranges back to the works of Löfler (1988), Leith and Ellenbecker (1979), or (Schmidt, 1998). While these investigations used

simplified models of the filter (e.g. homogenous conditions), recent developments regarding measurement technology and simulative studies give a deeper and “local” insight regarding the internal conditions within the filter house and thus offer optimization approaches for filter operation.

Heck et al. performed simulative investigations into the operating behavior of an industrial baghouse (1117 filter elements) and the flow conditions of the clean gas side, indicating different filter loading and, consecutively, different wear on the individual filter bags depending on filter position (Heck et al., 2016; Heck and Becker, 2022). In addition to spatial differences, the filtration velocity may vary across the length of the filter element according to the simulations of Park et al. (2019). Many simulative works have been performed in order to improve cleaning performance of surface filters. Andersen et al. (2016), performed simulations including the experimental validation of the jet-pulse during filter regeneration, showing the relevance of the venturi nozzle and the flow pattern of the pressurized air (Klein et al., 2009). Similar investigations were led by e.g. Li et al. (2016), who also investigated the gas flow dynamics of the jet-pulse. Qiu et al. (2021), numerically investigated the pulse-jet cleaning of pleated filter cartridges that offer higher filter areas compared to bag filters but pose different challenges, as they are more prone to patchy cleaning (Dittler et al., 2002). Similar investigations were led by Chen et al. (2017) or Kang et al. (2020). Fundamental studies on the loading of filter media and cake formation can also be found in the literature (e.g. Zhang et al., 2020). While the conclusions of these simulative studies may be transferred to the practical application, experimental investigations remain an important means to investigate the operating and emission behavior of pulse-jet cleaned filters under praxis-relevant conditions (Saleem et al., 2012; Simon et al., 2014).

Many different factors affect the overall dust emission of a surface filter (e.g. filter medium, dust properties, operating parameters) [Schmidt (1998); VDI, (2010)]. Highly efficient filter media e.g. with membrane surfaces enable plant operators to achieve almost zero emission (Imminge and Krug, 2019). However, in real baghouses, leaks of the filter medium or the plenum plate, the seams of the filter medium or damaged/incorrectly installed filter bags can greatly contribute to the total dust emission of the facility. As a result, a continuous baseline dust emission occurs in addition to emission peaks due to jet-pulse cleaning (Qin et al., 2006; Bach and Schmidt 2007; Kurtz et al., 2017).

Regarding the particle emission contribution, even small defects can significantly increase the overall dust emission. Bach and Schmidt (2007), showed the significant increase in dust concentration through pinholes in a filter test rig Kurtz et al. (2017), performed similar investigations in a small scale baghouse filter and found a high increase in particle emission for leak areas that were only a small fraction (about 1 ppm) of the total installed filter area. Li et al. (2022), modeled the operation behavior of a test filter system for different leak ratios/pinhole sizes, where model and experiment were in good agreement. The reliable detection and identification of leaks and particle emission hotspots is one of the key challenges in the filter industry.

Li et al. (2020), demonstrated the capability of optical fiber sensors to detect leaks in a baghouse filter with high certainty. The leak diameters were in the region of multiple millimeters ranging into the centimeter region, which are considerable diameters and represent a high degree of damage of the filter bag.

Simon et al. (2010), performed investigations regarding the (local) flow-profile of baghouse filters. However, the bags were intact and the study did not focus on the detection of damaged bags, but rather the overall impact of transitory air flows during stable filter operation.

A cost efficient method to potentially monitor the particle emission of individual filter bags, or at least a subset of all installed

filter bags, are low-cost PM-sensors. Ostermeyer et al., 2020, showed the capabilities of low-cost PM-sensors for spatial emission monitoring in a different emission application (brake dust). Previous publications have proven the sensors are capable of reliably measuring the qualitative emission behavior of baghouse filters, both in a modified filter test rig according to (DIN ISO 11057, 2016) and in a small scale baghouse filter (Schwarz et al., 2018; Bächler et al., 2019a, 2019b). For membrane filter media with sealed seams (low emission level and nearly ideal emission behavior), the typical emission peak after jet-pulse cleaning was detected after the regeneration of the corresponding bag. Additionally, different spatial emission levels could be distinguished when introducing a single filter bag with open seams (non-membrane medium) into the membrane media installation in the baghouse (Bächler et al., 2020).

This study expands upon these results and shows the different local PM emission behavior of two types of filter bag (two filter media with regular, non-sealed, seams), as well as their PM evolution over multiple filtration cycles for different levels of regeneration intensities, by simultaneous measurement employing low-cost PM-sensors to demonstrate the potential of spatial emission monitoring in filtration applications. The technology might help to identify spatial particle emission hotspots (one of the most common reasons for plant shutdowns) and thus improve process monitoring for plant operators.

2. Experimental set-up, procedures and materials

2.1. Pilot plant scale baghouse and process parameters

Contrary to typical lab-scale filter tests, where circular filter coupons are investigated (DIN ISO 11057, 2016), the experiments have been conducted in a pilot scale testing facility equipped with nine filter bags (diameter 11.7 cm; length: 125 cm). The blow pipe above the outlet of each filter bag has been equipped with a low-cost sensor of the model OPC-N3 from the manufacturer Alphasense for local and simultaneous PM measurement (Fig. 1).

A radial blower creates a circulating air flow through the testing facility. The average filter face velocity (total volume flow related to total filter area) has been adjusted to 120 m/h (total volume flow rate of approx. 510 m³/h). The air flow is loaded with test dust at two different locations. New dust is added from a dust silo in addition to previously separated test dust, which is mostly recirculated to enable a steady supply of dust over multiple hours of the experiment and economic operation of the testing facility. An extinction measurement monitors the raw-gas concentration and was calibrated to a gravimetric raw gas concentration of approximately 5 g/m³. Dust is separated at the filter bags, causing an increase in differential pressure between raw gas side and clean gas side. Filter regeneration was time controlled with adjustable cycle times. For the highest cycle time of 120 s, a low decrease of volume flow due to limitations of the radial blower could be observed (approx. 12% reduction in volume flow). At each cleaning event, a single bag was regenerated (“bag by bag”), starting at filter bag 1 and ending with filter bag 9 according to Fig. 1. The jet-pulse causes detachment of the filter cake from the filter medium, resulting in a decrease in differential pressure and the typical ‘saw-toothed’ differential pressure profile of pulse-jet cleaned surface filters (Löffler, 1988).

The operating parameters as well as the experimental procedure are summarized in Fig. 2. During the initial filtration cycles, aging effects of the filter medium are to be expected. Therefore, the whole experimental procedure is repeated after the initial series of 90 cycles to gain a solid data foundation for different operation points. During further experiments after the main procedure, effects like variations in tank pressure (3 bar, 5 bar, 8 bar – values based on

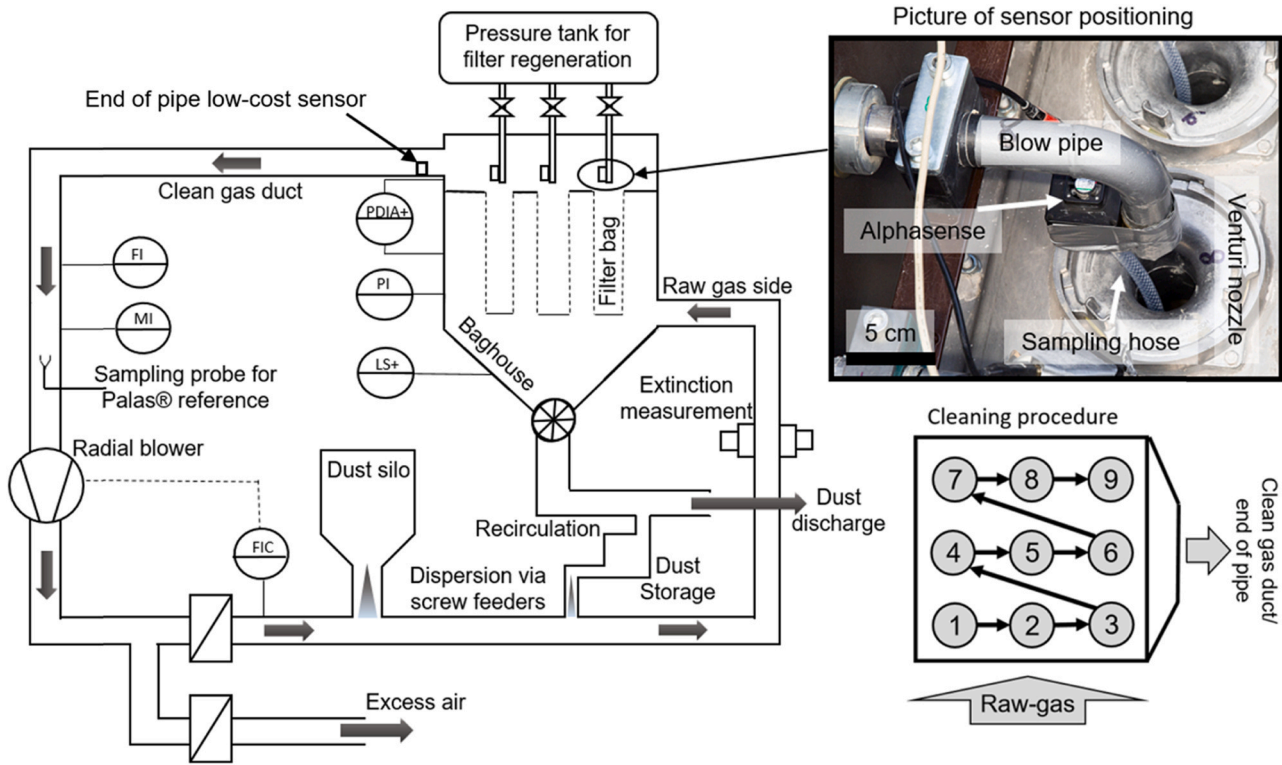


Fig. 1. Flow sheet of the pilot scale baghouse with nine filter bags, photograph of sensor positioning and scheme of the cleaning procedure.

operator experience) were investigated in order to identify emission sources or enable direct comparison between Palas® reference & low-cost PM-sensor (see chapter 2.2). The presented findings are qualitative and semi quantitative, so that trends and the overall emission evolution are discussed.

The employed test dust was PURAL SB® from the manufacturer Sasol ($x_{50,3} \approx 45 \mu\text{m}$; $\rho_{\text{solid}} = 2800 \text{ kg/m}^3$; $n = 1.64 (-)$). Note that the size distribution of the test dust may vary depending on the exact batch of the manufacturer. The dust is free flowing and does not tend to agglomerate, causing a higher particle penetration through filter media compared to agglomerating dusts (Kurtz et al., 2017; Sobich et al., 2018).

2.2. Aerosol measurement technology

Two different types of aerosol spectrometers were employed in this study. A costly state-of-the-art precision laboratory Palas® Promo®2000 aerosol spectrometer in combination with a welas®2100 sensor serves either as the reference for validation of local measurements or for end of pipe particle emission monitoring. For local & simultaneous measurement of the particle concentration at the outlet of each filter bag, a low-cost sensor of the type OPC-N3 from the manufacturer Alphasense has been fixed to the blow pipe. Each sensor was equipped with an additional sampling hose of 10 cm length, extracting the sample flow at (or close to) the edge of

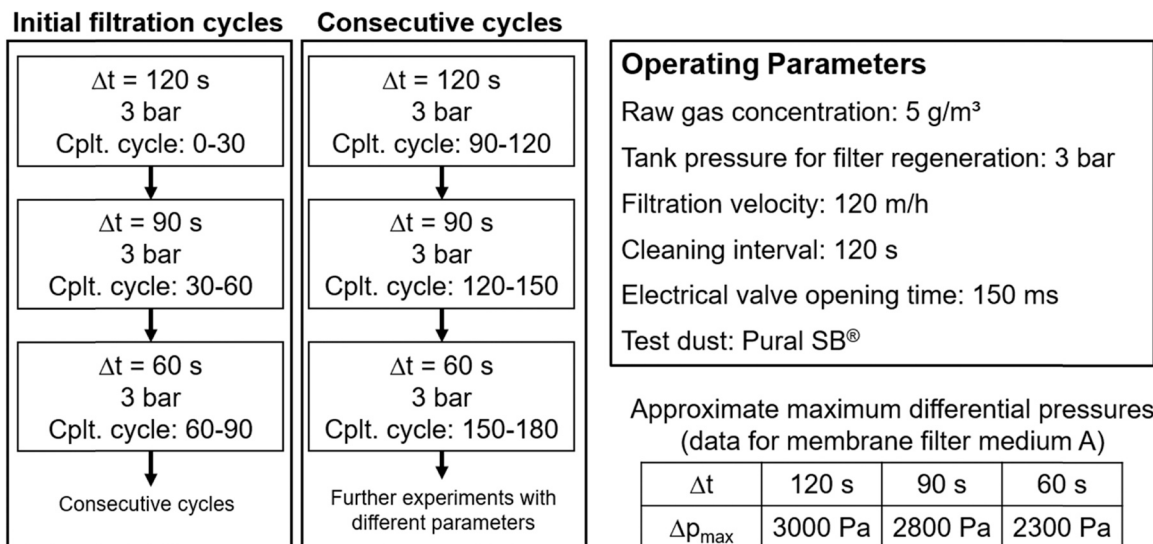


Fig. 2. Experimental procedure and summary of operating parameters.

Table 1
Sensor specifications [Alphasense (2018); Palas®, (2020)].

Device	OPC-N3	Promo® 2000 with welas® 2100
Manufacturer	Alphasense	Palas®
Measurements	Mass based concentration: PM ₁ , PM _{2.5} , PM ₁₀ ; Count rate and size resolved particle counts	Mass and number based total concentration, size distributions, size resolved PM _x conversion
Detectable size range	0.35–40 µm	0.2–10 µm; 0.3–17 µm; 0.6–40 µm (user selectable)
Size categorization	24 bins	64 bins per decade
Maximum concentration	Mass based: 2000 µg/m ³ 0.84% coincidence probability at 1000 #/cm ³	5 · 10 ⁵ #/cm ³
Approximate cost (including required cables & connectors)	400 €	> 30.000 €
Length x Width x Height	75 mm × 45 mm x 63.5 mm	245 mm × 100 mm x 80 mm (welas® sensor only)
Response time	≈ 1 s	≈ 1 s
Volume flow	5.5 l/min (inlet flow) 280 ml/min (sample flow)	5 l/min (inlet flow)
Configuration	ρ _{particle} = 2800 kg/m ³ n _{aerosol} = 1.5 (-) Spherical particles	ρ _{particle} = 2800 kg/m ³ n _{aerosol} = 1.59 (-) Spherical particles

the smallest cross-section of the venturi insert (see Fig. 1). Sensor specifications are displayed in Table 1. Though the sampling can have an effect on the performance of low-cost PM-sensors (Bezantakos et al., 2021), there have been no significant complications regarding measurement performance.

Particle density was considered in the configuration of both measurement devices, other settings were left at their default state or could not be altered. The low-cost sensors were not calibrated against the reference device. Prior measurements at ambient conditions showed negligible deviations between the individual low-cost PM-sensors.

The sensor sample flow-rate logged by the Alphasense sensor during the experiment in the baghouse filter showed strong deviations compared to the specified flow-rate given in the datasheet. According to the manufacturer, the flow-rate is determined applying a time-of flight method. During ideal filter operation, where no particles penetrate the filter medium due to the dust cake, there is a zero concentration level on the clean gas side. During this period, the sensor logs a constant flow-rate. The flow-rate varies during particle emission peaks and is higher compared to the specified flow-rate. This, understandably, puts the overall quantitative accuracy of the low-cost PM-sensor into question. The goal of this investigation is to evaluate differences in emission level, qualitative effects and semi quantitative trends regarding the particle emission behavior of surface filters. We selected PM_{2.5} as reference value for the emission, as it is a common value that can be found when evaluating the performance of low-cost PM-sensors (Kang et al., 2021). For some sensors, it is unclear whether the determined PM₁₀ output is calculated from internal data processing or indeed measured via size resolved PM conversion (Budde et al., 2018). As the Alphasense sensor also offers size resolved particle counts, PM₁₀ would also be an adequate value for comparison. Nonetheless, the impact of few bigger particles would influence PM₁₀ concentrations more strongly and PM_{2.5} is not prone to these larger fluctuations.

2.3. Filter media

Two different filter media with different properties have been employed in this investigation. The properties of the two filter media are listed in Table 2.

Filter medium A is a membrane filter medium with an ePTFE membrane laminated on the upstream side, causing a low air permeability and high separation efficiency of the surface of the filter

medium. Medium B is a spunbond filter medium and its properties are more similar to conventional needle felts. The two filter media were already investigated in a previous publication in a filter test rig, where medium A showed a lower emission level, as is expected due to the membrane surface (Bächler et al., 2019a, 2019b). The filter media are assembled in the form of filter bags. Due to the manufacturing confectional process, the filter bags have seams that are a known source of particle emissions for pulse-jet cleaned filters (Kurtz et al., 2017; Lacerda et al., 2019). The seams of the filter bags have not been sealed with sealing paste or tape. The filter media have not been aged prior to the investigation, so that effects of filter aging (storage of particles in the filter matrix) are expected during the initial filtration cycles (see Fig. 2). The correct installation of filter bags is of high importance in order to avoid continuous particle emissions. Therefore, the filter bags come with double beaded ring clamps to enable tight sealing between raw gas side and clean gas side. Due to their different properties, different particle emission dynamics can be investigated by application of these two different media.

3. Results and discussion

When employing low-cost PM-sensors as (spatial) particle emission control for pulse-jet cleaned filters, it is important to validate the measurement technology by measurement of predictable trends. Thus, effects like filter aging, different emission levels based on different cycle times and/or filter media and the dependence of the particle emission and tank pressure for filter regeneration, are investigated in the following chapters, using low-cost PM-sensors to monitor the spatially and temporally resolved particle emissions.

3.1. Spatio-temporal emission behavior during the initial filtration cycles

As shown in Fig. 2, factory new filter bags of uniform type (either medium A or medium B) have been installed inside the baghouse for separate experimental runs. Filter aging, meaning the storage of particles inside the filter medium during prolonged filter operation, has a severe effect on filter performance, both with regards to the differential pressure and separation efficiency. With increasing amount of stored particles, the separation efficiency and the differential pressure of the medium itself increase. This effect is considered in standards for filter testing of surface filter media, where an aging procedure is performed (DIN ISO 11057, 2016).

Table 2
Specifications of filter media.

Medium	Area weight/gm ⁻²	Thickness/mm	Permeability (200 Pa)/ ldm ⁻² min ⁻¹	Fiber material & remarks
A	500	1.9	30	PPS (heat set) with laminated ePTFE membrane
B	240	1	100	PES, PA, hydro entangled microfilaments

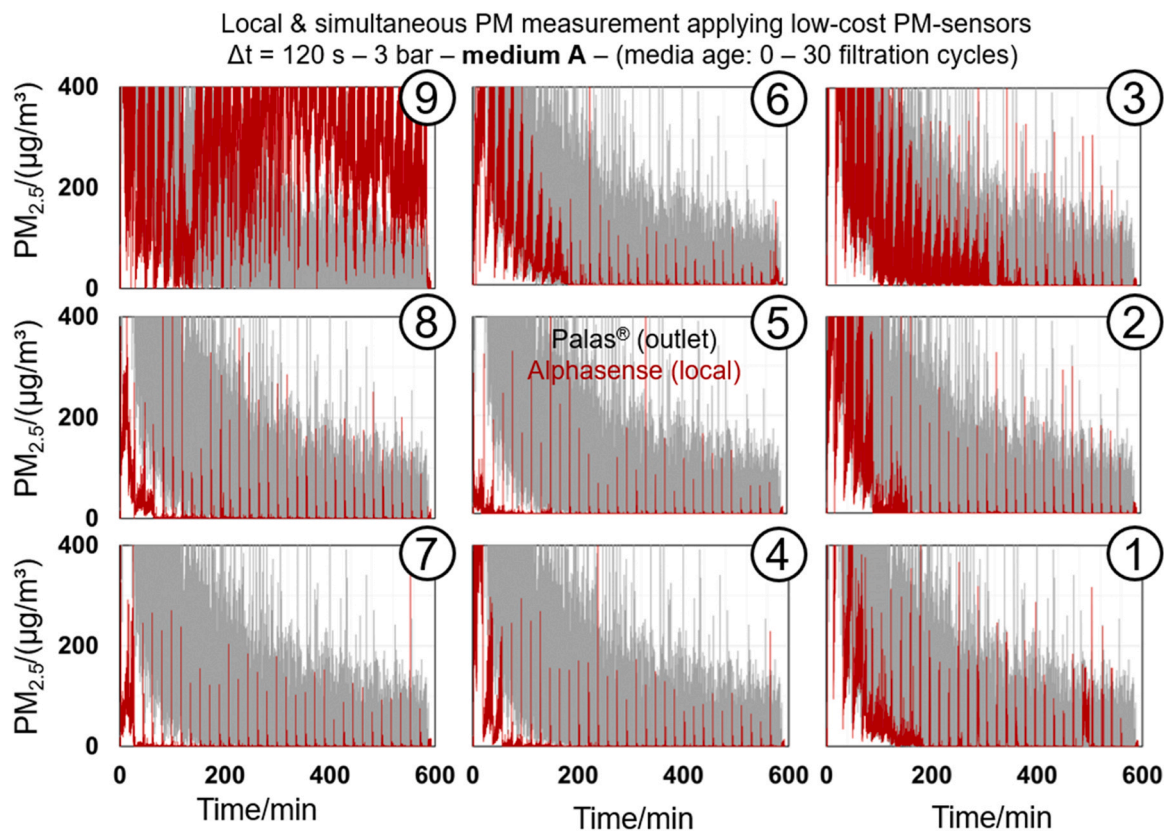


Fig. 3. Spatially resolved $\text{PM}_{2.5}$ measurement employing nine low-cost sensors (one at each individual filter bag) and comparison with the detected total emission by the Palas® reference on the clean gas side for the initial filtration cycles of medium A. The number indicates the corresponding filter bag in the baghouse.

The particle emissions, which were measured at the outlet of each individual filter bag by low-cost sensors and the total emission detected by the Palas® reference during the initial filtration cycles for membrane medium A are displayed in Fig. 3. Note that the aerosol measurement equipment yields concentrations and a direct comparison between the concentrations of local and total emissions is not accurate due to, mixing and dilution effects and the change of flow-conditions on the clean gas side due to different dust loads on the individual filter bags (Bächler et al., 2020; Simon et al., 2010). Fig. 3 shows the experimental data according to the procedure in Fig. 2 for the initial loading stage, where a dust cake is formed on the new bags and high particle penetration occurs. Each diagram shows the PM evolution of the entire experimental run at the measurement position of the corresponding filter bag (positions 1–9). The emission peaks at the later stages (e.g. after 300 min) only occur for a time duration of several seconds. Thus, the diagram depicts the spatially resolved overall particle emission behavior for the corresponding experiment.

The particle emission shows a decreasing trend for the initial filtration cycles. At the beginning, a continuous emission occurs at each filter bag. After several cycles, only a defined emission peak, indicating the regeneration of the corresponding bag, is detected. Here, the individual behavior is different for each installed filter bag. This is potentially caused by differences of individual bags due to the manufacturing process of the filter media, the confectioning of the bag, or handling errors. Membrane surfaces are very fragile and

require careful handling to avoid damaging the structure and causing higher emissions, as the supporting fiber structure has a much lower separation efficiency. Position of the filter bag may also influence its particle emission, however due to the dominating continuous emission, no clear trend can be derived from the experiment and the number of filter elements is comparably low in comparison to large scale filter houses where position plays a larger role (Heck et al., 2022). The overall decreasing trend in particle emission correlates qualitatively well with the total particle emission detected in the clean gas duct by the Palas® reference at the outlet. After about 300 min (midway of 30 complete filtration cycles), most of the spatially detected particle emissions are rather low, resembling the ideal particle emission behavior of surface filters, where a particle emission peak occurs after jet-pulse cleaning due to cake removal and the particle penetration through the filter medium. Similar results were presented in a previous publication, where membrane filter media with sealed seams have been employed to display (close to) ideal emission behavior (Bächler et al., 2020). Bag number nine is an exception in this measurement, as a high local emission is detected by the Alphasense sensor mounted at the corresponding bag even after 30 cycles. This high continuous emission potentially dominates the total emission detected by the Palas® reference. However, the emission contribution of bag nine decreases further over time and later reaches a comparable low emission level (see chapter 3.2). The same observations can be made for medium B, where high continuous baseline emissions occur

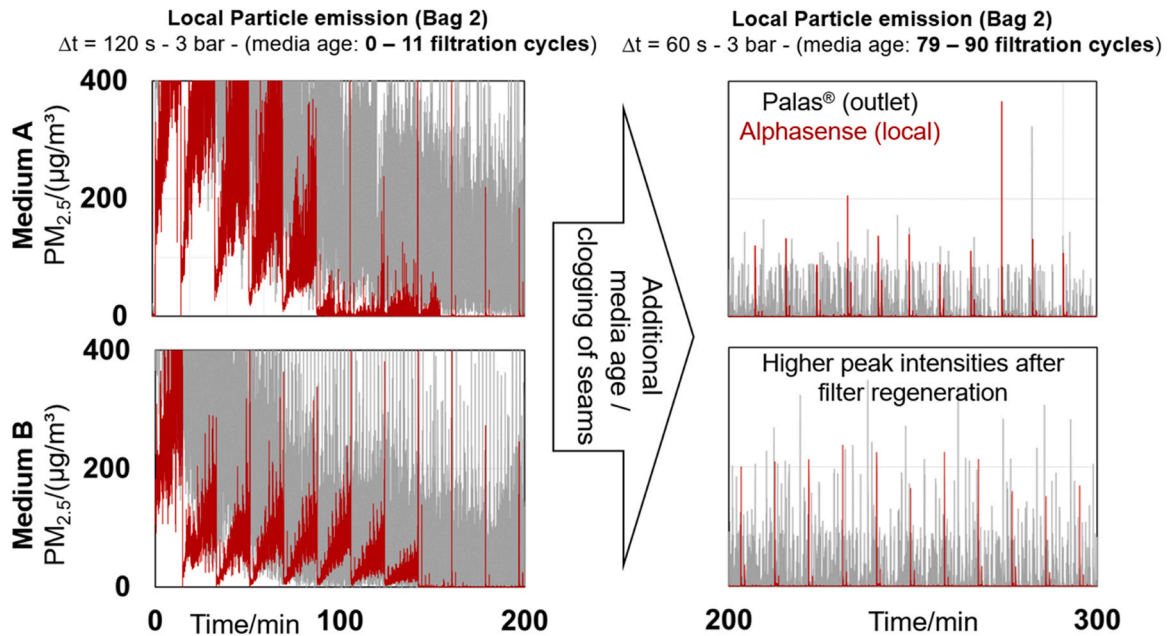


Fig. 4. Detail view of the particle emission of initial filtration cycles of an exemplary filter bag for both filter media and global emission compared to the end of the first measurement procedure (see Fig. 2).

during the initial stages. A more detailed comparison regarding the emission behavior of both filter media is discussed in chapter 3.2, where a stable emission level is reached due to filter aging.

To demonstrate the change in particle emission level of local and total emissions within the initial aging stage (up to about 100 cycles), Fig. 4 shows a comparison of the PM emission behavior of the first filtration cycles of the $\Delta t = 120$ s and the final filtration cycles of the $\Delta t = 60$ s experiment (set of initial filtration cycles – compare Fig. 2) of an exemplary individual filter bag for both filter media.

The continuous particle emission decreases to a zero level within a few cycles and defined peaks can be detected with increasing media age for both filter media. This PM evolution is a clear indication that the filter bag has been installed correctly and that correct filter installation with double beaded ring clamps enable low particle emission levels with an ideal emission behavior, where particle penetration through the filter medium is the dominating source of particle emissions (Binnig et al., 2009). There is an indication regarding different emission levels when comparing local and total emissions of filter medium A and B, where the peaks of the membrane medium are slightly lower. In the next chapter, the overall PM evolution for both filter media will be compared.

3.2. Spatio-temporal particle emission behavior at increased media age for both filter media and detection of temporal “random” continuous emission hotspots

After the initial filtration cycles, where effects of filter aging were clearly visible, another set of experiments with identical cycle times were performed (Fig. 2). Here, the particle emission level has decreased and in most cases, resembles ideal emission behavior similar to filter test rigs (detection of emission peak after filter regeneration only). Comparing the overall particle emission behavior and the PM evolution displayed in Figs. 3 and 5, the difference between media ages becomes apparent, thus demonstrating the capabilities of the low-cost PM-sensor to measure qualitatively correct trends in particle emission for the overall baghouse filter.

In addition to the differences in media age, differences between the two filter media regarding their spatio-temporal particle

emission behavior can be found. Fig. 6 displays the emission behavior of the nine filter bags of medium B for the local particle emissions detected by the low-cost PM-sensor and the total emission detected by the reference after an identical number of filtration cycles (90 – 120 cycles).

Due to the high separation efficiency of the membrane layer, the spatial and total particle emissions are lower for medium A. One indication is the peak height, which is approx. $100 \mu\text{g}/\text{m}^3$ for the majority of detected peaks at filter medium A and larger than $200 \mu\text{g}/\text{m}^3$ for filter medium B. Additionally, even though filter medium B has been aged significantly and reaches a zero level during the filtration phase in most cases, there is a higher occurrence of local continuous particle emissions, which appear and disappear, seemingly at random, at individual filter bags. The origin of these particle emissions is discussed further in the next chapter.

Regarding the overall particle emission and its particle size distributions for both filter media, a direct comparison between locally detected size distributions and outlet distribution is not accurate, due to spatially different flow conditions and different settings and specifications of the optical parameters (e.g. refractive index) of the different devices. However, an additional Alphasense sensor was installed on the clean gas side for measurement of the total emission and direct comparison at similar flow conditions ($W_{\text{filtration}} = 120 \text{ m}^3/\text{h}$) (Fig. 7).

The particle size distributions are qualitatively in good agreement and enable the distinction between the two filter media from the size distribution. Quantitative differences regarding particle counts are significant especially for the smallest size bin of the low-cost PM-sensor. Note that the counting efficiency of the reference decreases in the lower size bins and that the most penetrating particle size is at the lower end of reliable optical measurement (Bächler et al., 2022). The detected average PM emission decreases with increasing cycle time, as the averaging interval of the emission peaks increases but the number of individual cleaning events (30 complete cycles) remains constant and differences in peak height are negligible in comparison. While the low-cost PM-sensor overestimates the $\text{PM}_{2.5}$ concentration compared to the reference, the particle concentrations are in the same order of magnitude for both devices, offering semi quantitative information on the emission level

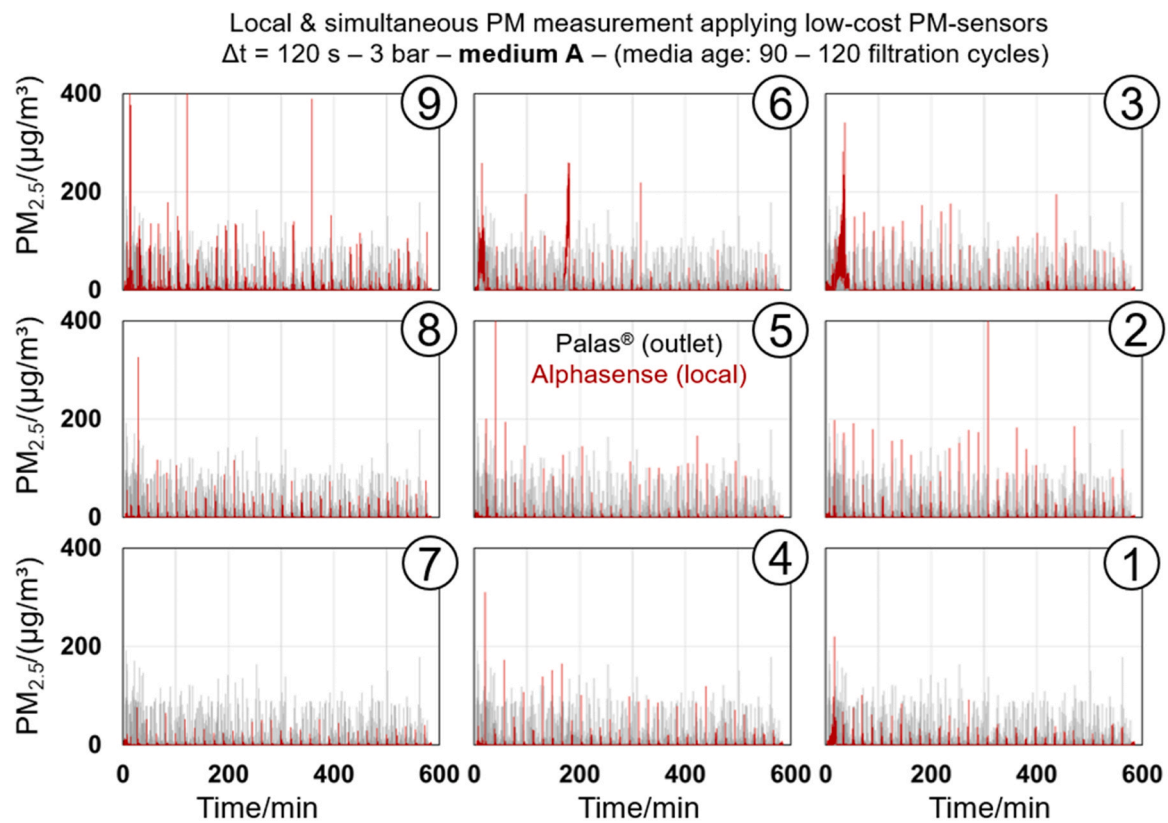


Fig. 5. Spatially resolved $\text{PM}_{2.5}$ measurement employing nine low-cost sensors (one at each individual filter bag) and comparison with the detected outlet emission by the Palas® reference on the clean gas side for medium A at an increased age of the filter medium. The number indicates the corresponding filter bag in the baghouse.

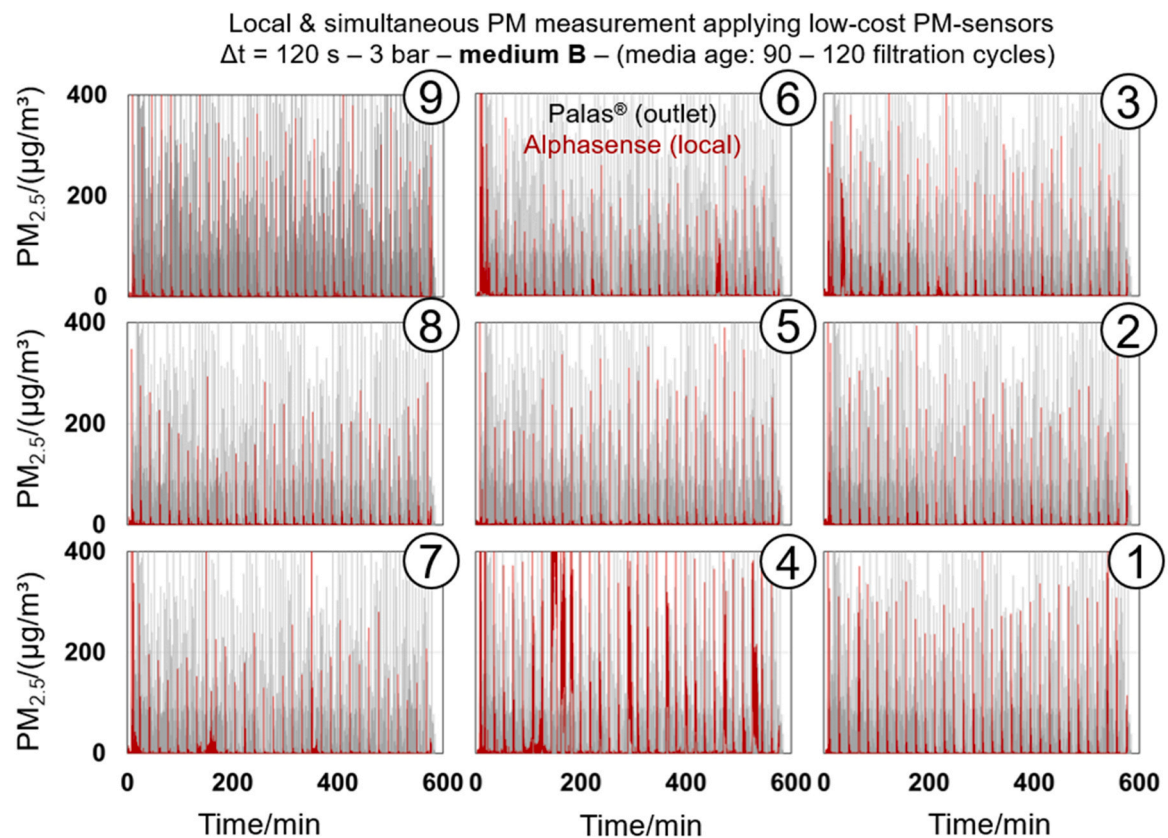


Fig. 6. Spatially resolved $\text{PM}_{2.5}$ measurement employing nine low-cost sensors (one at each individual filter bag) and comparison with the detected outlet emission by the Palas® reference on the clean gas side for medium B at an increased age of the filter medium. The number indicates the corresponding filter bag in the baghouse.

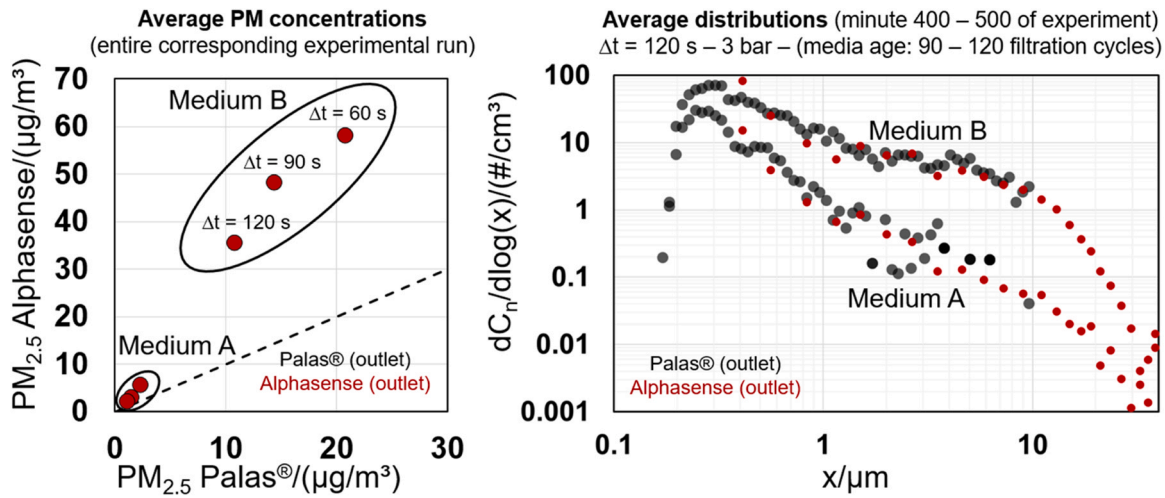


Fig. 7. Comparison of the average concentration and the particle size distribution of the total emission (additional low-cost PM-sensor installed end of pipe/outlet) for both filter media (compare Fig. 5 and Fig. 6).

and showing the general suitability of low-cost PM-sensors as “end of pipe” measurement technology.

In order to demonstrate the capabilities of low-cost PM-sensors to detect temporal particle emission hotspots, the obtained dataset has been evaluated further and locally detected randomly occurring continuous emissions have been allocated to a respective particle emission at the end of the pipe. Fig. 8 shows exemplary data for the majority of cases, where the origin of particle emission detected in the clean gas duct can be identified in one specific local measurement applying low-cost PM-sensors. Note that sometimes it can be

difficult to correlate local and total particle emissions, since additional emission sources (e.g. residual dust in the pipes, tiny leaks in the filter house, etc.) can have an impact that is not monitored by low-cost PM-sensors. Additionally, there are cases where a continuous particle emission occurs simultaneously at multiple bags, so that not a singular main emission source contributes to the total emission. This holds especially true for medium B, where high local continuous emissions were detected at bag 4 across all measurements. Therefore, in Fig. 8 only the membrane filter medium is considered.

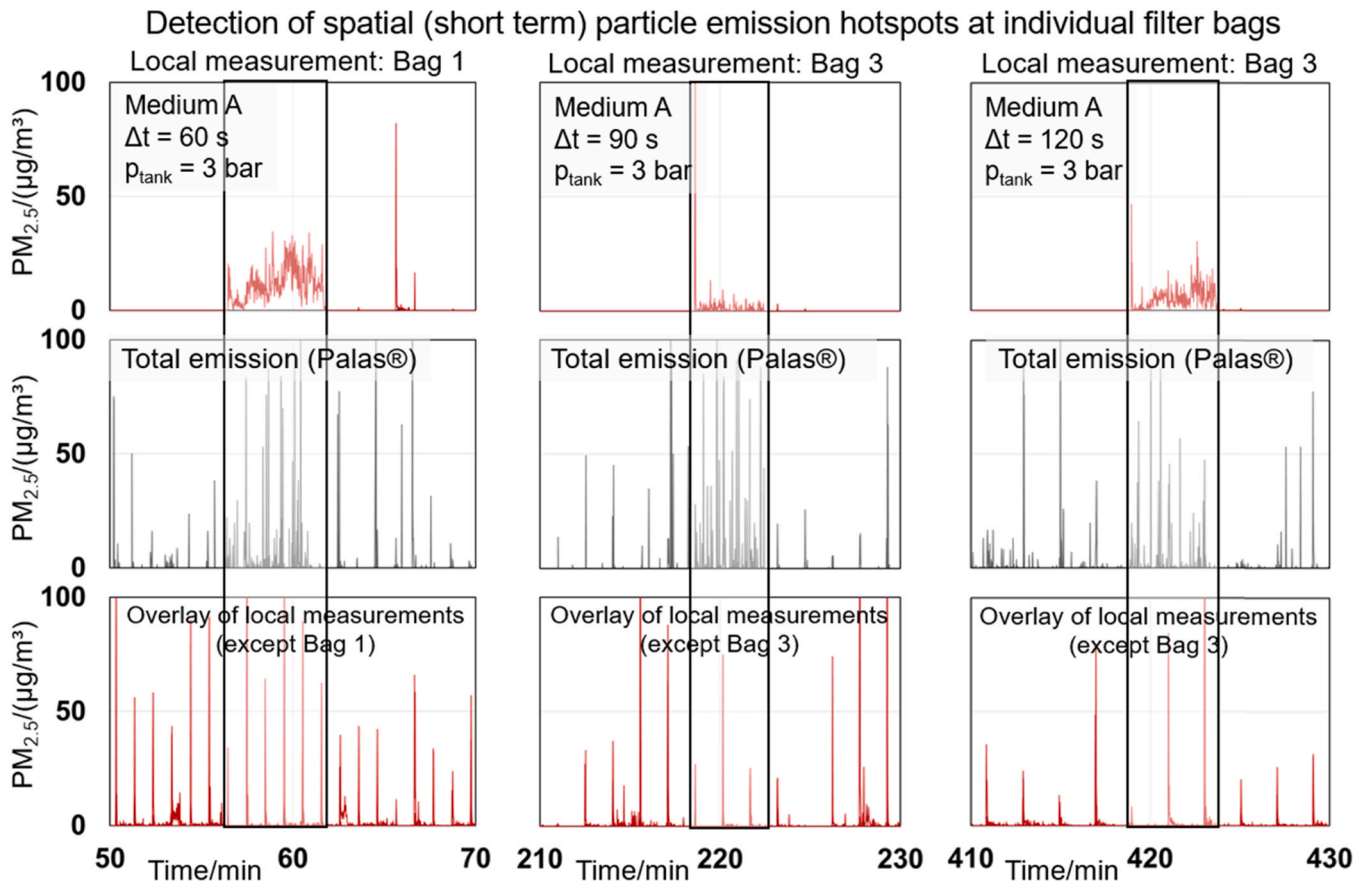


Fig. 8. Temporal continuous emissions for selected measurement intervals (detail view of regions with “random” continuous emissions).

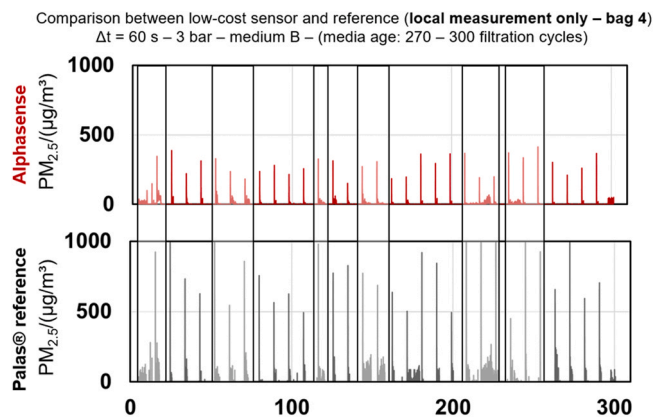


Fig. 9. Direct comparison between the low-cost PM-sensor and the reference at an individual filter bag.

Additional measurements have been performed where both, the reference and the low-cost sensor, were deployed at the same filter bag to enable direct comparison between devices. The result of 30 filtration cycles is displayed in Fig. 9. Many distinct PM emission characteristics correspond well between the two devices (e.g. continuous particle emissions are detected by both devices – see framed areas in Fig. 9). Key differences are the exact concentration values that deviate strongly, especially considering the lower height of emission peaks detected by the low-cost PM-sensor. The only event with significant qualitative difference occurs around 175 min time, where only the reference detects a continuous particle emission. Due to the transient nature of particle emissions detection of an emission peak for several seconds only (Bächler et al., 2020) the exact determination of peak height is a metrological challenge.

3.3. Effect of pulse intensity on the intensity and the frequency of cycle dependent continuous emissions for both filter media

For the determination of the origin of cycle dependent continuous emissions, experiments at an increased age of the filter medium have been performed with different pulse intensities (tank pressure for filter regeneration). According to Kurtz et al. (2016), the total emission increases with increasing tank pressure. Simultaneous monitoring enables an in-depth evaluation regarding the source of the increased emissions.

Fig. 10 presents the spatial emission profile for two test runs at different tank pressures for the membrane filter medium. An increased tank pressure leads to an increase of the total particle emission, mainly caused by temporarily occurring continuous emissions originating from individual filter bags (e.g. bag 9, bag 6, bag 3, etc.).

Measurements for medium A and B were repeated at a higher media age using the PALAS® reference (local measurement of the emission of bag 4). Fig. 11 shows a comparison of measurements at varying tank pressures for both media. Both media show an increase of peak PM emission after filter regeneration with increasing tank pressures. Additionally, intensity and frequency of cycle dependent continuous particle emissions increase. The effect can also be observed regarding particle size distributions, illustrated by a concentration shift to higher concentration regions with almost no change in most penetrating particle size (MPPS at lower end of reliable optical detection). The deviations of the local PSD of the low-cost PM-sensors seems to be higher at increased emission levels for higher particle diameters with low numbers of counting events.

In a previous publication where filter bags with sealed seams were investigated, temporarily occurring continuous emissions with high intensity were practically nonexistent at tank pressures of 5 bar

(Bächler et al., 2020). Measurements at 8 bar tank pressure for filter bags with sealed seams also showed no significant increase in cycle dependent continuous emissions. Therefore, this spatio-temporal emission behavior can be linked to the seams of the filter medium. Kurtz et al. (2017) investigated the relevance of seams regarding their emission contribution. By sealing the seam, the emission could be greatly reduced. Especially during the initial filtration cycles, the seams of the filter medium are particle emission hotspots. Considering non-membrane filter media, there is a high amount of dust storage during operation especially in the upper layers of the filter medium (Höflinger et al., 2007). Due to higher air permeability of the stitching holes, there is also an increased penetration and storage of particles in the region around the seams, clogging them. Due to high intensity jet-pulses (in this case 5 or 8 bar), particles can be released from the previously clogged seams. Thus, increased particle penetration through the seam can re-occur, causing a temporary continuous emission until seams are sufficiently clogged. Increased flow velocities through stitching holes during pulse-jet cleaning can overcome adhesive forces that bind particles on the fiber support structure below the membrane (Löffler, 1972). Fig. 12 shows SEM images of the seams of the filter bag before and after filter operation, showing high amounts of particle agglomerates in the region around the seam thread for the used filter bag, where the media surface has been damaged by stitching holes. The visible fiber matrix is covered with particles, reducing the effective pore diameter. This qualitatively corresponds to the simulative work of Tao et al., who simulated clogging of fibrous filters consisting of the buildup of particle chains that can bridge (and subsequently clog) the space between fibers (Tao et al., 2020).

Charvet et al. (2016), demonstrated that after clogging of pores in granular bed filters, some holes remain unblocked, as increased fractions of the total flow (high velocities), pass through individual pores. The overall characteristic of their system is comparable and can be transferred to filter bags with stitching holes. Lacerda et al., 2019, also discussed the significance of seams regarding an increase in particle penetration through the stitching holes even after long term operation in a filter test rig. This effect might be different for more cohesive test dusts, and more realistic operation conditions regarding increased temperatures and humidity or longer operation duration, where the seams may clog irreversibly.

Overall, the findings demonstrate the suitability of spatial PM monitoring for baghouse filters. Potential scenarios for application in the industry include individual bags equipped with low-cost PM-sensors in order to detect continuous emissions. If a continuous emission appears and does not disappear after several cleaning cycles and/or lowering of pulse intensity for jet-pulse cleaning, a permanent damage (e.g. leak or pinhole) is most likely responsible for the constant particle flux. Correct filter installation and selection of tank pressures can significantly lower the particle emission level, which has been shown by local PM monitoring.

4. Summary and outlook

The spatio-temporal emission behavior of filter bags manufactured from two different types of filter media was investigated in a pilot-plant scale baghouse filter by equipping each filter bag with a commercially available low-cost PM-sensor (OPC-N3 from the manufacturer Alphasense) for local and simultaneous particle emission monitoring. Two different types of filter bags (membrane medium and spunbonded fabric) with regular seams were employed to show differences in the respective particle emission behavior. The measurement behavior of the sensors was compared to the emission detected by an elaborate Palas® optical particle counter. The low-cost PM-sensors showed the same trends regarding the detected (spatial) PM evolution for several emission characteristics (e.g. filter aging,

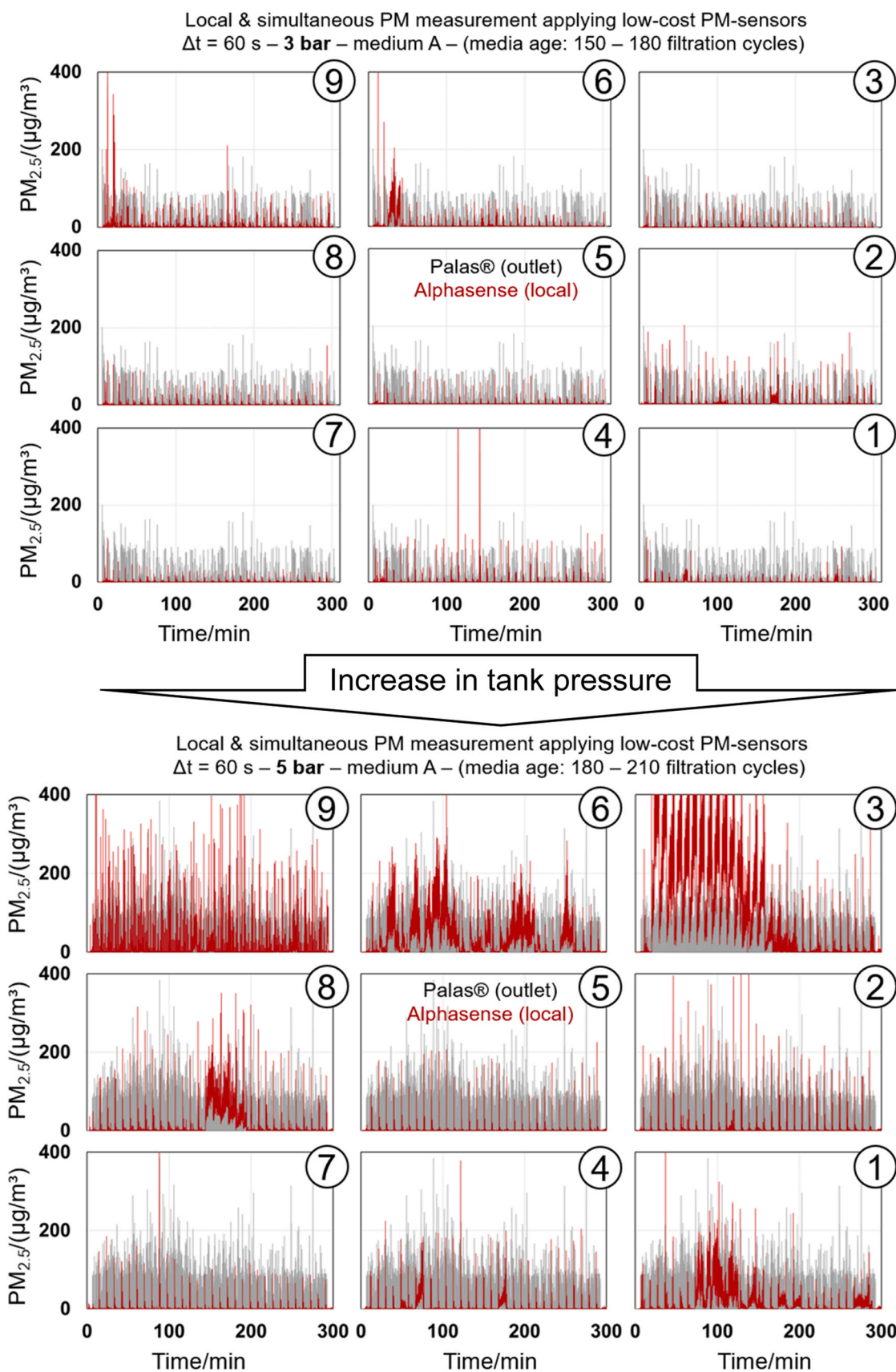


Fig. 10. Spatially resolved $PM_{2.5}$ measurement employing nine low-cost sensors (one at each individual filter bag) and comparison with the detected total emission by the Palas® reference on the clean gas side for medium A for two different tank pressures. The number indicates the corresponding filter bag in the baghouse.

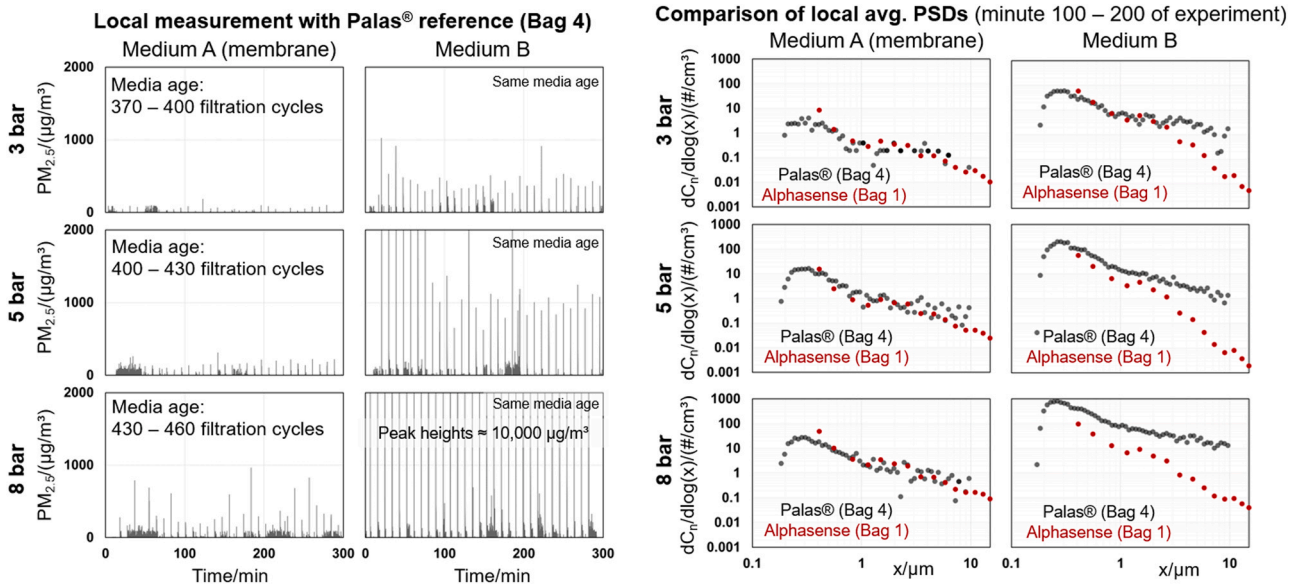


Fig. 11. Local particle emission measurement at a singular filter bag (bag 4) applying the Palas® reference for different tank pressures and comparison of particle size distributions.

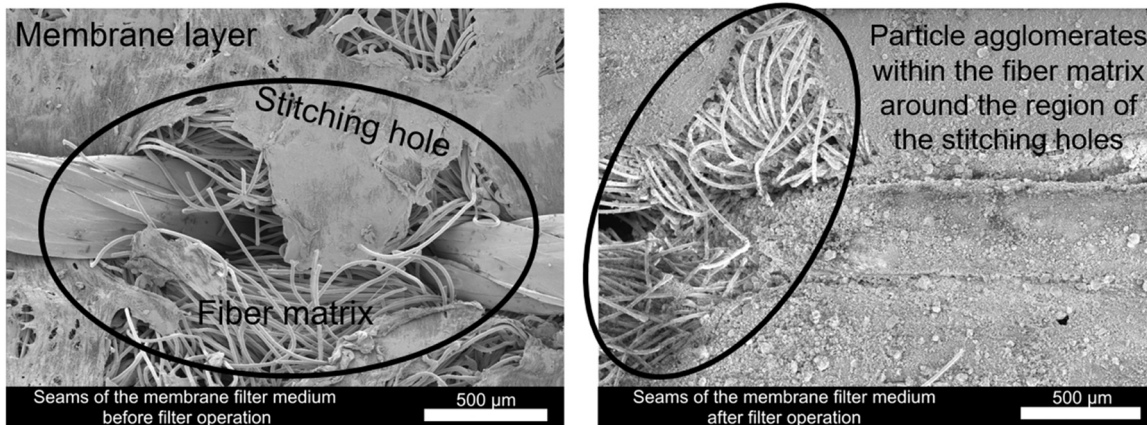


Fig. 12. SEM images of the seam region of filter medium A before (left) and after (right) operation in the baghouse filter.

different filter media, variation in tank pressure for filter regeneration) typical for pulse-jet cleaned filters.

During the initial filtration cycles of the factory-new bags, a rapid decrease of particle emission can be detected both locally (measurement via low-cost PM-sensors) and for the global outlet dust emission of the baghouse (measurement via Palas® optical particle counter as reference), indicating filter aging and clogging of the seams. After several cleaning cycles, the emission decreases close to ideal behavior, where only a particle emission peak after filter regeneration occurs at the corresponding filter bag. Quantitative differences between the spunbond medium and the membrane filter medium can be shown both by application of local PM monitoring via low-cost sensors and the total emission detected by the reference. The peak heights of the membrane medium are lower due to the high separation efficiency of the membrane surface. In addition to particle emission peaks caused by particle penetration through the filter medium after detachment of the dust cake via jet-pulse cleaning, “random” continuous emissions may appear and disappear at individual filter bags over the course of filter operation.

This spatio-temporal particle emission dynamic seems to be strongly influenced by the tank pressure for filter regeneration. Higher intensity pressure pulses cause an increase in the frequency

of local continuous emissions and in peak height of the emission peaks. A likely source of this temporarily occurring continuous emission are the seams of the filter bag. The seams are clog during filter operation (especially during the initial filtration cycles), most significantly at lower tank pressures. Higher intensity pressure pulses cause the release of particles from the previously clogged seam, thus enabling renewed particle penetration. SEM inspections of the membrane filter medium around the region of the seams confirmed high amounts of deposited particulate matter on the fibrous support structure at regions where the membrane is damaged due to the stitching holes.

The results demonstrate the feasibility of applying optical sensors for emission monitoring of baghouse filters. Short and long term local emission hotspots can be identified through spatial PM monitoring with high temporal resolution. This is not considered by state of the art measurement of the total dust emission in baghouse filters. Known trends regarding the particle emission behavior were shown applying cheap PM-sensors (e.g. high separation efficiency of membrane filter media, increased emissions at higher tank pressures, high particle penetration through seams of the filter bag). Concluding, the sensors are suitable for the qualitative characterization of the spatial and total particle emission of pulse-jet cleaned filters.

In further investigations, the quantitative accuracy of the low-cost PM-sensors will be evaluated considering local flow-conditions for the calculation of an emitted dust mass from the locally obtained particle concentrations.

With regards to the industrial application, long term stability and lifetime of the sensors has to be taken into account. During ideal filter operation, low-emission levels can be achieved. The process conditions (e.g. temperature, humidity, gas composition) are current limitations for the use of commercially available low-cost PM-sensors. The ultimate goal of this research is to transfer conclusions from spatially resolved measurements to optimize operation and maintenance of baghouse filters.

Acknowledgements

We acknowledge the financial support and close cooperation of Filterkonsortium at KIT. Filterkonsortium at KIT unites leading companies in the fields of fiber and media production, assembly, plant engineering and measurement technology with the research activities of the research group Gas-Particle-Systems of the Institute of Mechanical Process Engineering and Mechanics (MVM). The members of Filterkonsortium at KIT are as follows: BWF Tec GmbH & Co. KG, ESTA Apparatebau GmbH & Co. KG, Evonik Fibres GmbH, Freudenberg Filtration Technologies SE & Co. KG, Junker-Filter GmbH, MANN+HUMMEL GmbH, PALAS GmbH, Sick AG. We acknowledge the collaboration of Grigor Vrhovac for his help in conducting the experiments.

Declaration of Competing Interest

The authors declare that they have no known competing financial interests or personal relationships that could have appeared to influence the work reported in this paper.

References

- Zhang, Q., Horst, D., Schmidt, E., 2020. Evaluation of tensile adhesion strength in simulated dust cakes on fabric filters. *Chem. Technol.* 44, 359–364. <https://doi.org/10.1002/ceat.201900541>
- Alphasense, 2018. (<http://www.alphasense.com/index.php/products/optical-particle-counter>). (Accessed 20 March 2020).
- Andersen, B.O., Nielsen, N.F., Walther, J.H., 2016. Numerical and experimental study of pulse-jet cleaning in fabric filters. *Powder Technol.* 291, 284–298. <https://doi.org/10.1016/j.powtec.2015.12.028>
- Bach, B., Schmidt, E., 2007. Influence of leaks in surface filters on particulate emissions. *J. Hazard. Mater.* 143 (3), 673–676. <https://doi.org/10.1016/j.jhazmat.2007.01.093>
- Bächler, P., Meyer, J., Dittler, A., 2022. Measurement of transient nanoparticle emissions of pulse-jet cleaned filters applying an engine exhaust particle sizer. *Aerosol Sci. Technol.* <https://doi.org/10.1080/02786826.2022.2027335>
- Bächler, P., Meyer, J., Dittler, A., 2019a. Characterization of the emission behavior of pulse-jet cleaned filters using a low-cost particulate matter sensor. *Gefährst. Reinhalt. Luft.* 79 (11–12), 443–450. <https://doi.org/10.37544/0949-8036-2019-11-12-49>
- Bächler, P., Szabadi, J., Meyer, J., Dittler, A., 2020. Simultaneous measurement of spatially resolved particle emissions in a pilot plant scale baghouse filter applying distributed low-cost particulate matter sensors. *J. Aerosol Sci.* 150, 105644. <https://doi.org/10.37544/0949-8036-2019-11-12-49>
- Bächler, P., Meyer, J., Dittler, A., 2019b. Investigation of low-cost PM-sensors regarding the suitability for emission measurement for pulse-jet cleaned filters. Conference paper at FILTECH 2019 – The Filtration Event (Cologne).
- Bezantakos, S., Costi, M., Barmounis, K., Antoniou, P., Voulerakos, P., Keleshis, C., Sciare, J., Biskos, G., 2021. Qualification of the Alphasense optical particle counter for inline air quality monitoring. *Aerosol Sci. Technol.* 55 (3), 361–370. <https://doi.org/10.1080/02786826.2020.1864276>
- BImSchG Bundesministerium für Justiz und Verbraucherschutz: Gesetz zum Schutz vor schädlichen Umwelteinwirkungen durch Luftverunreinigungen, Geräusche, Erschütterungen und ähnliche Vorgänge (Bundes-Immissionsschutzgesetz - BImSchG). (<https://www.gesetze-im-internet.de/bimsg/index.html>). (Accessed 11 January 2019).
- Binnig, J., Meyer, J., Kasper, G., 2009. Origin and mechanisms of dust emission pulse-jet cleaning filter media. *Powder Technol.* 189 (1), 108–114. <https://doi.org/10.1016/j.powtec.2008.06.012>
- Budde, M., Schwarz, A., Müller, T., Laquai, B., Streibl, N., Schindler, G., Riedel, T., Dittler, A., Beigl, M., 2018. Potential and limitations of the low-cost SDS011 particle sensor for monitoring urban air quality. *Prosci. Dust* 2018 (5), 6–12. <https://doi.org/10.14644/dust.2018.002>
- Charvet, A., Wingert, L., Bardin-Monnier, N., Pacault, S., Godoy, C., Ribeyre, Q., Thomas, D., 2016. Visualization of airborne nanoparticle deposits onto spherical collectors. *Sep. Purif. Technol.* 172 (2017), 119–129. <https://doi.org/10.1016/j.seppur.2016.07.045>
- Chen, S., Wang, Q., Chen, D.R., 2017. Effect of pleat shape on reverse pulsed-jet cleaning of filter cartridges. *Powder Technol.* 305, 1–11. <https://doi.org/10.1016/j.powtec.2016.09.013>
- DIN ISO 11057 DIN ISO 11057:2012–05, 2016. Air quality – Test method for filtration characterization of cleanable filter media (ISO 11057:2011).
- Dittler, A., Ferer, M.V., Mathur, P., Djuranovic, P., Kasper, G., Smith, D.H., 2002. Patchy cleaning of rigid gas filters – transient regeneration phenomena comparison of modelling to experiment. *Powder Technol.* 124 (1–2), 55–66. [https://doi.org/10.1016/S0032-5910\(01\)00481-8](https://doi.org/10.1016/S0032-5910(01)00481-8)
- Löffler, F., 1988. *Staubabscheiden*. Georg Thieme, Verlag Stuttgart, New York.
- Heck, U., Becker, M., Riefler, N., Fritsching, U., 2016. Micro-Macroscopic filter modelling based on computational fluid dynamics (CFD). Conference paper at FILTECH 2016 – The Filtration Event (Cologne).
- Heck, U., Becker, M., 2022. CFD modelling of a bag filter plant for flue gas cleaning under consideration of flow shift and particle deposition relocations. Conference paper at FILTECH 2022 – The Filtration Event (Cologne).
- Imming, H.J., Krug, P., 2019. Cleanable filter media go close to zero emission. Conference paper at FILTECH 2019 – The Filtration Event (Cologne).
- Kang, F., Cheng, H., Leng, H., Zen, S., Xu, Z., Li, X., Lü, J., Lin, L., Chen, H., 2020. Performance optimization of rectangular flat pleated filter with slit nozzle for dust cleaning. *Powder Technol.* 376, 320–331. <https://doi.org/10.1016/j.powtec.2020.06.035>
- Höflinger, W., Rud, H., Mausitz, G., 2007. Estimation of the particle penetration and the dust holding capacity of different surface-treated needle felts. *Sep. Purif. Technol.* 58 (2007), 256–261. <https://doi.org/10.1016/j.seppur.2007.03.021>
- Kang, Y., Aye, L., Ngo, T.D., Zhou, J., 2021. Performance evaluation of low-cost air quality sensors: a review. *Sci. Total Environ.*, 151769. <https://doi.org/10.1016/j.scitotenv.2021.151769>
- Klein, G.-M., Schrooten, T., Neuhaus, T., Kräbs, R., 2009. *Energieeffiziente jet-pulse-entstaubungsanlagen*. *Gefährst. Reinhalt. Luft.* 5.
- Kurtz, O., Meyer, J., Kasper, G., 2017. The contribution of small leaks in a baghouse filter to dust emission in the PM_{2.5} range – a system approach. *Particology* 30 (40–52). <https://doi.org/10.1016/j.partic.2016.08.001>
- Kurtz, O., Meyer, J., Kasper, G., 2016. Influence of filter operating parameters on fine dust emissions from pulse-cleaned filter bags. *Chem. Eng. Technol.* 39 (3), 435–443. <https://doi.org/10.1002/ceat.201500340>
- Leith, D., Ellenbecker, J., 1979. Theory for pressure drop in a pulse-jet cleaned fabric filter. *Atmos. Environ.* 14, 845–885. [https://doi.org/10.1016/0004-6981\(80\)90141-9](https://doi.org/10.1016/0004-6981(80)90141-9)
- Li, H., Choi, J., Li, B., Kim, I., Heo, J., 2016. Numerical analysis on the gas flow dynamics from a rectangular slot-nozzle for pulse cleaning of filter unit. *Powder Technol.* 297, 330–339. <https://doi.org/10.1016/j.powtec.2016.04.040>
- Li, J., Lu, X., Wang, W.F., 2020. Leak monitoring and localization in baghouse filtration system using a distributed optical fiber dynamic air pressure sensor. *Opt. Fiber Technol.* 57, 102218. <https://doi.org/10.1016/j.yofte.2020.102218>
- Li, J., Wu, Q., Huang, Y., Sun, Z., Li, J., Wu, D., 2022. Particulate matters filtration by filter medium with pin holes: modeling and experimental verification. *Process Saf. Environ. Prot.* 158, 282–290. <https://doi.org/10.1016/j.psep.2021.12.012>
- Löffler, F., 1972. *Abblasen von an Filterfasern abgeschiedenen Feststoffteilchen*. *Verfahrenstechnik* 6, 3–7.
- Mausitz, G., Secklehner, A., Hagn, S., 2018. The DeCONOX process - an example of advanced exhaust gas cleaning technology in the Austrian cement industry. *Cem. Int.* 16 (2), 34–53.
- Ostermeyer, G.-P., Sandgaard, M., Otto, J., Brandt, S., Finke, B., Schilde, C., Kwade, A., 2020. Measurement of Dynamic Signature of Brake Emissions on a Pin-On-Disc Tribotester with Low-Cost Particulate Sensors. Conference paper at EuroBrake 2020 – EB2020-EBS-029 (Barcelona). (<https://doi.org/10.46720/EB2020-EBS-029>).
- Lacerda, C. R., Andrade, B. K. S. A., Aguiar, M. L., 2019. Collection efficiency of a bag after 3 years of use in a bag filter. Conference paper at FILTECH 2019 – The Filtration Event (Cologne).
- Palas® (<https://www.palas.de/product/promo2000>). (Accessed on 20 March 2020).
- Park, S., Joe, Y.H., Shim, J., Park, H., Shin, W.G., 2019. Non-uniform filtration velocity of process gas passing through a long bag filter. *J. Hazard. Mater.* 365, 440–447. <https://doi.org/10.1016/j.jhazmat.2018.10.098>
- Qin, W., Dekermenjian, M., Martin, R.J., 2006. Prediction of particulate loading in exhaust from fabric filter baghouses with one or more failed bags. *J. Air Waste*

- Manag. Assoc. 56 (8), 1177–1183. <https://doi.org/10.1080/10473289.2006.10464541>
- Qiu, J., Wu, D., Chen, D.R., Li, J., 2021. Reverse pulsed-flow cleaning of pleated filter cartridges having an inner pleated filter cone. *Process Saf. Environ. Prot.* 146, 481–489. <https://doi.org/10.1016/j.psep.2020.11.025>
- Saleem, M., Krammer, G., Khan, R.U., Tahir, M.S., 2012. Influence of operating parameters on cake formation in pilot scale pulse-jet bag filter. *Powder Technol.* 224, 28–35. <https://doi.org/10.1016/j.powtec.2012.02.016>
- Schmidt, E., 1998. Abscheidung von Partikeln aus Gasen mit Oberflächenfiltern, Fortschritt-Berichte der VDI-Zeitschriften, Reihe 3, 546. VDI Verlag, Düsseldorf.
- Schwarz, A.D., Meyer, J., Dittler, A., 2018. Opportunities for low-cost particulate matter sensors in filter emission measurements. *Chem. Eng. Technol.* 41 (9), 1826–1832. <https://doi.org/10.1002/ceat.201800209>
- Simon, X., Bémer, D., Chazelet, S., Thomas, D., Régnier, R., 2010. Consequences of high transitory airflows generated by segmented pulse-jet cleaning of dust collector filter bags. *Powder Technol.* 201 (1), 37–48. <https://doi.org/10.1016/j.powtec.2010.02.036>
- Simon, X., Bémer, D., Chazelet, S., Thomas, D., 2014. Downstream particle puffs emitted during pulse-jet cleaning of a baghouse wood dust collector: influence of operating conditions and filter surface treatment. *Powder Technol.* 261, 61–70. <https://doi.org/10.1016/j.powtec.2014.04.028>
- Tao, R., Yang, M., Li, S., 2020. Effect of adhesion on clogging of microparticles in fiber filtration by DEM-CFD simulation. *Powder Technol.* 360, 289–300. <https://doi.org/10.1016/j.powtec.2019.09.083>
- Sobich, S., Meyer, J., Dittler, A., Kasper, G., 2018. Baghouse filtration: a praxis-relevant media parameter to determine an emissions level of a pulse-jet cleanable filter. Conference paper at FILTECH 2018 – The Filtration Event (Cologne).
- VDI 3677:2016-11, Filtering Separators – Surface Filters, VDI 3677: 2010.
- Wiegleb, G., 2016. Gasmestechnik in Theorie und Praxis. Springer Vieweg, Wiesbaden, pp. 2016. <https://doi.org/10.1007/978-3-658-10687-4>

Publication V

Title: Operating Behavior of Pulse Jet-Cleaned Filters Regarding Energy Demand and Particle Emissions – Part 1: Experimental Parameter Study

Authors: Peter Bächler, Jörg Meyer, Achim Dittler

Journal: Chemical Engineering and Technology

Year of Publication: 2023

Volume and Issue: 46 (8)

Page Numbers: 1689-1697

Reference: [Bächler et al., 2023b]

Abstract:

Filter operation of a pilot-scale baghouse filter was evaluated under energy and particle emission criteria. Evaluation of the required total power for filter operation takes into account the fan power as well as the consumption of pressurized air. Filter face velocity, raw-gas concentration, and tank pressure for regeneration were varied for several cycle time settings to identify the minimum power. Cycle times shorter than at minimum power are not feasible due to increased dust emissions and no additional energetic benefit. Cycle times longer than at minimum power may lower the dust emissions at the cost of increased power consumption. Lowering filter face velocity can greatly lower the power consumption of baghouse filters, having implications on filter layout.

Peter Bächler*
Jörg Meyer
Achim Dittler


Operating Behavior of Pulse Jet-Cleaned Filters Regarding Energy Demand and Particle Emissions – Part 1: Experimental Parameter Study

Filter operation of a pilot-scale baghouse filter was evaluated under energy and particle emission criteria. Evaluation of the required total power for filter operation takes into account the fan power as well as the consumption of pressurized air. Filter face velocity, raw-gas concentration, and tank pressure for regeneration were varied for several cycle time settings to identify the minimum power. Cycle times shorter than at minimum power are not feasible due to increased dust emissions and no additional energetic benefit. Cycle times longer than at minimum power may lower the dust emissions at the cost of increased power consumption. Lowering filter face velocity can greatly lower the power consumption of baghouse filters, having implications on filter layout.

Keywords: Energy optimization, Filtration, Particle emissions, Process efficiency, Pulse jet-cleaned filters

Received: February 03, 2023; *revised:* March 24, 2023; *accepted:* May 11, 2023

DOI: 10.1002/ceat.202300080

 This is an open access article under the terms of the Creative Commons Attribution License, which permits use, distribution and reproduction in any medium, provided the original work is properly cited.



Supporting Information
available online

1 Introduction


Increasing process efficiency and minimizing the power consumption of industrial processes is one of many important measures to lower carbon dioxide emissions to lessen the impact of climate change and staying economically sustainable when facing rising energy costs. Pulse jet-cleaned filters have remained a key technology for dust separation in many industrial processes for several decades and have kept their relevance to this day [1]. The application spectrum for baghouse filters ranges from industrial processes (e.g., cement or aluminum production, food sector, wood processing [2–6]) to smaller-scale applications (e.g., incineration plants, dedusting systems for worker protection [7, 8]).

The operation of filters often follows a strict framework (e.g., Δp - or Δt -controlled criterion for filter regeneration)¹⁾ [9] and a re-evaluation of filter operation regarding energy aspects has the potential to improve process efficiency in the future [10]. While the research foundations for pulse jet-cleaned filters have been laid in the past by, e.g., Löffler [11] or Leith and Ellenbecker [12], present filter operation under demanding conditions still poses its individual challenges [13]. To list some examples, (nano-)particles can cause clogging of the filter material with particulate matter so that the differential pressure increases drastically and the filtration of a protective pre-coat prior to the nanoparticle aerosol might be necessary [7, 14, 15].

High temperatures and toxic gases push the limits of conventional (e.g., polyester needle-felt) filter media and rigid ceramic filter elements have to be used [16–18].

The operation of pulse jet-cleaned filters – while simple on first glance – offers room for highly flexible cleaning and operation strategies that impact particle emissions and the power consumption. During filter operation, particles are separated primarily on the surface of the filter medium, causing the formation of a dust cake with high separation efficiency and an increase in differential pressure. After a regeneration criterion is met (e.g., exceeding of a maximum differential pressure Δp_{\max} or a cycle time Δt), a jet pulse from the clean gas side causes the rapid deformation of the filter element and subsequent cake detachment [9]. This leaves the filter medium prone to particle penetration for a short duration (hence causing an “emission peak”) until a sufficient dust cake has been deposited on the surface of the medium [19].

The biggest contributors regarding power consumption of filter operation are the consumption of pressurized air P_{reg} for filter regeneration and the fan power P_{fan} caused by the differential pressure due to the flow through the filter medium and the filter cake [10, 20, 21]. Both of these contributions are

Peter Bächler  <https://orcid.org/0000-0001-9172-5880>
(peter.baechler@kit.edu), Dr.-Ing. Jörg Meyer, Prof. Dr.-Ing. habil.
Achim Dittler
Karlsruhe Institute of Technology, Institute of Mechanical Process
Engineering and Mechanics, Strasse am Forum 8, 76131 Karlsruhe,
Germany.

1) List of symbols at the end of the paper.

dependent on each other. Higher pulse intensities (e.g., tank pressures for filter regeneration p_{tank}) and shorter time durations between regenerations Δt_{cycle} may lead to a lower differential pressure through better and more frequent cake detachment, but in turn, the consumption of pressurized air rises. Increased tank pressures are known to lead to higher dust emissions as, e.g., seams of the filter element cannot clog sufficiently and remain a source for particle penetration, but may grant a lower residual differential pressure after regeneration due to improved cake detachment [19, 22–24].

Klein et al. [21] have shown the relevance of the efficiency of the nozzle geometries for the jet pulse and discussed the power consumption of pulse jet-cleaned filters. According to Klein et al., roughly 15 % of the required power is caused by the consumption of pressurized air. The remaining 85 % can be attributed to the differential pressure (roughly 11 % housing, 59 % filter cake, 8 % residual pressure drop of the filter medium, 7 % lateral flow through the bag) between raw-gas side and clean-gas side. While the investigation was based on a certain application scenario (filter face velocity: 1 m min^{-1} , length of the bag 6 m, and tank pressure for regeneration 6 bar) it serves as a general guideline [21].

In another study, Ho et al. determined an economically optimal cycle time of 10 s for pulse jet-cleaned filters (pleated filter) on an industrial scale [25]. Krammer et al. also performed investigations regarding an optimal cycle time for filter operation, whereby the optimization criterion was focused on differential pressure levels [26]. Caputo and Pelagagge examined the economic optimum for baghouse filters, identifying optimal filtration velocities for certain filtration times [27]. While the economic situation is market-dependent, an energy evaluation has the advantage of universal applicability even for fluctuating energy prices.

From an emissions perspective, modern (membrane) filter media may provide (almost) zero emission levels [28]. Mainly leaks of the filter medium or the plenum plate, small defects of the filter medium, or the seams of the filter element due to the manufacturing process can cause increased particle emissions [29–31]. In the context of the current draft of the Common Waste Gas Treatment in the Chemical Sector-Best Available Techniques Reference Document (WGC-BREF), a restriction of dust emissions for fabric filters of 5 mg m^{-3} (in case of dust mass flows $> 0.05 \text{ kg h}^{-1}$ at each stack with unique conditions at the outlet) is discussed [32]. In case of a bag failure or unfavorable operation conditions, these limits could potentially be exceeded. Conventional emission monitoring is performed at the outlet of the filter house, e.g., via gravimetric measurement or triboelectric sensors or “filter guards” [33].

The identification of leaks can be performed, e.g., with the help of fluorescent dust for visual identification during a plant shutdown. Innovative sensor technology has been proposed by Li et al. in the form of an optical fiber sensor to identify damaged filter elements [34]. In previous publications, the suitability of the identification of leaks and spatial emission monitoring by application of scattered-light-based particulate matter (PM) sensors has been discussed in detail demonstrating the potential of improved emission monitoring in filtration applications [28, 35, 36].

This study, consisting of two individual articles, aims to combine the two most prominent performance indicators of

filter operation, namely, the required power for filter operation and particle emissions, to enable a better evaluation of beneficial operation settings and favorable cycle times. In this first article, the operation of a small-scale baghouse filter is discussed under energy-related and particle emission-related criteria. The power consumption of the baghouse filter is calculated according to equations proposed by Höflinger and Laminger [2, 14] (compare Sect. 2.3). The second article will deal with the modeling of filter operation applying and expanding on the calculation basics introduced by Löffler [11]. Modeling has the potential to improve the layout of baghouse filters and check existing plants regarding energy-efficient operation as well as validating the experimental results.

2 Experimental Setup, Materials, Measurement Technology, and Experimental Methodology

2.1 Pilot Plant-Scale Baghouse Filter

The experiments have been performed in a small-scale baghouse filter (Fig. 1) with a total of nine filter bags (4.14 m^2 installed filter area).

A radial blower creates a circulating air flow through the testing facility. Dust is added at two separate points: new dust is added from a silo to enable a constant particle size distribution and already separated dust is recirculated to grant long-term economic operation. The raw-gas dust concentration is monitored via an extinction measurement before entering the filter house. The extinction measurement has been calibrated for several gravimetric concentration levels (dispersion via screw-feeders with varying rotational speed). After entering the filter house, dust is separated from the air flow at the surface of the filter medium. Each filter bag can be regenerated individually (cleaning of approx. 1/9th of installed filter area for each regeneration). During the experiments, a time-controlled regeneration algorithm was selected so that a single filter bag is regenerated after a time interval Δt_{cycle} following a “bag-by-bag” cleaning pattern. The total particle emission penetrating the filter bags after regeneration is monitored employing a highly developed laboratory aerosol spectrometer (Promo[®] 2000 with *welas*[®] 2100 sensor) from the manufacturer Palas[®].

Several different parameters have been adjusted and evaluated regarding their energy demand (respectively required power for filter operation) and particle emission. Tab. 1 gives an overview on the varied and constant process parameters.

2.2 Filter Medium and Test Dust

The employed filter medium was a polyester needle-felt with a singed upstream side. Specifications of the filter medium are summarized in Tab. 2. Prior to the experiments, the filter bags were aged up to 300 complete filtration cycles each so that particle emissions and residual pressure drop of the filter elements are stabilized and any consecutive filter aging effects are negligible compared to the variations performed in the parameter study [23]. The filter medium is representative for commonly

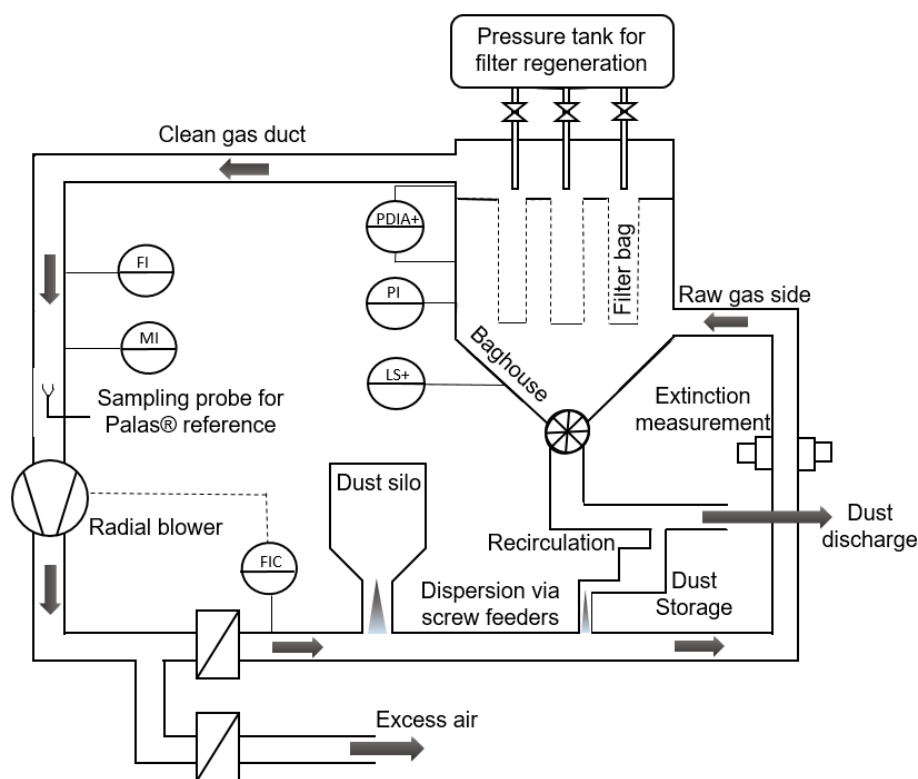


Figure 1. Schematic overview of the baghouse filter (operating parameters listed in Tab. 1) – image modified from [28].

Table 1. Varied and constant process parameters for the study.

Parameter	Value
Filter face velocity [cm s ⁻¹]	2, 2.5, and 3.3
Raw-gas concentration $c_{\text{raw-gas}}$ [g m ⁻³]	15, 30, and 40
Tank pressure p_{tank} [bar]	3 and 6
Cleaning interval Δt_{cycle} [s]	10–180
Electrical valve opening time [ms]	150
Filter medium	Needle felt (compare Tab. 2)
Test dust	PURAL SB [®]

Table 2. Specifications of the needle-felt filter medium.

Parameter	Value
Area weight [g m ⁻²]	600
Thickness [mm]	2
Permeability (at 200 Pa) [L dm ⁻² min ⁻¹]	70
Fiber material and remarks	PE, singed upstream side

used needle-felt filter media used in the industrial applications. The bags have a length of 125 cm and a diameter of 11.7 cm, what is on the lower end of typical bag geometries.

The test dust PURAL SB[®] is an alumina monohydrate powder from the manufacturer Sasol[®]. A more in-depth evaluation of the test dust, including the particle size distribution across a wider range (from 10 nm to 200 μm) measured by different instruments, can be found in a previous publication [37]. The test dust has a mass median diameter of approx. 35 μm as determined by laser diffraction. The dust is free-flowing and does not tend to agglomerate, causing a significant fine-dust fraction in the dispersed state. Thus, the dust tends to cause high emissions during filter tests.

Note that the reported data in this publication is only valid for this system of test dust and filter medium. Different dust properties and types of filter media, e.g., membrane filter media, may lead to different conclusions regarding optimal process parameters.

2.3 Methodology for the Evaluation of Filter Operation under Energy-Related and Particle Emission-Related Criteria

Höflinger et al. proposed a method to evaluate filter media based on energy criteria in a filter test rig based on DIN ISO 11057 [38]. They took into account the differential pressure across the filter medium as well as the consumption of pressurized air from the jet pulse by applying the following equation in order to calculate the total power consumption of filter operation P_{Filter} (equation modified from [10, 20]):

$$P_{\text{Filter}} = \dot{V} \Delta p_{\text{Filter}} + \frac{V_{\text{Tank}} \Delta p_{\text{Tank}}}{\Delta t_{\text{cycle}}} \quad (1)$$

where \dot{V} is the volume flow through the filter, Δp_{Filter} is the differential pressure between raw-gas side and clean-gas side, V_{Tank} is the volume of the vessel containing the pressurized air, Δp_{Tank} is the pressure drop within the vessel caused by releasing the jet pulse for filter regeneration, and Δt_{cycle} the time interval between filter regenerations or cleaning frequency. The equation can be split into two separate parts, representing the required fan power due to the differential pressure across the

filter medium and the dust cake and the required average power consumption of the jet-pulse cleaning.

$$P_{\text{Filter}} = P_{\text{fan}} + P_{\text{reg}} \quad (2)$$

$$P_{\text{fan}} = \dot{V} \Delta p_{\text{Filter}} \quad (3)$$

$$P_{\text{reg}} = \frac{V_{\text{Tank}} \Delta p_{\text{Tank}}}{\Delta t_{\text{cycle}}} \quad (4)$$

The equation itself can be transferred and used aside from filter testing to estimate the required energy demand for bag-house filters. The underlying experimental procedure was presented at the Filtech 2023 conference [39]. To evaluate filter operation based on the energy consumption, the determination of an average differential pressure Δp_{Filter} is necessary for a certain set of parameters. The pressure drop during the jet pulse Δp_{Tank} has to be determined for individual tank pressures and valve opening times (constant valve opening time of 150 ms in this study).

The cycle time has been adjusted during each experimental run for each parameter, ranging from a maximum cycle time (e.g., 180 s) down to 10 s (longest possible sequence: 180 s → 150 s → 120 s → 90 s → 60 s → 45 s → 30 s → 20 s → 10 s) to create several differential pressure levels. Note that longer cycle times above 90 s are at the upper limit of the capacity of the radial blower of the testing facility for the highest adjusted filter face velocity of 3.3 cm s^{-1} and the volume flow may decrease by approx. 10 % during the cycle. Therefore, the starting point of the sequence was adjusted dependent on the corresponding parameters, ensuring that an energetic optimum could be identified for each setting.

The exact cycle times within the sequence (after selecting an initial starting cycle time) were kept constant for each experiment and set of parameters, starting at the highest cycle time ranging down to the lowest cycle time of 10 s. The average differential pressure and the average particle emission were determined from the experimental data at the end of the corresponding cycle time setting to gain a representative value.

For the determination of an average power consumption of the pressurized air for filter regeneration, the pressure drop Δp_{Tank} was determined in a preliminary experiment for multiple tank pressures. The volume of the tank V_{Tank} is 0.011 m^3 so that the calculation of the energy consumption for filter regeneration P_{reg} is possible. More information regarding the experimental procedure can be found in the Supporting Information.

Fig. 2 displays a summary of the determination of a characteristic

operation curve for filter operation by combining the total required power for filter operation (consisting of P_{fan} and P_{reg}) and the particle emission. $PM_{2.5}$ concentrations were selected as benchmark values for the particle emission, as the fine dust fraction is of significant importance regarding human health and was also presented in older studies when measuring the emission with scattered-light based low-cost PM sensors [28, 35, 36]. $PM_{2.5}$ represents the fine dust fraction of the emission (classification of particles following a separation curve with a cut size of $2.5 \mu\text{m}$). Plotting the total energy consumption versus the particle emission yields the operation curve.

The operation curve enables the identification of favorable operation regions at (or close to) the minimum power. A more detailed guideline on how to read the operation curve can be found in the Supplementary Information. In general, operation points on the right side of the power minimum (red line – higher energy consumption and higher emissions) are unfavorable. To the left of the power minimum (green line), emissions are lower at the cost of a certain increase of fan power, as the contribution of pressurized air consumption becomes (almost) negligible. Exceeding feasible cycle times may yield an increasingly high total power consumption that outweighs the lower dust emission due to less frequent regenerations. Note that the low spectrum of employed cycle times (e.g., 10 and 20 s) borders unstable operation (almost constant regeneration of a large fraction of installed filter area and no cake formation) and thus, is not praxis-relevant [40].

The results of the study are within reasonable agreement with the publication by Klein et al. [21], where approximately 15 % of the total power can be allocated to filter regeneration and the remaining 85 % can be attributed to the differential pressure across housing and filter. The contributions of fan power and filter regeneration to the total power at the corre-

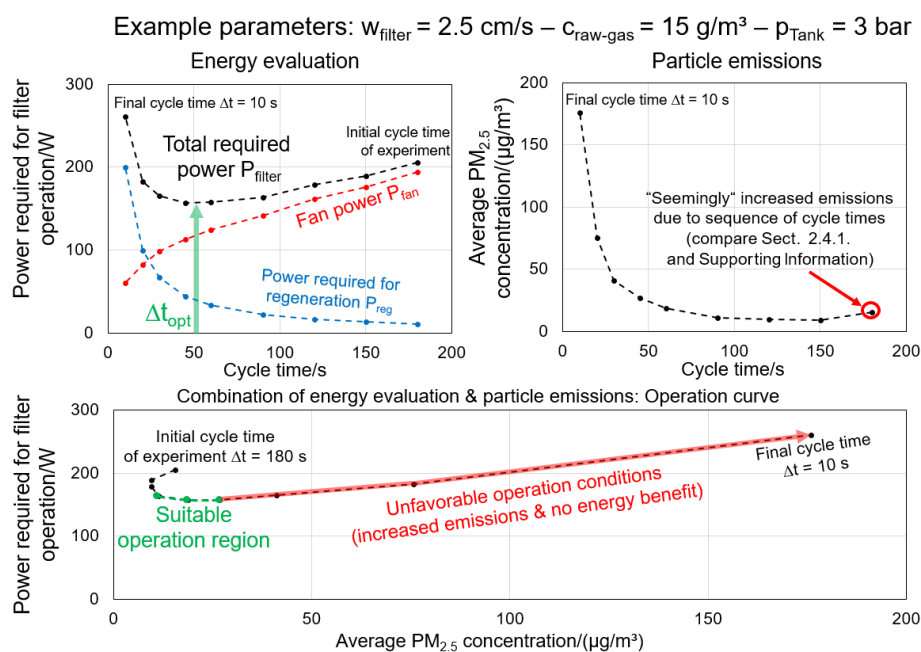


Figure 2. Evaluation of filter operation based on power consumption and particle emissions for a certain set of parameters ($w_{\text{filter}} = 2.5 \text{ cm s}^{-1}$, $c_{\text{raw-gas}} = 15 \text{ g m}^{-3}$, $p_{\text{Tank}} = 3 \text{ bar}$).

sponding minimum are ranging between 60–80 % fan power and 40–20 % filter regeneration for the experiments. Note that the determined fan power does not include fan efficiencies or electrical efficiencies, so that the actual contribution would be somewhat higher and a little closer to the data reported by Klein et al.

3 Results and Discussion

3.1 Variation of Raw-Gas Concentration

Different cycle time settings were adjusted at a constant tank pressure for filter regeneration of 3 bar and a filter face velocity of 2 cm s^{-1} at varying raw-gas concentration levels. The operation curves of the experiments were derived according to Sect. 2.3 and are displayed in Fig. 3.

A shift towards higher power requirements occurs with an increase in raw-gas concentration (global trend of operation curves) due to thicker dust cakes. Adjusting the cycle times cannot offset the increment in differential pressure due to the increased dust load on the filter bags. The region close to the power minimum is of actual interest regarding viable settings for filter operation. The power minimum for lower raw-gas concentrations is located at a lower overall power consumption

combined with longer cycle times so that filter regeneration is required less frequently. From an emissions perspective, all operation curves are in a similar region ($PM_{2.5}$ emission lower than $30 \mu\text{g m}^{-3}$ at the optimum). Particle emissions are lower for the shorter cycle times, mainly 10 and 20 s, at higher raw-gas concentrations. Increased dust load causes the rapid formation of a dust cake even for the shorter cycle times what may seem beneficial at first, however, the shorter cycle times of 10 and 20 s are far outside an energetically suitable operation region.

Fig. 4 shows the potential benefit of incorporating energy criteria into the evaluation of filter operation via a detail view of the region around the power minimum.

At the region close to the power minimum, small adjustments regarding the cycle time Δt_{cycle} may significantly impact particle emissions and power consumption. In the figure, the green lines represent a favorable increase in cycle time, where emissions can be lowered significantly at almost no increase in total power. Purple lines indicate a reasonable decrease in particle emission when compared to the additional power requirement. Red lines display unfavorable shifts in cycle times with significantly increased power consumptions with negligible impact on particle emissions.

As an example, the energetic optimum at 15 g m^{-3} raw-gas concentration can be identified at 90–60 s, where there is no

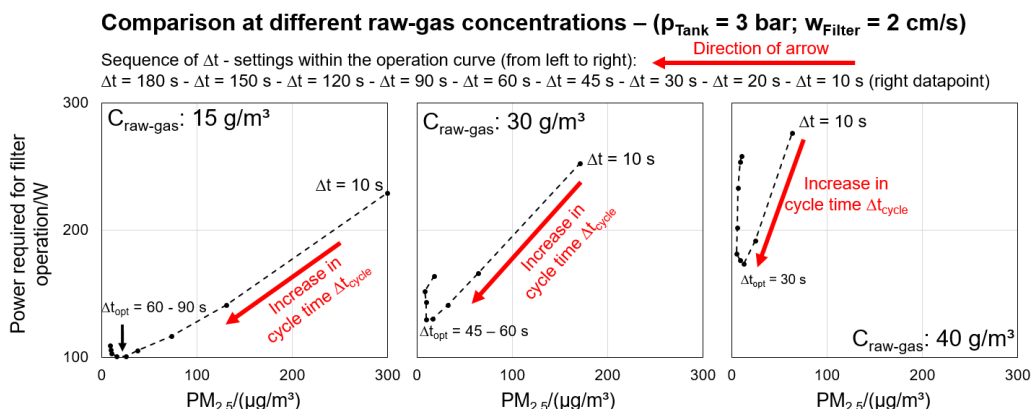


Figure 3. Operation curve of filter operation at different raw-gas concentrations ($w_{\text{filter}} = 2 \text{ cm s}^{-1}$, $p_{\text{Tank}} = 3 \text{ bar}$).

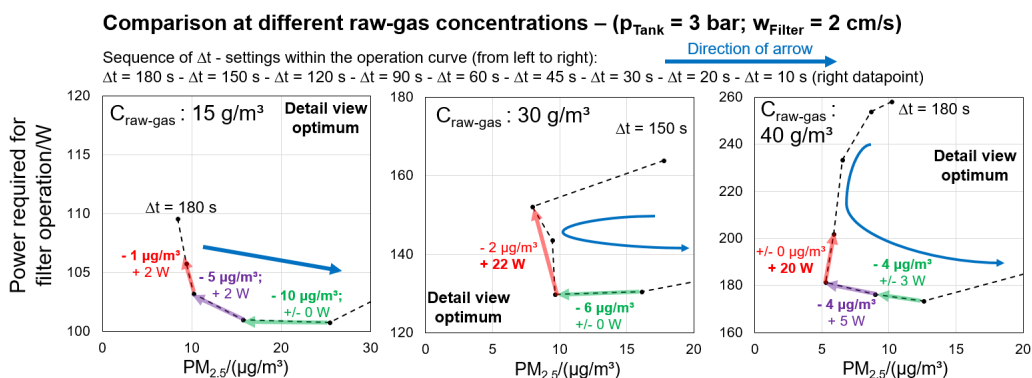


Figure 4. Detail view of the power minimum of the operation curves at different raw-gas concentrations ($w_{\text{filter}} = 2 \text{ cm s}^{-1}$, $p_{\text{Tank}} = 3 \text{ bar}$).

significant difference between the total power at both cycle times. Thus, the longer cycle time of 90 s is overall preferable, due to less frequent regenerations and lower particle emissions. In order to further lower particle emissions, the cycle time could be increased further to 120 s. While the energetic investment is moderate, if not negligible, the decrease in particle emission is significant. A further increase from 120 s to 150 s is not sensible, as the energetic investment increases further but the impact on dust emissions is rather low compared to the previous step from 90 s to 120 s).

Summarizing, an increase in raw-gas concentration shifts the power minimum towards higher overall power consumption at a shorter cycle time, making more frequent regenerations more feasible. At the corresponding filter face velocity of 2 cm s^{-1} , the cycle times were sufficiently long in order to not suffer exceedingly high dust emissions.

3.2 Variation of Filter Face Velocity

After the variation of raw-gas concentration, the filter face velocity has been varied for two distinct levels of raw-gas concentration (15 and 30 g m^{-3}). Since the filter face velocity is defined as the total volume flow divided by the available filter area, adjusting the filter face velocity in the baghouse filter is only possible by changing the volume flow (constant installed filter area). Due to the direct correlation between flow velocity and pressure drop, the required power has been related to the total volume flow in Fig. 5 to grant directly comparable conditions (specific energy demand in Wh m^{-3}).

The results at the corresponding filter face velocities are qualitatively similar to the previous chapter at 2 cm s^{-1} filter face velocity. At the higher raw-gas concentration, the operation curve is shifted towards higher power consumptions and the power minimum is shifted towards shorter cycle times (more frequent regeneration). The results are in line with the investigations of Saleem et al. where increased filter face velocities led to shorter cycle times and a higher specific cake resistance for a Δp -controlled filter operation [41]. The particle emission in the relevant

operation region (cycle times equal to or larger than the cycle time at the minimum) are at a low level with (almost) negligible differences regarding the varied parameters.

A lower filter face velocity is highly beneficial from an energy point of view. Lowering the filter face velocity would potentially allow for higher raw-gas concentrations (similar level of operation curves at 30 g m^{-3} and lower filter face velocity compared to 15 g m^{-3} and the next-higher filter face velocity). Longer cycle times are also beneficial from a wear and materials perspective, as less frequent regenerations can prolong the lifetime of filter elements. A summary of the power consumptions at the minimum with the corresponding cycle time can be found in Sect. 3.3 in Fig. 6.

Following the energy evaluation, economic aspects would have to be taken into account. The findings give major implications to the layout of filter houses regarding the required filter area. Facing rising energy costs, installing a larger amount of filter area to keep the filter face velocity as low as possible compared to the typical layout guidelines, e.g., stated in VDI3677 [42], might be feasible. However, additional filter area of course also causes additional investment and maintenance costs when replacing filter elements. Increasing the filter area is in most cases retroactively not possible for existing filter houses and the volume flow of an industrial facility is (in most cases) fixed and cannot be varied. Some industrial filters operate under a fan with constant rotary speed. Here, it might be beneficial to lower the rotary speed to save energy, if process stability is not in danger.

3.3 Variation of Tank Pressure for Filter Regeneration

The experiments presented in Sect. 3.2 were repeated at a higher tank pressure for filter regeneration (6 bar compared to 3 bar) to demonstrate the effect on particle emissions and total power of raising the regeneration intensity.

The power minimum of the corresponding experimental parameters is summarized in Fig. 6. When increasing the tank

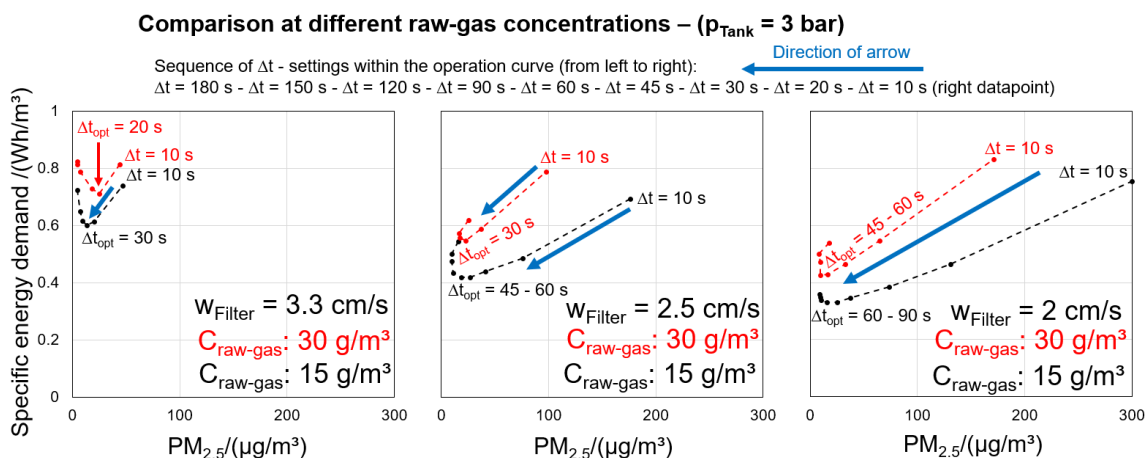


Figure 5. Operation curve of filter operation at different raw-gas concentrations (15 and 30 g m^{-3}) and filter face velocities ($2, 2.5, 3.3 \text{ cm s}^{-1}$).

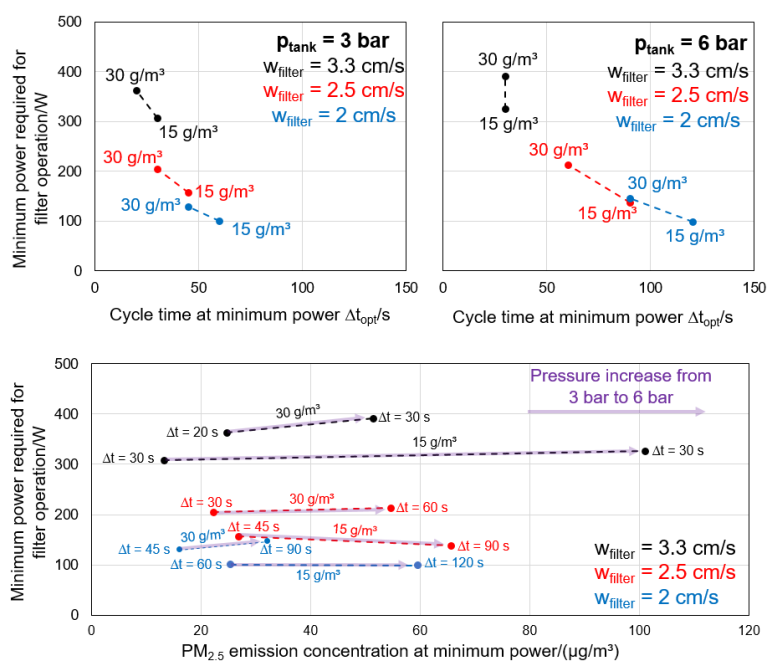


Figure 6. Comparison of cycle times at minimum power regarding energy demand and particle emissions for two different tank pressures (3 and 6 bar) at varying raw-gas concentrations and filter face velocities. In case of a less pronounced power minimum (multiple datapoints), only a single datapoint is displayed (compare Figs. 3 and 5).

pressure, the power requirement due to the jet pulse/filter regeneration rises according to Eq. (4), as the pressure drop Δp_{tank} within the pressure vessel becomes higher.

The bottom image in Fig. 6 clearly demonstrates the potential emission problems of raising the tank pressure. Despite the longer cycle times at the power minimum for the 6-bar measurements, the particle emission increases by approx. a factor of 2. There is almost no benefit of raising the tank pressure from an energy point of view, as the differences in total power between the individual settings are almost negligible. The cycle times of the 6 bar tank pressure are approximately higher by a factor of 2 for the filter face velocities of 2.5 and 2 cm s^{-1} . Less frequent regenerations are, in theory, beneficial from a wear and materials perspective. However, the higher pulse intensity also increases the wear on the filter element, so that there is no obvious benefit. According to the results of Tsai et al. [22], increasing the tank pressure above certain limits does not significantly lower the residual pressure difference after regeneration. There may be more beneficial pulse intensities from an energy perspective. Additional data for 4.5 bar tank pressure and a raw-gas concentration of 30 g m^{-3} is reported in the Supporting Information.

Summarizing, increasing the tank pressure for filter regeneration overall lowered the contribution of the required fan power (lower dif-

ferential pressure level) due to a more thorough cleaning of the filter element and lower residual pressures after filter regeneration. The additional energetic investment due to increased pressures mitigated the benefit of a lower differential pressure level. While higher tank pressures shifted the energetic optimum to higher cycle times, the particle emissions were greatly increased due to the higher pulse intensity so that raising the tank pressure above certain limits is never recommended outside certain scenarios, e.g., regeneration issues or conglutination of filter elements.

4 Summary and Outlook

The operation of a pulse jet-cleaned filter was evaluated in a pilot-scale baghouse filter taking into account power consumption and particle emission. The power required for filter operation was determined according to the equations proposed by Höflinger et al., considering the fan power (product of volume flow and average differential pressure for a set of parameters) and an average power representing the consumption of pressurized air for jet-pulse cleaning. Particle emissions were measured using an optical aerosol spectrometer.

Several different parameters were varied. The main results of the parameter study are summarized in Tab. 3. Note that the results are based on investigations using a single type of filter medium (needle-felt) and test dust (free-flowing/non-agglomerating). Different dust properties and filter media may lead to different conclusions; however, the qualitative observations should be valid for many applications.

Higher raw-gas concentrations and higher filter face velocities led to qualitatively similar results in the form of an increase of the total power consumption due to higher differential pressure levels and a decrease in the cycle time at minimum power (more frequent regenerations). The differences in particle emission were negligible at feasible operation regions and sufficiently long cycle times. Raising the tank pressure did not offer energetic benefits, as the lower power requirement due to lower differential pressure levels got mitigated by increased power consumption of the higher intensity pressure pulse.

Table 3. Summary of the results of the parameter variation.

Parameter variation increase of:	Total power consumption	Cycle time at the power minimum	Particle emission
Raw-gas concentration	Increase	Decrease More frequent regeneration	Constant at relevant operation region
Filter face velocity	Increase	Decrease More frequent regeneration	Constant at relevant operation region
Tank pressure	(Almost) constant	Increase Less frequent regeneration	Increase

The results demonstrate the importance of taking into account energy criteria when evaluating filter operation. While many results may seem evident (e.g., an increase in raw-dust concentration requires a decrease in cycle time in order to remain at a feasible differential pressure level), the exact quantification of energetically beneficial operation points can put current operation strategies into question and offer a perspective on optimization potential.

Many industrial filters follow more or less strict operation frameworks. Incorporating these results into operation strategies, e.g., monitoring raw-gas concentrations, and dynamically adjusting the cycle time towards favorable conditions may improve the energy efficiency of pulse jet-cleaned filters.

In part 2 of this study, the experimental results of this article will be implemented in modeling of filter operation applying and enhancing the calculation basics by Löffler [11]. This has the potential to give layout advice regarding filter operation and help plant operators predict and optimize the energy demand of their filter when changing existing parameters.

Supporting Information

Supporting Information for this article can be found under DOI: <https://doi.org/10.1002/ceat.202300080>.

Acknowledgment

The authors acknowledge the financial support and close cooperation of Filterkonsortium at KIT. Filterkonsortium at KIT unites leading companies in the fields of fiber and media production, assembly, plant engineering, and measurement technology with the research activities of the research group Gas-Particle-Systems of the Institute of Mechanical Process Engineering and Mechanics (MVM). The members of Filterkonsortium at KIT are as follows: BWF Tec GmbH & Co. KG, ESTA Apparatebau GmbH & Co. KG, Evonik Fibres GmbH, Freudenberg Filtration Technologies SE & Co. KG, Junker-Filter GmbH, MANN+HUMMEL GmbH, PALAS GmbH, Sick AG. We acknowledge that part of the materials (Sect. 2.3) and parts of the Supporting Information have been first presented at FILTECH 2023. Open access funding enabled and organized by Projekt DEAL.

The authors have declared no conflict of interest.

Symbols used

$c_{\text{raw-gas}}$	[g m ⁻³]	raw-gas dust concentration
Δp	[Pa]	differential pressure
Δp_{filter}	[Pa]	differential pressure between raw-gas side and clean gas side across the filter medium (including the dust cake)
Δp_{tank}	[bar]	pressure drop in the pressure vessel supplying the pressurized air for the jet pulse
P_{fan}	[W]	fan power

P_{filter}	[W]	total energy consumption of filter operation
$PM_{2.5}$	[μg m ⁻³]	fine dust fraction of the emission (classification of particles following a separation curve with a cut size of 2.5 μm)
P_{reg}	[W]	energy consumption due to filter regeneration/consumption of pressurized air
$\Delta t/\Delta t_{\text{cycle}}$	[s]	time interval between regenerations of each individual filter element (if each of the nine filter elements was regenerated, it is referred to as a “complete filtration cycle”)
Δt_{opt}	[s]	cycle time at the power minimum of an operation curve
\dot{V}	[m ³ h ⁻¹]	volume flow
V_{tank}	[m ³]	volume of the pressure vessel supplying the pressurized air for the jet pulse
w_{filter}	[cm s ⁻¹]	filter face velocity

References

- [1] W. Peukert, A. Bück, *Chem. Ing. Tech.* **2022**, *95* (1–2), 19–25. DOI: <https://doi.org/10.1002/cite.202200159>
- [2] X.-L. Huang, A. M. El Badawy, M. Arambewela, R. Adkins, T. Tolaymat, *Chemosphere* **2015**, *134*, 25–30. DOI: <https://doi.org/10.1016/j.chemosphere.2015.03.033>
- [3] J. O. Litchwark, J. Winchester, J. J. Nijdam, *Powder Technol.* **2015**, *284*, 379–386. DOI: <https://doi.org/10.1016/j.powtec.2015.06.056>
- [4] J. Wilanowicz, W. Grabowski, M. Andrzejczak, A. Chromiec, *Procedia Eng.* **2013**, *57*, 1269–1277. DOI: <https://doi.org/10.1016/j.proeng.2013.04.160>
- [5] X. Simon, D. Bémer, S. Chazelet, D. Thomas, *Powder Technol.* **2014**, *261*, 61–70. DOI: <https://doi.org/10.1016/j.powtec.2014.04.028>
- [6] M. G. Cora, Y.-T. Hung, *Environ. Qual. Manage.* **2002**, *11* (4), 53–64. DOI: <https://doi.org/10.1002/tqem.10041>
- [7] S. Schiller, H. J. Schmid, *Powder Technol.* **2015**, *279*, 96–105. DOI: <https://doi.org/10.1016/j.powtec.2015.03.048>
- [8] F. Schott, G. Baumbach, D. Straub, H. Thorwarth, U. Vogt, *Biomass Bioenergy* **2022**, *163*, 106520. DOI: <https://doi.org/10.1016/j.biombioe.2022.106520>
- [9] K. T. Hindy, *Atmos. Environ.* **1986**, *20* (8), 1517–1521. DOI: [https://doi.org/10.1016/0004-6981\(86\)90240-4](https://doi.org/10.1016/0004-6981(86)90240-4)
- [10] W. Höflinger, T. Laminger, *Energy Sustainability* **2013**, *4*, 145–155. DOI: <https://doi.org/10.2495/ESUS130121>
- [11] F. Löffler, *Staubabscheiden*, Georg Thieme, Stuttgart **1988**.
- [12] D. Leith, M. J. Ellenbecker, *Aerosol Sci. Technol.* **1982**, *1* (4), 401–408. DOI: <https://doi.org/10.1080/02786828208958604>
- [13] W. Peukert, C. Wadenpohl, *Powder Technol.* **2001**, *118* (1–2), 136–148. DOI: [https://doi.org/10.1016/S0032-5910\(01\)00304-7](https://doi.org/10.1016/S0032-5910(01)00304-7)
- [14] N. Khirouni, A. Charvet, D. Thomas, D. Bémer, *Process. Saf. Environ.* **2020**, *138*, 1–8. DOI: <https://doi.org/10.1016/j.psep.2020.02.040>
- [15] E. H. Tanabe, P. M. Barros, K. B. Rodrigues, M. L. Aguiar, *Sep. Purif. Technol.* **2011**, *80* (2), 187–195. DOI: <https://doi.org/10.1016/j.seppur.2011.04.031>

- [16] A. Dittler, H. F. Umhauer, *Powder Technol.* **2001**, *120* (3), 223–231. DOI: [https://doi.org/10.1016/S0032-5910\(01\)00280-7](https://doi.org/10.1016/S0032-5910(01)00280-7)
- [17] G. Ahmadi, D. H. Smith, *Aerosol Sci. Technol.* **2002**, *36* (6), 665–677. DOI: <https://doi.org/10.1080/02786820290038357>
- [18] J.-H. Kim, Y.-C. Kim, J.-H. Choi, *Korean J. Chem. Eng.* **2016**, *33*, 726–734. DOI: <https://doi.org/10.1007/s11814-015-0211-y>
- [19] J. Binnig, J. Meyer, G. Kasper, *Powder Technol.* **2009**, *189* (1), 108–114. DOI: <https://doi.org/10.1016/j.powtec.2008.06.012>
- [20] W. Höflinger, T. Laminger, *J. Taiwan Inst. Chem. Eng.* **2019**, *94*, 53–61. DOI: <https://doi.org/10.1016/j.jtice.2017.07.035>
- [21] G.-M. Klein, T. Schrooten, T. Neuhaus, R. Kräbs, *Gefahrstoffe – Reinhalt. Luft* **2009**, *5*, 20633.
- [22] C.-J. Tsai, M.-L. Tsai, H.-C. Lu, *Aerosol Sci. Technol.* **2000**, *35* (2), 211–226. DOI: <https://doi.org/10.1081/SS-100100152>
- [23] O. Kurtz, J. Meyer, G. Kasper, *Chem. Eng. Technol.* **2016**, *39* (3), 435–443. DOI: <https://doi.org/10.1002/ceat.201500340>
- [24] C. R. de Lacerda, P. Bächler, A. D. Schwarz, R. Sartim, M. L. Aguiar, A. Dittler, *Chem. Eng. Technol.* **2022**, *45* (7), 1354–1362. DOI: <https://doi.org/10.1002/ceat.202200132>
- [25] C.-L. Ho, Y.-C. Tang, W.-C. Chiu, *Appl. Sci.* **2021**, *11* (22), 10941. DOI: <https://doi.org/10.3390/app112210941>
- [26] G. Krammer, A. Kavouras, A. Anzel, *Chem. Eng. Technol.* **2003**, *26* (9), 951–955. DOI: <https://doi.org/10.1002/ceat.200303032>
- [27] A. C. Caputo, P. M. Pelagagge, *Environ. Prog.* **2000**, *19* (4), 238–245. DOI: <https://doi.org/10.1002/ep.670190410>
- [28] P. Bächler, J. Szabadi, J. Meyer, A. Dittler, *J. Aerosol Sci.* **2022**, *150*, 105644. DOI: <https://doi.org/10.1016/j.jaerosci.2020.105644>
- [29] B. Bach, E. Schmidt, *J. Hazard. Mater.* **2007**, *144* (3), 673–676. DOI: <https://doi.org/10.1016/j.jhazmat.2007.01.093>
- [30] O. Kurtz, J. Meyer, G. Kasper, *Particuology* **2017**, *30*, 40–52. DOI: <https://doi.org/10.1016/j.partic.2016.08.001>
- [31] J. Li, Q. Wu, Y. Huang, J. Li, D. Wu, *Process. Saf. Environ.* **2022**, *158*, 282–290. DOI: <https://doi.org/10.1016/j.psep.2021.12.012>
- [32] K. Daginnus, T. Marty, N. V. Trotta, T. Brinkmann, A. Whitfield, S. Roudier, *Best Available Techniques (BAT) Reference Document for Common Waste Gas Management and Treatment Systems in the Chemical Sector: Industrial Emissions Directive 2010/75/EU (Integrated Pollution Prevention and Control)*, JRC131915, European Union, Luxembourg **2023**. <https://data.europa.eu/doi/10.2760/220326>
- [33] G. Wiegleb, *Gasmestechnik in Theorie und Praxis*, Springer, Wiesbaden **2016**. DOI: <https://doi.org/10.1007/978-3-658-10687-4>
- [34] J. Li, X. Lu, W. F. Wang, *Opt. Fiber Technol.* **2020**, *57*, 102218. DOI: <https://doi.org/10.1016/j.yofte.2020.102218>
- [35] P. Bächler, V. Löschner, J. Meyer, A. Dittler, *Process. Saf. Environ.* **2022**, *160*, 411–423. DOI: <https://doi.org/10.1016/j.psep.2022.02.005>
- [36] P. Bächler, J. Meyer, A. Dittler, *Chem. Ing. Tech.* **2023**, *95* (1–2), 178–188. DOI: <https://doi.org/10.1002/cite.202200116>
- [37] P. Bächler, J. Meyer, A. Dittler, *Aerosol Sci. Technol.* **2022**, *56*, 394–402. DOI: <https://doi.org/10.1080/02786826.2022.2027335>
- [38] DIN ISO 11057, *Air Quality – Test Method for Filtration Characterization of Cleanable Filter Media*, Beuth, Berlin **2016**.
- [39] P. Bächler, J. Meyer, A. Dittler, On the trade-off between energy efficiency and particle emissions for pulse jet-cleaned filters, *Filtech 2023*, Cologne, February **2023**.
- [40] H. Leubner, U. Riebel, *Chem. Ing. Tech.* **2003**, *75* (1–2), 82–86. DOI: <https://doi.org/10.1002/cite.200390027>
- [41] M. Saleem, G. Krammer, R. U. Khan, M. S. Tahir, *Powder Technol.* **2012**, *224*, 28–35. DOI: <https://doi.org/10.1016/j.powtec.2012.02.016>
- [42] VDI 3677 Blatt 1, *Filtering Separators – Surface Filters*, Beuth, Berlin **2010**.

Supporting Information

Operating Behavior of Pulse Jet-Cleaned Filters Regarding Energy Demand and Particle Emissions – Part 1: Experimental Parameter Study

Peter Bächler*, Jörg Meyer, Achim Dittler

DOI: 10.1002/ceat.202300080

Correspondence: Peter Bächler (peter.baechler@kit.edu), Karlsruhe Institute of Technology, Institute of Mechanical Process Engineering and Mechanics, Strasse am Forum 8, 76131 Karlsruhe, Germany.

Additional context regarding experimental procedure to determine fan power and particle emission for the individual Δt -settings

For the evaluation of certain cycle times regarding their energy consumption and particle emission, it is necessary to determine the average differential pressure and the average dust emission. Here, different cycle times were adjusted in a fixed sequence according to Fig. S1.

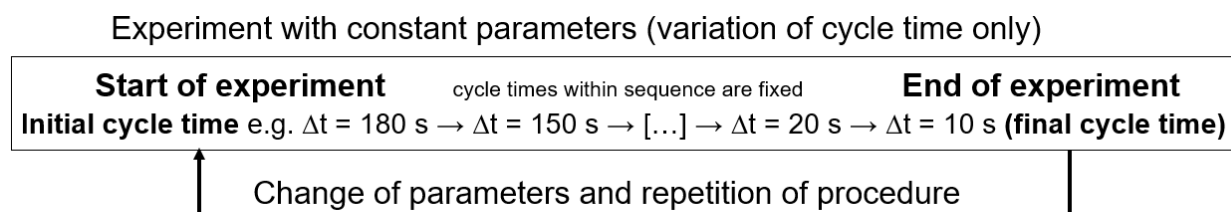


Figure S1. Schematic overview of the experimental procedure including the cycle time sequence.

The sequence within an experiment always started at the highest cycle time (e.g., 180 seconds or 150 seconds for most cases). The individual cycle times between the selected initial cycle time and the final cycle time of 10 seconds were fixed for each experiment (longest possible sequence: 180 s \rightarrow 150 s \rightarrow 120 s \rightarrow 90 s \rightarrow 60 s \rightarrow 45 s \rightarrow 30 s \rightarrow 20 s \rightarrow 10 s).

Fig. S2 shows the Δp -data for an exemplary experimental run, where average differential pressures could be determined for each of the adjusted cycle times. The average was calculated towards the end of each Δt -settings, where the differential pressure level has reached an (almost) steady state.

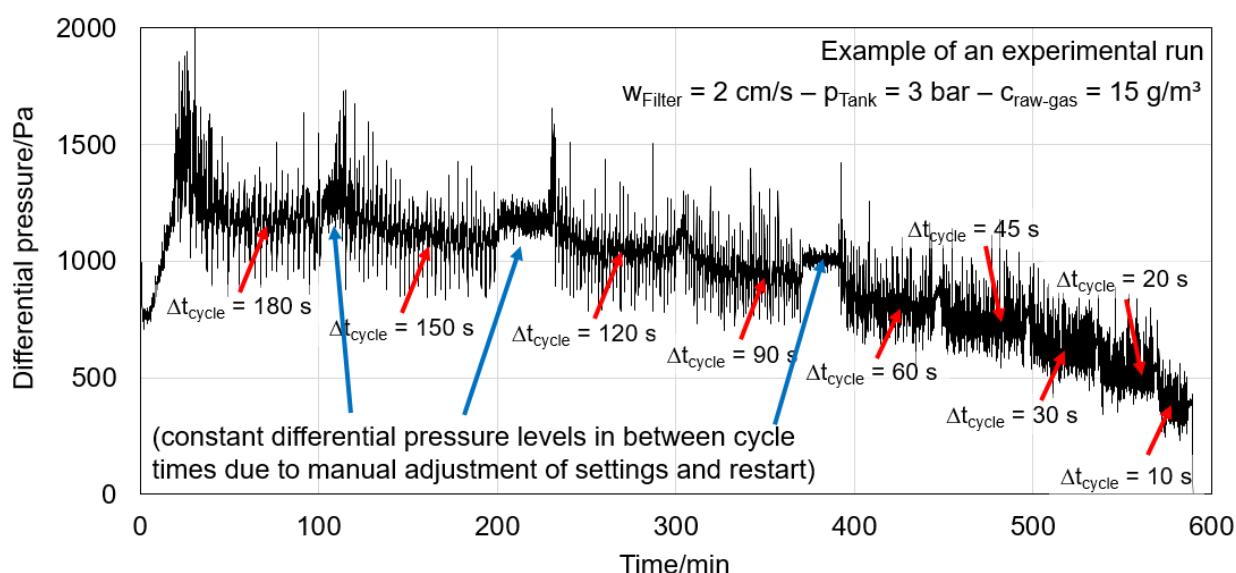


Figure S2. Exemplary data of the differential pressure generated during an experiment (adapted from [39]).

The particle emission data was extracted following the same procedure as shown in Fig. S3. Due to the experimental procedure shown in Fig. S1, a measurement artifact may occur for the initial Δt -setting. Due

to the frequent cleaning of the preceding experimental run at the 10 second setting (bordering on unstable filter operation), emission levels have to stabilize and the filter medium (including the seams) takes time to adjust until it is sufficiently clogged. More information on the implications regarding the particle emission behavior at shorter cycle times can be found in the subsequent chapter.

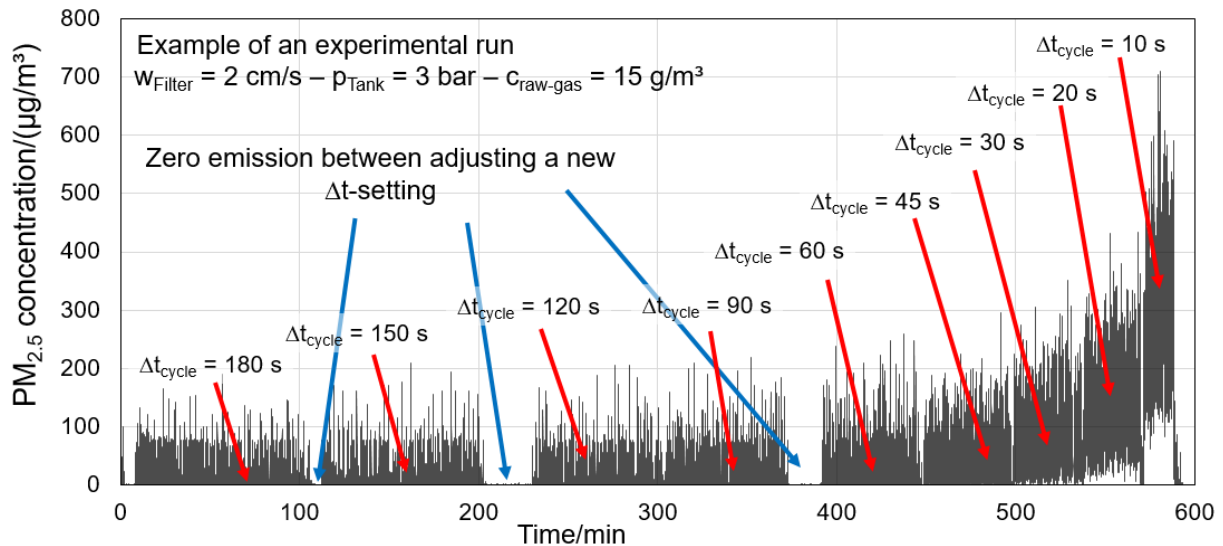


Figure S3. Exemplary data of the particle emission concentration generated during an experiment (adapted from [39]).

Thus, the longest cycle time could potentially be discarded. Note that the longest cycle time (as well as the shortest cycle time of 10 seconds) is not relevant for the power minimum and merely serves as the framework for the investigation. In general, no more than five Δt -settings would be necessary to correctly display relevant operation regions.

Implications on particle emissions due to the experimental procedure

In addition to energy criteria, the particle emission penetrating the filter medium is of key importance when evaluating filter performance. Assuming a well maintained baghouse, where no major leaks enable a continuous particle emission [29, 30, 31, 36], particles may only penetrate the filter medium directly after filter regeneration for a short time duration until a sufficient dust cake is formed (emission peak) [19, 28]. While the particle emission depends strongly on the employed filter medium, the pulse intensity (pressure level of the jet-pulse) and cycle time are key parameters. Higher pressures and shorter time intervals generally result in higher average dust emissions.

Past research has shown the dominant role that seams of the filter element may have on the dust emission if the pulse intensity is too high for sufficient clogging [24]. A similar problem may occur for short cycle times, as the filter element is regenerated so frequently, that cake formation is only possible sporadically (e.g., 90 seconds time difference between regenerations of the same bag for Δt_{cycle} of 10 seconds) and there is a frequent wear on the bag causing unstable conditions. This can lead to increased emissions when switching cycle times from a short cycle time to a longer cycle time, as a specific time is required in order for seams and small defect to clog sufficiently. Due to the experimental sequence, this may lead to seemingly higher emissions for the longest initial cycle time (e.g., 180 seconds) and is a measurement artifact based on the experimental procedure. Note that the artifact does not impact the power minimum

relevant to filter operation and the data point for the longest cycle time could potentially be dismissed accordingly.

Furthermore, short cycle times lead to an emission characteristic, where particle penetration is possible simultaneously through multiple filter bags, as shown in Fig. S4.

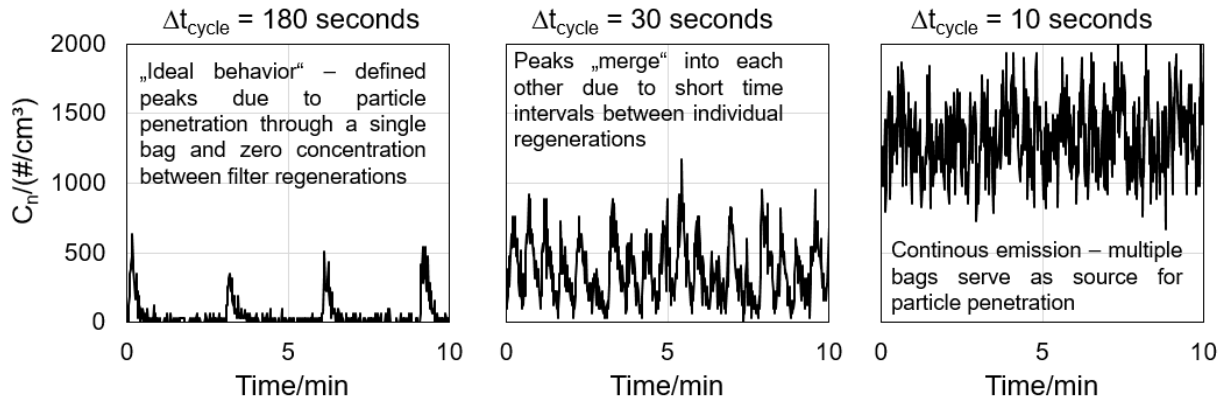


Figure S4. Characteristic particle emission behavior for pulse-jet cleaned filters at different cycle times (adapted from [39]) – example parameters: ($w_{\text{filter}} = 2$ cm/s – $c_{\text{raw-gas}} = 15$ g/m³ – $p_{\text{Tank}} = 3$ bar).

In case of sufficiently long cycle times (left image of Fig. S4), clearly distinct emission peak can be identified after the regeneration of the corresponding bag (or in case of many industrial baghouse filters) or row of filters. This behavior was shown in past research via spatial PM-monitoring for very long cycle times. Each regeneration event that is detected on the clean gas side can be allocated to the regeneration of the corresponding filter element [28]. Until a sufficiently thick dust layer is deposited on the filter element, particles can penetrate the filter bag. If the cycle time approaches the decay time of the emission peak, the peaks caused by individual regenerations begin to merge into one another (center image of Fig. 3). In case of the shortest cycle time, regeneration occurs so frequently, that continuous emissions are detected on the clean gas side, as particle penetration may occur during multiple bags at once. Individual peaks cannot be distinguished. In general, this scenario should be avoided, as emissions are high and no sufficient cake formation is possible. Additionally, troubleshooting and leak identification is more difficult, as particle bypass through a leak also causes a continuous emission with a similar characteristic. When a leak occurs during filter operation, it merely causes an increase of the total continuous emission and not a significant difference in the overall emission characteristic, what makes troubleshooting (e.g., via triboelectric sensors or “filter guards” as end of pipe measurement technology) not as evident [36]. Kurtz et al. also underlined the importance of a sufficient cycle time from an emissions perspective [23].

Determination of the energy consumption of the jet-pulse

According to Eq. (4) of the main article, the pressure drop in the pressure vessel supplying the pressurized air for the jet-pulse is necessary to calculate the energy consumption for each jet-pulse. Measurements at different tank pressures were performed to experimentally determine the pressure drop at a fixed valve opening time of 150 ms and different tank pressures. It was ensured, that the absolute pressure drop (without instantaneous refilling of the pressure vessel during the jet-pulse due to automatic pressure control) was obtained by decoupling the pressure vessel from the pressurized air distribution grid.

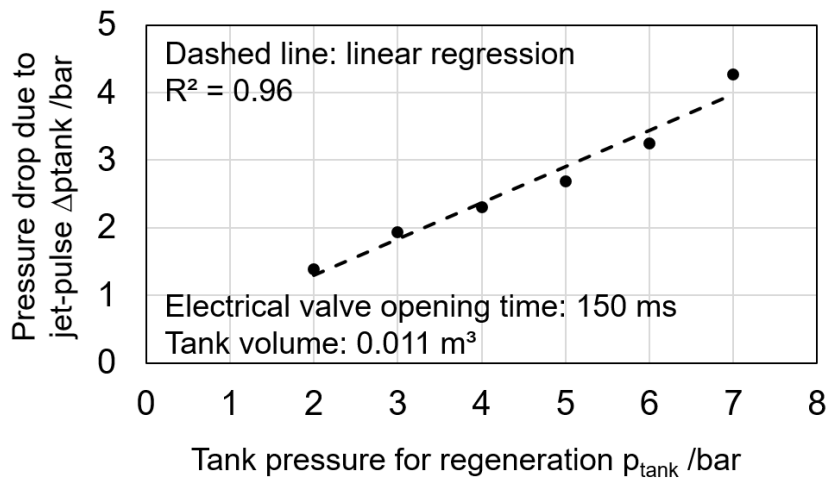


Figure S5. Pressure drop in the pressure tank for filter regeneration due to the jet-pulse as a function of regeneration pressure.

Multiplying the pressure drop in Fig. S5 with a volume of the pressure vessel of 0.011 m^3 and dividing with the cycle time according to Eq. (4) of the main manuscript yields the average power consumption of filter regeneration.

Additional explanation on how to read operation curves for filter operation

Fig. S6 shows in detail how to read and interpret the operation curve obtained from the experimental data. The sequence of cycle time always starts with an initial cycle time (longest cycle time). Afterwards, the consecutive cycle times are adjusted in order of the sequence during the experimental run, ending with the shortest cycle time of 10 seconds.

The cycle time increases from the right end of the operation curve (10 second cycle time) to the left end (initial cycle time – typically 180 or 150 seconds depending on operating parameters).

The 10 second cycle time results in unfavorable conditions, as energy consumption and emissions are very high due to the (almost) constant cleaning of the filter elements. Ideally, an operation point would be located close to the origin of the diagram at low emissions and low energy consumption. The region of interest consists in most cases of several data points, where in between an energetic minimum can be identified.

Sequence of Δt - settings within the operation curve (read from left to right): $\Delta t = 180 \text{ s} - \Delta t = 150 \text{ s} - \Delta t = 120 \text{ s} - \Delta t = 90 \text{ s} - \Delta t = 60 \text{ s} - \Delta t = 45 \text{ s} - \Delta t = 30 \text{ s} - \Delta t = 20 \text{ s} - \Delta t = 10 \text{ s}$ (final data point)

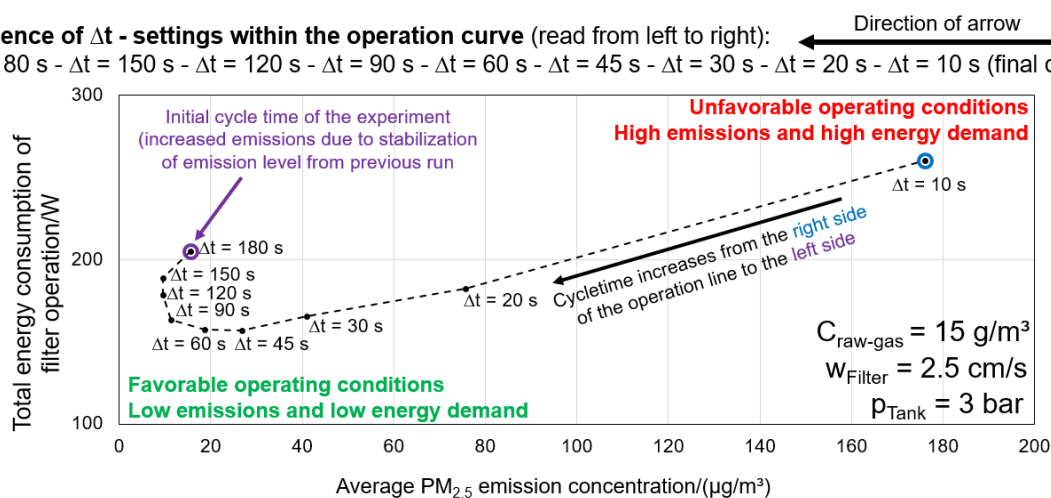


Figure S6. Guideline on how to read the filter operation curve for an exemplary set of parameters.

Additional experimental data regarding the variation of tank pressure (Sect. 3.3. of the main article)

Since the increase from 3 bar to 6 bar tank pressure is quite significant, an intermediate tank pressure of 4.5 bar was adjusted for the 30 g/m³ raw-gas concentration and the filter face velocities of 2 cm/s and 2.5 cm/s to offer additional context. The results are displayed in Fig. S7. From an energetic perspective, the tank pressure of 4.5 bar offers a slight benefit for the 2.5 cm/s measurement. However, the emission is still significantly increased so that the trade-off between lower energy demand and higher emissions is not worth it.

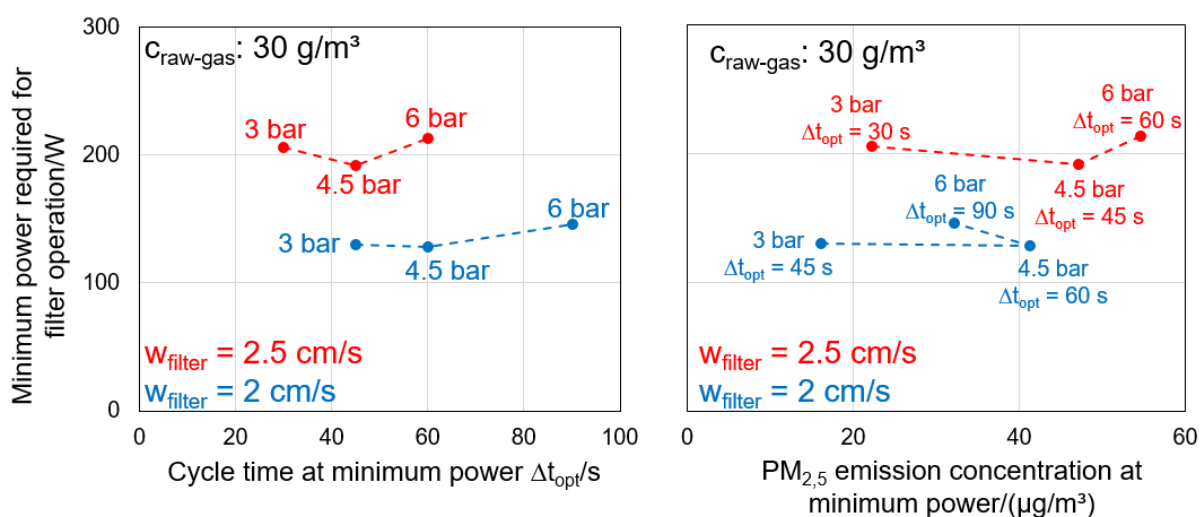


Figure S7. Comparison of power consumption and particle emission at the energetic optimum for several tank pressures at 30 g/m³ and two filter face velocities.

Regarding the operation curve (right diagram), a decrease of particle emission from 4.5 bar to 6 bar at the power minimum is noticeable for the 2 cm/s measurement. Due to the longer cycle time of the 6 bar measurement, the emission is lower compared to the 4.5 bar measurement at 60 seconds cycle time at the power minimum.

Publication VI

Title: Operating Behavior of Pulse Jet-Cleaned Filters Regarding Energy Demand and Particle Emissions – Part 2: Modeling

Authors: Peter Bächler, Jörg Meyer, Achim Dittler

Journal: Chemical Engineering and Technology

Year of Publication: 2024

Volume and Issue: 47 (4)

Page Numbers: 722-731

Reference: [Bächler et al., 2024a]

Abstract:

Baghouse filters applied for gas cleaning are subject to digitalization concepts, including process modeling and the development of digital twins in order to improve energy efficiency and lower particle emissions. Modeling equations from literature were adapted to match experimental data from part 1 of this study to calculate the effect of varying filter face velocities, dust concentrations or tank pressures on energy demand and particle emissions. Based on the model approaches, an operation curve that enables the evaluation of filter operation regarding the trade-off between energy demand and particle emissions can be constructed. The identification of energetically optimal cycle times and favorable operation regions is possible due to the extensive experimental framework of the model.

Peter Bächler*
Jörg Meyer
Achim Dittler


Operating Behavior of Pulse Jet-Cleaned Filters Regarding Energy Demand and Particle Emissions – Part 2: Modeling

Baghouse filters applied for gas cleaning are subject to digitalization concepts, including process modeling and the development of digital twins in order to improve energy efficiency and lower particle emissions. Modeling equations from literature were adapted to match experimental data from part 1 of this study to calculate the effect of varying filter face velocities, dust concentrations, or tank pressures on energy demand and particle emissions. Based on the model approaches, an operation curve that enables the evaluation of filter operation regarding the trade-off between energy demand and particle emissions can be constructed. The identification of energetically optimal cycle times and favorable operation regions is possible due to the extensive experimental framework of the model.

Keywords: Energy optimization, Filtration, Particle emission, Process efficiency, Pulse jet-cleaned filters

Received: August 31, 2023; *revised:* October 23, 2023; *accepted:* January 16, 2024

DOI: 10.1002/ceat.202300409

 This is an open access article under the terms of the Creative Commons Attribution License, which permits use, distribution and reproduction in any medium, provided the original work is properly cited.



Supporting Information
available online

1 Introduction

Baghouse filters are widely applied in industrial gas cleaning processes in order to separate particles from dust-laden gas streams. While in technical applications on the industrial scale stable filter operation is paramount, operation strategies are rarely optimized and the filters are merely a necessity to meet emission standards, protect downstream operation units or enable product recovery. Guidelines such as VDI 3677 offer layout advice for filter houses regarding, e.g., the selection of filter media and the required filter area for certain applications [1].

Nonetheless, baghouse filters are complex systems in which the operation control greatly influences the energy demand and the particle emissions of the facility [2, 3]. During filter operation, particles are primarily separated at the surface of the filter elements, causing increases in cake thickness, flow resistance, and, consequently, differential pressure. Filter regeneration (e.g., via jet pulse) is typically initiated after fixed time intervals (Δt -controlled regeneration) or after exceeding a differential pressure limit (Δp -controlled regeneration) [4]. Typically, not all installed filter elements are regenerated simultaneously; rather, individual bags or individual rows of filter elements are regenerated after meeting the regeneration criterion. Thus, the dust mass deposited on the filter elements is not evenly distributed among all filters and the flow resistance of the different elements may vary greatly. This causes a spatially and temporally variable flow profile through the baghouse filter, where the total volume flow splits depending on the flow resistance of the individual filter elements, resulting in a total

differential pressure between the raw-gas side and the clean-gas side [5, 6]. This behavior is, e.g., not considered in the filter testing standard DIN ISO 11057, where a constant volume flow passes through the filter medium for the entire test procedure and the entire filter area (compared to a subset of the installed filter elements) is regenerated via jet pulse cleaning [7].

The time interval between regeneration events, or the corresponding cake formation, dictates the particle emission behavior. Due to the (almost) perfect separation characteristics of the dust cake, particle penetration through the filter medium is only possible directly after filter regeneration. With sufficient cake formation, the emission quickly declines to a zero level, hence causing an “emission peak” [8]. Longer time intervals between regenerations enable lower average dust emissions at the trade-off of larger differential pressures. Shorter time durations can lower the differential pressure level, where a higher consumption of pressurized air and increased emissions have to be taken into account [2, 9].

In part 1 of this study, experiments were performed in a small-scale baghouse filter with nine filter bags in order to identify feasible operation points regarding the power requirement for filter operation and the corresponding dust emissions [2]. The total power for filter operation was determined as the

M.Sc. Peter Bächler (peter.baechler@kit.edu), Dr.-Ing. Jörg Meyer, Prof. Dr.-Ing. habil. Achim Dittler
Karlsruhe Institute of Technology, Institute of Mechanical Process Engineering and Mechanics, Straße am Forum 8, 76131 Karlsruhe, Germany.

sum of the fan power and the compression energy for the consumption of pressurized air, according to equations shown by Höflinger and Laminger [9]. The optimal cycle times in order to operate at the power minimum were identified for various parameters (filter face velocity, raw-gas concentration, tank pressure). Filter operation at cycle times shorter than the power minimum is not feasible, due to higher dust emissions at no energy benefit. Increasing the cycle time beyond certain limits can significantly increase the differential pressure and the total power, where the benefit of slightly lower particle emissions does not justify the energetic investment. An increase in tank pressure (6 bar vs. 3 bar) for filter regeneration enables a less frequent regeneration (approximately doubled cycle time) at a similar power minimum, with the trade-off of significantly increased dust emissions. Lowering the filter face velocity (or increasing the filter area) can help to lower the overall power consumption of filtration processes. In the context of digitalization, process modeling and the development of digital twins becomes increasingly relevant [10–12].

Modeling of the operating behavior of cleanable filter media ranges back to the mid and late 20th century [13, 14]. An in-depth literature review would exceed the scope of this study and many primary sources were summarized by Löffler [4]. One of the most seminal publications is the work by Leith and Ellenbecker [15]. The total differential pressure across a surface filter medium is typically calculated via the specific resistance of a filter medium K_{medium} and the specific resistance of the dust layer K_{cake} . The coefficients can be derived from experimental data. However, universal applicability is not guaranteed for every process condition and the coefficients are highly dependent on the type of filter medium and dust [16–18].

A fairly recent noteworthy publication is the work of Klein et al. [19], who presented a calculation tool for the economic optimization of baghouse filters based on model equations. Here, the differential pressure of the filter housing, the dust cake, the filter medium, and the regeneration system including nozzle type and tank pressure were taken into account to identify favorable cycle times regarding the required power for filter operation. The corresponding particle emissions were not taken into account.

In-depth modeling and simulation of the transient separation behavior of surface filters were performed, e.g., by Schmidt and Zhang who focused on cake formation on the micro-scale [20–22]. Full-scale computational fluid dynamics (CFD) simulations to predict the flow and operation behavior of large-scale pulse jet-cleaned filters were presented by Heck and Becker [23].

Part 2 of this study combines the model approach for the layout of surface filters summarized by Löffler [4] and the methodology presented in part 1 of the study [2], which is based on the energy evaluation of filter media presented by Höflinger and Laminger [9].

2 Modeling of Filter Operation under Consideration of Energy Consumption and Particle Emissions

2.1 Basic Equations for the Layout of Pulse Jet-Cleaned Filters (Ideal Conditions)

While the overall calculation basics for the determination of the differential pressure of a pulse jet-cleaned filter are well documented in the literature (e.g. [4, 24, 25]), the corresponding sources are out of print or difficult to obtain outside of university environments. Thus, this section serves as a repetition of the fundamental equations for the calculation of ideal filter behavior for baghouse filters with multiple filter elements. Assumptions for the calculation include no additional pressure drop due to the housing, homogenous flow conditions, constant process parameters, and an incompressible filter cake. Fig. 1 shows a schematic image illustrating the calculation steps described in this section.

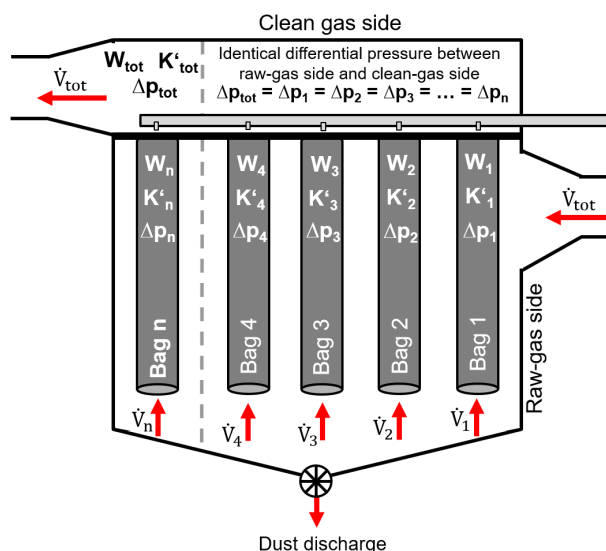


Figure 1. Schematic image of a model filter house with n filter elements.

The well-known “filter equation” enables the calculation of the differential pressure between the raw-gas side and the clean-gas side across a single filter element i as a function of the specific filter medium and cake resistances, K_{medium} and K_{cake} , as well as the deposited dust mass on the filter element W_i and the filter face velocity $w_{\text{filter},i}$.

$$\Delta p_{\text{Filter}} = (K_{\text{medium}} + K_{\text{cake}} \cdot W_i(t)) \cdot w_{\text{filter},i} = (K_{\text{medium}} + K_{\text{cake}} \cdot W_i(t)) \cdot \frac{\dot{V}_i}{A_i} \quad (1)$$

In case of a constant and time-independent filter face velocity (e.g., in case of a single filter element or filter tests with a single circular filter sample – 100% cleaning efficiency), the differential pressure increases linearly (due to typically low filter face velocities) with the deposited dust mass.

The complexity of the calculation increases in case of real baghouse filters with multiple rows of filter elements (Fig. 1). The deposited dust mass $W_i(t)$ decreases (or in this case is set to zero) due to cake detachment after a regeneration criterion is met. This causes different loading states of the individual filter elements, dependent on the regeneration strategy. Each filter element (or row of filter elements in case of a row-by-row cleaning procedure) has an individual resistance constant K'_i .

$$K'_i = (K_{\text{medium}} + K_{\text{cake}} \cdot W_i(t)) \quad (2)$$

An overall resistance constant K'_{tot} can be calculated for the entire baghouse filter and all filter elements n (assuming $A_i = \text{const.}$) in order to determine the differential pressure between the raw-gas side and the clean-gas side.

$$K'_{\text{tot}} = \frac{n}{\sum_{i=1}^n \frac{1}{K_i}} \quad (3)$$

$$\Delta p_{\text{Filter}} = K'_{\text{tot}} \cdot w_{\text{filter}} = K'_{\text{tot}} \cdot \frac{\dot{V}_{\text{tot}}}{A_{\text{tot}}} \quad (4)$$

Since the differential pressure between the raw-gas side and the clean-gas side corresponds to the differential pressure across each filter element, the total volume flow \dot{V}_{tot} is divided among the filter elements dependent on the flow resistance K_i .

$$\dot{V}_i = \frac{\Delta p_{\text{Filter}} \cdot A_i}{K_i} \quad (5)$$

The load on the filter elements increases after each time increment $\Delta t_{\text{increment}}$ according to the raw-gas concentration and the corresponding volume flow through the filter element. This assumes a perfect separation of particles on the filter surface (complete deposition of incoming particle mass on the filter surface). This assumption holds true for most cases of filter operation, where the raw-gas concentrations are in the region of several gram per cubic meter and the emission is (at least) one magnitude lower (maximum emission concentration for fabric filters according to the recent WGC BREF of 5 mg m^{-3} for emitted dust mass flows larger than 50 g h^{-1} [26]).

$$W_i(t + \Delta t_{\text{increment}}) = W_i(t) + \frac{\dot{V}_i}{A_i} \cdot c_{\text{raw-gas}} \cdot \Delta t_{\text{increment}} \quad (6)$$

Filter regeneration is typically initiated after a preset differential pressure is exceeded (Δp -controlled regeneration) or a time interval has passed (Δt -controlled operation). Here, a Δt -controlled approach was selected similar to the experimental study. After exceeding a cycle time Δt_{cycle} , the deposited dust mass is reduced to zero. This assumes that the regeneration causes a complete cake detachment of the corresponding filter element.

$$W_i(t) \rightarrow 0 \quad (7)$$

After the determination of the deposited dust mass $W_i(t)$, the time is increased by the time increment $\Delta t_{\text{increment}}$.

$$t = t + \Delta t_{\text{increment}} \quad (8)$$

This procedure can be repeated for a selected number of time increments in order to model temporally resolved filter

operation. A “steady state” condition is reached relatively quickly so that the average differential pressure for a certain set of parameters does not change significantly. For this study, 20 000 time increments of 1 s each were selected for the creation of each dataset, whereby an average differential pressure for each set of parameters was calculated from the mean of the last 5000 s. An example dataset showing the results for a single set of input parameters can be found in the Supporting Information.

2.2 Calculation Parameters for the Validation of the Experiments

The calculation parameters for part 2 of the study were adapted from the previous experiments and are summarized in Tab. 1. Note that these values are mainly relevant for Sect. 3 and the validation of the model from experimental data.

Table 1. Calculation parameters.

Parameter	Value
Filter face velocity w_{filter} [cm s^{-1}]	2, 2.5, and 3.3
Raw-gas concentration $c_{\text{raw-gas}}$ [g m^{-3}]	15 and 30
Cleaning interval Δt_{cycle} [s]	10–180
Number of filter elements n [-]	9
Total filter area [m^2]	4.14
K_{medium} [Pa s m^{-1}]	10 000–44 000
K_{cake} [Pa m s g^{-1}]	111

The value for K_{cake} could be reliably extracted from uniformly loading the filter elements, starting from a point where all filter elements were recently regenerated without any deposited dust mass ($W = 0$). While K_{medium} can be determined in a similar manner (for $W_i = W_{\text{tot}} = 0 \rightarrow \Delta p = w_{\text{filter}} \times K_{\text{medium}}$), the actual medium resistance may vary during filter operation. For example, the regeneration pressure can play a role in the residual pressure drop after filter regeneration due to effects like patchy cleaning [27]. As a result, K_{medium} is the main optimization parameter to better describe the experimental data by the model in Sect. 3.1.1.

2.3 Consideration of the Energy Consumption of Filter Operation

In order to determine the required power for filter operation, the fan power and the compression energy to compensate for the pressure drop in the pressure vessel due to filter regeneration were calculated. These equations were used by Höflinger and Laminger [9] in order to evaluate filter media based on energy criteria in a past study, as well as in part 1 of this study [2].

$$P_{\text{Filter}} = P_{\text{fan}} + P_{\text{reg}} \quad (9)$$

$$P_{\text{fan}} = \dot{V}_{\text{tot}} \cdot \Delta p_{\text{Filter}} \quad (10)$$

$$P_{\text{reg}} = \frac{V_{\text{tank}} \cdot \Delta p_{\text{tank}}}{\Delta t_{\text{cycle}}} \quad (11)$$

The pressure drop in the vessel Δp_{tank} was determined experimentally for different regeneration pressures according to part 1 of the study, and the volume of the vessel V_{tank} is 0.011 m^3 .

2.4 Modeling of Particle Emissions for Filter Regeneration

The particle emission of pulse jet-cleaned filters follows a distinct behavior. Directly following filter regeneration, particles may penetrate the filter medium. The medium itself is commonly optimized regarding its surface properties (e.g., laminated membrane on the upstream side, singed upstream side, calendered, etc.) to enable a quick formation of a dust cake on the surface. After sufficient cake formation (deposited dust mass on filter element $W_i(t)$), the emission drops to a zero level due to the high separation efficiency of the dust cake.

Löffler [4] offers the following equation according to Valentin for the calculation of the (total) separation efficiency linked to the transient particle emission behavior. κ and δ are empirical constants:

$$\eta = 1 - \exp\{-\kappa \cdot W_i(t)^\delta\} \quad (12)$$

The transient particle emission concentration can consecutively be calculated as follows:

$$c_{\text{clean-gas}} = c_{\text{raw-gas}} \cdot (1 - \eta) = c_{\text{raw-gas}} \cdot \exp\{-\kappa \cdot W_i(t)^\delta\} \quad (13)$$

According to this function, there is a fixed amount of particulate matter that is emitted after filter regeneration, provided the area weight increases far enough within a complete filtration cycle for the efficiency to reach values close to unity. If the same filter element is regenerated before the emission drops to zero, cake formation is interrupted and the emission peaks early at the single filter element, causing higher average dust emissions within a filtration cycle and a transient “continuous emission”. The time duration during which particles are emitted and the shape of the emission peak depend strongly on the process conditions and the filter medium [28]. Emission peaks taken from filter tests with, e.g., membrane filter media offer only brief durations of several seconds where an emission can be detected. Higher raw gas concentrations and filter face velocities create a higher dust load on

the filter elements and, thus, a faster increase of $W_i(t)$ and a sharper decline of the emission peak.

While the experimental data would offer a sufficient dataset to model the transient behavior of the total dust emissions from online measurements, the goal of the study is to model the overall trends presented in part 1 of the investigation. In-depth modeling of the dust emission would exceed the scope of this study. Regarding closer insights, Zhang [22] recently showed experimental data and calculation approaches detailing the transition from depth filtration mechanisms directly after filter regeneration to surface filtration and cake build-up.

Thus, a simpler modeling approach is selected instead to predict the total dust emission and its behavior as a function of the cycle time. The total cumulative emitted dust mass per filter area (EDM) can be calculated from online measurements of the clean-gas particle concentration $c_{\text{clean-gas}}(t)$ according to Eq. (14).

$$EDM = \int_{t_{\text{start}}}^{t_{\text{end}}} c_{\text{clean-gas}}(t) \cdot \frac{\dot{V}_{\text{tot}}}{A_{\text{tot}}} dt = w_{\text{filter}} \cdot \int_{t_{\text{start}}}^{t_{\text{end}}} c_{\text{clean-gas}}(t) dt \quad (14)$$

Similarly, size-resolved determination of the emitted dust mass is possible by considering the weighted particulate matter concentration PM_x (Eq. (15)).

$$EDM_{PM_x} = \int_{t_{\text{start}}}^{t_{\text{end}}} PM_x(t) \cdot \frac{\dot{V}_{\text{tot}}}{A_{\text{tot}}} dt = w_{\text{filter}} \cdot \int_{t_{\text{start}}}^{t_{\text{end}}} PM_x(t) dt \quad (15)$$

For the experimental dataset of part 1, the emitted dust mass was calculated from the $PM_{2.5}$ concentration curves.

$$EDM_{PM_{2.5}} = \int_{t_{\text{start}}}^{t_{\text{end}}} PM_{2.5}(t) \cdot \frac{\dot{V}_{\text{tot}}}{A_{\text{tot}}} dt = w_{\text{filter}} \cdot \int_{t_{\text{start}}}^{t_{\text{end}}} PM_{2.5}(t) dt \quad (16)$$

As previously stated, each regeneration event causes the penetration of a distinct amount of particulate matter. In order to validate this assumption, Fig. 2 shows the cumulative emission

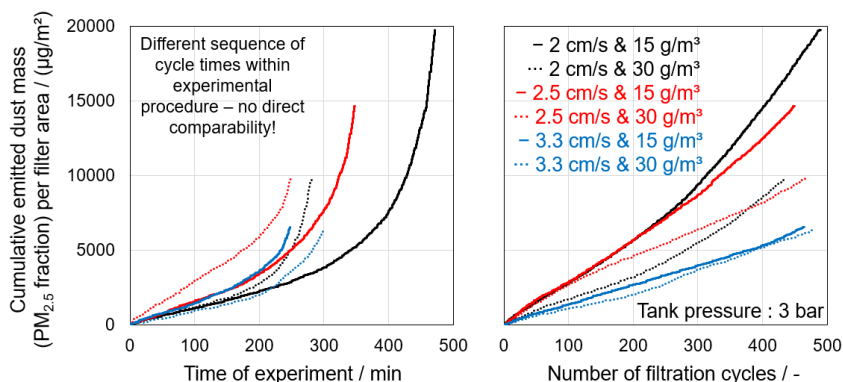


Figure 2. Cumulative emitted dust mass of the $PM_{2.5}$ fraction as a function of the time (left) and the number of filtration cycles (right) for each experiment (compare part 1 of the study) at a tank pressure of 3 bar.

ted particulate matter per filter area ($EDM_{PM_{2.5}}$) over the course of an experimental run for all experiments at 3 bar tank pressure as a function of the time (left) and the number of filtration cycles (right). In part 1 of this study, average $PM_{2.5}$ concentrations were used as benchmark values to quantify particle emissions due to their health-related relevance and comparability to past studies, where scattered light-based low-cost sensors were used that only have limited output values. Note that, due to the high separation efficiency of pulse jet-cleaned filters, the vast majority of the particle emission is part of the $PM_{2.5}$ fraction anyway. Emissions at the beginning of an experimental run at a higher cycle time were not considered in the diagram due to higher dust emissions caused by the experimental procedure (compare part 1 of the study). Values at the increased tank pressure of 6 bar can be found in the Supporting Information.

Note that shorter cycle times cause a higher number of filtration cycles in a shorter time duration and therefore a more frequent emission of particulate matter. This leads to a higher slope at the end of the experiment (left diagram), where a state of almost constant regeneration ($\Delta t_{\text{cycle}} = 10$ s) is reached. When relating the emitted dust mass to the number of filtration cycles instead of the absolute time, the emission increases linearly with increasing number of filtration cycles, validating the assumption of a “fixed” amount of particulate matter being released after each regeneration. Deviations from the linear behavior seem to be prevalent in measurement data with a slower cake formation (e.g., at lower filter face velocities and raw-gas concentrations). Due to the more frequent regenerations, the volume flow passing the recently regenerated filter element is not as high and the flow profile is comparably even. A characteristic $EDM_{PM_{2.5}}$ value can be extracted from the slope of the diagram (intercept=0). The data for 6 bar tank pressure can be found in the Supporting Information.

In an ideal case, the average emission concentration of the clean gas can be calculated according to Eq. (17). Note that the corresponding clean-gas concentration may also be a weighted PM_x concentration depending on the used emitted dust mass.

$$c_{\text{clean-gas}} = \frac{EDM \cdot A_{\text{tot}}}{\dot{V}_{\text{tot}} \cdot \Delta t_{\text{cycle}}} = \frac{EDM}{w_{\text{filter}} \cdot \Delta t_{\text{cycle}}} \quad (17)$$

To account for real behavior, an empirical coefficient γ can be introduced to improve the correlation between the measurement data and the model.

$$c_{\text{clean-gas}} = \frac{EDM}{w_{\text{filter}} \cdot \Delta t_{\text{cycle}}^\gamma} \quad (18)$$

To comply with part 1 of the study, clean-gas concentrations were calculated from the $PM_{2.5}$ size fraction of the emitted dust mass.

$$PM_{2.5} = \frac{EDM_{PM_{2.5}}}{w_{\text{filter}} \cdot \Delta t_{\text{cycle}}^\gamma} \quad (19)$$

Summarizing, there is a hyperbolic behavior of the global dust emission and the cycle time in between individual filter regenerations. Introducing the “EDM” coefficient enables the prediction of particle emissions as a function of cycle time/regeneration efficiency for a certain set of parameters.

3 Results and Discussion

3.1 Validation of Experimental Data Applying the Modified Model Equations

In the consecutive sections, the experimental data from part 1 of this study is modeled applying the equations described in Sect. 2.

3.1.1 Modeling of Real Differential Pressure Behavior

The differential pressure between the raw-gas side and the clean-gas side is the main result following the layout equations from Löffler [4]. Following ideal assumptions, the resistances K_{cake} and K_{medium} are sufficient to model filter operation. However, real filter behavior may deviate from the ideal assumptions (e.g., patchy cleaning, non-homogenous flow conditions, compression of the dust cake, etc.), and experimentally determined resistances under defined conditions can vary during actual filter operation [17, 18].

Hence, the medium resistance K_{medium} was varied between 10 000 and 44 000 Pa s m⁻¹ in order to determine the corresponding values for different sets of parameters. Fig. 3 shows the experimental data (connected data points) in a field of calculated differential pressure values for different filter medium resistances. At increased tank pressures, the medium resistance is lower, indicating a better filter regeneration, where the residual pressure drop is lower compared to the softer regeneration at a lower tank pressure. The concave behavior is in

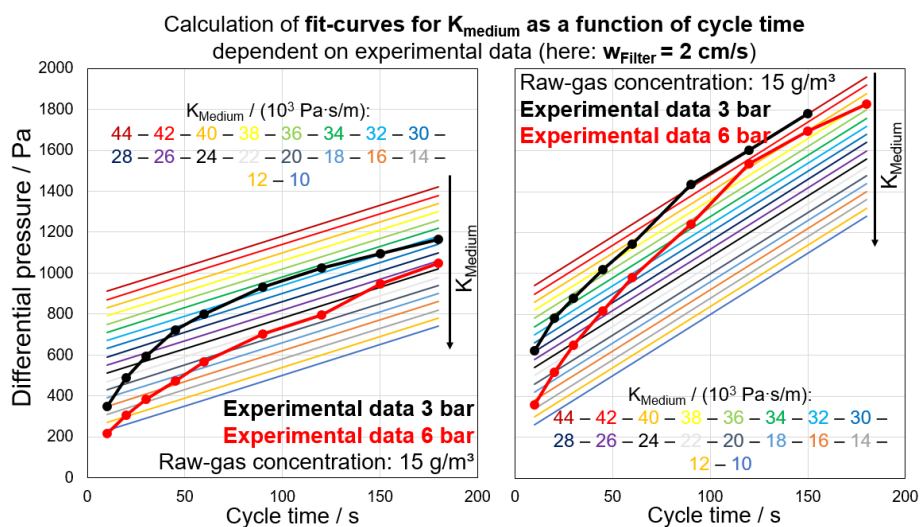


Figure 3. Comparison of experimental data ($w_{\text{filter}} = 2$ cm s⁻¹; $p_{\text{tank}} = 3$ bar; $c_{\text{raw-gas}} = 15$ and 30 g m⁻³) and model calculations varying the filter medium resistance K_{medium} .

agreement with investigations by Saleem et al. [17] who reported the differential pressure as a function of the deposited dust mass.

Out of the medium resistances, fit functions can be derived for each set of parameters to determine an empirical fit for the data. Each data point at the corresponding cycle time matches a corresponding filter medium resistance according to Fig. 3. A logarithmic fit yielded high regression coefficients for each set of experimental parameters when plotting the resistance coefficient K_{medium} as a function of the cycle time. Note that this data-driven approach enables a high agreement between model and experiment. Applying higher-degree polynomial functions would further increase the regression coefficient at the cost of a more complex set of parameters for the model. However, extrapolation would prove much more difficult due to the “arbitrary” mathematical regression within and outside of the set of experimental cycle times.

Fig. 4 shows the corresponding logarithmic fit functions and the resulting scatter plots from the calculation of Δp values for the experimental parameters at 2 cm s^{-1} filter face velocity. The

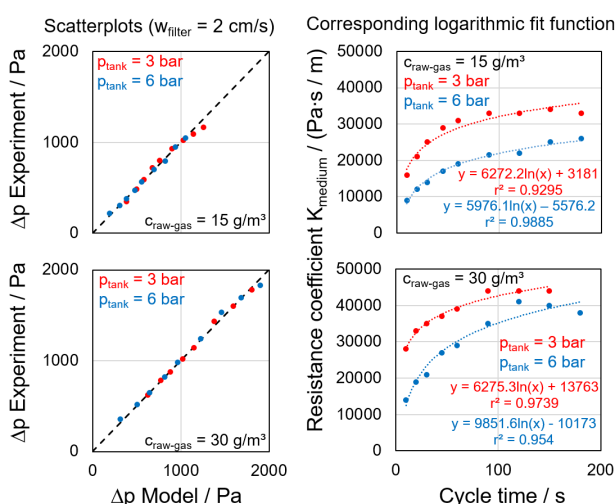


Figure 4. Scatter plots and corresponding logarithmic fit function for the dataset at 2 cm s^{-1} (fit functions for the rest of the dataset can be found in the Supporting Information).

logarithmic cycle time-dependent fit functions accurately predict the experimental data. Due to the large amount of available data, the calculation of the differential pressure behavior is possible for a wide range of parameters. The regression coefficients are sufficiently high (lowest r^2 of 0.8823) and the remaining fit functions for each set of parameters can be found in the Supporting Information.

Due to the data-driven approach when determining the fit functions, very high correlations between experiment and model can be achieved, as expected. Of course, the optimized fit of the experimental framework comes at the trade-off of limited general accuracy outside of the experimental framework. However, the tight-knit experimental framework still enables interpolation and not only modeling of experimentally captured sets of parameters. Examples can be found in the Supporting Information.

3.1.2 Modeling of the Required Power for Filter Operation

After the determination of the differential pressure for each set of parameters (compare Fig. 4), the required power for filter operation can be calculated following Eqs. (9)–(11). Taking into account the required power for filter regeneration P_{reg} as presented in part 1 of this study, the total power can be determined. Fig. 5 displays the calculation of the total power and the identification of the power minimum for one set of example parameters ($w_{\text{filter}} = 2 \text{ cm s}^{-1}$; $p_{\text{tank}} = 3 \text{ bar}$; $C_{\text{raw-gas}} = 15$ and 30 g m^{-3}). The calculation results for the missing parameters (compare the full parameter set in Fig. 4) can be found in the Supporting Information.

Since the energy consumption due to filter regeneration is taken directly from experimental data, the error made from the calculation of the differential pressure is significantly lower at shorter cycle times, where the total power requirement is dominated by the contribution of filter regeneration. The identification of the broad region of the power minimum is accurately represented by the model calculations where the benefit of a higher temporal resolution of the model equations enables the exact quantification of the corresponding cycle time at minimum power. The experimental data covers relevant operation

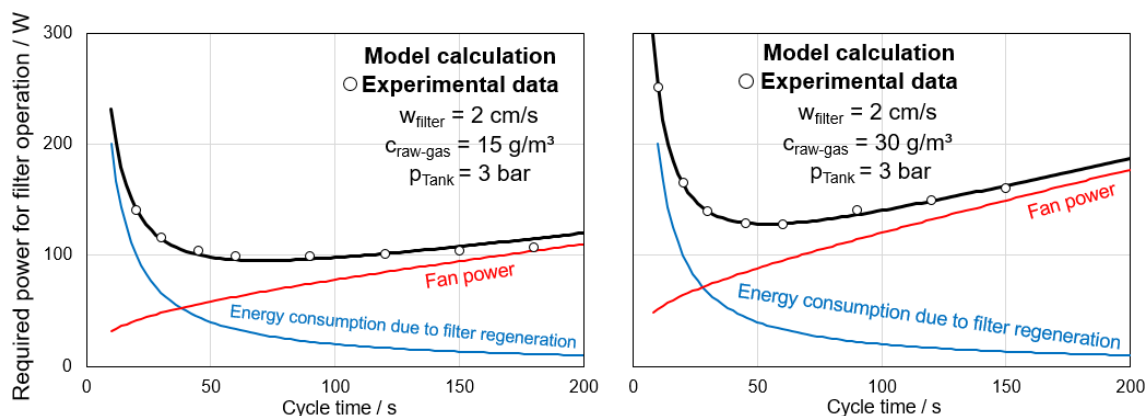


Figure 5. Comparison of experimental data ($w_{\text{filter}} = 2 \text{ cm s}^{-1}$; $p_{\text{tank}} = 3 \text{ bar}$; $C_{\text{raw-gas}} = 15$ and 30 g m^{-3}) and model calculations regarding the required power for filter operation.

regions ranging from shorter cycle times up to exceedingly long cycle times. The results are in qualitative agreement with the economic optimization performed by Klein et al. [19]. Extrapolation outside of the range of experimentally tested cycle times has to be handled with caution, but the logarithmic fit functions for K_{medium} at least yield plausible values as the contribution of filter regeneration to the total power.

3.1.3 Modeling of Particle Emissions

The particle emission is mainly independent of the cycle time and mostly dependent on other process conditions. Note that the experimental dataset offers data based on a single filter medium (at a single stage of filter life) with a single test dust and is not universally applicable. The greatest impact of particle emissions in this study is the tank pressure for filter regeneration (3 bar vs. 6 bar). For the calculation of particle emissions, the average emitted dust mass of the $PM_{2.5}$ fraction was determined from the slopes of the individual curves shown in Fig. 2 for a tank pressure of 3 bar. Afterwards, empirical coefficients γ were determined based on the average $EDM_{PM_{2.5}}$ value via minimizing the sum of absolute error between model and experiment for each set of parameters, to enable a better corre-

lation between experiment and model. The exact values for $EDM_{PM_{2.5}}$ and γ can be found in the Supporting Information.

Fig. 6 shows a comparison between the modeled particle emissions and the experimental data for the entire set of parameters at 3 bar.

The key importance of modeling particle emissions is the overall trend in order to identify the transition point between increasingly high dust emissions and the lower emission level at higher cycle times. While particle emissions are highly dependent on many different factors (e.g., tank pressures for regeneration, filter medium, leak-free operation, filter age, etc.) and the presented emitted dust masses are not universally applicable, the hyperbolic behavior of particle emissions with increasing cycle time has to be taken into account when operating and during the layout of baghouse filters.

3.2 Calculation of Operation Curves

Combining the model results of Sects. 3.1.2 and 3.1.3 enables the calculation of operation curves to evaluate filter operation based on power demand and particle emissions (Fig. 7). The agreement between the experimental data and the model is sufficiently high in the region of interest around the power

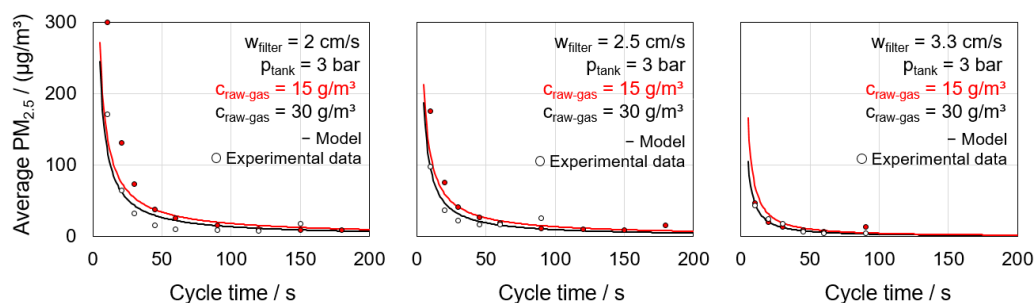


Figure 6. Modeling of particle emissions for the entire set of experimental parameters based on the determination of the emitted dust mass ($EDM_{PM_{2.5}}$) for 3 bar tank pressure and an individual empirical coefficient γ for each set of parameters.

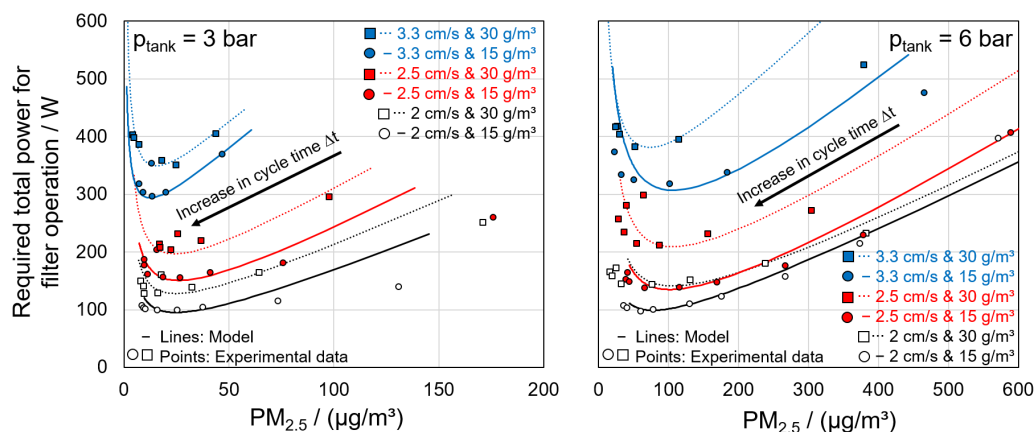


Figure 7. Modeled operation curves for the complete set of parameters and comparison to experimental data from part 1 of this study.

minimum. Values at either end of the experimentally tested cycle times show higher deviations.

Similarly to the experimental parameter study presented in part 1, suitable cycle times can be identified. Cycle times shorter than at the power minimum should be avoided due to increased consumption of pressurized air with no power benefit and higher particle emissions. Cycle times longer than at power minimum offer lower particle emissions at the trade-off of higher differential pressures and higher power requirements. Due to the hyperbolic behavior of particle emissions, slightly increasing the cycle time may already significantly lower the particle emissions. However, selecting increasingly long cycle times can significantly increase the power required for filter operation, with negligible effects on particle emission. Comparing the two tank pressures shows the difference in particle emissions, where the higher tank pressure requires longer cycle times to approach a zero-emission concentration.

While there are quite significant deviations and not all data points are perfectly represented by the model, especially when considering particle emissions, which were modeled semi-empirically, the overall levels calculated by the model are in good agreement. Fig. 8 shows the relevant region of (or around)

the power minimum at the corresponding cycle time Δt_{opt} for the experiment and the model. If no distinct power minimum could be taken from the experiments, both relevant data points are displayed.

Regarding the power for filter operation, all values are almost exactly on the same level, where the model offers an increased resolution regarding cycle times that cannot be achieved experimentally. Regarding particle emissions, the main importance is to reach a “stable emissions level” and the quantitative differences do not necessarily play a role in actual filter operation. The overwhelming trend of increased emissions with increased tank pressure is portrayed correctly, although the model does overestimate particle emissions at the power minimum.

4 Summary and Outlook

In part 2 of this study, the experimental data of part 1 was taken as a framework for process modeling. The transient differential behavior was modeled applying equations found in the literature [4, 15] and adapted to enable higher agreement with the experimental data. Here, the medium resistance K_{medium} was

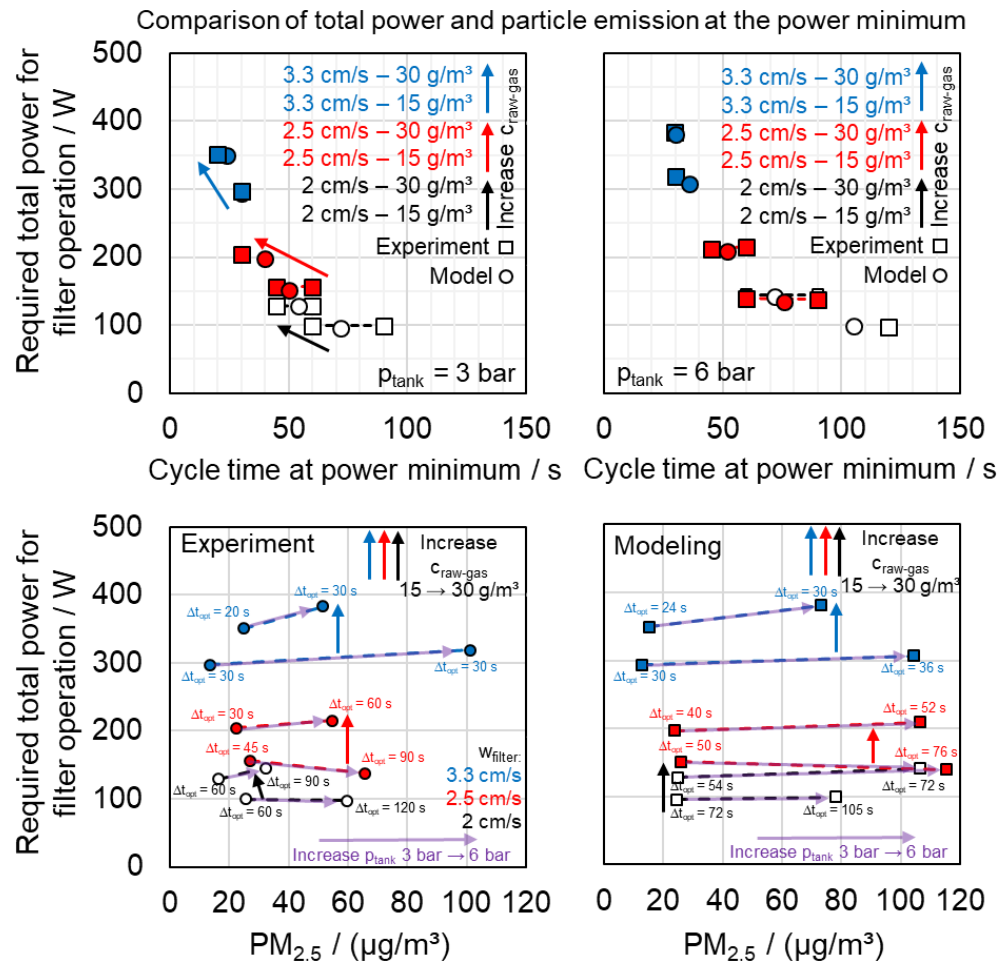


Figure 8. Comparison of model and experiment for the total power and $PM_{2.5}$ emissions as a function of the cycle time at the power minimum for each set of parameters.

selected as flexible optimization parameter based on the cycle time, and logarithmic fit functions were derived to calculate differential pressures. The required power for filter operation was calculated as the sum of fan power and compression energy, representing the consumption of pressurized air as proposed by Höflinger and Laminger [9]. A hyperbolic dependence of particle emissions and cycle time was derived from the experimental data. Combining the energy consumption and particle emission yields operation curves at certain process parameters that enable the evaluation of filter operation and the identification of suitable operation regions. The results may help plant operators to avoid unfavorable filter operation, to improve the filter layout and shows the potential for the development of digital twins for pulse jet-cleaned filters.

Supporting Information

Supporting Information for this article can be found under DOI: <https://doi.org/10.1002/ceat.202300409>.

Data Availability Statement

Data available on request from the authors. The data that support the findings of this study are available from the corresponding author upon reasonable request.

Acknowledgments

We acknowledge the financial support and close cooperation of Filterkonsortium at KIT. Filterkonsortium at KIT unites leading companies in the fields of fiber and media production, assembly, plant engineering, and measurement technology with the research activities of the research group Gas-Particle-Systems of the Institute of Mechanical Process Engineering and Mechanics (MVM). The members of Filterkonsortium at KIT are as follows: BWF Tec GmbH & Co. KG, ESTA Apparatebau GmbH & Co. KG, Freudenberg Filtration Technologies SE & Co. KG, Junker-Filter GmbH, MANN+HUMMEL GmbH, PALAS GmbH. Open access funding enabled and organized by Projekt DEAL. [Correction added on 08 February 2024 after online publication: Figure 1,4 and 7 are updated in this version.]

The authors have declared no conflict of interest.

Symbols used

A_i	$[m^2]$	filter area of a single filter element
A_{tot}	$[m^2]$	total filter area
$c_{clean-gas}$	$[\mu g m^{-3}]$	clean-gas concentration
$c_{raw-gas}$	$[g m^{-3}]$	raw-gas concentration
EDM	$[\mu g m^{-2}]$	total emitted dust mass per filter area
EDM_{PM_x}	$[\mu g m^{-2}]$	emitted dust mass per filter area for a certain size fraction PM_x
K_i'	$[Pa s m^{-1}]$	total resistance of a filter element

K'_{tot}	$[Pa s m^{-1}]$	equivalent resistance of all filter elements
K_{cake}	$[Pa m s g^{-1}]$	specific dust cake resistance
K_{medium}	$[Pa s m^{-1}]$	filter medium resistance
n	$[-]$	number of filter elements
Δp	$[Pa]$	differential pressure
Δp_{filter}	$[Pa]$	differential pressure between the raw-gas side and the clean-gas side
p_{tank}	$[bar]$	tank pressure for filter regeneration
Δp_{tank}	$[Pa]$	pressure drop within the pressure vessel due to filter regeneration
P_{Filter}	$[W]$	total power required for filter operation
P_{fan}	$[W]$	fan power
P_{reg}	$[W]$	energy consumption due to filter regeneration
PM_{tot}	$[\mu g m^{-3}]$	total mass concentration of particulate matter (emission)
PM_x	$[\mu g m^{-3}]$	mass concentration of a particle size fraction (e.g. $PM_{2.5}$)
r^2	$[-]$	regression coefficient
t	$[s]$	time
t_{start}	$[s]$	starting time for integration (here: start of experiment)
t_{end}	$[s]$	end time for integration (here: end of experiment)
Δt and Δt_{cycle}	$[s]$	time interval between regenerations of each individual filter element
$\Delta t_{increment}$	$[s]$	time increment
Δt_{opt}	$[s]$	time interval between regenerations at the power minimum
\dot{V}_i	$[m^3 s^{-1}]$	volume flow through a single filter element
\dot{V}_{tot}	$[m^3 s^{-1}]$	total volume flow
V_{tank}	$[m^3]$	volume of the pressure vessel for filter regeneration
w_{filter}	$[m s^{-1}]$	average/nominal filter face velocity
$w_{filter,i}$	$[m s^{-1}]$	local filter face velocity at a single filter element
W_i	$[g m^{-2}]$	separated/deposited dust mass on a filter element

Greek symbols

γ	$[-]$	empirical coefficient (calculation of PM)
δ	$[-]$	empirical coefficient (separation efficiency)
κ	$[m^{2\delta} g^{-\delta}]$	empirical coefficient (separation efficiency)
η	$[-]$	separation efficiency

References

- VDI 3677 Blatt 1, Filtering Separators – Surface Filters, Beuth Verlag, Berlin 2010.
- P. Bächler, J. Meyer, A. Dittler, *Chem. Eng. Technol.* **2023**, 46 (8), 1689–1697. DOI: <https://doi.org/10.1002/ceat.202300080>

- [3] O. Kurtz, J. Meyer, G. Kasper, *Chem. Eng. Technol.* **2016**, *39* (3), 435–443. DOI: <https://doi.org/10.1002/ceat.201500340>
- [4] F. Löffler, *Staubabscheiden*, Georg Thieme Verlag, Stuttgart **1988**.
- [5] X. Simon, D. Bémer, S. Chazelet, D. Thomas, R. Régnier, *Powder Technol.* **2010**, *201*, 37–48. DOI: <https://doi.org/10.1016/j.powtec.2010.02.036>
- [6] P. Bächler, J. Szabadi, J. Meyer, A. Dittler, *J. Aerosol Sci.* **2022**, *150*, 105644. DOI: <https://doi.org/10.1016/j.jaerosci.2020.105644>
- [7] DIN ISO 11057, Air quality – Test method for filtration characterization of cleanable filter media, Beuth Verlag, Berlin **2012**.
- [8] J. Binnig, J. Meyer, G. Kasper, *Powder Technol.* **2009**, *189* (1), 108–114. DOI: <https://doi.org/10.1016/j.powtec.2008.06.012>
- [9] W. Höflinger, T. Laminger, *Energy Sustainability* **2013**, *4*, 145–155. DOI: <https://doi.org/10.2495/ESUS130121>
- [10] T. Sinn, P. Menesklou, H. Nirschl, M. Gleiß, *Chem. Eng. Sci.* **2023**, *277*, 118858. DOI: <https://doi.org/10.1016/j.ces.2023.118858>
- [11] H. K. Baust, S. Hammerich, H. König, H. Nirschl, M. Gleiß, *Separations* **2022**, *9* (9), 248. DOI: <https://doi.org/10.3390/separations9090248>
- [12] F. Rhein, L. Hibbe, H. Nirschl, *Eng. Comput.* **2023**. DOI: <https://doi.org/10.1007/s00366-023-01809-8>
- [13] W. Solbach, *Staub – Reinhalt. Luft* **1969**, *1*, 24–28.
- [14] R. Dennis, H. A. Klemm, *J. Air Pollut. Control Assoc.* **1980**, *30* (1), 38–43. DOI: <https://doi.org/10.1080/00022470.1980.10465912>
- [15] D. Leith, M. J. Ellenbecker, *Atmos. Environ.* **1980**, *14* (7), 845–852. DOI: [https://doi.org/10.1016/0004-6981\(80\)90141-9](https://doi.org/10.1016/0004-6981(80)90141-9)
- [16] E. Schmidt, *Chem. Ing. Tech.* **1995**, *67* (4), 464–467. DOI: <https://doi.org/10.1002/cite.330670409>
- [17] M. Saleem, G. Krammer, M. S. Tahir, *Powder Technol.* **2012**, *228*, 100–107. DOI: <https://doi.org/10.1016/j.powtec.2012.05.003>
- [18] Z. Potok, T. Rogozinski, *Sustainability* **2020**, *12* (12), 4816. DOI: <https://doi.org/10.3390/su12124816>
- [19] G.-M. Klein, T. Schrooten, T. Neuhaus, *Chem. Ing. Tech.* **2012**, *84* (7), 1121–1129. DOI: <https://doi.org/10.1002/cite.201100251>
- [20] E. Schmidt, *Powder Technol.* **1996**, *86* (1), 113–117. DOI: [https://doi.org/10.1016/0032-5910\(95\)03044-1](https://doi.org/10.1016/0032-5910(95)03044-1)
- [21] Q. Zhang, D. Horst, E. Schmidt, *Chem. Ing. Tech.* **2020**, *92* (3), 275–281. DOI: <https://doi.org/10.1002/cite.201900116>
- [22] Q. Zhang, *Chem. Ing. Tech.* **2022**, *94* (4), 572–584. DOI: <https://doi.org/10.1002/cite.202100053>
- [23] U. Heck, M. Becker, CFD modelling of a bag filter plant for flue gas cleaning under consideration of flow shift and particle deposition relocations, presented at *Filtech – the Filtration Event*, Cologne **2022**.
- [24] E. Schmidt, *Abscheidung von Partikeln aus Gasen mit Oberflächenfiltern*, Fortschritt-Berichte der VDI-Zeitschriften, Reihe 3, 546, VDI Verlag, Düsseldorf **1998**.
- [25] E. Schmidt, Dust separation, in *Ullmann's Encyclopedia of Industrial Chemistry*, Wiley-VCH, Weinheim **2023**. DOI: https://doi.org/10.1002/14356007.b02_13.pub3
- [26] European Commission, Joint Research Centre, K. Daginnus, T. Marty, N. Valeria Trotta, et al., *Best available techniques (BAT) reference document for common waste gas management and treatment systems in the chemical sector: Industrial Emissions Directive 2010/75/EU (integrated pollution prevention and control)*, Publications Office of the European Union, Luxembourg **2023**. <https://data.europa.eu/doi/10.2760/220326>
- [27] A. Dittler, M. V. Ferer, P. Mathur, P. Djuranovic, G. Kasper, D. H. Smith, *Powder Technol.* **2002**, *124* (1/2), 55–66. DOI: [https://doi.org/10.1016/S0032-5910\(01\)00481-8](https://doi.org/10.1016/S0032-5910(01)00481-8)
- [28] P. Bächler, J. Meyer, A. Dittler, *Gefahrstoffe – Reinhalt. Luft* **2019**, *79* (11/12), 433–450. DOI: <https://doi.org/10.37544/0949-8036-2019-11-12-49>

Supporting Information

Operating Behavior of Pulse Jet-Cleaned Filters Regarding Energy Demand and Particle Emissions, Part 2: Modeling

Peter Bächler*, Jörg Meyer, Achim Dittler

DOI: 10.1002/ceat.202300409

Correspondence: Peter Bächler (peter.baechler@kit.edu), Karlsruhe Institute of Technology, Institute of Mechanical Process Engineering and Mechanics, Straße am Forum 8, 76131 Karlsruhe, Germany.

WILEY-VCH

Example dataset showing the results of the model calculation regarding differential pressure (chapter 2.1 of main manuscript)

The results for the model calculation applying the equations summarized in chapter 2.1 of the main manuscript are shown in figure S1.

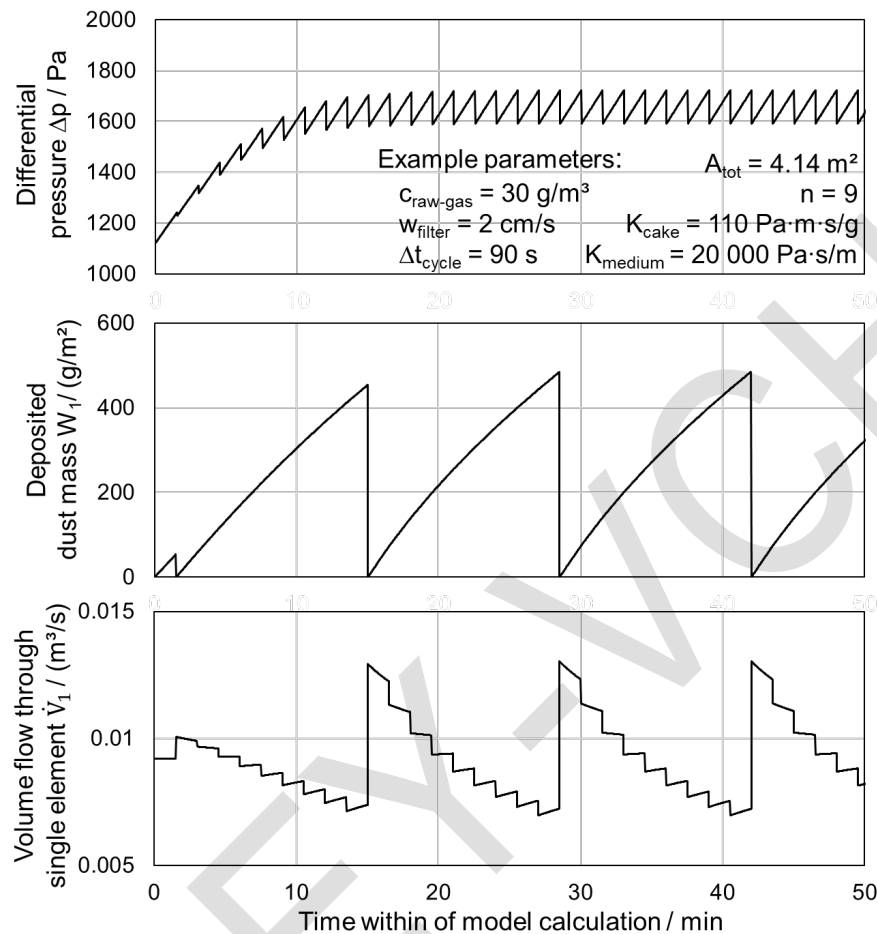


Figure S1. Results of differential pressure, deposited dust mass and volume flow through the single filter element for an example set of parameters

The differential pressure shows the characteristic saw-toothed pattern for pulse-jet cleaned filters. During the course of a complete filtration cycle (duration between the corresponding regenerations of a filter element – here: filter element 1), the deposited dust mass increases. Due to the time-controlled regeneration mode, it takes several cycles until the parameters (e.g. differential pressure) reach a stable level. The volume flow through the filter element changes over the course of an individual filtration cycle. If the filter element has recently been regenerated, the volume flow is high and lowers over the course of a filtration cycle due to the fast formation of a dust-cake and the increase in flow resistance. After reaching a specific dust load on the filter, the volume flow increases through the individual filter element, as other elements have a lower deposited dust mass due to a more recent regeneration. This behavior has also been observed experimentally in a past publication during flow measurements at the individual filter bag [6]. While for the selected parameters (especially medium resistance), the increase in differential pressure is explicitly linear, a more concave differential pressure curve is the result for smaller differences between cake and medium resistances.

Logarithmic fit functions for the entire set of parameters

In chapter 3.1.1 of the main manuscript, a modeling approach for the real differential pressure behavior of the small scale pulse-jet cleaned filter is introduced. Here, the filter medium resistance K_{medium} is selected as the free parameter for optimization and a logarithmic fit-function is derived in order to determine the filter medium resistance as a function of cycle time for each set of parameters. Due to the data-driven approach and the high regression coefficients of the fit-functions, an accurate calculation of the differential pressure in comparison to the experimental data is achieved. Figure S2 summarizes the corresponding functions and the regression coefficients for the entire dataset.

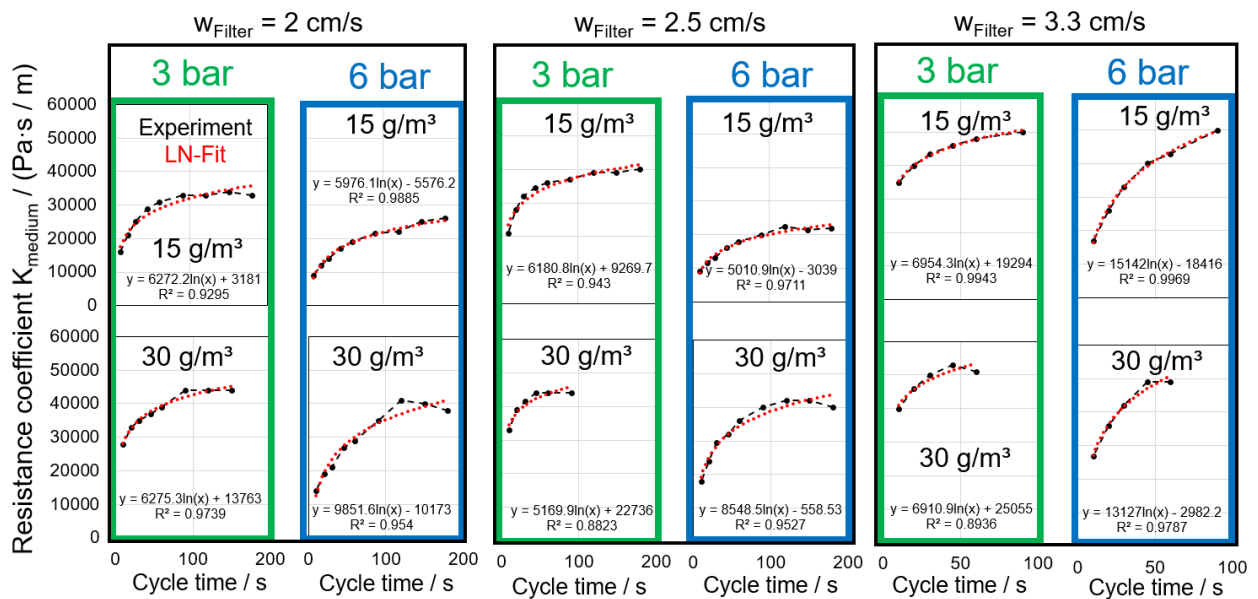


Figure S2. Logarithmic fit-function for the determination of filter medium resistance as a function of cycle time.

Determination of the power minimum for the dataset

The total power for filter operation can be calculated as the sum of fan power and the compression energy related to cycle time (equivalent value for pressurized air consumption). At shorter cycle times and frequent regenerations, the contribution of the pressurized air consumption is considerable. At longer cycle times, the fan power dominates the required total power for filter operation. A distinct power minimum regarding total power and a corresponding cycle time can be identified. Figure S3 – S5 show the required power for filter operation as a function of cycle time for the remaining sets of parameters that are not part of the main manuscript.

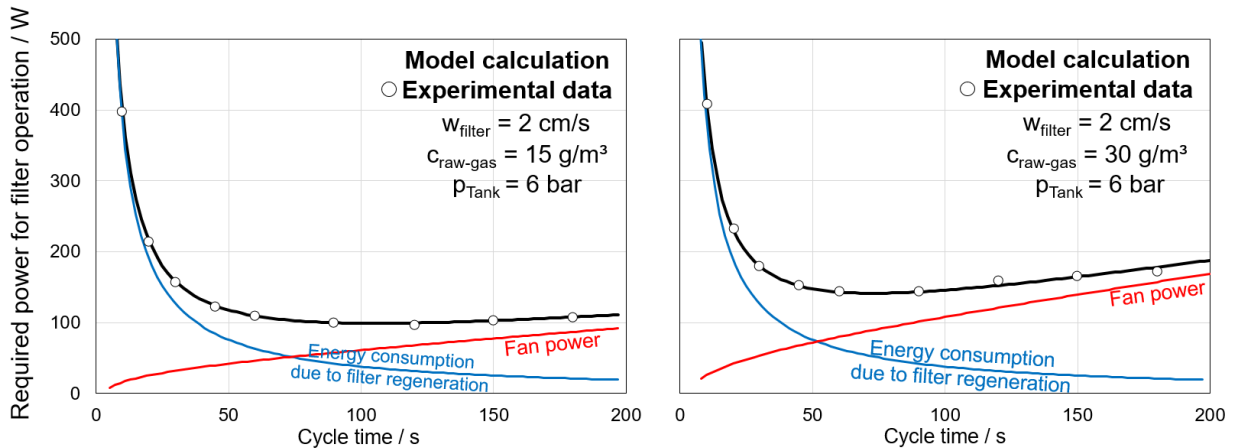


Figure S3. Comparison of experimental data ($w_{\text{filter}} = 2 \text{ cm/s}$; $p_{\text{tank}} = 6 \text{ bar}$; $C_{\text{raw-gas}} = 15$ and 30 g/m^3) and model calculations regarding the required power for filter operation

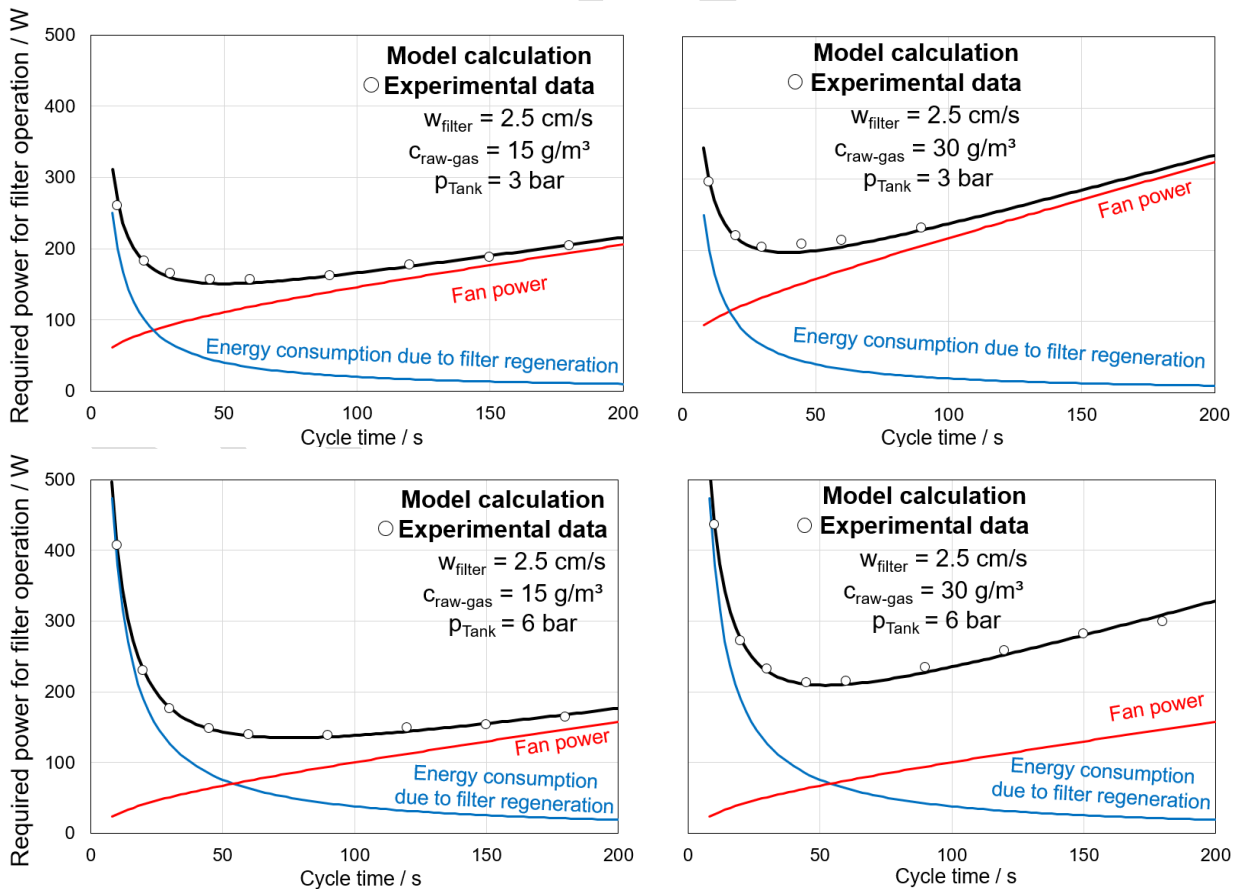


Figure S4. Comparison of experimental data ($w_{\text{filter}} = 2.5 \text{ cm/s}$; $p_{\text{tank}} = 3$ and 6 bar ; $C_{\text{raw-gas}} = 15$ and 30 g/m^3) and model calculations regarding the required power for filter operation

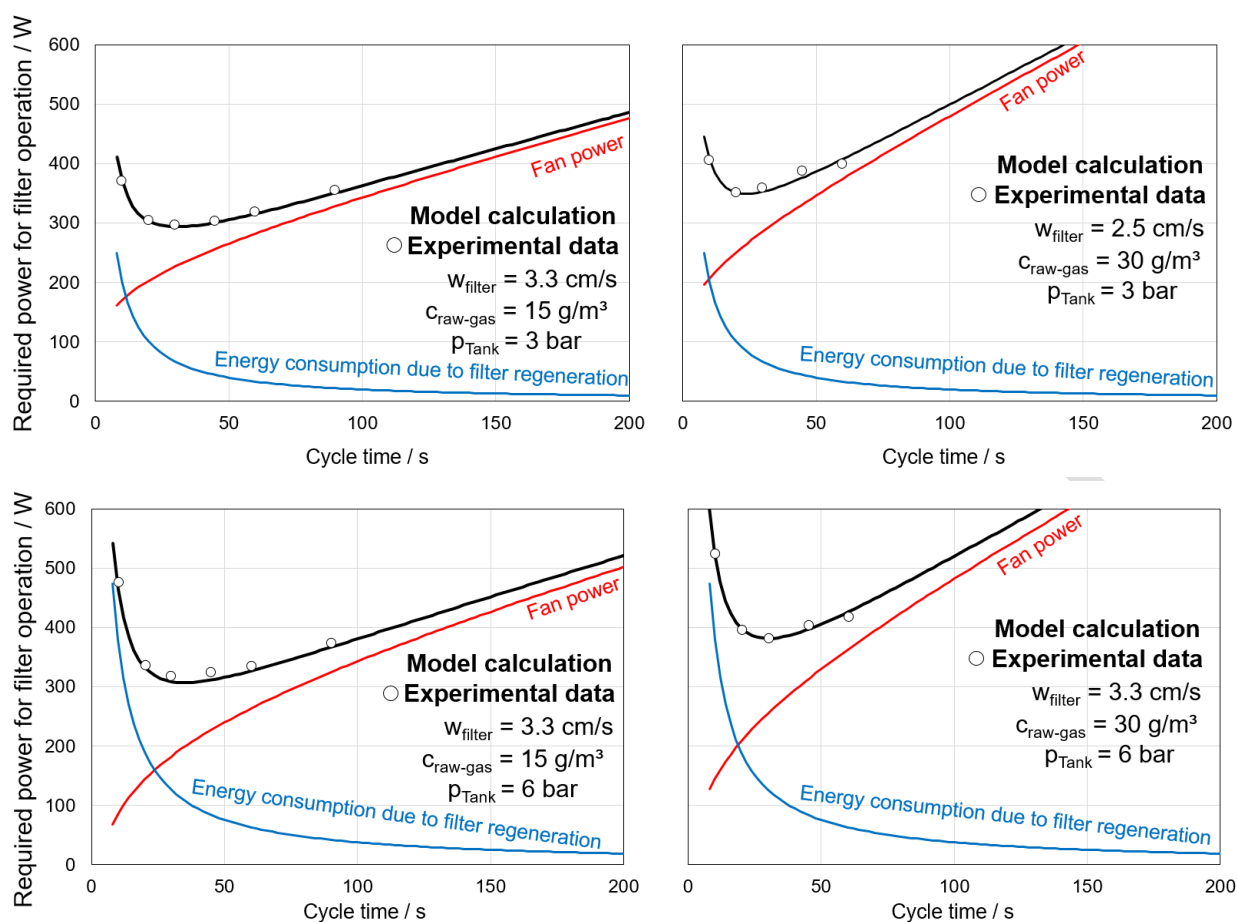


Figure S5. Comparison of experimental data ($w_{\text{filter}} = 3.3 \text{ cm/s}$; $p_{\text{tank}} = 3$ and 6 bar ; $c_{\text{raw-gas}} = 15$ and 30 g/m^3) and model calculations regarding the required power for filter operation

In general, an increase in raw-gas concentration leads to a shift of higher overall power consumption and shorter energetically favorable cycle times. Increasing the filter face velocity has the same qualitative effect on the power consumption, where shorter cycle times are more energetically favorable and the overall power increases with increasing filter face velocity. Increasing the tank pressure for filter regeneration lowers the fan power at the trade-off of higher pressurized air consumption so that the impact on total power is almost negligible. However, the power minimum shifts to longer cycle times so that less frequent regeneration is more feasible.

The agreement between experimental data and the model is very good, as can be expected from the data-driven model approach. Since the energy consumption due to the pressurized air is directly taken from experimental data (compare part I of the study), the overall error from the differential pressure calculation is even smaller when considering total power.

Interpolation outside of the experimentally tested set of parameters

While the extensive set of parameters already covers a wide set of typical parameters for filter operation, the experiments serve merely as a framework of potential process conditions. Raw-gas concentrations, cycle times and tank pressures may very well vary during operation. With the help of the model and the logarithmic fit-functions, intermediate input parameters can be interpolated.

An example is displayed in figure S6, where the experimentally derived fit functions for an intermediate raw-gas concentration of 22.5 g/m^3 at a filter face velocity of 2 cm/s and a tank pressure of 3 bar is compared to the experimental framework at 15 g/m^3 and 30 g/m^3 raw-gas concentration.

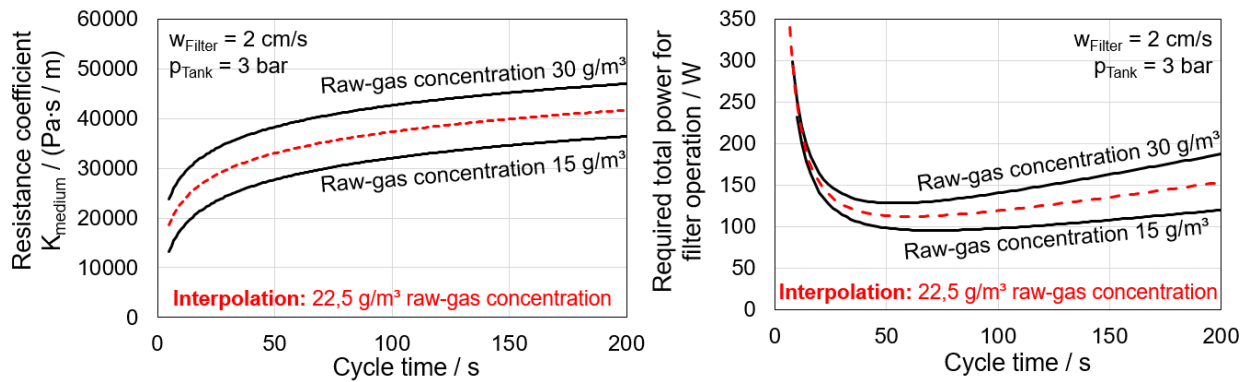


Figure S6. Interpolation of the required power for filter operation for a raw-gas concentration (22.5 g/m^3) not covered by experimental data

Applying linear regression of the parameters of the logarithmic fit functions shown in figure S2 enables the determination of operating condition inside the experimental framework. In this example (raw-gas concentration exactly halfway between the upper and lower limit of the experimental framework), the interpolated curve is exactly in the middle of the model data based on experimental data (linear interpolation). While linear interpolation might not exactly predict real filter operation, the result of the calculation is reasonable. Note that in this example, only one parameter (raw-gas concentration) was interpolated. Due to the extensive set of experimental data, a wider array of input parameters is possible (namely varying filter face velocities and tank pressures).

Figure S7 shows another example, where experimental data at 4.5 bar tank pressure (at 2 cm/s filter face velocity and 30 g/m^3 - compare SI of part I of this study) is compared to an interpolation following the model equations where no fit-function was derived for this specific set of parameters.

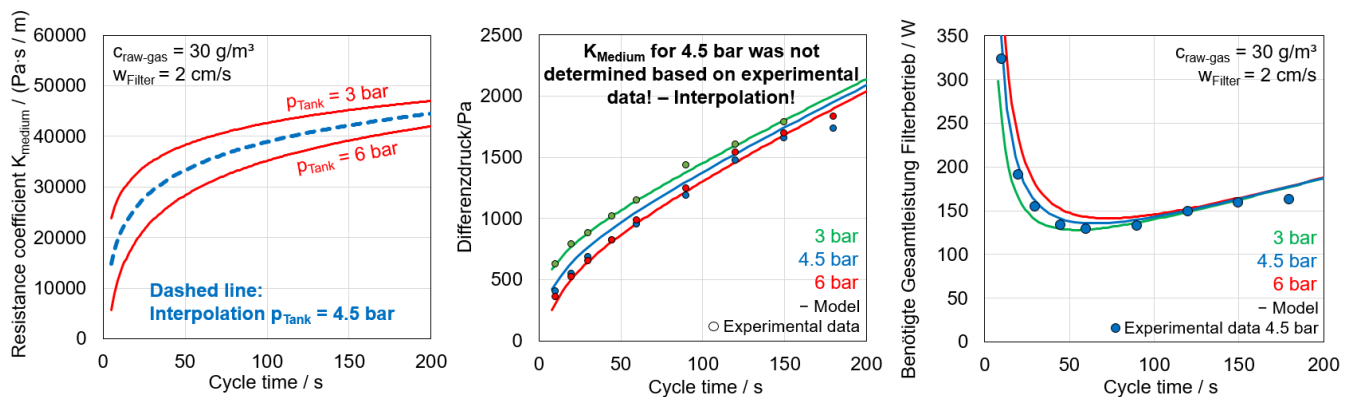


Figure S7. Interpolation of the required power for filter operation for experimental data not covered by the model framework (4.5 bar tank pressure)

Note that the experimentally determined differential pressures are on a similar level compared to the 6 bar experiment. This shows that increasing the tank pressure beyond certain limits does not enhance the resulting pressure drop due to cake detachment. Yet, the model – following an interpolation between 3 and 6 bar fit-functions - results in an intermediate differential pressure level between the two sets of parameters that serve as framework for the fit-function. When considering the power requirement, this error is not as pronounced due to the impact of the tank pressure on the total power consumption and still offers a reasonable agreement.

Summarizing, the tight-knit experimental framework offers the potential for interpolation and the model is the precursor to a digital twin, where filter operation and the impact of a shift in input-parameters on filter operation can be calculated and predicted.

Further context on modeling particle emissions

Linear behavior of the cumulative emitted dust mass per filter area as a function of the number of filtration cycles is also valid for the increased tank pressures at 6 bar (figure S8).

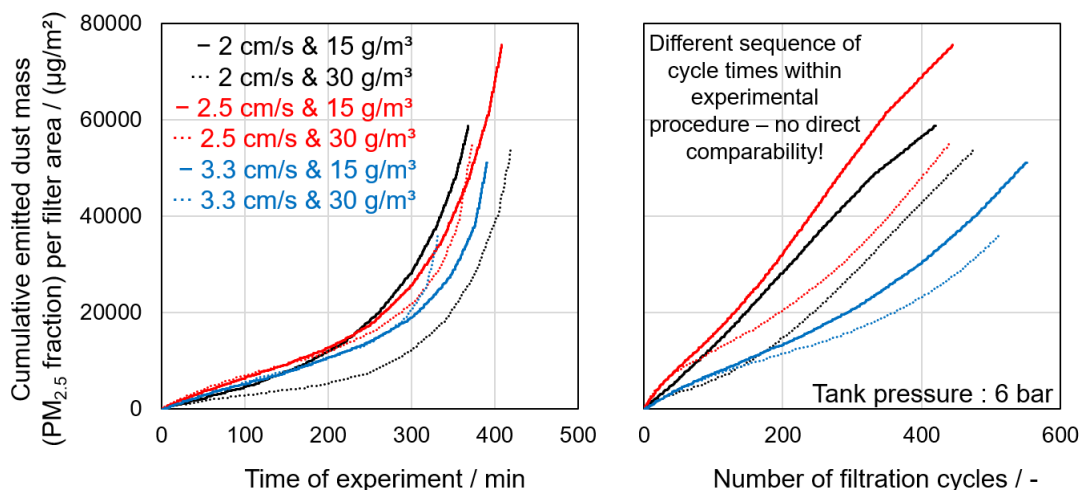


Figure S8. Cumulative emitted dust mass of the PM_{2.5} fraction as a function of time (left) and number of filtration cycles (right) for each experiment (compare part 1 of the study) at a tank pressure of 6 bar

As mentioned in the main manuscript, the slopes of each set of parameters (figure S8 – right) were extracted following linear regression (intercept = 0). Afterwards, out of the determined EDM_{PM_{2.5}} values, an average EDM_{PM_{2.5}} was calculated. The average EDM_{PM_{2.5}} serves as one parameter of the hyperbolic function describing the particle emission (eq. 18 main manuscript). The second (empirical) parameter γ was determined via minimizing the absolute error between model calculation. Minimizing the sum of least squares would improve the correlation at shorter cycle times and higher emissions, that are mostly out of interest for the actual application. The parameters are summarized in table S1.

Table S1. Results for the determination of the hyperbolic function describing the particle emission

p_{tank} / bar	w_{filter} / (cm/s)	$C_{\text{raw-gas}}$ / (g/m ³)	EDM _{PM_{2.5}} / (µg/m ²)	coefficient γ / -	Average EDM _{PM_{2.5}} / (µg/m ²)
3	2	15	32	0.90	23
		30	21	0.97	
	2.5	15	33	0.91	
		30	25	0.99	
	3.3	15	15	1.18	
		30	13	1.21	
6	2	15	142	0.91	108
		30	91	0.92	
	2.5	15	168	0.87	
		30	112	0.94	
	3.3	15	76	0.96	
		30	59	1.12	

The emission data for 6 bar tank pressure was left out of the main manuscript and is shown in figure S9.

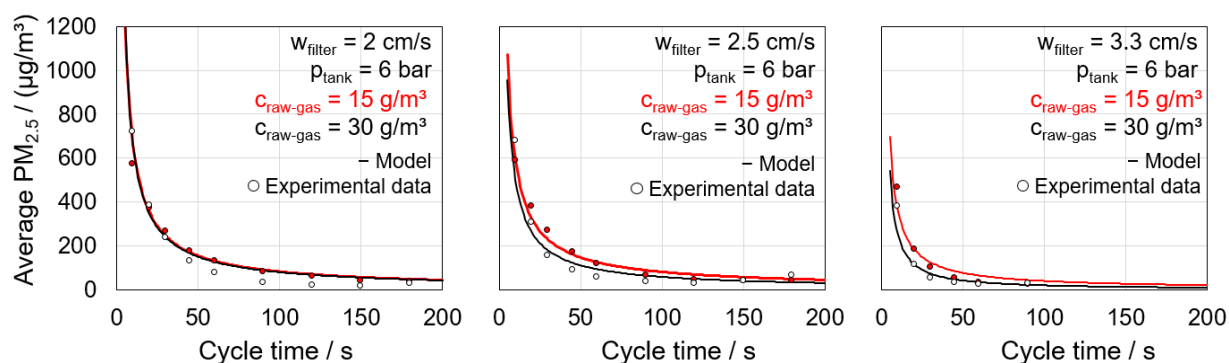


Figure S9. Modeling of particle emissions for the entire set of experimental parameters based on the determination of emitted dust mass ($\text{EDM}_{\text{PM}_{2.5}}$) for 6 bar tank pressure and an empirical coefficient γ for each set of parameters

Applying polynomial regression and generating empirical values for $\text{EDM}_{\text{PM}_{2.5}}$ from the experimental data would also have been possible and would lead to an even higher agreement between model and experiment. The selected approach is based on experimental data and only semi-empirical compared to an all out regression with no consideration to the physical behavior.

ACKNOWLEDGEMENTS

This dissertation is the result of my work as a research associate at the Institute of Mechanical Process Engineering and Mechanics (MVM) at the Karlsruhe Institute of Technology.

First of all, I want to thank Prof. Dr.-Ing. habil. Achim Dittler for his supervision, scientific input and his trust in me. Thank you for encouraging me to pursue an academic career and enabling me to work on many different interesting projects. I cannot say how much I have learned in the past years and how much I grew as a person and an engineer. Thank you for granting me this unique opportunity.

I also want to express my gratitude towards Prof. Dr.-Ing. habil. Eberhard Schmidt for the co-supervision of my thesis.

Acknowledgements go to the “Filterkonsortium at KIT” that set the scope for my research and financed my work. I am truly grateful for the chance to work on a praxis-relevant topic. Thank you to all the members of Filterkonsortium for the numerous project meetings, critical discussions and the personal and scientific input.

Thank you, Jörg Meyer for the countless discussions, the help in the lab and your shared know-how on pulse-jet cleaned filters and measurement technology. I really learned a lot from you and our work together, especially during our unforgettable field measurements at the biomass incineration plant in Günzburg.

My greatest thanks goes to the unsung heroes of this work. Thank you to all students that supported me within the scope of their Bachelor or Master thesis or as research assistants.

Thank you, Tolga Yildiz, Bora Bulut, Julia Szabadi-Fuchs, Daniel Arnauld Sokoundjou Fotsing, Vanessa Löschner, Enes Akdas, Marius Kuhn, Grigor Vrhovac, Akin Filiz, Onur Gazel, Ahmet Kükrek, Linda Kiefer and Jakob Knisley. Thank you for your time, dedication and trust in me and my supervision. Working together with every one of you has been the most enjoyable part of my employment as a research associate.

I also want to mention some of my dear friends and former colleagues. Thank you Thomas Penner and Almuth Schwarz for our runs in “Oberwald”, your enthusiasm for Whisky and for bearing with me through all the highs and lows. Thank you Shukhrat Sobich for introducing me to the filter test rig and helping me get started with the experiments. Thank you Christian Straube for your good humor and to Johannes Deichmann for providing sufficient amounts of oat-drink for our coffee breaks. Thank you Manas Mokashi for many pleasant lunch breaks. Thank you Camila de Lacerda for the fruitful and interesting collaboration. Thank you to all the other doctoral candidates of the GPS group – on some days you were somewhat of a second family and my time here would not have been the same without you.

Acknowledgements also go to the countless technicians at MVM from the electrical and mechanical workshop, the particle measurement lab and the GPS group. Thank you Uwe Albrecht and Friedhelm Klingel for all your help and the stories from the “old days”. Thank you Maik Hof for managing everything electric and Labview-related during my research.

Furthermore, I want to thank Prof. Dr.-Ing. Elke Schweers for showing me the way in the right direction after I completed my Master's degree. When you talked about "particle counting" during my studies, I initially thought it was supposed to be a joke. I could not have guessed where all this would take me.

Thanks also goes to Prof. Dr.-Ing. Wilfried Schütz from the University of Applied Sciences Bremerhaven, without whom I would not be the engineer I am today. Thank you for the many lessons (especially regarding the most important engineering software "Microsoft Excel"). Thank you very much for enabling me to hold my own lectures at Hochschule Bremerhaven.

I also want to thank my family, especially my parents Brigitte and Michael Bächler who encouraged me to pursue an engineering career in the first place, when I did not really know where to go.

Finally, I want to thank my wife Celine. This document is long enough as is, so I will keep these last lines relatively short. Thank you for being such a lovely, kind-hearted and affectionate person. I never want to miss you in my life. You are wonderful!

Peter Bächler, May 2024

LIST OF PUBLICATIONS

Peer reviewed publications

Bächler, P., Weis, F., Kohler, S., Dittler, A., (2024). Exploratory measurements of ambient air quality in a residential area applying diffusion charge based UFP monitor. *Gefahrstoffe – Reinhaltung der Luft*, 84 (1-2), 15-22, <https://doi.org/10.37544/0949-8036-2024-01-02-17>

Bächler, P., Meyer, J., Dittler, A., (2024). Operating Behavior of Pulse Jet-Cleaned Filters Regarding Energy Demand and Particle Emissions – Part 2: Modeling. *Chemical Engineering & Technology*, 47 (4), 722-731, <https://doi.org/10.1002/ceat.202300409>

Bächler, P., Meyer, J., Ligotski, R., Krug, P., Dittler, A., (2024). Measurement of transient nanoparticle emissions of a municipal biomass incineration plant equipped with pulse-jet cleaned filters. *Process Safety and Environmental Protection*, 184, 601-614, <https://doi.org/10.1016/j.psep.2024.02.013>

Bächler, P., Meyer, J., Dittler, A., (2023). Spatially Resolved Online Leak Detection in a Baghouse Filter Applying Low-Cost PM-Sensors. *Chemie Ingenieur Technik*, 95 (1-2), 178-188, <https://doi.org/10.1002/cite.202200116>

Bächler, P., Meyer, J., Dittler, A., (2023). Operating Behavior of Pulse Jet-Cleaned Filters Regarding Energy Demand and Particle Emissions – Part 1: Experimental Parameter Study. *Chemical Engineering & Technology*, 46 (8), 1689 – 1697, <https://doi.org/10.1002/ceat.202300080>

Bächler, P., Meyer, J., Dittler, A., (2022). Measurement of transient nanoparticle emissions of pulse-jet cleaned filters applying an engine exhaust particle sizer. *Aerosol Science & Technology*, 56 (4), 394 – 402, <https://doi.org/10.1080/02786826.2022.2027335>

Bächler, P., Löschner, V., Meyer, J., Dittler, A., (2022). Process integrated monitoring of spatially resolved particle emissions of a baghouse filter using a network of low-cost PM-sensors. *Process Safety and Environmental Protection*, 160, 411 – 423, <https://doi.org/10.1016/j.psep.2022.02.005>

Lacerda, C., R., Bächler, P., Schwarz, A., D., Sartim, R., Aguiar, M., L., Dittler, A., (2022). Impact of Seams on the Operating Behavior of Surface Filters Regarding Particle Emissions. *Chemical Engineering & Technology*, 45 (7), 1354 – 1362, <https://doi.org/10.1002/ceat.202200132>

Bächler, P., Müller, T., K., Warth, T., Yildiz, T., Dittler, A., (2021). Impact of ambient air filters on PM concentration levels at an urban traffic hotspot (Stuttgart, Am Neckartor). *Atmospheric Pollution Research*, 12 (6), 101059, <https://doi.org/10.1016/j.apr.2021.101059>

Bächler, P., Szabadi, J., Meyer, J., Dittler, A., (2020). Simultaneous measurement of spatially resolved particle emissions in a pilot plant scale baghouse filter applying distributed low-cost particulate matter sensors. *Journal of Aerosol Science*, 150, 105644, <https://doi.org/10.1016/j.jaerosci.2020.105644>

Bächler, P., Meyer, J., Dittler, A., (2019). Characterization of the emission behavior of pulse-jet cleaned filters using a low-cost particulate matter sensor. *Gefahrstoffe – Reinhaltung der Luft*, 79 (11-12), 443-450, <https://doi.org/10.37544/0949-8036-2019-11-12-49>

Conference Talks

Bächler, P., Meyer, J., Dittler, A., (2024) Methodik und Ergebnisse einer Feldmesskampagne zur Messung transienter Nanopartikelemissionen hinter einem Oberflächenfilter an einer Hackschnitzelverbrennungsanlage. Conference talk at Jahrestreffen der DECHEMA-Fachgruppen Abfallbehandlung und Wertstoffrückgewinnung und Gasreinigung (Dresden)

Bächler, P., Löschner, V., Meyer, J., Dittler, A., (2023) Optimierung des Betriebs von druckstoßgereinigten Oberflächenfiltern unter Einbezug von Energieverbrauch und Partikelemission. Conference talk at Jahrestreffen der DECHEMA-Fachgruppen Aerosoltechnik, Gasreinigung, Mehrphasenströmung und Partikelmesstechnik (Paderborn)

Bächler, P. Meyer, J., Dittler, A., (2023). On the trade-off between energy efficiency and particle emissions for pulse-jet cleaned filters. Conference paper at FILTECH 2023 – The Filtration Event (Cologne)

Bächler, P., Löschner, V., Meyer, J., Dittler, A., (2022) Emissionsbasierte Optimierung des Betriebs von Oberflächenfiltern auf Basis der lokalen Erfassung von Partikelemissionen. Conference talk at Jahrestreffen der ProcessNet-Fachgruppen Abfallbehandlung und Wertstoffrückgewinnung, Energieverfahrenstechnik, Gasreinigung, Hochtemperaturtechnik und Rohstoffe (Bamberg)

Bächler, P. Meyer, J., Dittler, A., (2022). Identification of particle emission hotspots in baghouse filters via spatially resolved PM measurement. Conference paper at FILTECH 2022 – The Filtration Event (Cologne)

Löschner, V., Bächler, P., Meyer, J., Dittler, A., (2021) Origin of spatio-temporal particle emissions of surface filters due to clogging and release of particles from previously clogged seams of individual filter bags due to jet-pulse cleaning. Conference talk at AFS FILTCON 2021 (virtual conference)

Bächler, P., Löschner, V., Meyer, J., Dittler, A., (2021) On the spatio-temporal particle emission behavior of pulse-jet cleaned surface filters via measurement of the emission contribution of individual filter bags with low-cost particulate matter sensors. Conference talk at AFS FILTCON 2021 (virtual conference)

Bächler, P., Löschner, V., Meyer, J., Dittler, A., (2021) Optimierung von Oberflächenfiltern auf Basis der online Messung lokaler Partikelemissionen und Berücksichtigung des Energieverbrauchs. Conference talk at Jahrestreffen der ProcessNet-Fachgruppen Gasreinigung und Partikelmesstechnik (virtual conference)

Bächler, P., Meyer, J., Dittler, A., (2020). Digitalisierung in der Filtertechnik: Simultane Messung der lokalen Partikelemission von Schlauchfilteranlagen mittels kostengünstigen Feinstaubsensoren. Conference talk at Online Industrieworkshop: „Digitalisierung in der Trenntechnik“ (virtual conference)

Bächler, P., Szabadi-Fuchs, J., Meyer, J., Dittler, A., (2020) Einsatz von low-cost PM-Sensoren zur Messung der lokalen Partikelemission einzelner Filterschläuche in einer Filteranlage im Technikumsmaßstab. Conference talk at Jahrestreffen der ProcessNet-Fachgruppen Computational Fluid Dynamics und Gasreinigung (Bamberg) – Poster award

Bächler, P. Meyer, J., Dittler, A., (2019). Investigation of low-cost PM-sensors regarding the suitability for emission measurement for pulse-jet cleaned filters. Conference paper at FILTECH 2019 – The Filtration Event (Cologne)

Bächler, P., Schwarz, A., D., Meyer, J., Dittler, A., (2019). Innovative Ansätze zur Verwendung von Low-Cost PM-Messtechnik: Neuartige Möglichkeiten der Emissionsbestimmung von Oberflächenfiltern bei der Gasreinigung. Conference talk at Jahrestreffen der ProcessNet-Fachgruppen Mechanische Flüssigkeitsabtrennung und Gasreinigung (Bamberg)

Publication I

Verification of the contribution from the co-authors

Title: Characterization of the emission behavior of pulse-jet cleaned filters using a low-cost particulate matter sensor

Journal: Gefahrstoffe – Reinhaltung der Luft

Authors: Peter Bächler, Jörg Meyer, Achim Dittler

Position in the dissertation:

The content of this paper has been included in Chapter 4.1 and 7.

Contribution of Peter Bächler:

Conceptualization, Methodology, Validation, Investigation, Writing – Original Draft, Visualization

Contribution of Jörg Meyer:

Conceptualization, Writing – Review and Editing

Contribution of Achim Dittler:

Conceptualization, Writing – Review and Editing, Supervision

Publication II

Verification of the contribution from the co-authors

Title: Spatially Resolved Online Leak Detection in a Baghouse Filter Applying Low-Cost PM-Sensors

Journal: Chemie Ingenieur Technik

Authors: Peter Bächler, Jörg Meyer, Achim Dittler

Position in the dissertation:

The content of this paper has been included in Chapter 4.2 and 7.

Contribution of Peter Bächler:

Conceptualization, Methodology, Validation, Investigation, Writing – Original Draft, Visualization

Contribution of Jörg Meyer:

Conceptualization, Writing – Review and Editing

Contribution of Achim Dittler:

Conceptualization, Writing – Review and Editing, Supervision

Publication III

Verification of the contribution from the co-authors

Title: Simultaneous measurement of spatially resolved particle emissions in a pilot plant scale baghouse filter applying distributed low-cost particulate matter sensors

Journal: Journal of Aerosol Science

Authors: Peter Bächler, Julia Szabadi-Fuchs, Jörg Meyer, Achim Dittler

Position in the dissertation:

The content of this paper has been included in Chapter 5.1 and 7.

Contribution of Peter Bächler:

Conceptualization, Methodology, Validation, Investigation, Writing – Original Draft, Visualization

Contribution of Julia Szabadi-Fuchs:

Methodology, Investigation

Contribution of Jörg Meyer:

Conceptualization, Writing – Review and Editing

Contribution of Achim Dittler:

Conceptualization, Writing – Review and Editing, Supervision

Publication IV

Verification of the contribution from the co-authors

Title: Process integrated monitoring of spatially resolved particle emissions of a baghouse filter using a network of low-cost PM-sensors

Journal: Process Safety and Environmental Protection

Authors: Peter Bächler, Vanessa Löschner, Jörg Meyer, Achim Dittler

Position in the dissertation:

The content of this paper has been included in Chapter 5.2 and 7.

Contribution of Peter Bächler:

Conceptualization, Methodology, Validation, Investigation, Writing – Original Draft, Visualization

Contribution of Vanessa Löschner:

Methodology, Investigation

Contribution of Jörg Meyer:

Conceptualization, Writing – Review and Editing

Contribution of Achim Dittler:

Conceptualization, Writing – Review and Editing, Supervision

Publication V

Verification of the contribution from the co-authors

Title: Operating Behavior of Pulse Jet-Cleaned Filters Regarding Energy Demand and Particle Emissions – Part 1: Experimental Parameter Study

Journal: Chemical Engineering & Technology

Authors: Peter Bächler, Jörg Meyer, Achim Dittler

Position in the dissertation:

The content of this paper has been included in Chapter 6.1 and 7.

Contribution of Peter Bächler:

Conceptualization, Methodology, Validation, Investigation, Writing – Original Draft, Visualization

Contribution of Jörg Meyer:

Conceptualization, Writing – Review and Editing

Contribution of Achim Dittler:

Conceptualization, Writing – Review and Editing, Supervision

Publication VI

Verification of the contribution from the co-authors

Title: Operating Behavior of Pulse Jet-Cleaned Filters Regarding Energy Demand and Particle Emissions – Part 2: Modeling

Journal: Chemical Engineering & Technology

Authors: Peter Bächler, Jörg Meyer, Achim Dittler

Position in the dissertation:

The content of this paper has been included in Chapter 6.2 and 7.

Contribution of Peter Bächler:

Conceptualization, Methodology, Software, Validation, Investigation, Writing – Original Draft, Visualization

Contribution of Jörg Meyer:

Conceptualization, Writing – Review and Editing

Contribution of Achim Dittler:

Conceptualization, Writing – Review and Editing, Supervision